NASA-CR 72250

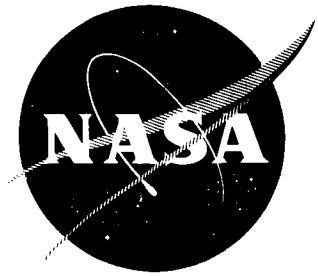

THREE STAGE POTASSIUM TEST TURBINE

FINAL DESIGN - VOLUME II - MECHANICAL DESIGN

By

H. E. Nichols

R. W. Fink

W. F. Zimmerman

prepared for
NATIONAL AERONAUTICS AND SPACE ADMINISTRATION
CONTRACT NAS 3-8520

SPACE POWER AND PROPULSION SECTION
MISSILE AND SPACE DIVISION
GENERAL ELECTRIC
CINCINNATI, OHIO 45215

Requests for copies of this report should be referred to:

National Aeronautics & Space Administration
21000 Brookpark Road
Cleveland, Ohio 44135
Attn: Contracting Officer
Space Power Systems Procurement Section
MS 500-309

DESIGN OF A THREE-STAGE POTASSIUM VAPOR TURBINE

Volume II

MECHANICAL DESIGN

by

H.E. Nichols
R.W. Fink
W.F Zimmerman

Program Manager
E. Schnetzer

March 20, 1967

Prepared For

NATIONAL AERONAUTICS AND SPACE ADMINISTRATION

Contract NAS 3-8520

Technical Management
NASA - Lewis Research Center
Nuclear Power Technology Branch
J.P. Joyce, Technical Manager

SPACE POWER AND PROPULSION SECTION
MISSILE AND SPACE DIVISION
GENERAL ELECTRIC COMPANY
CINCINNATI, OHIO 45215

CONTRIBUTORS

The following General Electric Company SPPS personnel contributed substantially to the mechanical design work described in this report.

I. Bates	Drafting
R. Conley	Drafting
L. Cumbers	Engineering Calculations
D. Engleby	Materials Selection and Fabrication Methods
R.W. Fink	Mechanical Design, Analysis, and Engineering Coverage to Drafting
A. Groh	Manufacturing Engineering
W. Herdliska	Drafting
H. Nichols	Responsibility for Mechanical Design
W.H. Kearns	Welding Methods and Design
C. Kelly	Drafting
N. Knue	Instrumentation
B.L. Moor	Mechanical Design Analysis
D. Pritchett	Drafting Supervision and Planning
E. Schnetzer	Program Manager
W. Townsend	Quality Control Engineering
W. Zimmerman	Materials Engineering Responsibility

TABLE OF CONTENTS

TABLE OF CONTENTS (Cont'd)

LIST OF TABLES

LIST OF FIGURES

LIST OF FIGURES (Cont'd)

LIST OF FIGURES (Cont'd)

LIST OF FIGURES (Cont'd)

LIST OF FIGURES (Cont'd)

LIST OF FIGURES (Cont'd)

LIST OF FIGURES (Cont'd)

LIST OF FIGURES (Cont'd)

LIST OF FIGURES (Cont'd)

I. INTRODUCTION

This report presents the final design of the three-stage potassium vapor turbine. This effort, for the design and fabrication of the turbine, was initiated on June 5, 1966, under NASA contract NAS 3-8520, and is to be completed on December 5, 1967. This report comprises the mechanical design effort corresponding to the major milestone as defined under Section E, Exhibit "A" of the contract,* requiring the final design to be submitted eight months after date of contract. The turbine discussed herein is designed for a 15,000 hour life at 1550°F inlet temperature, and a total-to-static pressure ratio of 7.9. The rotational speed is 18,250 RPM, (as defined under item 3 of the listing of design specifications in Section II). These conditions comprise what is termed throughout this report as "design-point" operation.

The turbine is similar in its overall geometry and concept to the two-stage potassium vapor turbine which was successfully designed and tested on contract NAS 5-1143. This testing was completed in September 1966, (References 1, 2, 3, 4), following which the two-stage turbine was removed from the test facility, allowing the existing test facility to be used with some modifications, in the present three-stage turbine program.

The three-stage turbine described herein incorporates much of the design philosophy of the two-stage turbine, and also reflects design knowledge and experience gained during the previous program. Numerous minor changes have been incorporated into the basic structural components (such as bearing housing) as well as the various major changes involving such items as new turbine wheel materials, and the incorporation of turbine tip shrouds. Table I provides a comparison of significant parameters of design and operation between the two-stage and three-stage turbines.

The design described herein comprises two phases (or main turbine configurations) as follows:

Phase I Assembly with tip-shrouded turbine blades (cast U-700 and machined molybdenum).

---

* See DESIGN SPECIFICATIONS

Phase II Assembly with non tip-shrouded turbine blades (all machined from bar stock).

The Phase I assembly will constitute the first build-up of the turbine, and will be employed during the performance and endurance test. The duration of these tests are as follows:

Checkout and Performance testing: 100-to-200 hours
Endurance test: 5000 hours

The endurance test will follow performance testing with a brief shutdown to inspect blading with borescope. During the Phase I testing, moisture extraction will not be employed in the turbine, and the extraction ports in the casing will be closed-off, accordingly.

The Phase I assembly is the primary design vehicle discussed herein, since it constitutes the most severe stress condition in the rotor (which in general, is the region of limiting turbine stress). The blade and wheel stresses for unshrouded blades are obviously lower, due to lower blade centrifugal forces.

However, complete stress and vibration analyses, and the full set of drawings of turbine components, including flowpath and main assembly drawing (Figure 109), are included for the Phase II (unshrouded assembly) as well as for the Phase I (shrouded) design.

An activity sequence (PERT) chart of the program is shown in Figure 1.

II. DESIGN SPECIFICATIONS

Following are the major design specifications for the three-stage turbine, as defined under items A and B of Exhibit "A" of the contract.

A. DESIGN SPECIFICATIONS

1. The three-stage turbine shall be designed for installation and test in the existing 3000 KW facility without major facility modifications. The identical startup drive, power absorption and support hardware developed under Contract NAS5-1143 shall be used.

2. The turbine shall be designed for a range of inlet vapor temperatures from 1450° to 1550°F, inlet total to exit static pressure ratios from 3.6 to 15.5 and rotational speeds up to 19,500 RPM.

3. The turbine shall have a life of 15,000 hours at an inlet vapor temperature of 1550°F and a rotational speed of 18,250 RPM.

4. The first two stages shall be designed to provide potassium vapor with 8% to 10% wetness into the third stage. Turbine pressure ratio shall be chosen for maximum turbine efficiency, consistent with the wetness.

5. Rotor blade shrouds shall be considered for the first two stages as a means to improve efficiency.

6. The third stage shall be designed for an exit vapor pressure equal to, or greater than 2 psia.

7. The outlet guide vanes, if required, shall be designed so as to prevent choking and to take the swirl out of the exit vapor flow.

8. Rotor blades for stages two, and three shall be dovetailed to each rotor disk to permit removal and replacement of blades.

9. Curvic couplings shall be used to mate each rotor disk.

10. A single tie bolt shall be used to mate each rotor disk.

11. The turbine shall be overhung from the oil-lubricated pivot-pad radial-support bearing and the duplex ball axial-thrust bearing developed under Contract NAS5-1143.

12. The dynamic oil-to-potassium seal developed under Contract NAS5-1143 shall be used for the three-stage turbine.

B. ANALYSIS

1. A detailed turbine harmonic speed analysis shall be performed to determine critical rotational speed ranges. The analysis method presented in NACA TN 4373 shall be used to prevent rotor blade excitation at their natural frequency, which would result in high blade stresses.

2. Detailed turbine thermal and stress plots shall be calculated for inlet vapor temperatures of 1500°F and 1550°F, a rotational speed of 18,250 RPM and the pressure ratio defined in paragraph A., above that will provide the maximum potassium-vapor wetness at the inlet to the third stage.

.
.
.
.
.
.

E. FINAL DESIGN SUBMISSION AND APPROVAL

The contractor shall submit the final turbine design to the NASA Project Manager not later than eight (8) months after date of contract. NASA approval or changes will be specified not later than ten (10) working days after submission. The final design document shall include, but not be limited to, the following:

1. Complete detailed mechanical design drawings of the turbine components, assembly and installation in the 3000 KW facility.

2. Graphical and tabular summary of predicted fluid performance.

3. Detailed turbine thermal and stress plots.

4. Detailed turbine harmonic speed analysis.

5. Material choice for each components, including its process specification.

6. Location, type and calibration procedure for instrumentation.

7. A list of hardware to be procured and that had been procured.

III. INTEGRATED TURBINE DESIGN

General

A cross-sectional drawing of the three-stage Phase I turbine is shown in Figure 2, and a trimetric view is shown in Figure 3. The main assembly is shown in Figure 109. The assembly drawing shows three combinations of turbine hardware groups, including both Phase I and Phase II (shrouded and unshrouded) turbine assemblies and with condensate extraction included for the Phase I design (included as group 3). The turbine comprises three axial flow stages, overhung from an oil-lubricated pivoted-pad bearing and double ball thrust bearing arrangement, similar to the two-stage potassium turbine. Separation of oil and potassium is accomplished by the combined hydrodynamic seal and argon buffer seal shown between the third rotor stage and pivoted-pad bearing. The fluid-dynamic design of the first two stages is identical with that of the two-stage turbine, and the third stage is similar in its mechanical construction, also employing dovetails for attachment of the turbine blades. As indicated above, the third stage has been designed for moisture extraction, which could be incorporated into the turbine test schedule at a later date (and shown as an alternate design on the assembly drawing of Figure 109 and as discussed later), with the intention of obtaining measured data indicative of improved turbine performance and erosion resistance in ultimate space turbomachinery. As indicated previously, during initial testing, the moisture extraction slot will be closed-off as shown in Figure 2. Moisture extraction requires tip shrouds on the turbine blades to collect the moisture for directing it into the casing slot, a technique similar to the approach used in existing General Electric steam turbines. In addition, the tip shrouds minimize the fluid-dynamic losses associated with large tip clearances, and therefore, in the first two stages also, tip shrouds have been included as a step towards increased performance (Phase I design).

The use of dovetail connections for the turbine blades is necessary to allow insertion of blades of various materials for erosion testing, and interchangeability of blades throughout testing. The same dovetail

form is employed on all three stages (first-stage turbine of the General Electric J85 turbojet engine). The turbine rotor stages are held together by a central tie bolt and are indexed to each other by curvic-coupling face teeth. The turbine casings are separated by a horizontally split weld-flange. The radial end-flanges are welded during assembly to the exhaust scroll, and to the aft flange of the inlet duct (bullet nose) assembly.

The turbine exhaust scroll comprises a diffusion section which transitions from axial-to-radial flow, and then dumps the flow into a peripheral plenum collector which directs it around and downward into the test facility condenser below the turbine. No outlet guide vane is used in the turbine exhaust region.

Instrumentation is attached to the turbine by welded connections through tubes which extend from the inlet duct, casing, and scroll regions, and which are fabricated as part of the basic components during their manufacture. Disassembly of any of the turbine components inside the casing will require cutting of the instrumentation lines (pressure taps and thermocouples) as was performed during the two-stage turbine testing.

The nozzle diaphragms are brazed assemblies and are installed into the turbine casings by rabbeted connections. They are held in place by the bolted-in turbine tip seal rings which provide honeycomb running surfaces against the rotor blade tips.

The pivoted-pad bearing - shaft sleeve assembly is very similar to that of the two-stage turbine, except for a number of minor refinements. Also, the double ball thrust bearing assembly is preloaded axially by a belleville spring washer to prevent shifting of the rotor from startup to full running conditions. Lubrication of both bearing systems is done by flow lines extending through the bearing sump region. Reliability and accessibility of the lubrication lines to the pivoted-pad bearings have been improved over the two-stage turbine design, as discussed later. Sealing of the aft bearing sump region is accomplished by a standard carbon face rubbing seal.

The design improvements made to the bearing housing structure, which incorporates all of the main flow tubes in-and-out of the bearing and seals region, comprise mainly increases in the welding accessibility and reliability of the tubes, and an improvement of the heat shield (bellows expansion assembly) covering these tubes. Also, selection of number, size, and location of the individual flow tubes has been judiciously investigated.

Throughout the assembly, all rabbeted connections where flange welding is required, have been provided with shim surfaces, to allow for ease of repair and remachining of these surfaces between major disassemblies of the turbine.

The bearing sleeve and hydrodynamic seal rotating assembly are held onto the shaft by a belleville spring-loaded locknut, which is provided with an accurate rabbet for maintaining concentricity with the shaft.

The coupling on the aft end of the turbine is designed to eliminate the large splined teeth which were employed in the two-stage turbine coupling. The coupling design is not included as part of this contract. However, since it must be integrated with the components on the aft end of the shaft, a preliminary design of the coupling is shown on the turbine assembly, shown in Figure 2 . The coupling shown employs a flexing membrane similar to a bellows convolution, and when combined with a similar configuration on its other end, accommodates misalignment by flexation of these membranes. This coupling more closely approximates a non-lubricated coupling which would be required in an actual space turbine. Such couplings are presently manufactured and sold commercially. The major design effort here will be that of effectively fitting it to the turbine and waterbrake end shafts to provide ease of assembly and to prevent axial constraint (and over stress) of the membranes.

A list of all manufacturing drawings of the turbine components and their numbers designation is given in Figure 108. In addition, copies of all these drawings are included in Figures 109 through 182. A list of all major turbine components to be procured and the numbers of each to be obtained are given in Table II.

Materials Selection

The fabrication materials for the significant turbine components are shown in Figure 4 and are listed below:

Component	Material		Max. Temp. at Design Point (°F)
First-stage wheel	TZM		1434
Second-stage wheel	TZM		1319
Third-stage wheel	Modified Astroloy		1216
First-stage blades	U-700C*		1445
Second-stage blades	U-700C*		
	TZM (molybdenum)		1335
	TZC (molybdenum)		
Third-stage blades	U-700C*		
	TZM		1230
	TZC		
Blade fasteners	Rene' 41	1st	1445
		2nd	1335
		3rd	1230
Shaft	A-286		1065
Tie Bolt	U-700		1439
Nozzle Partitions	L-605	1st	1497
		2nd	1372
		3rd	1255
Exhaust Scroll	Type 316 SS		1169
Turbine Casing (Fwd Flange Weld)	Type 316 SS		1378
Bearing Housing (Fwd End)	Type 316 SS		852

* Wrought U-700 blades machined from bar stock will be available as a backup.

The materials listed above were selected based upon either (1) their successful use in the previous two-stage turbine under similar design conditions or (2) their necessity for meeting the 15,000-hour design life requirements. The rotating parts, particularly, were affected by the longer design life requirement and the desirability of utilizing replaceable blades.

The only significant departure from the contigent of materials used in the two-stage turbine is in the first two rotor stages, where TZM is being used as the wheel material instead of U-700, as on the two-stage turbine. The third turbine stage wheel is made of Modified Astroloy, which is quite similar in composition to U-700.* All major structural containment parts are made of type 316 stainless steel, and the shaft is made of A286. The tie bolt is U-700. All the stage one blades are made of U-700, while the stage two and stage three blades both comprise an assortment of U-700, TZM, and TZC blades (four TZC blades and four TZM blades in each stage, with the remainder being U-700).

• Design Data

The typical compositions of the various alloys are given in Table III. Design information is found for the various material properties in the figures indicated below:

Data	Figure
0.2% yield strength versus temperature	5
Ultimate strength versus temperature	6
Elongation versus temperature	7
Modulus of elasticity versus temperature	8
0.2% creep stress: Parameter Plot	9
Master rupture stress: Parameter Plot	10
Coefficient of thermal expansion versus temperature	11

The heat-treat condition of the alloy for which design data are presented is designated by a reference number which is referenced in detail in Table IV.

• TZM Wheel Forgings

The evaluation of one of six TZM pancake forgings supplied by NASA for use in the first two stages of the turbine is reported in detail in Appendix A. It was concluded that the forgings were adequate, but that

* See Table III.

their low brittle-to-ductile transition temperature, particularly in the area of the curvic coupling, was cause for concern during manufacturing and handling. It is recommended that backup forgings be procured using improved forging techniques intended to assure improved grain flow conditions near the curvic coupling.

• TZM Wheel Broaching

In addition to preliminary dovetail broaching trials which were performed on a section of a NASA TZM wheel forging by Walbar Machine Products, Inc., of Peabody, Mass., and which are reported in Appendix A, a TZM broaching machinability experiment was performed to select machining speeds, tool configurations, cutting tool materials, and lubricants. The results of this broaching study on TZM are reported in Appendix B.

It was concluded from the above study that (1) tool life should be sufficient for broaching more than 100 wheel slots, (2) a surface finish of 30-50 rms can be achieved, (3) some surface smearing of metal will occur to a depth of about one mil, and (5) a steel backup plate is necessary to prevent breakout along the back surface of the broached slots.

• Modified Astroloy Wheel Forgings

The formation of sigma phase in U-700 alloy (or in Modified Astroloy, which has a similar composition as seen in Table III) can cause loss of room temperature ductility; it is, therefore, desirable to minimize the possibility of sigma phase formation in the third-stage U-700 (or Modified Astroloy) wheels.

Sigma phase rarely forms in nickel-base alloys heated under stress for long duration at temperatures under 1400°F. Since the third-stage wheel operates well below this temperature, the possibility of sigma phase formation in that stage is very minor even in an alloy of specific composition prone to sigma phase formation. A factor (in addition to temperature) which has an influence on sigma phase formation is the composition of the alloy matrix from which sigma phase might form. A

method for calculating the tendency for an alloy to form sigma phase has been described by Woodyatt, Sims, and Beattie.* It treats the original composition of the alloy in a mathematical way, ascribing various elements in the proper amounts to form the various precipitating phases in a sequential order according to their relative stability. In the analysis, an electron vacancy number N_v is calculated for the alloy from the original composition. This number is a measure of the tendency of that alloy composition to form sigma phase; if it is above 2.32, sigma phase will form (if it is below 2.32, sigma phase will not form).

In the previous operation of the two-stage turbine, the Astroloy wheels had an N_v of 2.57, well above the maximum permissible value of 2.32 for sigma phase resistant material. Nevertheless, these turbine wheels performed well during test, but they were not immediately available for destructive analysis and evaluation of sigma phase formation after the test.

Sigma phase was found, however, only in first stage U-700 alloy blades operated for 3000-5000 hours in the two-stage turbine in that specific alloy composition, which was prone to sigma phase formation. Since the formation of sigma phase requires temperatures above 1400°F, there was no evidence of sigma phase in the second-stage blades, which operated at only 1314°F. Sigma phase was evidenced in the first-stage blades, both metallographically and as indicated by low ductility at room temperature; these blades operated above 1400°F.

Since the third-stage astroloy wheels will be operated well below 1400°, they, like the second-stage blades in the two-stage turbine, should not be affected by sigma phase formation.

---

*Woodyatt, L.R., Sims, C.T., and Beattie, H.J., Jr., "Prediction of Sigma-Type Phase Occurrence from Compositions in Austenitic Superalloys," Trans. Met. Soc. A.I.M.E., V 236, No. 4, pp. 519-27.

It would have been desirable, but not essential, to procure the third-stage wheels from a U-700 composition with N_v less than 2.32 (sigma phase resistant); however, the immediate availability of Modified Astroloy wheels (successfully used in jet engine applications) prompted its selection even though the N_v of the available heat was 2.4.

A comparison of the compositions and heat treatments for the superalloy wheels used in the earlier two-stage turbine and in the present three-stage turbine is shown in Table V. Five forgings have been ordered, one for mechanical test evaluation and machinability studies and four for potential use as wheels.

• Cast U-700 Blades

When the two-stage turbine was designed, the decision on fabrication of blades was made after considering cast, forged, and machine-from-bar stock blades. At that time castings were neither well-developed nor in extensive use in jet engines; forged blades require extensive lead times, die rework, and removal of forging flash which resulted in the immediate availability of less accurate airfoils than required for development purposes. Consequently, the machined-from-bar stock approach was used in the two-stage turbine with the intent of securing accurate airfoils, in minimum numbers, at lowest total cost. The experience in procuring the first set of blades was poor in that deflection of the blades and tool wear resulted in blade inaccuracies; however, a second set of blades procured from an alternate vendor was good.

For the three-stage turbine, forged blades are again rejected for the same reasons as above and the fact that the number of blades to be produced does not justify the costs and effort.

The difficulty of preparing shrouded U-700 blades machined-from-bar stock supported the decision to use castings for the shrouded blades. However, a set of unshrouded U-700 blades will be machined-from-bar stock, presently on hand, as a backup to the cast blades.

The considerable improvements which have been made in castings, their widespread use in current jet engines, their relative lower costs, their high reproducibility, and their nominal delivery lead times made the selection of cast U-700 blades with shrouded tips a highly promising one. The casting technology for superalloy blades has improved considerably in the last 5-6 years. Higher mold preheat temperatures, lower metal superheat during casting, the use of grain-refining inoculants in molds, the control of alloys for improved ductility by the PHACOMP method, and newer heat treatment methods have resulted both in finer grain size control and improved ductility in cast blades and in improvements in casting precision.

The design, quality control measures, and precurement practices associated with the cast blades will follow those which have been used successfully in the application of cast blades to aircraft gas turbines.

For example, (1) blades will be purchased P.T.L.O. (prior to layout inspection). This basis of purchase requires that the vendor produce metallurgically sound blades and that the customer assume the risk, in the first set of blades produced, that the geometric definition of the blades will be adequate. This eliminates the necessity of a reiteration period for modification of the blade pattern and the casting of a second set of components; and it could save as much as ten to fourteen weeks in the schedule. A sufficient number of parts for immediate use would be available; but if the blade pattern required rework, an additional manufacturing cycle would be required to obtain parts for use. (2) All material will be procured from a single heat of PHACOMP controlled U-700 prepared by vacuum induction and/or vacuum consumable-electrode remelt methods. (3) Precision vacuum investment casting will be used. (4) Careful nondestructive evaluation by X-ray and fluorescent penetrant methods will be used to eliminate blades which might have critical defects, particularly along leading and trailing edges where surface defects might initiate vibratory fatigue or thermal cycle fatigue failures. (5) Grain size control requires that there be no sharp transition in grain size, no columnar grains in the circular airfoil

or dovetail areas, and that the average grain size in the airfoil by 1/16 inch or less. (6) A total of thirty tensile test specimens will be prepared from the same heat and will be used in documenting the original properties of the cast blades at the turbine stage temperatures and at the same conditions after 1000 hours aging in vacuum at stage test conditions. (7) The cast U-700 erosion inserts will be prepared from the same heat and at the same time as the U-700 cast blades.

• Refractory Alloy Blades

Both TZM and TZC molybdenum alloy blades were tested in the two-stage turbine; these blades were made by a process of rough electrical-discharge machining of the airfoil surfaces followed by hand-benching to bring the airfoil surfaces to final dimension and to remove surface stock containing the last traces of electrical-discharge machining surface imperfections. This same process will be used in machining the TZC and TZM molybdenum blades for the three-stage turbine.

The difficulties in achieving room-temperature ductility in processing TZC to bar stock are indicated in Figure 12. In rolling TZC to 3/4-inch thick plate, it was necessary first to hot-roll at 2900°F in order to get some initial work into the material and to prevent cracking at the lower cold-working temperatures. Because of this it was not possible to achieve a high degree of cold work in the final 3/4-inch thick plate; as a result, the room-temperature ductilities were low.

Figure 13 shows the stability of the various carbide phases and is helpful in understanding the reasons for the lack of ductility in this material. At the melting temperature the carbon is in solid solution; such distribution of carbon results in a matrix of low ductility at room temperature. Long duration heat treatments in the 3000-3100°F temperature range, as occasioned by extrusion or rolling operations, tends to permit the precipitation of unfavorably dispersed Mo_2C carbides which result in lower hot strength and poor ductility. This precipitate is favored by

the strain induced in hot rolling. Processing operations in the range above 3000°F should be minimized; on the other hand, warm working of the TZC in the 2400°F range (1) produces strain in the alloy which encourages the precipitation of a highly dispersed TiC strengthening phase, (2) eliminates room-temperature embrittling carbon from the matrix, and (3) provides hot cold-work strengthening of the matrix.

As an indication of more optimized processing of TZC, Figure 14 illustrates the good room-temperature ductility which can be achieved in TZC when the material is worked to a large reduction in area at 2400°F with a minimum of higher temperature treatment. Ductilities above 10-15% elongation at room temperature were achieved without sacrificing strength. In material processed at lower degrees of cold work, long time aging at temperatures near 2600-2700°F will precipitate carbon from the matrix as carbon and room temperature ductility will also be improved, but the strength characteristics, both in tensile test and in rupture test, will decrease.

The TZC materials for the second and third-stage blades is being procured with a minimum of high temperature processing and with at least 72% reduction in area at 2400°F. Round bar stock 1-1/2 inches in diameter is being produced rather than plate or bar since cracking and alligatoring of the material during rolling is less likely when the material is well supported, as in rod-rolling; a less efficient use of material is involved, but the probability is better of producing sound material with good strength and adequate room-temperature ductility.

- Material Test Inserts

In addition to the refractory metal blades in stages two and three, inserts of various materials will be installed downstream of stage-three rotor and investigate the effects of liquid impingement. Twelve such inserts will be installed, including nickel, molybdenum, and columbium-base alloys. The materials to be tested are indicated in Table VI. Shown in Figure 15

is the arrangement of the erosion inserts in the third stage tip seal ring. The inserts will be flush with the outer wall of the flowpath and will extend forward over the trailing edge of the third stage rotor tip shroud. The tip seal ring will have a machined relief on the side of the insert from which the rotor blade approaches, as shown in Figure 15(b). The fluid which is slung off the trailing edge of the rotor tip shroud will impinge on the relieved side and the inner flush face of the insert as shown. The detail of this liquid impingement concept is shown in Figure 15(c). Previous experience (on the two-stage test turbine) indicated that the impingement area is located radially outward from the turbine blade along the exposed edge of the insert where the tip seal rim is relieved. Erosion of the insert is caused only by liquid which was part of the film on the blade surface. This film moves on the blade in a direction which deviates only two or three degrees from radial. The detail drawings of the assembled test inserts and tip seals are shown in Figure 160 and 167 for the shrouded and unshrouded blade designs.

Flowpath

Figures 16 and 17 show enlarged views of the turbine fluid-dynamic parts region, (for Phase I and Phase II design) and the turbine hot flowpath for Phase I is shown in Figure 18. This comprises the flowpath geometry for the design point conditions.* In the high velocity flow region (exhausting from each nozzle blade row) losses are minimized by radially extending the outer and inner extremities of the turbine rotor blade slightly beyond the flow stream lines, to prevent the flow from "tripping" over the blade platform and/or outer shroud band during its entry into the blade row. This results in approximately a 0.060 diametral over-size of the blade tip shroud, and a 0.010 inch diametral undersizing of the blade platform diameter. The third-stage blade tip shroud has a slight slope to facilitate the flow of collected liquid to the blade shroud trailing edge during moisture extraction

* 1550°F inlet temperature, 7.9 total-to-static turbine pressure ratio, and 18,250 RPM rotational speed as defined under item 3 of DESIGN SPECIFICATIONS.

testing. Figure 19 shows the cold flowpath necessary in fabricating the turbine components, to provide the hot flowpath of Figure 18 during high temperature operation. The apparent non-smooth character of the cold flowpath results from the relatively large differences in thermal expansion coefficients between the high-growth stator components (made of 316 stainless steel) and the low growth characteristics of the rotor components (made of TZM and U-700).

Figure 20 shows the corresponding hot and cold flowpath outer contour corresponding to the Phase II (unshrouded) design. The inner flowpath contours for hot and cold conditions are identical to those of Figures 18 and 19, respectively. Further detail information on specific blade geometry is given in Tables VII and VIII for the shrouded and unshrouded blades, respectively.

Inspection Ports

Prior to completing all tests in potassium vapor, it may be desirable to visually inspect the turbine critical fluid-dynamic regions (blades and tip seals) for overall mechanical integrity and/or any signs of gross deterioration. To consider removal from the facility and partial disassembly of the turbine for such routine inspection would not be justified in terms of cost and testing delay. Instead, means have been provided for inspecting the turbine by use of borescope extended inward through the casing between each blade row, as shown in Figure 21. This requires drilling through not only the casing, but judiciously through nozzle diaphragm shroud bands and honeycomb tip seals. The holes in the casing are sealed-off by capped tubes extending outward from each hole (see Figure 143). The borescope holes are 0.25 inches in diameter, to be used with 3/16 inch diameter borescopes. The possibility of inspecting the aft region of the turbine fluid dynamic region through the scroll inspection ports exists, is discussed later.

Design Criteria

Figure 22 defines the basic stress design criteria used for the overall mechanical design. The long-time operation of a space turbine with an uncooled rotor makes the problems of material creep and stress-rupture generally more limiting than the short-time properties of yield and ultimate strength. The stress- temperature-life relationship is based on the use of the Larson-Miller parameter, and the theory of failure employed is the Henky-vonMises minimum-energy-of-distortion theory. Figure 22 shows the allowable stress criteria for yield, creep, and rupture, stresses, and the assumptions for blade alternating stresses are defined.

Turbine Temperature Distribution

The calculation of an accurate overall turbine temperature distribution is a necessary prerequisite for the analysis of thermal stresses, and for differential thermal expansion calculations to establish proper clearances (for example, the flow paths described previously). Also, allowable stresses and other materials properties (obtained from the curves of Figures 5 through 11) are based upon the calculated temperatures.

Calculations of temperatures are performed using a computer program (THTC) which is based on a thermal-electrical analogy, wherein the turbine is subdivided into a series of material blocks or "nodes" and Kirchoff's laws are written about each node with heat flow instead of current as parameter. Figure 23 lists the assumptions and limiting conditions for the temperature distribution calculations performed herein. Figures 24 and 25 show the nodal pattern plots for both the rotor and the stator. Because of axial geometry of the turbine parts, the nodal plot can be shown in a single plane, with each node having a wedge shape, varying with radius (in the plane normal to the paper). All material surface-to-surface contacting

coefficients and convective coefficients of heat transfer between joining parts, are defined (and used for all the calculations included here) as shown in Figure 26 where the rotor and stator nodal plots are shown superposed. A temperature distribution was calculated for four operating conditions as follows:

1. 1550°F inlet temperature and pressure ratio 7.9 (design point)
2. 1550°F inlet temperature and pressure ratio 3.06 (high-temperature exhaust)
3. 1500°F inlet temperature and pressure ratio 7.9 (lower than design point temperature)
4. 1450°F inlet temperature and pressure ratio 12.6 (start-up condition)

The first condition represents design point operation, with its resulting temperature distribution indicated in Figure 27. The second condition (Figure 28) represents a "high exit temperature" condition wherein the exhaust temperature is highest, due to the low turbine pressure ratio. The third operating condition (Figure 29) represents a lower inlet temperature of 1500°F, but with design point pressure ratio, and the fourth condition (Figure 30) represents a still lower turbine inlet temperature condition and high pressure ratio, giving low turbine exhaust temperature, characteristic of startup conditions.

In addition to the steady-state temperature distributions indicated in the foregoing figures, thermal transient conditions are also calculated, (as representative of the startup operation), for each of the above conditions. Some of the results are shown for design point operation only, as indicated in Figures 31 through 35. These figures examine the possibility of problems of mechanical interference between rotor and stator and/or possible loosening the tie bolt during startup. These curves assume a 700°F environmental temperature throughout the turbine blade-wheel-nozzle region prior to startup (representing the electrical pre-heating of the turbine to minimize thermal shock and to obtain some ductility in the refractory metal parts at startup). The transient temperature calculation assumes that the full operating temperature environment is instantaneously imposed on the turbine

and maintained constant up-to, and throughout steady-state operation. This is somewhat more severe than an actual turbine start, and the transient temperature gradients are, therefore, conservative. Figure 35 indicates the transient temperature during start-up for various selected points along the rotor and tie bolt.

Figures 31, 32, and 33 show, for the design point conditions (1550°F inlet temperature and 7.9 total-to-static pressure ratio) the axial growth of the stator, rotor (shaft and wheels), and tie bolt as a function of distance forward from the thrust bearing at various increments of time after onset of vapor flow. Figure 34 shows the differential thermal expansion of the most critical locations along the turbine as a function of time after onset of vapor flow. These locations are at the axial clearance space between stator and forward face of the rotor, and at base of the head of the tie bolt, respectively. Obviously, unfavorable transient or steady-state thermal expansion opening or closure at these locations could produce axial rubs and/or loosening of the tie bolt. This figure indicates the general similarity in thermal growth as a function of time between tie bolt and rotor, thereby preventing thermal loosening. Also, the differential growth between rotor and stator is greatest at steady-state, for which condition the axial clearances have been adequately sized, as indicated later.

Figure 35 shows the transient temperature differences between tie bolt and rotor wheels (at their most massive sections) and indicates a maximum differential temperature (in the first stage wheel location) of about 200°F at 10 seconds. This distribution is acceptable.

Figures 36, 37, and 38 show steady-state axial elongation of stator, rotor, and tie bolt as a function of turbine length for the three off-design conditions. Figure 36 presents greater expansion, and Figures 37, and 38, less expansion than the design-point conditions.

Figure 39(a) shows the hot and cold radial and axial clearances which were set following the foregoing temperature distribution and thermal expansion analyses. Figure 39(b) incorporates these dimensions in the formal clearance drawing for the turbine, and Figure 39(c) shows the hot and cold fits of mating parts. Figure 40 shows the axial stack-up drawing for the critical fluid dynamic region of the turbine, based upon the nominal hot-and-cold axial clearances of Figure 39 and after inclusion of allowable manufacturing tolerances.

Critical Speed Analysis

The critical speeds for the turbine were calculated using the VAST (Vibration Analysis System) program, which is a computer program that identifies critical speeds by balance of potention and kinetic energies of the entire rotor-stator system. In this instance, the program analyzed the turbine, the turbine mounting structure, and the upstream duct (to the boiler) as a system. The computer technique is to break the turbine up into a large number of short segments, considering each incremental link as short beam, (shown conceptually in Figure 42) and with the rotor suspended in the stator by a series of springs (bearings). The bearings are mounted in their housings which are in turn connected to support structure. The natural frequencies of the support structure are also determined by considering them as supported by springs which simulate the flanged connections.

The assumptions employed in the analysis of the system critical speeds are indicated in Figure 41. Figure 43 shows the analytical model used to calculate the critical speeds for the three-stage turbine. The various basic structural parts are considered to be continuous spans (as numbered) connected together by the welded joints and/or bearing springs.

The turbine critical speeds are influenced by the major connections to external components such as the long upstream duct, and glove box, at its forward end, and the connection to the waterbrake load train system

through the flexible coupling. In this analysis, the upstream duct has been considered as part of the vibrating system. The flexible coupling-to-waterbrake is considered to be extremely soft in comparison to the remainder of the turbine, and is, therefore, ignored as a structural component. The critical speeds discussed here do not include critical speed analysis of the waterbrake-steam turbine drive train system which will be subsequently analyzed, and may ultimately affect the selection of the precise operating speed.

For this analysis, the spring constants for the pivoted pad bearing and the ball thrust bearings are considered to be 500,000 lb./in. and 1,000,000 lb./in. respectively, based on previous experience. Although investigation through a speed range of up to 20,000 RPM is adequate, the analysis was performed over a range from 0 to 50,000 RPM, and the various speeds and corresponding bending mode shapes identified are shown in Figure 44.

It can be seen that the rotor modes, the duct modes, and other modes are determined. Figure 44(a) shows the first natural frequency of the system duct wherein the turbine is active only as a mass on the duct.

Figure 44(b) shows the second natural frequency of the duct system. Here again, the turbine is active as only a mass on the duct. Figure 44(c) shows the third natural frequency of the duct system with the turbine still significant only as a mass. Figure 44(d) shows the first rigid-body critical of the rotor in its bearings (conical whirl). Here, the extended springs illustrate the potential energy storage associated with this condition. Figure 44(e) shows the fourth natural frequency of the duct. The mode shape was normalized on the basis of the duct amplitude. It can be seen that there is also some potential energy in the spring representing the pivoted pad bearing. Figure 44(f) shows the fifth natural frequency of the duct. Figure 44(g) shows the first natural frequency of the duct and turbine rotor systems. In this case, the combined system normalized on the rotor amplitude. Figure 44(h) shows the second natural frequency of the duct and turbine rotor systems. Figure 44(i) shows the second rigid body critical of the rotor

in its bearings (cylindrical whirl). Figure 44(j) shows the first bending mode of the rotor.

In addition to the above determination of the critical speeds of the entire turbine-ducting system, an investigation was performed to determine the effect of variations in the assumed spring constant of the pivoted pad bearing on the two important rigid body critical speed modes, (i.e. the conical whirl and cylindrical whirl modes) and the shaft first bending mode. For this analysis, the thrust bearing spring constant was maintained at 10^6 lb./in., and the pad bearing spring constant was varied between 5000 lb./in. and 500,000 lb./in. The turbine non-rotating structure was considered to be an infinite mass, thereby isolating the critical speeds of only the rotor in its springs (bearings). The results are shown in Figure 45, and can be compared with the corresponding rigid-body critical speeds of the previously-tested two-stage turbine. The latter critical speeds were borne out by testing (Reference 1). As expected, the rigid-body criticals for the three-stage turbine rotor are lower than those of the lighter-weight two-stage turbine. Also, it can be seen that for all the assumed pad bearing spring constants, the cylindrical whirl and shaft bending modes are above the turbine's maximum operating speed, and are, therefore, of no consequence.

A further investigation of the vibrational behavior of the tie bolt alone, indicated its first critical speed to be at 46,846 RPM, which is considerably above the operating range, and therefore, also of no significance.

IV. INDIVIDUAL COMPONENT DESIGN

The following discussion presents the results of the detailed design of individual turbine components and sub-assemblies of them, in combinations which affect the overall functioning capacity and mechanical integrity of the turbine. A geometric description of each part is included in the set of manufacturing drawings of Figures 109 through 180, which contains the major assembly drawing (Figure 109) showing both Phase I and Phase II design and a list of the detailed component parts and drawing numbers. Table XIII presents a listing of significant turbine physical and dynamic data, including the approximate weight of all the turbine components, and specifically, the length, bearing span, and C.G. location of the assembled rotor.

Rotor

• Blade Stress Analysis

The turbine blades of all three stages are designed with tip shrouds and dovetail connections, as indicated previously. Figures 46 through 48 show the rotor blade airfoil contours (actual inspection glassines). The intersection of the airfoil tip and the blade tip shrouds are shown for all three stages in Figure 49. The relative weight and centrifugal forces of the three stages of blades, based upon weight calculations from these glassines, are shown in Figure 50(a) and 50(b). These also indicate the total "rim loads" of all the blades on the respective turbine wheels for the wheel stress analysis discussed later.

Tables VII, VIII and IX contain a comprehensive summary of turbine rotor blade physical and dynamic data for all three stages, including Phase I (shrouded) and Phase II (unshrouded) design for both the superalloy and refractory metal blades.

Shown in Figure 51 is a photograph of a turbine blade pair as a "mock-up" tip shroud assemblage. The detail manufacturing drawings of all three stages of shrouded blades are shown in Figures 110 through 114, and Figures 115 through 119 show the Phase II unshrouded blades (for both U-700 and molybdenum blades).

The major stresses in the blades are in the dovetail region, and Figure 52 shows the general distribution of these stresses. Maximum blade stresses occur at the inner curvature of the top tang and in the turbine wheel, at the lowest neck section of the dovetail. These stresses are a combination of direct tensile stress (neck stress) and bending stress, considering the dovetail tang somewhat as a triangular beam, as shown. Analysis of the dovetail stresses is performed by a combination of graphical and analytical procedures. The dovetail is accurately described on a layout drawing where all dimensions and contact angles are determined. Then, based upon an analytical procedure (derived in part, from experimental stress analyses and employing techniques developed for, and used extensively in aircraft gas turbine design), the combined stresses are calculated. The wheel dovetail stress is always greater than that of the blade since the wheel carries not only the entire blade, but also the stub section of the wheel between blades. Construction of the graphic portion of the analysis is done using the actual dovetail glassines, shown in Figures 53 and 54 for the blade and wheel slot respectively. These are actual copies of the inspection tooling used during manufacture of the dovetail, and show the tolerance band allowable during manufacture. Figures 55 and 56 show the analytical breakdown of the wheel and blade dovetails for the calculation of weight used in the centrifugal force determination of Figures 50(a) and, 50(b), and in the dovetail stress calculations and turbine wheel stress analysis. Figures 57 through 66 show overall summaries of the stresses in the turbine blades, and wheel dovetails (for shrouded and unshrouded blades), including dovetail stresses, airfoil root stresses, and blade shroud stresses for the design-point speed of 18,250 RPM. Different summaries are given for the various materials (U-700 and molybdenum) and for the various stages. All of the individual dovetail stresses are shown, with the maximum combined stress in the fillet region as the life-limiting stress. All stresses in these charts may be ratioed by the square of the speed to determine stress levels at other operating speeds. Also, the operating temperatures (based upon design point

operation), and the resulting life of the blade and wheel for this combined stress are shown. Also shown are the airfoil root centrifugal stresses. The shroud stresses in Figures 57 through 61 were calculated by treating the shroud as a cantilever beam extending from the airfoil. The shroud is strengthened by three ribs, two of which are tip seal edges, and the center one which is designed as a blade shroud stiffener. The maximum compressive stresses occur along the top edges of the seal sections and the maximum tensile stress occurs directly below this, on the under surface of the shroud at the point where it joins the airfoil. The maximum values of each are indicated in the stress summary charts.

As seen in the blade stress summary figures, the stresses are highest where refractory materials are employed, but in all cases, the allowable life exceeds the 15,000 hour requirement. The most life-limiting stress is in the third stage (despite test's lower temperature) where the weaker astroloy is used in the turbine wheel (instead of molybdenum).

• Blade Vibration Analysis

All three stages of blades have been analyzed by computer for determination of their natural frequencies at rotating speeds of 0 and 20,000 RPM. One blade was also analyzed at 10,000 RPM, but merely verified a linear variation of natural frequencies between 0 and 20,000 RPM. The excitation frequency search range was 0-40,000 CPS. Assumptions and limits of the blade vibration analysis are listed in Figure 67. The analysis was made for both the Phase I (shrouded) and Phase II (unshrouded) blade design. The rotor blade physical section properties determined by the "General Blade Program" as part of this analysis are presented in Table IX.

Figures 68 through 73 show the blade frequency diagrams resulting from the analysis, for both the shrouded and unshrouded blades. In addition, Table X provides these results in tabular form indicating the calculated resonances of various blade vibrating modes. Superposed on the graphs are the loci of excitation pulses of 38, 44, and 46 per revolution, based upon the number of nozzles immediately preceding each rotor. These excitation

pulses are of somewhat academic interest however, since, as described later, the even-spacings of the nozzle vanes have been intentionally disrupted to eliminate these even-passing exciting frequencies. There are, as a result of this spacing, numerous other exciting frequencies of lower driving force imposed on the blades as discussed in the NACA TN 4373.

Due to the inherent stiffness of these turbine blades, the effects of centrifugal stiffening due to operation at 20,000 RPM were to increase the natural frequencies of the shrouded blades above those of 0 RPM only by the following percentages:

	1st Critical	2nd Critical	3rd Critical	4th Critical	5th Critical	6th Critical
Stage 1	+0.158%	+0.158%	+0.159%	+0.153%	-	-
Stage 2	+3.210%	+0.447%	+0.286%	+0.351%	+0.409%	-
Stage 3	+5.706%	+0.419%	+0.491%	+0.643%	+0.623%	+0.874%

In addition to the above analysis, shrouded blade mock-ups for preliminary vibration testing of the stage 1 and 2 blades were fabricated from previously used two-stage turbine blades (see Figure 74(a & b)). The mock-ups duplicated the assumptions used in making the computer analyses:

1. The blade dovetails were cut off at the upper tang contact point.
2. The dovetail was rigidly fixed to a massive block (2"x2"x3") by furnace brazing.
3. The extra length of the three-stage turbine blades was duplicated furnace brazing 0.040 in. blade-contour spaces to the blade tips.
4. Tip shroud pieces were milled to shape and silver-brazed to the airfoil spacers.
5. Tip shrouds were free.

Figures 74(c) and 74(d) show comparison between the calculated (and bench test, for shrouded design) resonances for various modes of vibration and for all three stages. Table X summarizes in tabular form, the results of the blade vibration analysis.

An assumption made in the computer analysis was that to simulate actual stiffness of the blade neck section, joining the dovetail to the airfoil, the platform was considered to be 68 percent of its true width: This is a judgement, based on previous experience.

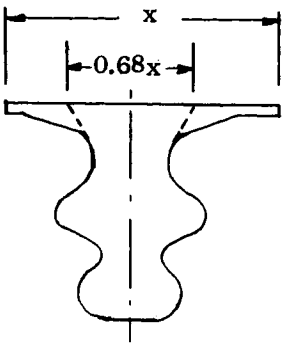

Material properties at operating temperatures were used in the computer analysis, while the bench tests were run at room temperature. Bench tests for the unshrouded blades were not performed, since the natural frequencies of the two-stage turbine blades are known from actual previous testing, and the first two stages of this turbine are the same as the two-stage turbine. A repetition of the bench tests with actual blades from all three stages will be made after the turbine test blades are received.

The correlation between the analytical and test results for the first flexural frequencies is considered good, although some deviations appear for the higher modes.

The intersections of the blade natural frequencies with the lines of exciting frequencies of Figures 68 through 73 indicate the lower limits of the operating speeds at which blade resonance can occur. Their upper limits will be set by the effective pulse pattern of the staggered nozzle configuration, which was designed to reduce the level of the excitation forces.

The low gas bending loads at design conditions (approximately 2 lbs. per blade) are factors in favor of minimizing chances of blade vibration problems. It is considered that the first flexural frequency would normally be the most dangerous one to experience at operating speed, and this is

clearly out of the range of excitation at design speed. The higher modes are typically more difficult to energize, and would probably require continuous operation exactly at their natural frequency to constitute a problem.

• Wheels

The overall wheel assemblage is shown in Figure 75, and the manufacturing drawings of the wheels are shown in Figures 121 through 123. Table XII presents a tabulated summary of geometric and dynamic data pertaining to the three turbine wheels. In addition to the wheel dovetail stress analysis discussed previously (with the blades), and shown in Figures 57 through 66, stresses were calculated for the main disk and curvic coupling regions. The turbine disk stress analysis was performed using the analytical models indicated in Figures 76 through 78, for the three stages. The wheels were divided into a number of radial stations, and the radius and thickness of the wheel was described for each of these stations to an "elastic disk" computer program which calculated radial, tangential, and overall effective stress (as defined previously in Figure 22) at each section for a prescribed rotation speed and previously calculated blade rim load (see Figures 50(a) and 50(b)). The disk is considered as a continuous member radially outward to the base of the dovetail slots, above which the centrifugal rim load is applied to the disk as a negative pressure. Thermal stresses are also calculable in this program but have not been included here due to the general uniformity of temperature throughout the disks (see Figures 27 through 30).

Figures 79 through 81 show the stress distributions as a function of radius for the three turbine wheels. The stresses in the stage 1 wheel included a superposition of rotational stress and a bending stress produced at the central bore due to the moment resulting from the axial force of the central tie bolt and the resisting forces through the curvic coupling torque cylinder. When these stresses are superposed, for the 11,000 lb. axial pull of the tie bolt, the central bore stress is approximately 42,000 psi. This is the stress at the cold initial assembly condition, and it is reduced

somewhat as the temperature of the turbine is increased, due to thermal expansion of the tie bolt which exceeds that of the shaft-wheel assembly. The bore stress after thermal expansion, (which reduces the tie bolt tension to 5500 lbs. at design point conditions) is 36,170 psi, and well within the allowable stress for 15,000 hours. The initial tension condition (cold) at build-up imposes a worse condition than that at temperature, since the initial stress is not only higher, but is acting on the TZM material in its least-ductile condition. This peak stress is quite local, being concentrated at the aft end of the central hole. On the forward end, the tie bolt axial load reduces the rotational stresses by an equal increment. Figures 80 and 81, showing the stage 2 and 3 wheel stress distribution, do not include any such bending effects. Superposed on each curve is the "average tangential stress", which is a measure of overall resistance to bursting failure, and is based upon the presumption that immediately prior to failure of a disk, the stresses tend to equalize themselves, approximating this average tangential stress. These average tangential stresses represent approximately 40% of the allowable stresses based upon 15,000 hour stress rupture of life, and are, therefore, safe.

The differential thermal expansion between the molybdenum wheels and the adjacent stainless steel and nickel based superalloys produces not only previously shown large tip clearance, but also requires a special design for the curvic coupling teeth.

As indicated previously, the three-stage turbine employs curvic coupling connections between all wheels and at their attachment to the shaft. The curvic couplings between the first and second stage wheels and between the third stage wheel and the shaft are the same standard full-barrel curvic coupling used on the two-stage turbine. The curvic coupling between the second stage wheel and the third stage wheel is a "half-barrel" design which will allow radial slippage, to account for differential thermal expansion. This is necessary because the second stage wheel is made of low-expanding TZM while the third stage wheel is made of higher expanding U-700 (see Figure 11)

with the overall effect of 0.011" differential radial expansion between room-temperature and design-point temperature operation. Figure 82(a) shows the basic geometric differences between the full barrel and half barrel curvic couplings, and Figure 82(c) defines the specific geometry used for each curvic joint. Table I of Figure 82(c) applies to the full barrel joints between the stage 1 and stage 2 wheels and between the stage 3 wheel and the shaft. Table II of Figure 82(c) applies to the half barrel curvic joint between the stage 2 and stage 3 wheels.

The design of the curvic between the first and second stage and between the third stage wheel and the shaft required only that a check be made to determine that the previous (two-stage turbine) tooth form could be used with a longer radial face, which has been increased from 0.200 in. to 0.300 in. for this turbine. A computer analysis was made by the manufacturer* to verify that the tooth form could be extended.

The half barrel curvic between the third stage wheel and second stage wheel was designed as nearly as possible to approximate a straight-sided tooth, which theoretically would allow radial slippage without producing eccentricity or adversely affecting the axial engagement of the coupling. During the transition to the thermally expanded condition, the curvic coupling will undergo an axial closure by an amount which depends upon the location of the chordal intersection point "e" (as shown in Figure 83). For the full barrel coupling form, the chordal intersection point of the tooth sides is at the center of the wheel, and therefore, "e" (and the corresponding axial closure due to differential thermal expansion of the wheels) is zero. The design problem was to minimize the axial closure (and therefore, to minimize "e") and to obtain the largest possible arc radius while maintaining; (1) the nonradial locking characteristics of the half-barrel design, (2) a relatively stubby tooth form for strength, and (3) ability to produce this tooth without exceeding a 13.5" cutting wheel diameter (which is the limiting capacity of machines currently available). Figure 84 shows the effect of the number of teeth on grinding wheel diameter, and it can be seen that 16 teeth would be made by a 12.5" diameter wheel. This curve was based on parameters which cause the grinding wheel locus to pass as nearly as possible

*Gleason Works, Rochester, N.Y.

except in the region of the refractory metal turbine wheels. Here, the thermal expansion of the tie bolt exceeds the growth of the molybdenum wheels by a significant amount (0.021 inch) and if the tie bolt were not initially stretched during assembly by a greater amount (0.041 in.), it would become loose during operation. Figure 87 shows the corresponding stress distribution throughout the tie bolt (changing with the varying diameters) and shows that during operation, the stresses drop to a value of approximately one-half the initial levels (due to thermal expansion) and are then well within the allowable stress envelope bounded by the 0.2% creep and 0.02% yield strength curves for U-700. Figure 34 indicates that during transient startup conditions, the thermal expansion of both tie bolt and shaft assembly are sufficiently similar, that at no time does the total thermal expansion of the bolt exceed or even approximate that of the shaft. Turbine shutdown transients are of no consequence here, since the temperature drop at shutdown requires approximately 12-to-15 hours, due to the effectiveness of the thermal insulation, and is, therefore, essentially at "steady-state" during the entire shutdown.

- Disk Brake

Although not designed in detail during this phase of the turbine program, consideration has been given to, and space is provided for the installation of a disk brake on the aft end of the turbine shaft, adjacent to the flexible membrane coupling (Figure 109). This figure shows a spacer (the detail drawing shown in Figure 173) which can be replaced by a disk, if installed, at a later time.

The disk brake will require considerable design and experimental development effort. Some experience was obtained on the two-stage potassium turbine on a disk brake, and qualitative knowledge was gained regarding necessary design approaches for a new design. In the previous installation, (shown configurationally in Figure 89) when the brake was actuated, the friction

between the pucks and the U-700 disk produced high surface heating which caused cracking and scoring of the disk surface in the heated zone and some shifting of disk material, resulting in an unacceptably high unbalance of 8 gram inches. Also, the lack of thermal mass in the disk allowed considerable heat conduction into the coupling region.

The disk design problem is one of severe thermal transients. During actuation, surface fluxes in the order of 5 $\frac{Btu}{in^2\ sec}$ are imposed on the surface of the rotating disk, and since the thermal conductivity of all high strength steels is relatively low, severe temperature gradients are produced at the disk surface during the period of brake actuation. In designing a disk brake, it will be necessary to provide means for removing disk surface heat (to minimize this thermal gradient) by utilizing some form of surface impingement cooling during the actuation period. The size and thickness of disk to be employed will have to be sufficient to provide a thermal mass which will absorb the unremoved heat without producing excessively high temperatures in the region of the coupling. Also, it will be necessary to identify materials with high thermal shock resistance, to prevent cracking of the disk surface. These materials must also possess sufficient strength to withstand the substantial centrifugal bore stresses at design speed. Also, the materials will have to resist melting, galling, or plastic deformation shifting of material with resulting rotor unbalances.

The material to best meet these requirements is as yet, unidentified. However, several ferritic or martensitic stainless alloys will possibly exhibit greater resistance to thermal cracking than the austenitic nickel-base U-700 disk used on the two-stage turbine, because of their greater thermal conductivity. For example, 17-22A(S) is used by the aircraft disk brake manufacturer who was consulted for applications where higher thermal conductivity and improved oxidation resistance are required. However, tests on disks of the size required for this turbine have been run to only 6000 RPM. It is possible that for the heat rates and speeds associated with a disk brake for this turbine, usage for one time only during emergency shutdown will have to be seriously considered, with replacement of the disk after each shutdown.

During consultation with the disk brake manufacturer, recommendations were obtained to employ a more abradable puck material than was used on the two-stage turbine. Despite possible improvements in material choices, however, the disk brake design will constitute a very challenging task.

While the THTC computer program calculates transient conditions, the analytical problem is complicated by the fact that convergence of the calculations is difficult to obtain with the extremely short time transients experienced in the actuation of the disk brake.

It is recommended that any analytical design program of a disk brake be combined with a minimum test program to prove the adequacy of the designed disk brake, its materials, and its cooling scheme, before actual installation into the potassium turbomachinery.

Stator

• Instrumentation

Figure 90(a) shows the turbine instrumentation stations for performance testing. Figure 90(b) shows the general stator design in the fluid-dynamic region, including a view of the typical interstage temperature instrumentation required for performance testing and for monitoring mechanical operation. Figure 16 also shows typical instrumentation ports in the casing. Table III of Reference 5 is a detailed list of turbine instrumentation. In general, it comprises thermocouples and static pressure taps at turbine inlet and exit, and between each blade row, both at the inner and outer flowpath surfaces, and additional total pressure taps at turbine inlet and exit. Figure 91 is the main instrumentation drawing, showing this instrumentation, its plane of location, and the detailed geometry of typical pressure tap and thermocouple well attachments to the casing and external ducting. In addition, the mechanical monitoring instrumentation (accelerometers, shaft proximity probes, bearing thermocouples, etc.) and its locating planes is also shown.

• Nozzle Diaphragms

The manufacturing drawings of the turbine nozzle vanes and diaphragm assemblies are shown in Figures 136 through 141. Table XI is a tabulated summary of geometric data regarding the nozzle vanes for all three stages. The vane manufacturing glassines are shown in Figures 92 through 94. Figure 95 shows an example of the layout work required for the incorporation of the pressure taps and thermocouples into the outer shroud bands of the nozzle diaphragms (shown for stage one). Figures 96 through 98 show the spacing of the nozzle vanes in all three nozzle diaphragm assemblies. Of significance is the fact that one-half of the vanes have been rotated through one-third of a vane space, as was done on the two-stage turbine (following the procedure as discussed in detail in NACA TN 4373) to minimize the possibility of resonant vibration of the turbine blades due to even passing frequency produced by vapor exhausting from the nozzles, as discussed previously. This results in the one wide gap and one narrow gap near the horizontal split line, as shown in Figures 96 through 98. The overall nozzle diaphragm assemblies are brazed, but incorporate welding of the instrumentation for greatest replaceability, if necessary, during testing.

• Inlet Duct and Exhaust Scroll

Figures 142 and 144 show the manufacturing drawings for the inlet duct and exhaust scroll. These components are similar in geometry to those used in the two-stage turbine program, but incorporate a greater amount of instrumentation. The inlet duct bullet nose is supported by four struts, and houses the first stage nozzle diaphragm and honeycomb tip seal. The exhaust scroll comprises a plenum of essentially constant rectangular cross-sectional at the lower region to mate with the 10 inch diameter condenser inlet duct. The exhaust scroll is provided with two access "portholes" in the top of its plenum to allow for inspection and/or access to instrumentation

if necessary. Also, the possibility exists for inspection of the aft face of the stage three turbine rotor blades and test material inserts by use of borescopes extended inward through these access ports.

• Casing

The manufacturing drawing of the turbine casing is shown in Figure 143. It is horizontally split, and connected to inlet duct and exhaust scroll by welded flanges. The welding sequence, including positioning tack-welds, used in closing the casing is shown in Figure 99(a). This sequence has been developed for minimum distortion during welding. The stage three casing region has been provided for moisture extraction to be installed at a later date, but is closed off for the first 5000 hours of turbine testing. The casing stress distributions of significance (in the flanges) are shown in Figure 99(b). This shows variations in stress as a function of turbine inlet temperature (with corresponding increase in internal pressure), and presumes a design-point pressure ratio of 7.9 in all cases. These stresses also presume 200 lbs. of axial load (aft) imposed on the turbine during all testing to prevent any buckling of the inlet duct resulting from thermal expansion. Superposed on these curves are the allowable stresses for 15,000 hours of operation according to the stress curve of Figure 10, and the actual maximum flange operating temperature.

As indicated previously, borescope ports will be added to the casing and inlet duct between each stage for visual inspection of critical fluid-dynamic parts (blades, vanes, wheels) at specified shutdown inspection points during the testing. Figure 21 is the layout drawing incorporating these borescope inspection ports. The design requires extending holes through the casings, tip seals, and nozzle diaphragm shroud bands in an assembled condition, as was done on the two-stage turbine program. Figure 143(c) shows the detail of the borescope inspection ports in the casing.

• Condensate Extraction

The moisture present at the exit of the third stage rotor at design point conditions (1550°F inlet, and 7.9 T-S pressure ratio) is nominally 13 percent. As an aid to increased performance and erosion resistance, and as indicated previously, condensate extraction has been designed into the third stage for possible testing following the 5000 hour test. The basic technical approach corresponds to that used in GE steam turbines, and the design of the moisture extraction slot in the casing is shown in Figure 100(b) and as group 3 in the turbine assembly drawing of Figure 109. The detail drawing of the condensate extraction manifold, which is inserted into the casing as an assembly, is shown in Figure 143(b).

The design of Figure 100(a) was also considered, and would possibly be employed in an actual space turbine due to its greater simplicity. However, to prevent any in- or out-leakage of liquid at the split horizontal flange, and to provide for replaceability of the moisture extraction device as an unit ring during this development program, the design shown in Figure 100(b) was selected.

In addition to moisture extraction off the blade trailing edge, sufficient room in the casing collecting cavity has been provided to allow extraction from the leading edge of radially-grooved rotor blades, as shown in Figure 101. However, no radially grooved blades are being designed or procured in this phase of the program, and no "forward blade" extracting components are being procured.

The employing of moisture extraction in the turbine requires the use of turbine tip shrouds, wherein the liquid collects on the inner diameter of the tip shroud and is slung outward from its trailing edge into the narrow collecting slot shown directly above. The casing is provided with this

peripheral slot and a collecting cavity with a "dam" which forces the rotating liquid outward through an exhausting pipe in the casing directly into the condenser. The components for condensate extraction will be designed, but will not be procured during the initial phase of the program.

• Bearing Housing Assembly

The bearing housing - shaft region of the turbine is similar to that of the two-stage turbine, but represents a number of improvements for greater reliability, ease of manufacture and accessibility during assembly. The bearing housing comprises the major structural assembly for support of the turbine rotor, and is the component from which the entire turbine is mounted in the test facility. It also contains all of the vital flow tubing to-and-from the bearings, hydrodynamic seal, and labyrinth purge seal regions between potassium and oil. The detail drawing of the bearing housing is shown in Figure 145 and its assembly with the hydrodynamic seal and pad bearing ring is shown in Figure 146. The position and number of all the flow tubes have been judiciously selected to provide for greatest reliability, necessary flow area, and the ease of drainage. The heat shield cover over the numerous tubes conducting flow in-and-out of the bearing and seal region has been increased in diameter to allow greater room for insertion of the tubes, and has been provided with a more generous thermal expansion bellows than was incorporated in the two-stage turbine. Also, the labyrinth seal surfaces of the bearing housing have been made for replacement of the copper subsurface by installation of a new copper-plated ring in case of necessary seal surface repair. Accessibility of oil supply tubes to the pad bearing has been improved, and improvements in cooling of the regions surrounding the pivoted pad bearing by using argon purge flow have also been incorporated into the design.

• Hydrodynamic Seal

The diameter of the hydrodynamic seal has been increased slightly (to 6.02 inches from a previous 5.88 inches, corresponding to the slightly larger third stage diameter) to provide for greater sealing ability. Figure 148 shows the detailed drawing of the hydrodynamic seal, and Figure 102 indicates its sealing capacity for 600°F and 900°F potassium as a function of speed. The lower curve indicates the point at which flow leakage from the seal occurs, and the upper curve is the Δp point at which all liquid is blown completely through the seal.

The "blow-through" pressure is the pressure differential which exists when the left static pressure drives the liquid interface on the left side of the stator disk to the 2.833 in. radius, while the right-hand liquid interface is at 1.941 in. radius. The "maximum sealing pressure" is the pressure differential which exists when the left-hand liquid interface is at 2.359 in. radius and the right-hand liquid interface is at 1.941 in. radius.

Figure 104 shows the temperature rise of potassium passing through the seal and absorbing the frictional power shown in Figure 103. This does not show the temperature rise of the liquid resulting from the considerable heat conducted from the hot vapor environment during actual testing.

The design of the hydrodynamic seal has been improved to allow welding to be used in its manufacture, in place of one previous brazing cycle. Also, the present design provides a greater reliability and ease of repair, if necessary.

• Thrust Bearing

The thrust bearing is shown in Figure 149. (Two such bearings, preloaded, are used.) Following are its specifications:

Manufacturer	Fafnir
Size	50 mm
Type	MM 210 VM 2 SMBR Split inner race, One piece - machined retainer
Contact angle 27°	
Outer ring curvature	52°
Inner ring curvature	51½°
Material	Races - 52100 vacuum melted steel Retainer - Silicon iron bronze, silver plated

Figure 105 shows the variation in axial bearing load associated with varying the overall turbine pressure ratios at the 1550°F design-point inlet temperature. The corresponding bearing operating life is shown, assuming an initial axial load (200 lbs.) sufficient to prevent any axial shifting of the rotor from the forward thrust condition at startup (due to the vacuum in the loop) to the rearward thrust at operating conditions (425 lbs.). Axial pre-loading of the bearings is accomplished by a belleville spring assembly. The thrust bearings are the same as incorporated in the two-stage turbine. As indicated above, they have a split inner race and a solid silicon-iron bronze (silver plated) ball retainer. The bearing life was calculated employing the available RECAP computer program, which basically employs the AFBMA bearing design analytical techniques, and includes the effects of ball centrifugal forces, contact angle, and several

other bearing geometry definitions. By using vacuum-melted material (52100 steel in this bearing) the calculated life of the bearing is increased by a factor of five. As indicated in Figure 105 the B10 life of this bearing is, therefore, 19,000 hours, which significantly exceeds the 5000 hour first endurance test life.

• Pivoted Pad Bearing

The detailed manufacturing drawings of the pivoted pad bearing and its associated parts are shown in Figures 150 through 155, and the pad bearing power consumption is shown in Figure 106 as a function of rotative speed. The power consumption was calculated using Figure 5 of Reference 7, which gives theoretical friction torque vs. Sommerfeld Number for Reynolds Numbers of 10-16,000; for a 4-pad tilting pad bearing without geometrical preload, each pad of 80° circumferential length, pivot pad location at the 55 percent point, and L/D = 1. The measured performance of similar bearings having geometrical preload compared favorably with their theoretical results. These calculations further compare well with test operating experience on a bearing of the same dimensions employed in the two-stage potassium turbine, as shown in Figure 17 of Reference 17.

The pad bearing lubrication lines are brought in through the aft end of the bearing sump, and extended forward through the sump region into each individual pad. The design is an improvement over the two-stage turbine in that a blind assembly of the lubrication tubes during turbine build-up is not required.

• Tip Seals

Shown in Figures 157 through 168 are the manufacturing drawings of the honeycomb turbine tip seals and interstage seals. These are machined type 316 stainless steel rings with brazed-in honeycomb of 0.005 inch material

thickness and 1/16 inch cell size. There are two sets of these tip seals, corresponding to the shrouded and unshrouded turbine blades, respectively. The general construction of all the seals is the same, but they differ in dimensions. Figures 162 and 167 show the assemblies of the stage three tip seal and blade erosion/corrosion test inserts, and the test inserts are shown in Figures 161 and 166 for the Phase I and Phase II design, respectively.

- Turbine Coupling Concept

A layout drawing of the proposed turbine coupling is shown in Figure 107. This incorporates a flexing membrane, which is more representative of the type of non-lubricated coupling which will be ultimately required for a space turbogenerator.

V. CONCLUSIONS

The conclusion is made that the turbine design presented herein is capable of 15,000 hours operation, and can operate for 5000 hours without replacement of any components. The new problems associated with the use of molybdenum wheels, and their low ductility and associated manufacturing problems constitute challenges, and the design of the shrouded turbine blades, in association with moisture extraction testing, promises new information regarding increased turbine performance and prevention of turbine erosion.

VI. REFERENCES

1. "Mechanical Design & Development of a Two-Stage Potassium Turbine", H. E. Nichols and R. W. Fink. Two-Stage Potassium Turbine Topical Report, Contract NAS 5-1143, Space Power and Propulsion Section, General Electric Company.

2. "Fluid Dynamic Design and Performance of Two-Stage Potassium Test Turbine", R. J. Rossbach, G. C. Wesling, Two-stage Potassium Turbine Topical Report, Contract NAS 5-1143, Space Power and Propulsion Section, General Electric Company.

3. "Materials Support of Performance and Endurance Tests", W. F. Zimmerman, J. W. Semmel, D. S. Engleby, R. B. Hand, Two-Stage Potassium Turbine Topical Report, Contract NAS 5-1143, Space Power and Propulsion Section, General Electric Company.

4. "Potassium Vapor Turbine Test Facility", S. E. Eckard, Two-Stage Potassium Turbine Topical Report, Contract NAS 5-1143, Space Power and Propulsion Section, General Electric Company.

5. "Design of a Three-Stage Potassium Turbine - Fluid Dynamic Design", (Vol. I) by R. J. Rossbach, G. C. Wesling, and W. F. Lemond. Three-Stage Turbine Report, Contract NAS 3-8520, Space Power and Propulsion Section, General Electric Company.

6. "Torsional and Axial Vibration System Analysis", T. G. Flach, J. A. Yuhas, R63FPD357, Advanced Engine and Technology Department, General Electric Company, October, 1963.

7. "Lubrication Analysis in Turbulent Regime", F. K. Orcutt, C. W. Ng, J. K. Vohr, E. B. Arwas, NASA CR-54259, MTI-65TR2, Contract NASw-1021, Second Quarterly Report, January 30, 1965.

8. "Mechanical Design and Systems Handbook", H. A. Rothbart, Editor-in-Chief, McGraw Hill Inc., 1964.

9. "Formulas for Stress and Strain", R. J. Roark, third edition, McGraw-Hill Book Company, Inc., 1954.

10. "Strength of Material, Part II Advanced Theory and Problems", S. Timoshenko, second edition, D. VonNostrand Company, Inc., 1941.

11. "Rolling Element Computer Analysis", C. B. Pineo, DF64SE82, Small Aircraft Engine Department, General Electric Company, October 10, 1964.

12. "General Analysis of Dovetail Blade Attachments", H. J. Macke, R59FPD611, General Electric Company, December 28, 1959.

REFERENCES

(Continued)

13. "Elastic Disc Stress Analysis and Design Program for IBM704", J. K. Casey, E. M. Gettel, C. L. Moore, General Electric Company, July 23, 1958.

14. "Multi-Shell: A Digital Computer Program for the Analysis of Shell of Revolution Structures Subject to Axisymmetric Loading", L. Beitch, General Electric Company, June 21, 1961.

15. "Program THTB for Analysis of General Transient Heat Transfer Systems", G. L. Stephens, D. J. Campbell, General Electric Company, April 21, 1961.

16. "Theoretical and Experimental Analysis of the Reduction of Rotor Blade Vibration in Turbomachinery Through the Use of Modified Stator Vane Spacing", R. H. Kemp, M. H. Hirschberg and W. C. Morgan, Technical Note 4373, NACA TN 4373, September, 1958.

17. "Operating Experience With an Oil-Lubricated High Speed Potassium Turbine Bearing", H. Ernst, General Electric Company ASME Paper 65-LUBS-10.

18. "Design Criteria for Rotary Seals for a Space Environment", Schnetzer, Ernst, McGrew, Phillips, Technical Report AFAPL-TR-65-89 Part I, AF Aero Propulsion Laboratory, AF Systems Command, WPAFB, September, 1965.

VII. TABLE I

COMPARISON OF TWO-STAGE AND THREE-STAGE TURBINES

	Two Stage	Three Stage
Date of Contract	May, 1961	June, 1966
Total Turbine Weight (lbs.)	350	451*
Rotor Weight (lbs.)	59.7	91.1*
Rotative Speed, RPM	18,250	18,250
Design Point Pressure Ratio (T-S)	3.47	7.9
Endurance Test Inlet Temp. (°F)	1500°F	1550°F
Endurance Point Mass Flow Rate (lb./sec.)	2.0	1.95
Rotor Critical Speed (Conical Whirl) RPM	14,331	9,987
Rotor Critical Speed (Cylindrical Whirl) RPM	41,831	37,580
Rotor Critical Speed (Shaft Bending) RPM	56,680	45,652
Total Rotor Length (Shaft End to Tie Bolt Head) (in.)	21.65	29.40
Available Life at Endurance Test Conditions (hrs.)	4,000	22,000
Approximate Distance From Thrust Bearing Shaft Shoulder to Rotor C.G., (in.)	8.6	13.25
Blade Configuration	unshrouded	shrouded or unshrouded
Flange Joining Method	welded	welded
Number of Performance Vapor Total Pressure Taps	18	14
Number of Performance Vapor Static Pressure Taps	23	46
Number of Performance Vapor Thermocouples (Fluid-Dynamic)	23	29
Total Number of Pieces of Turbine Instrumentation	174	182

* See Table XIII for detail weight breakdown.

TABLE II

TURBINE COMPONENTS TO BE PROCURED

	Description	Number to be Procured
Stator	Inlet Duct Assembly	1
	Turbine Casing Assembly	1
	Scroll Assembly	1
	Stage 1 Nozzle Diaphragm	1
	Stage 2 Nozzle Diaphragm	1
	Stage 3 Nozzle Diaphragm	1
	Tip Seal Stage 1	1
	Tip Seal Stage 2	1
	Tip Seal Stage 3	1
	Interstage Seal (Stage 1 to Stage 2)	1
	Interstage Seal (Stage 2 to Stage 3)	1
	Adopter Rings (Liquid Extraction)	1
	Refractory Metal Erosion Inserts (TZM, TZC, R41, U700)	24
	Spacers Shim Set (Stg. 1, Stg. 2, Stg. 3)	1
	Bolts	3 sets
Rotor	Tie Bolt	2
	Stage 1 Wheel (TZM)	2
	Stage 2 Wheel (TZM)	2
	Stage 3 Wheel (U700)	2
	Stage 1 Rotor Blades (Shrouded, U700)	75
	Stage 1 Rotor Blades (Unshrouded, U700)	75
	Stage 2 Rotor Blades (Shrouded, U700)	65
	Stage 2 Rotor Blades (Unshrouded, U700)	65
	Stage 2 Rotor Blades (Shrouded TZM)	8
	Stage 2 Rotor Blades (Unshrouded TZM)	8
	Stage 2 Rotor Blades (Shrouded TZC)	8
	Stage 2 Rotor Blades (Unshrouded TZC)	8

TABLE II (CONT'D)

	Description	Number to be Procured
Rotor	Stage 3 Rotor Blades (Shrouded TZM)	8
	Stage 3 Rotor Blades (Unshrouded TZM)	8
	Stage 3 Rotor Blades (Shrouded TZC)	8
	Stage 3 Rotor Blades (Unshrouded TZC)	8
	Stage 1 Rotor Blade Retainers (Set)	200 (3 sets + spares)
	Stage 2 Rotor Blade Retainers (Set)	200 (3 sets + spares)
	Stage 3 Rotor Blade Retainers (Set)	200 (3 sets + spares)
	Bar X Seal Retainer	1
	Bar X Seal	8
	Turbine Shaft	2
	Brake Disk	2
	Hydrodynamic Seal Assembly	2
Bearing Housing Assy.	Journal Bearing Sleeve	4
	Pad Bearing Assembly	2
	Ball Bearing Assembly	16
	Ball Bearing Housing Assembly	1
	Bearing Housing	1
	Carbon Face Seal	6

TABLE IV

HEAT TREAT CONDITIONS OF VARIOUS TURBINE MATERIALS

Code No.	Materials	
1	A 286	1650°F - 2 hours, O.Q.; 1325°F - 16 hrs., A.C.
2	L-605	2225°F - 12 min., A.C.
3	L-605	above + 1400°F - 16 hrs., A.C.
4	U-700 W*	2135°F - 4 hrs., A.C.; 1975°F - 4 hrs., A.C.; 1550°F - 24 hrs., A.C.; 1400°F - 16 hrs., A.C.
5	U-700 C	2100°F - 2 hrs., A.C.; 1400°F - 16 hrs., A.C.
6	U-700 C	2125°F, 2 hrs. - F.C. 100°F/hr. to 1975 - A.C.; 1400°F - 16 hrs., A.C.
7	Rene' 41	1975°F - 1/2 hr., W.Q.; 1975 - 1/2 hr., A.C. 1400°F - 16 hrs., A.C.
8	Type 316 SS	Annealed 1950°F - A.C.
9	TZM	Stress relieved 2200°F - 1 hr.
10	TZC	Stress relieved 2400°F - 1 hr.

* Properties of modified astroloy are similar.

TABLE V

COMPARISON OF CHEMICAL ANALYSIS AND HEAT TREATMENTS FOR SUPERALLOY TURBINE WHEELS USED IN THE TWO-STAGE AND THREE-STAGE TURBINES

	Chemical Analysis - %							
Two-Stage Turbine	C	B	Cr	Co	Mo	Ti	Al	Ni
Astroloy (S&C-1)	.03/.10	.005/.04	14/17	15/19	4.5/6.0	2.8/3.8	4.5/5.0	Bal
Astroloy Wheel	.10	.031	14.3	15.6	5.1	3.33	4.23	Bal
Actual N_V = 2.57*								
Three-Stage Turbine								
Modified Astroloy (C50TF3)	.03/.09	.02/.03	14/16	16/18	4.5/5.5	3.35/3.65	3.85/4.15	Bal
Modified Astroloy Wheel	.085	.023	14.99	16.83	5.14	3.52	4.21	Bal
Actual N_V = 2.41*								

Heat Treatment	
Two-Stage Turbine Wheels	Three-Stage Turbine Wheels
2135°F for 4 hours, AC 1975°F for 4 hours, AC	1975 - 2100°F** for 4 hours - Oil or Salt Quench 1600°F for 8 hours, AC
1550°F for 12 hours, AC	1800°F for 4 hours, AC
1400°F for 16 hours, AC	1200°F for 24 hours, AC
	1400°F for 8 hours, AC

* N_V 2.32 is desired for resistance to sigma phase which may form at temperatures above 1400°F.

** Selected temperature for each heat based upon minimum gamma prime solution temperature.

TABLE VI

EROSION/CORROSION MATERIAL

INSERTS TO BE TESTED*

U-700 C	(two inserts)
U-700 W	(two inserts)
TZC	(two inserts)
TZM	(two inserts)
Rene' 41	(two inserts)
AISI Type 316 Stainless Steel	(two inserts)

* See Figures 162 and 167 for detailed installation.

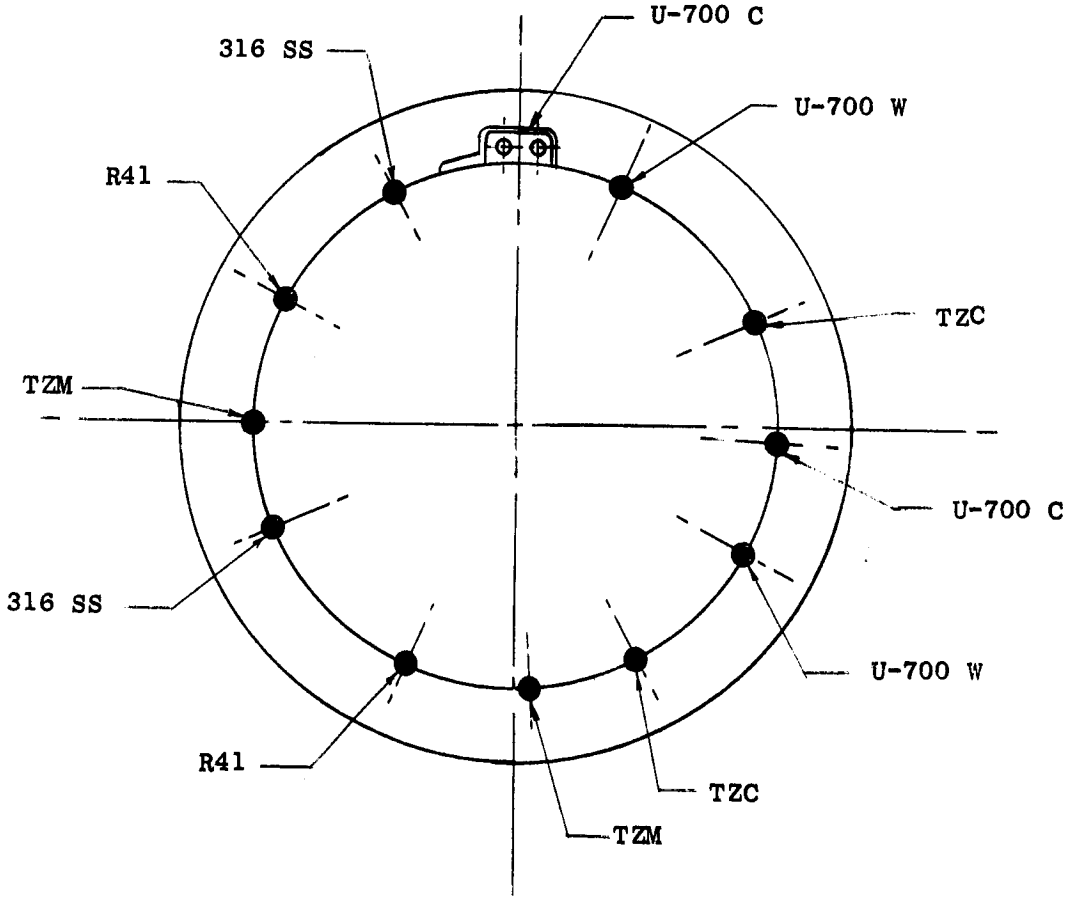

TABLE VII

THREE-STAGE TURBINE BLADE DATA

Phase I (Shrouded Blade)

Rotor

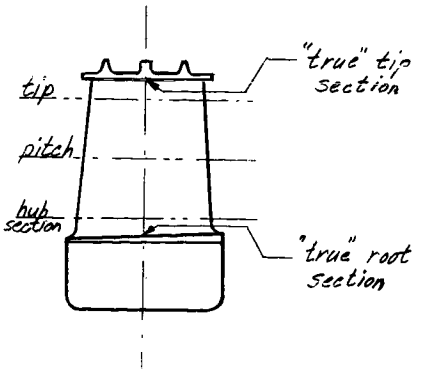

	Stage 1	Stage 2	Stage 3
Total number of blades in stage	62	60	52
Airfoil base (where it joins platform) cross-sectional area ($in.^2$)	0.108	0.133	0.119
Airfoil root section area ($in.^2$)	0.104	0.121	0.113
Airfoil pitch section area ($in.^2$)	0.084	0.100	0.103
Airfoil tip section area ($in.^2$)	0.0632	0.0771	0.0889
Hub section diameter	7.520	8.00	8.22
Pitch section diameter	8.160	8.80	9.26
Tip section diameter	8.800	9.60	10.30
Nominal throat dimension (d_o) at hub section	0.147	0.173	0.268
Nominal throat dimension (d_o) at pitch section	0.161	0.194	0.283
Nominal throat dimension (d_o) at tip section	0.186	0.230	0.308
Airfoil contour dimensional tolerance	$\pm$0.003	$\pm$0.003	$\pm$0.003
Nominal airfoil trailing edge thickness (in.)			
Airfoil tip (where it joins shroud) area ($in.^2$)	0.0592	0.0936	0.0858
Blade tip (where it joins shroud) dia. (in.)			
Airfoil height (in.)	0.768	0.9978	1.309
Total blade height (dovetail bottom to shroud seal tip) (in.)	1.273	1.485	1.826
Blade axial length (dovetail projected length) (in.)	0.795	0.915	1.000
Tip-to-root airfoil area ratio (shroud-to-platform)	0.549	0.706	0.722
Total weight of one blade with shroud (U-700) (grams)	18.53	25.92	33.88
Total weight of one blade with shroud (TZM or TZC) (grams)	——	33.33	43.55

TABLE VII (Cont'd)

(Shrouded Blades)

	Stage 1	Stage 2	Stage 3
Centrifugal force of one blade (U-700)* (lb.)	1529	2239	3240
Centrifugal force of one blade (TZM or TZC)* (lb.)	——	2879	4166
"g" load of one blade* (g's)	38,188	44,602	45,221
Total disk rim load (incl. wheel stubs & fasteners and based on U-700 blades only)* (lb.)	6399	8532	9921
Size of machining blank (TZM or TZC) (in.)	5/8" x 1 1/2" rectangular for TZM 1 1/2" dia. round for TZC		
Shroud weight (U-700) gram	1.883	2.394	3.987
Airfoil weight (U-700) gram	9.189	14.580	19.178
Dovetail weight (U-700) gram	7.458	8.952	10.711
Shroud weight (TZM) gram	——	3.078	5.126
Airfoil weight (TZM) gram	——	18.746	24.657
Dovetail weight (TZM) gram	——	11.510	13.771

* all dynamic data are given for 18,250 rpm.

TABLE VIII

THREE-STAGE TURBINE BLADE DATA

Phase II (Unshrouded Blade)

Rotor

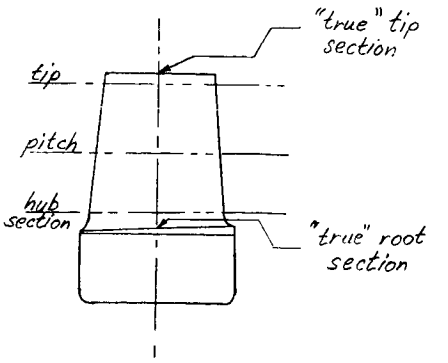

	Stage 1	Stage 2	Stage 3
Total number of blades in stage	62	60	52
Airfoil base (where it joins platform) cross-sectional area ($in.^2$)	0.108	0.133	0.119
Airfoil root section area ($in.^2$)	0.104	0.121	0.113
Airfoil pitch section area ($in.^2$)	0.084	0.100	0.103
Airfoil tip section area ($in.^2$)	0.0632	0.0771	0.0889
Hub section diameter	7.520	8.00	8.22
Pitch section diameter	8.160	8.80	9.26
Tip section diameter	8.800	9.60	10.30
Nominal throat dimension (d_o) at hub section	0.147	0.173	0.268
Nominal throat dimension (d_o) at tip section	0.186	0.230	0.308
Airfoil contour dimensional tolerance (in.)	$\pm$0.003	$\pm$0.003	$\pm$0.003
Airfoil true tip area ($in.^2$)	0.0590	0.0752	0.0862
Airfoil contour dimensional tolerance	$\pm$0.003	$\pm$0.003	$\pm$0.003
Blade true tip dia. (in.)	8.870	9.69	10.483
Airfoil height (in.)	0.7643	0.9895	1.2915
Total blade height (dovetail bottom to true tip) (in.)	1.1504	1.3774	1.6819
Blade axial length (dovetail projected length) (in.)	0.795	0.915	1.000
Tip-to-root airfoil area ratio (shroud-to-platform)	0.549	0.706	0.722
Total weight of one blade (U-700) gram	16.758	23.136	29.348
Total weight of one blade (TZM or TZC) gram	21.547	29.747	37.733
Centrifugal force of one blade (U-700)* lb.	1356	2004	2860

*all dynamic data are given for 18,250 rpm.

TABLE VIII (Cont'd)

(Unshrouded Blades)

	Stage 1	Stage 2	Stage 3
Centrifugal force of one blade (TZM or TZC)* lb.	1743	2577	3677
"g" load of one blade* (g's)	35,171	38,777	42,939
Total disk rim load (inc. wheel stubs & fasteners and based on U-700 blades only)* lb/circumference	5870	7992	9024
Size of machining blank (U-700) (in.)	3/4" x 1 1/4" rectangular bar		
Size of machining blank (TZM or TZC) in.)	5/8" x 1 1/2" rectangular for TZM 1 1/2" dia. round for TZC		
Nominal airfoil trailing edge thickness (in.)	0.015	0.015	0.015

*all dynamic data are given for 18,350 rpm.

TABLE X

SYNOPSIS OF THREE-STAGE TURBINE BLADE VIBRATION ANALYSES

(Search Limit 40KCPS)

Stg.	S or U(1)	RPM	1st Crit.CPS RPM(2)	2nd Crit.CPS (RPM)	3rd Crit. CPS (RPM)	4th Crit.CPS (RPM)	5th Crit.CPS (RPM)	6th Crit.CPS (RPM)
1 (38 Noz)	S	0	4,055 (6,400)	18,263	19,430	33,906		
		20K	4,061	18,292	19,461	33,958		
	U	0	5,300 (8,410)	20,560	25,811			
		20K	5,360	20,581	25,834			
2 (46 Noz)	S	0	2,523 (3,310)	10,505 (13,750)	11,502 (15,040)	19,925	25,632	
		20K	2,604	10,552	11,535	19,995	25,737	
	U	0	3,533 (4,630)	11,826 (15,460)	18,167 (23,740)	(3)	(3)	
		20K	3,611	11,857	18,192			
3 (44 Noz)	S	0	1,618 (2,220)	6,515 (8,930)	8,180 (11,200)	14,017 (19,280)	21,307	30,787
		20K	1,740	6,592	8,243	14,141	21,447	31,056
	U	0	2,121 (2,920)	7,655 (10,480)	10,156 (13,900)	17,166 (23,594)	22,396	32,988
		20K	2,236	7,717	10,214	17,282	22,498	33,214

Notes: (1) S = Shrouded, U = Unshrouded

(2) $N = \frac{20\ C_o}{\frac{n}{3} - C_{20}+C_o}$ where

C_o = Critical frequency at 0 RPM, KCPS.
C_{20} = Critical frequency at 20 KRPM, KCPS.
N = Critical speed, KRPM.
n = No. of nozzle blades
(N > 25 KRPM not calculated)

(3) Search limit 30 KCPS.

TABLE XI

THREE-STAGE TURBINE BLADE DATA

Stator

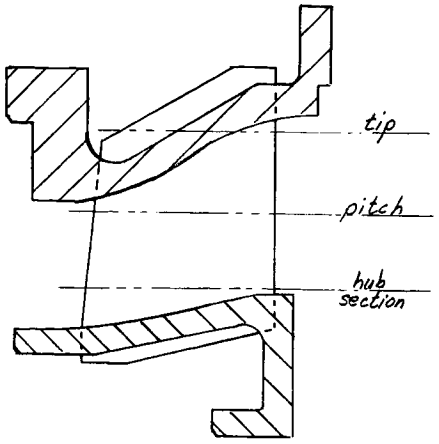

	Stage 1	Stage 2	Stage 3
Total number of vanes in stage	38	46	44
Airfoil cross-sectional area (constant) $in.^2$	0.223	0.189	0.2045
Airfoil true axial chord (in.)	1.056	0.964	1.050
Trailing edge thickness (in.)	0.015	0.015	0.015
Airfoil contour dimensional tolerance (in.)	$\pm$0.004	$\pm$0.004	$\pm$0.004
Nominal throat dimension (d_o) at hub section	0.1665	0.1725	0.2118
Nominal throat dimension (d_o) at pitch section	0.1700	0.1835	0.2462
Nominal throat dimension (d_o) at tip section	0.1735	0.1945	0.2800
Hub section diameter	7.520	8.00	8.22
Pitch section diameter	8.16	8.80	9.33
Tip section diameter	8.80	9.60	10.44
Root-to-tip section nominal twist (degrees)	5°30'	4°45'	1°40'
Vane turbine angle (degrees)	76.3	73.8	68.5

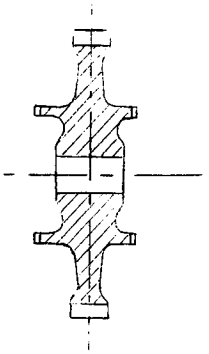

TABLE XII

TURBINE WHEEL DATA

	Stage 1	Stage 2	Stage 3
Wheel material	TZM	TZM	Modified Astroloy
Outer diameter (in.)	6.6114	6.884	7.0194
Bore diameter (in.)	1.0	1.0	1.0
Hub width (in.)	1.4	1.515	1.63
Rim Width (in.)	0.798	0.92	1.0
Neck Width (in.)	0.452	0.511	0.58
Pitch diameter of curvic coupling (in.)	3.450	3.450	3.450
Depth of dovetail slot (in.)	0.348	0.348	0.348
Total wheel cross-sectional area ($in.^2$)	4.94	5.59	6.084
Wheel polar mass moment of inertia ($Wr.^2$)	76.79	115.67	117.5
Total rim load (on uncut portion of wheel (lb.)/ in of circumference	6,369	8,430	9,752
Total bursting force acting on cross-sectional area (lb.)	99,350	127,669	127,762
Wheel weight (lb.)	9.261	10.840	9.252

Table XIII. Turbine Physical and Dynamic Data.

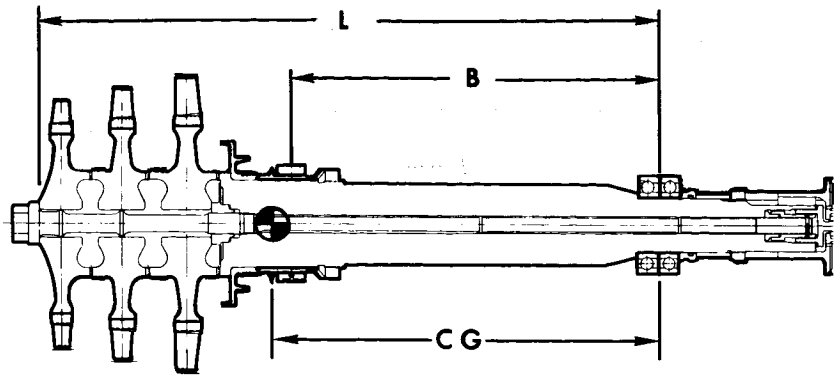

Mass Polar Moment of Inertia for Entire Rotor - WR^2 ($lb\text{-}in^2$)	396
Bearing Span "B" (in.)	13.547
Total Rotor Thrust-Bearing-to-End Span "L" (in.)	22.734
Overhang Ratio L/B	1.678
Distance from Thrust Bearing Centerline to Rotor CG (in.)	14.03

TURBINE WEIGHT

Component		
• Stator		
Inlet Duct		62.5 lbs.
Casing		58.0 lbs.
Scroll		100.0 lbs.
Nozzle Diaphragms		28.0 lbs.
Tip Seals and Interstage Seals		9.9 lbs.
	Sub Total	258.4 lbs.
• Rotor		
Tie Bolt		2.5 lbs.
Shaft		32.9 lbs.
Stage 1 Wheel and Blades		14.2 lbs.
Stage 2 Wheel and Blades		17.7 lbs.
Stage 3 Wheel and Blades		16.5 lbs.
Aft End Bearings and Fasteners and Sleeves		7.2 lbs.
	Sub Total	91.0 lbs.
• Bearing Housing Assembly		
Bearing Housing		51.5 lbs.
Hydrodynamic Seal		11.0 lbs.
Pad Bearing Assembly		12.5 lbs.
Ball Bearing Assembly		26.8 lbs.
	Sub Total	101.8 lbs.
	TOTAL TURBINE WEIGHT	451 lbs.

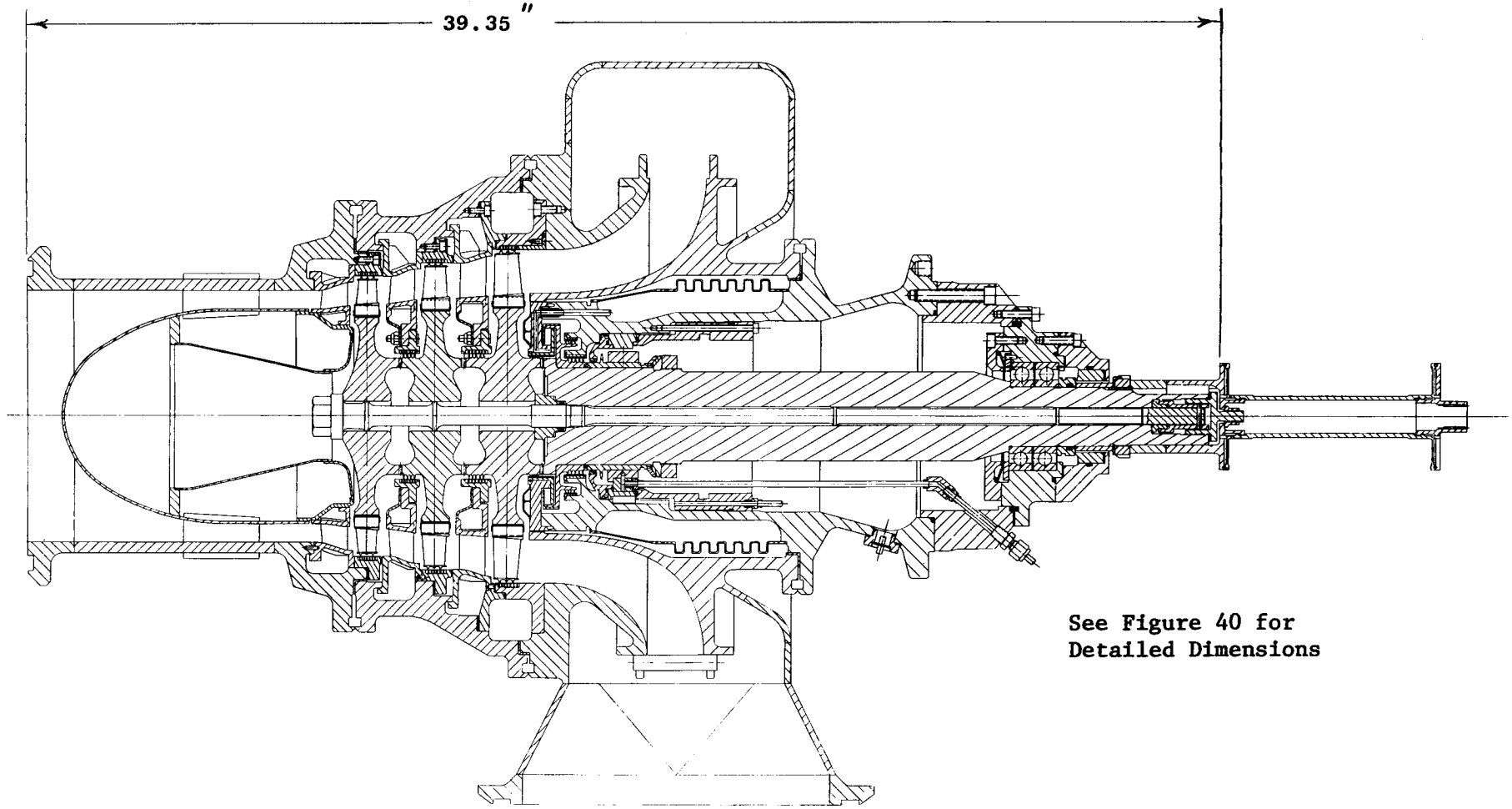

Figure 2. Turbine Assembly.

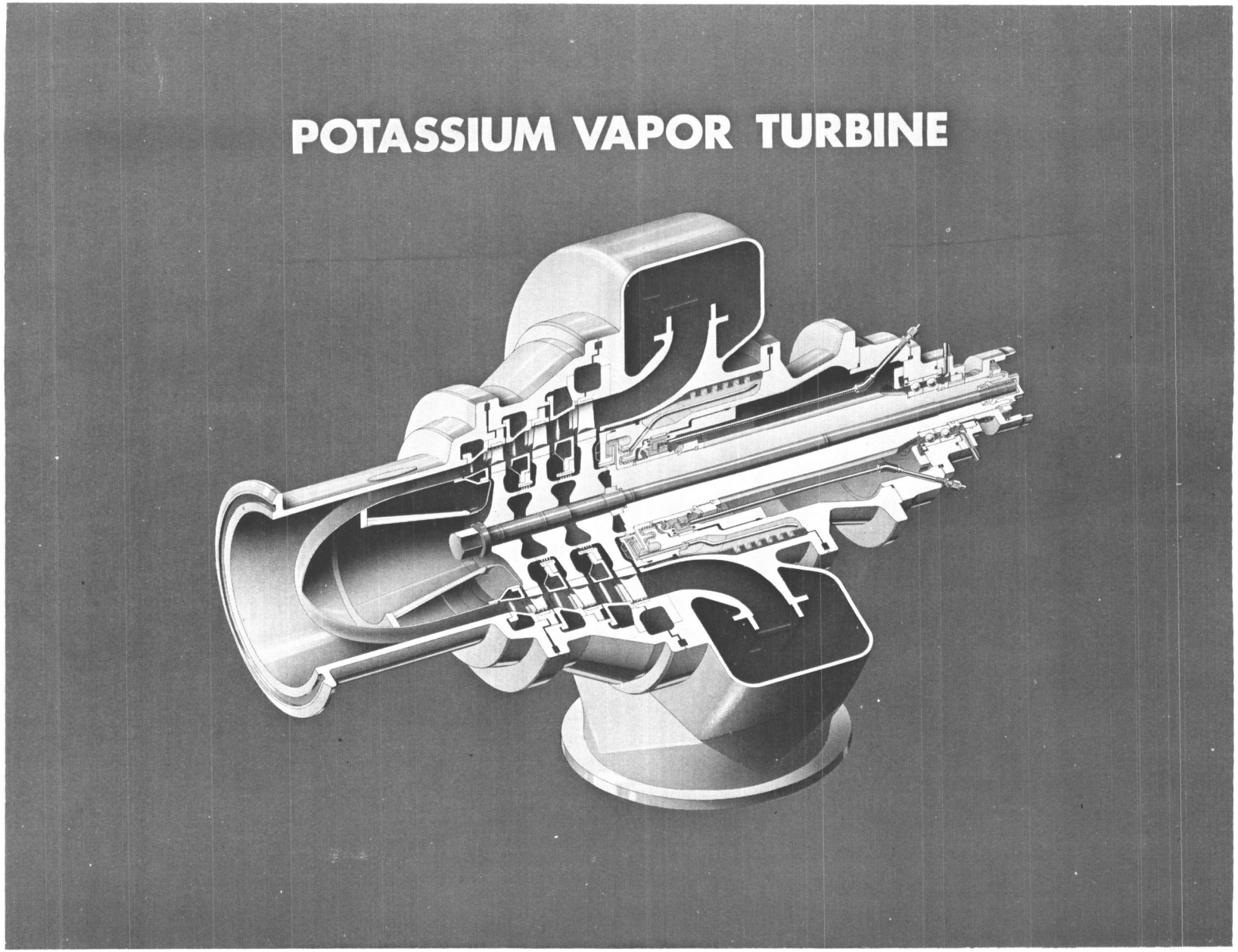

Figure 3. Three Stage Turbine Assembly.

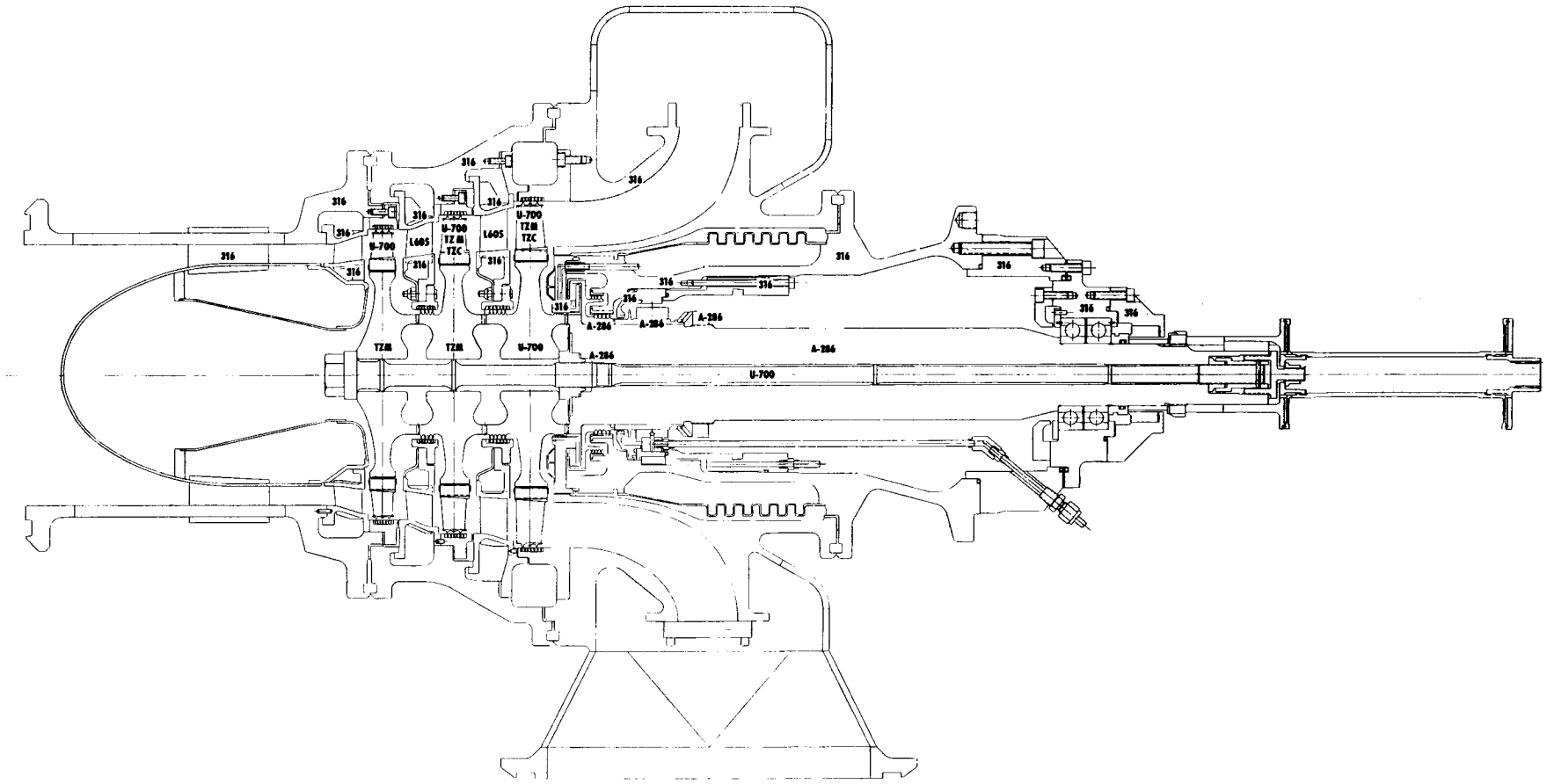

Figure 4. Fabrication Materials.

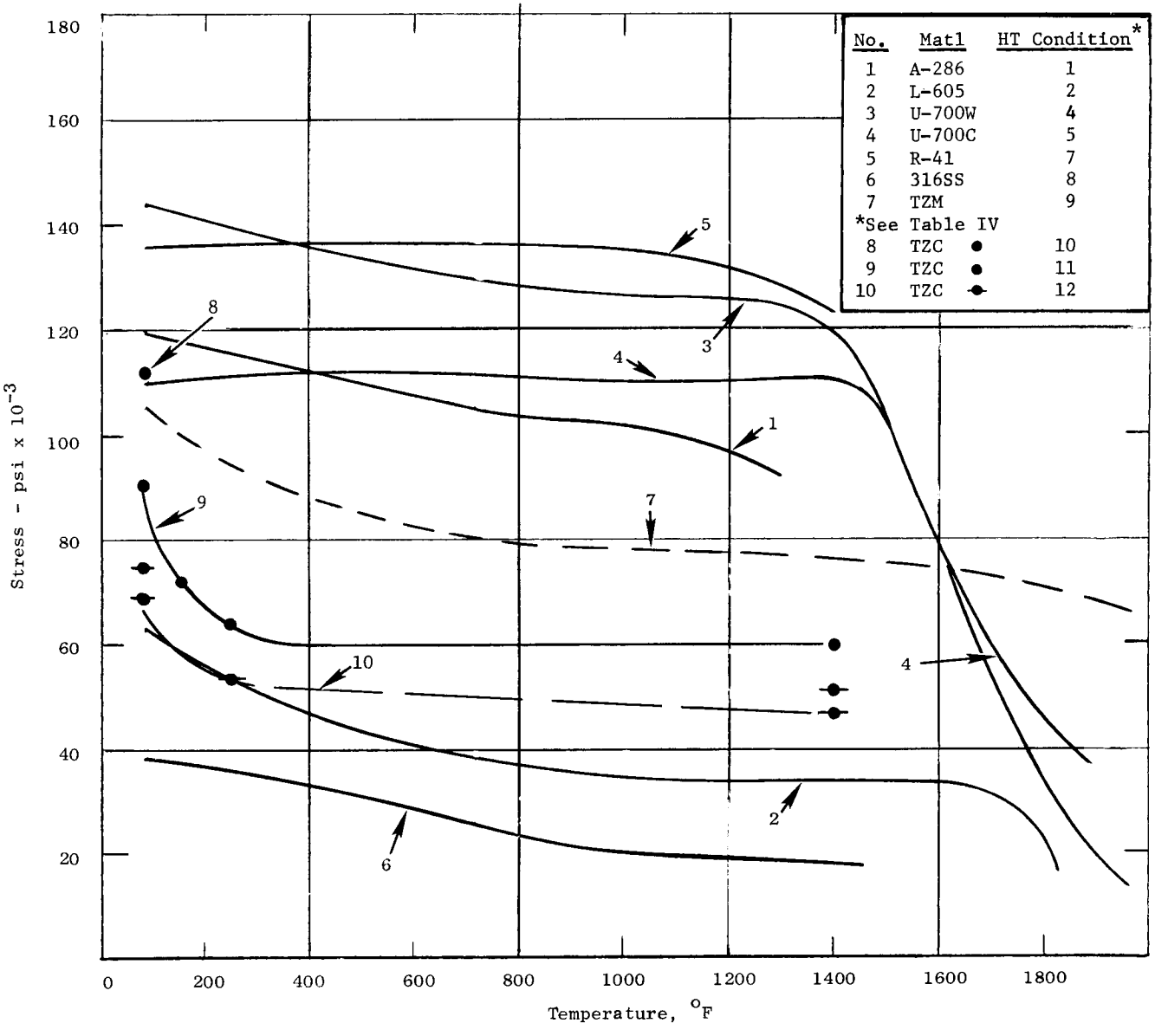

Figure 5. 0.2% Yield Strength of Various Turbine Materials Vs. Temperature.

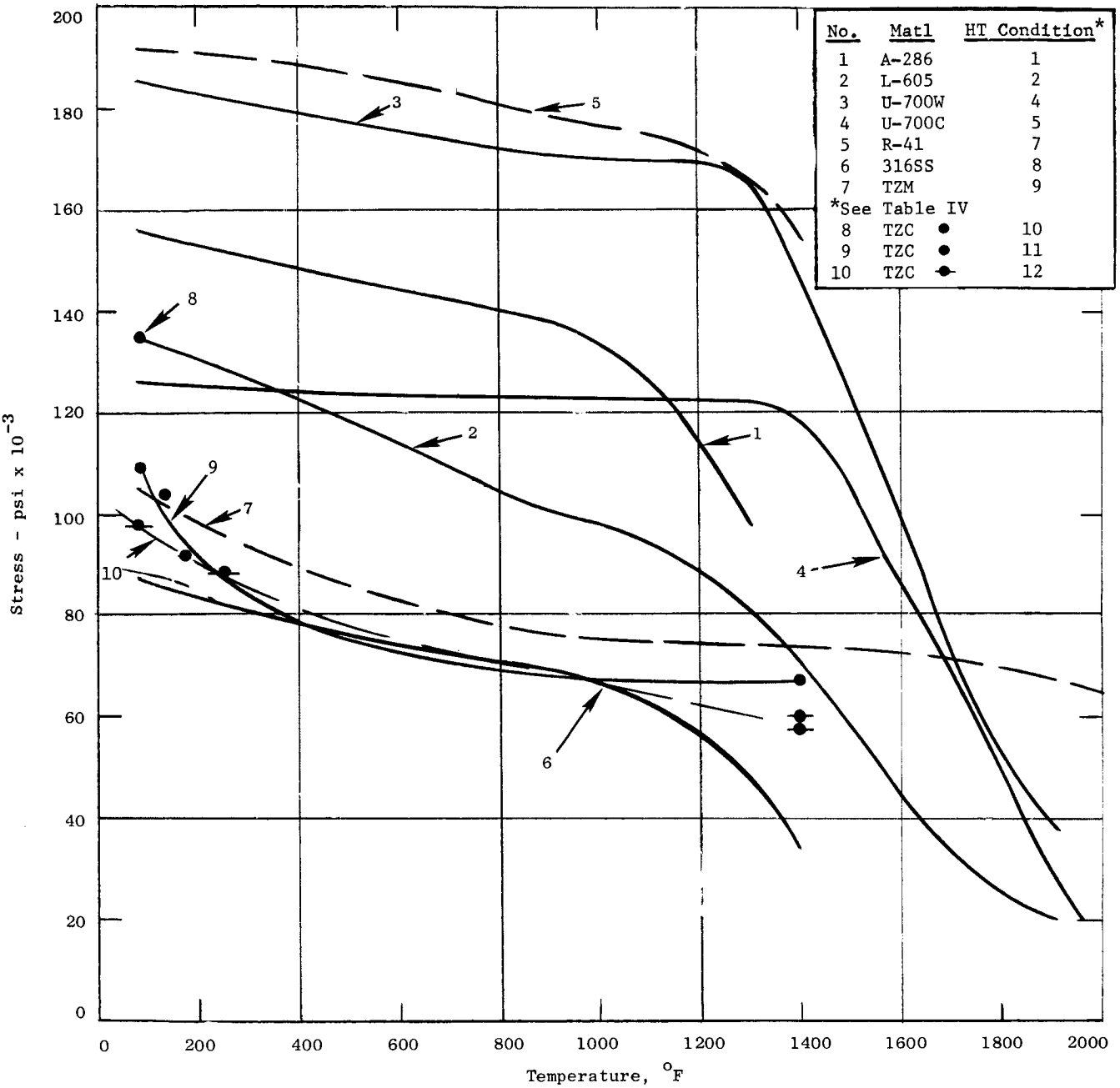

Figure 6. Ultimate Tensile Strength of Various Turbine Materials Vs. Temperature.

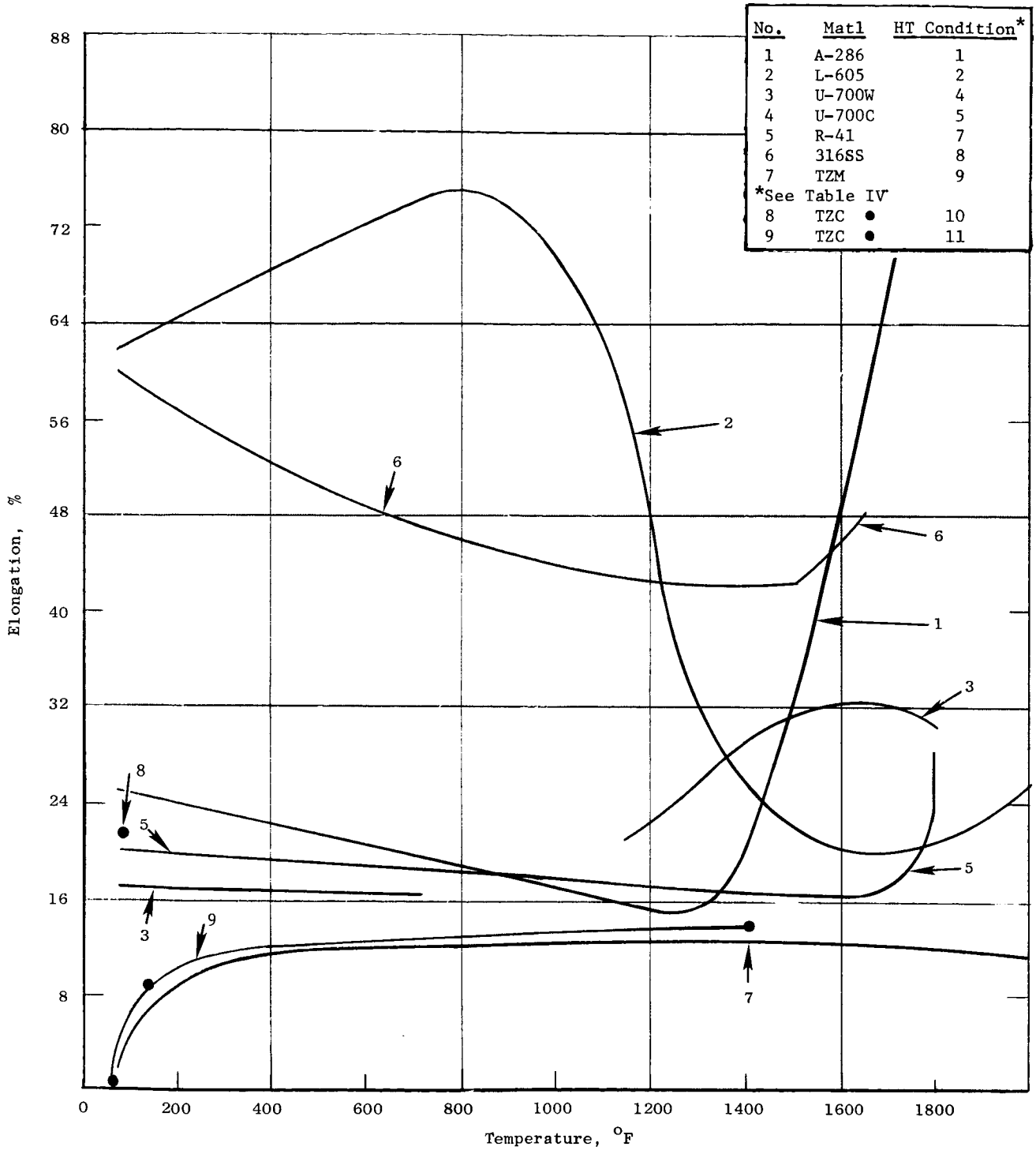

Figure 7. Tensile Elongation of Various Turbine Materials Vs. Temperature.

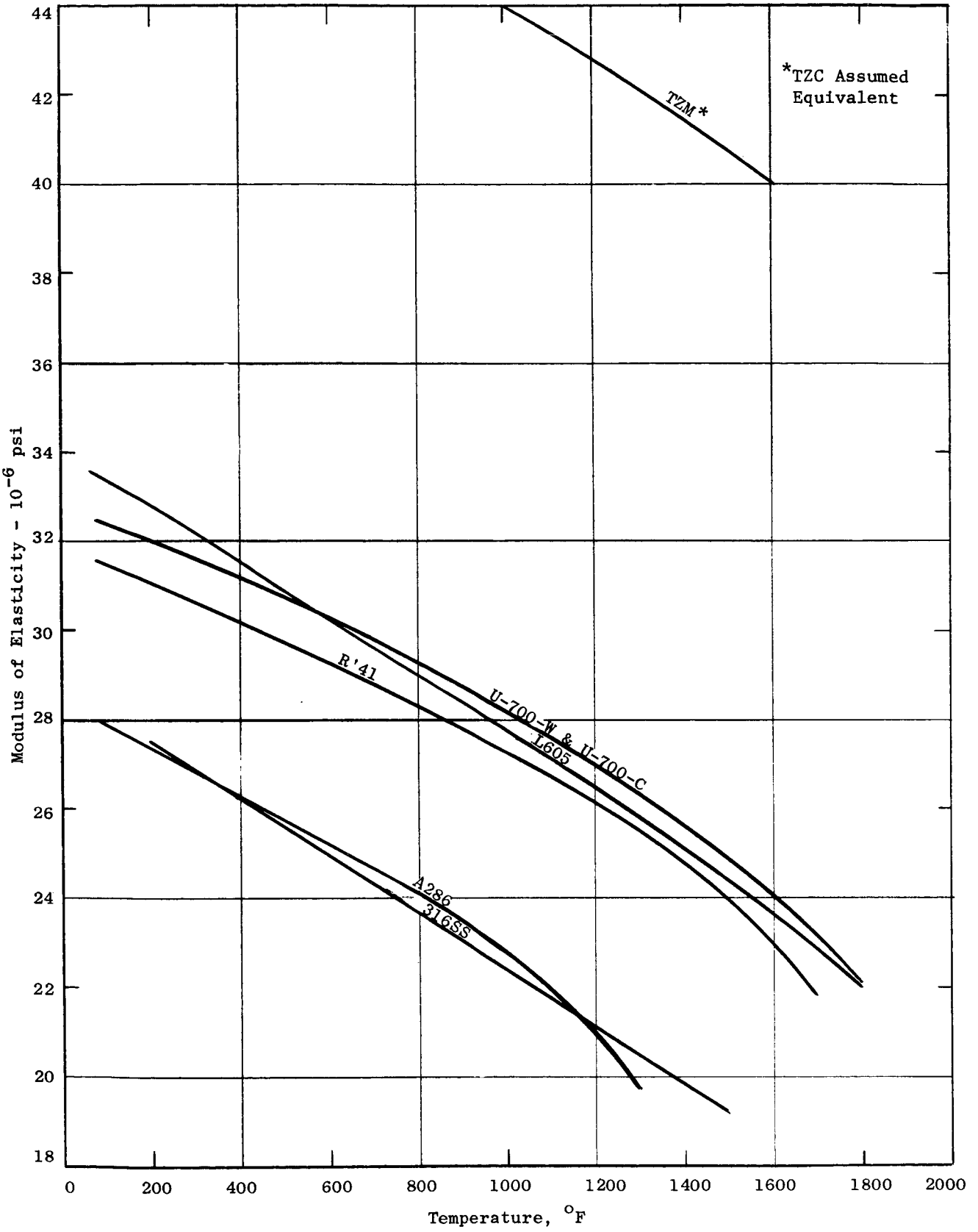

Figure 8. Modulus of Elasticity of Various Turbine Materials Vs. Temperature in Heat Treated Condition.

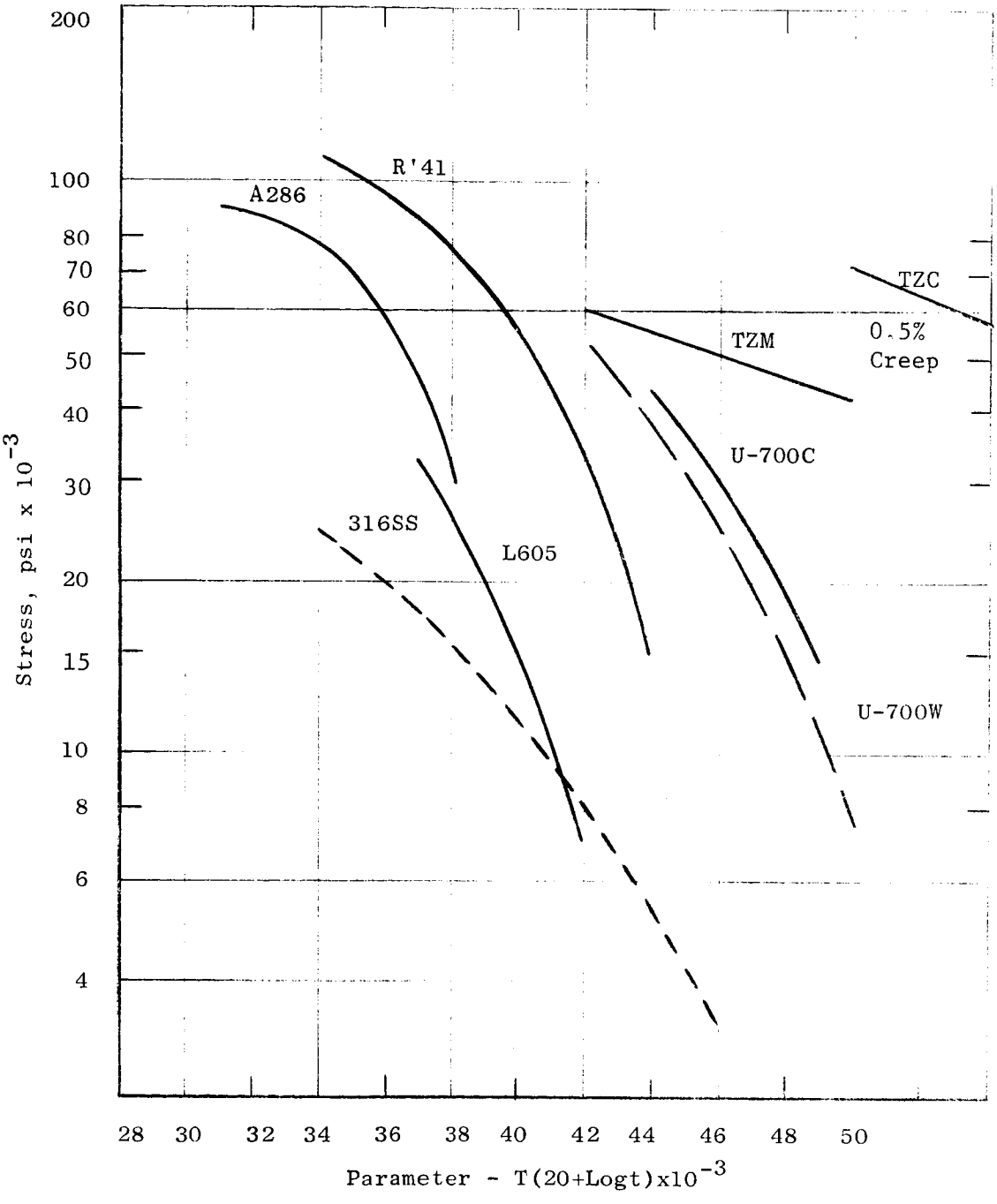

Figure 9. Parameter Plot of 0.2% (Average Values) Creep Stress for Various Turbine Materials in Heat Treated Conditions

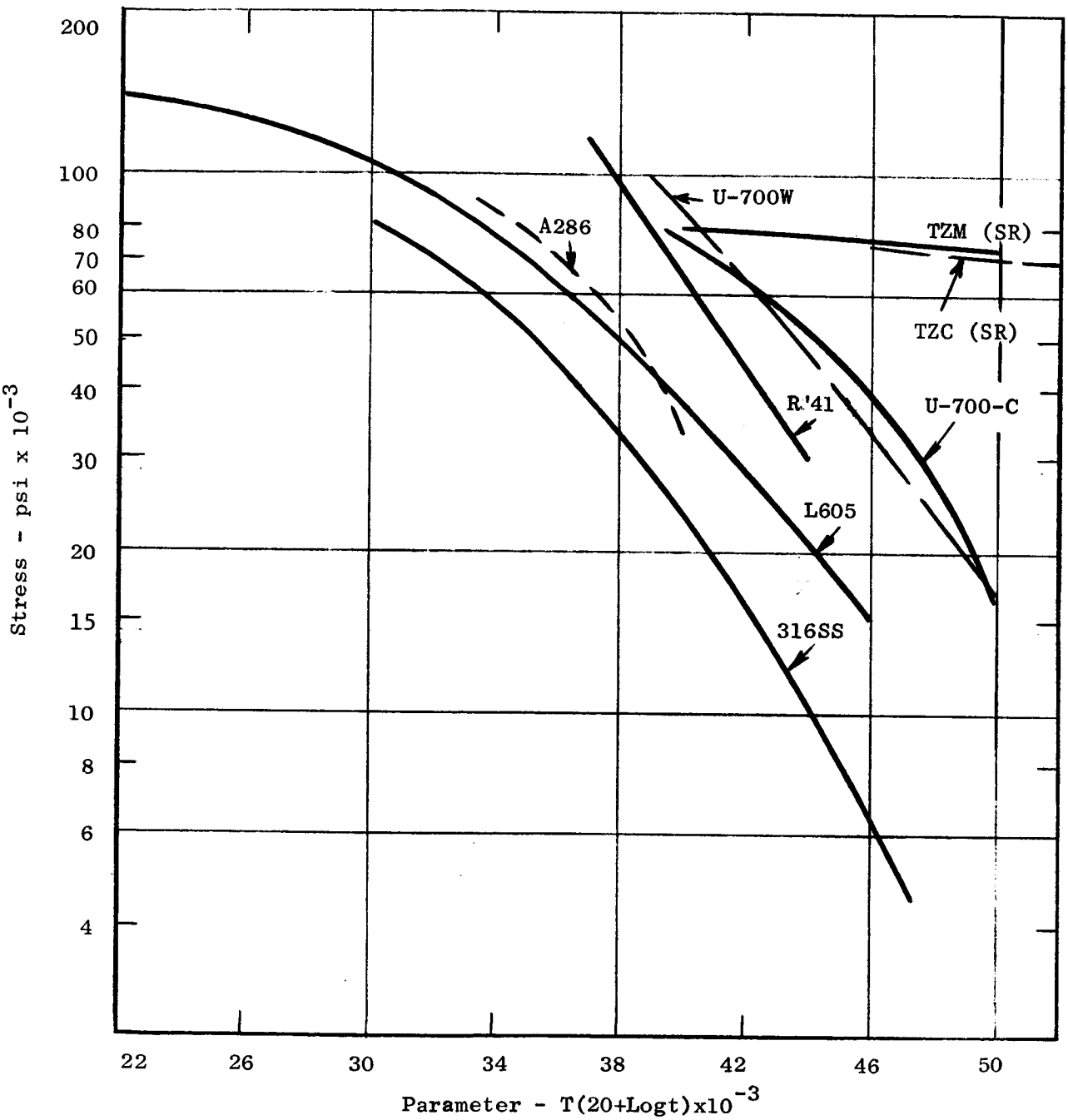

Figure 10. Parameter Plot of Rupture Stress for Various Turbine Materials in Heat Treated Condition. (Average Values)

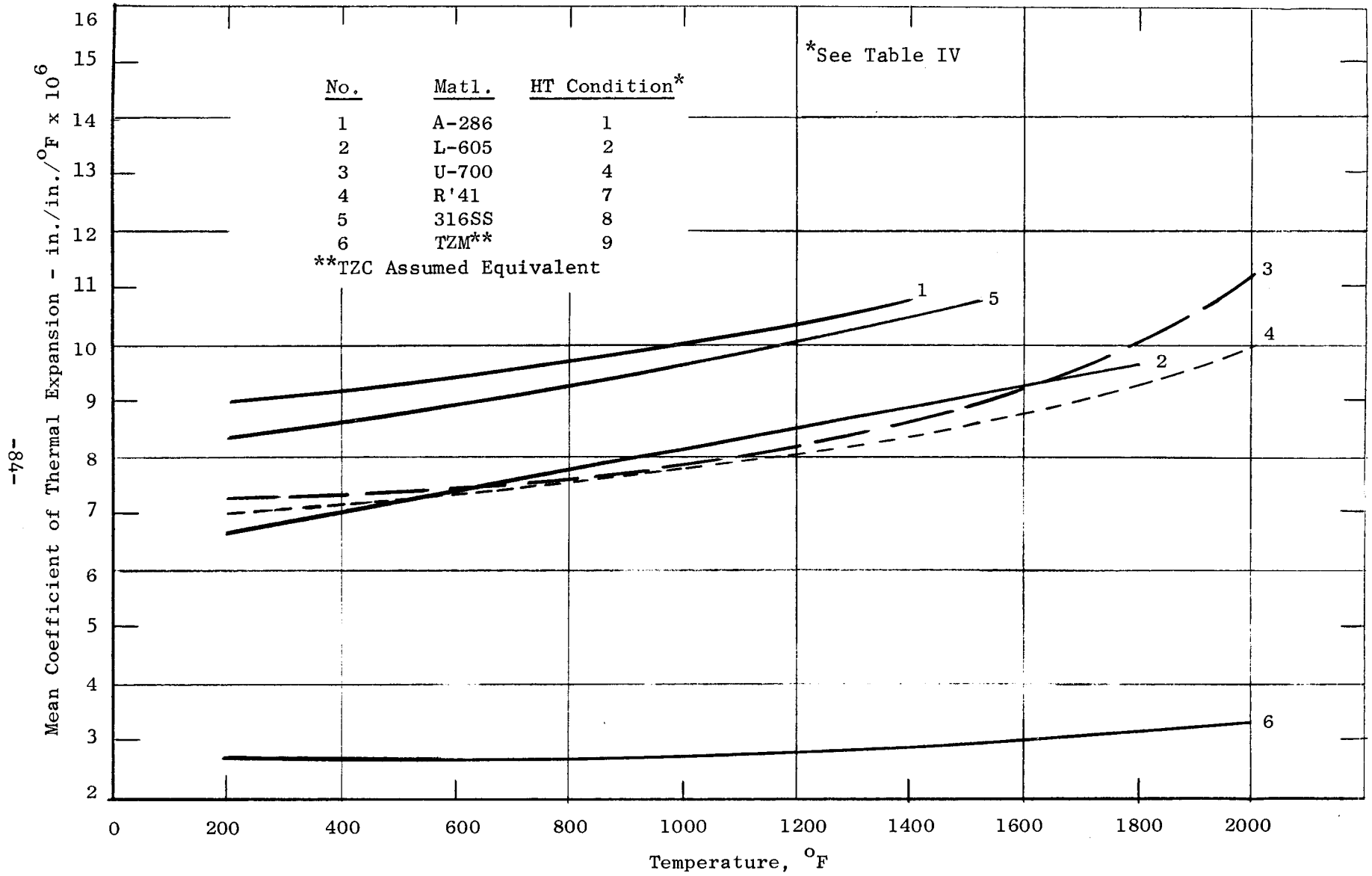

Figure 11. Mean Coefficient of Thermal Expansion of Various Turbine Materials Versus Temperature.

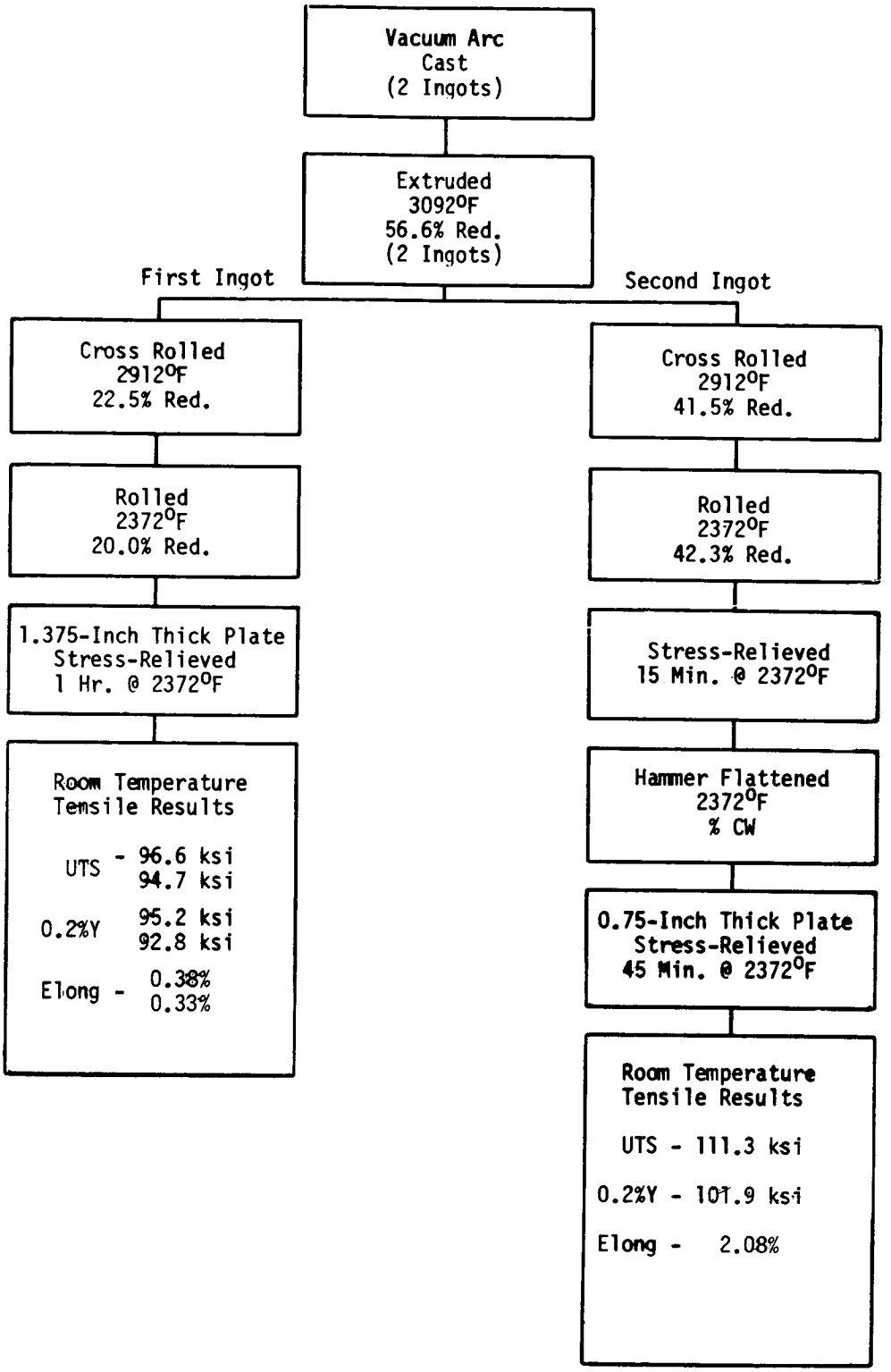

Figure 12. Processing History of 1.375-Inch and 0.75-Inch Thick Mo-TZC Alloy Plate Produced by GE-LMCD.

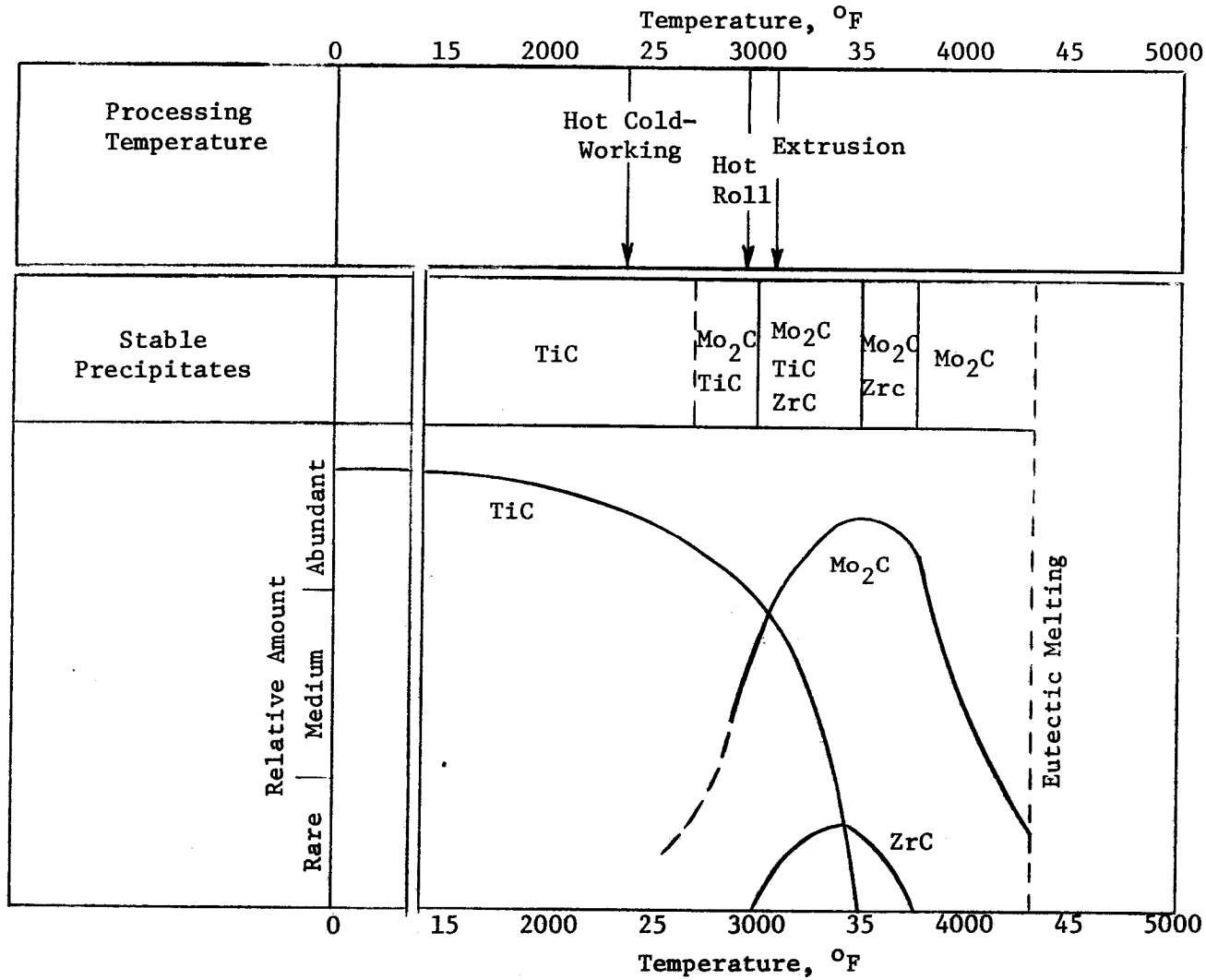

Figure 13. Approximate Carbide Stability Ranges in Mo-TZC Alloy.

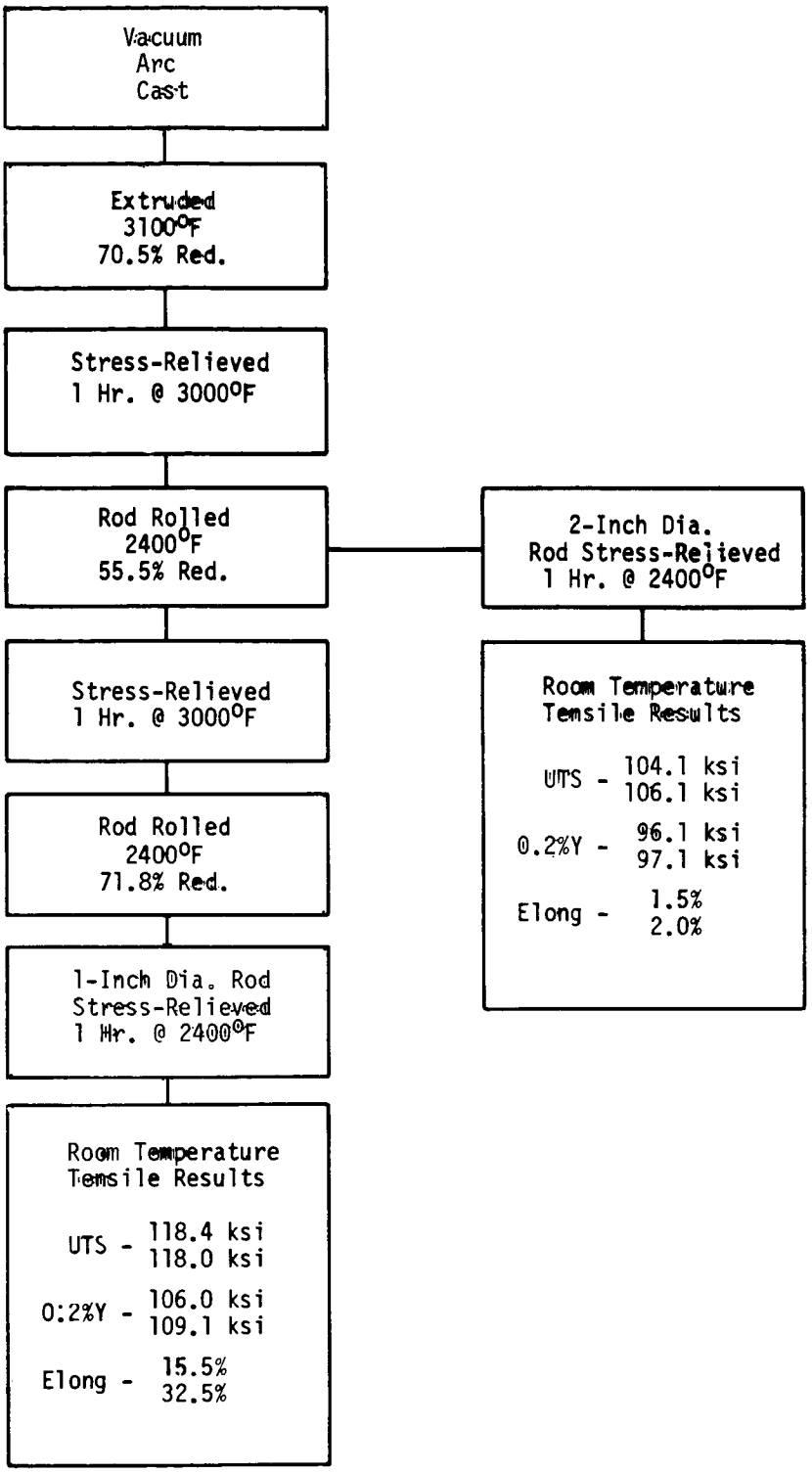

Figure 14. Processing History of 2-Inch and 1-Inch Diameter Mo-TZC Alloy Rod Produced by Climax.

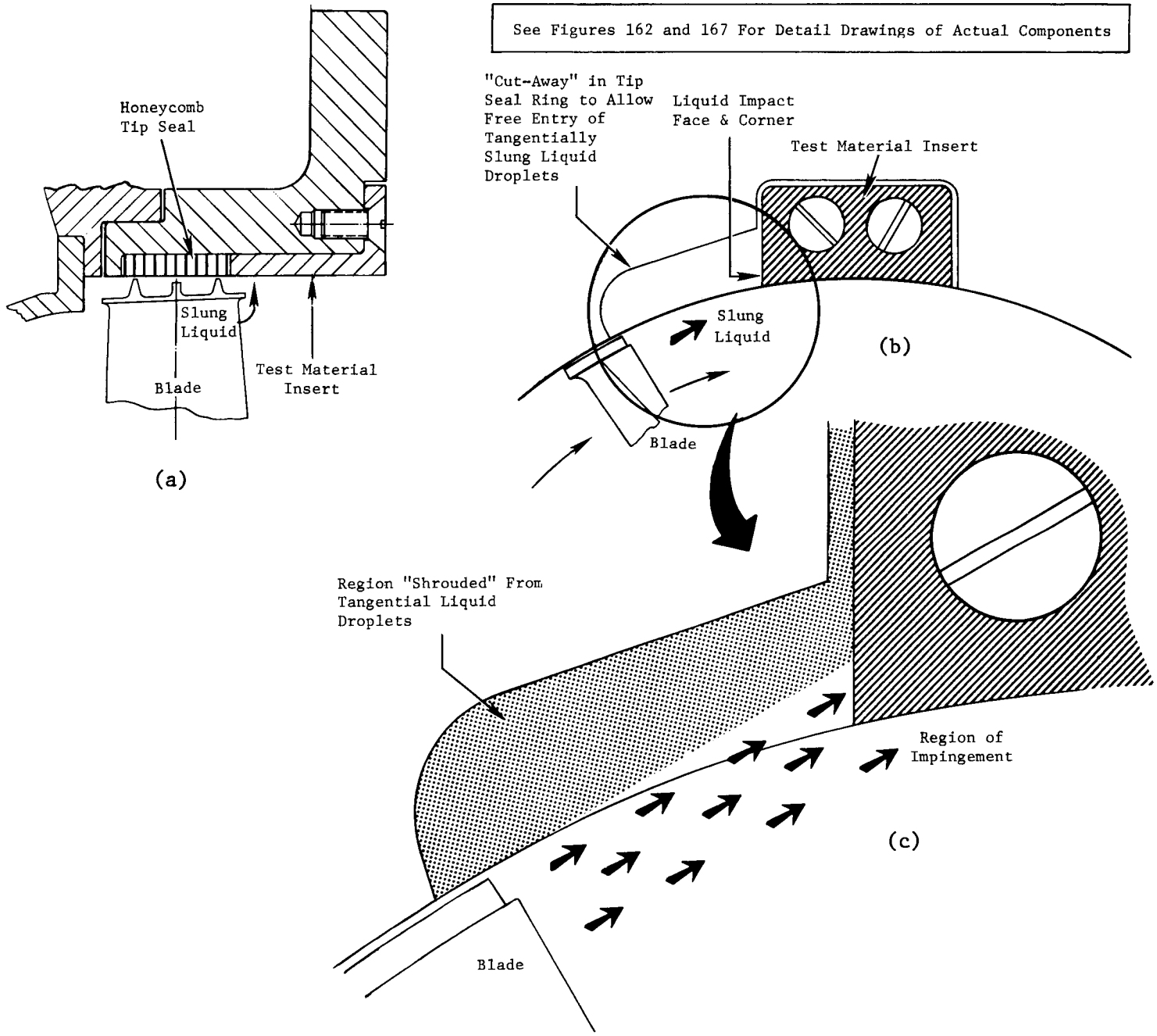

Figure 15. Installation of Corrosion/Erosion Test Material Inserts Aft of Stage 3 Rotor.

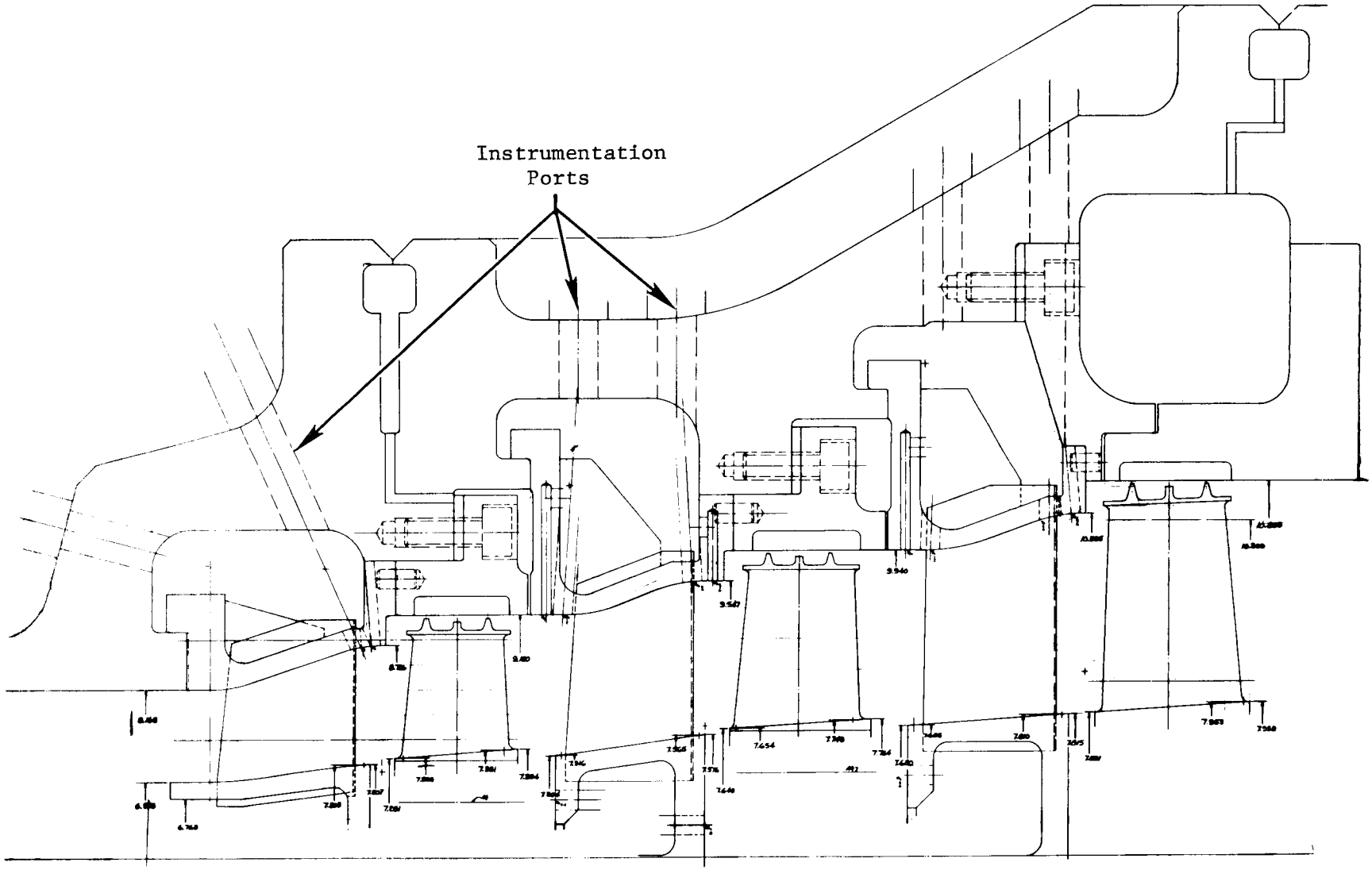

Figure 16. Turbine Fluid - Dynamic Region. (Phase I, Shrouded Design)

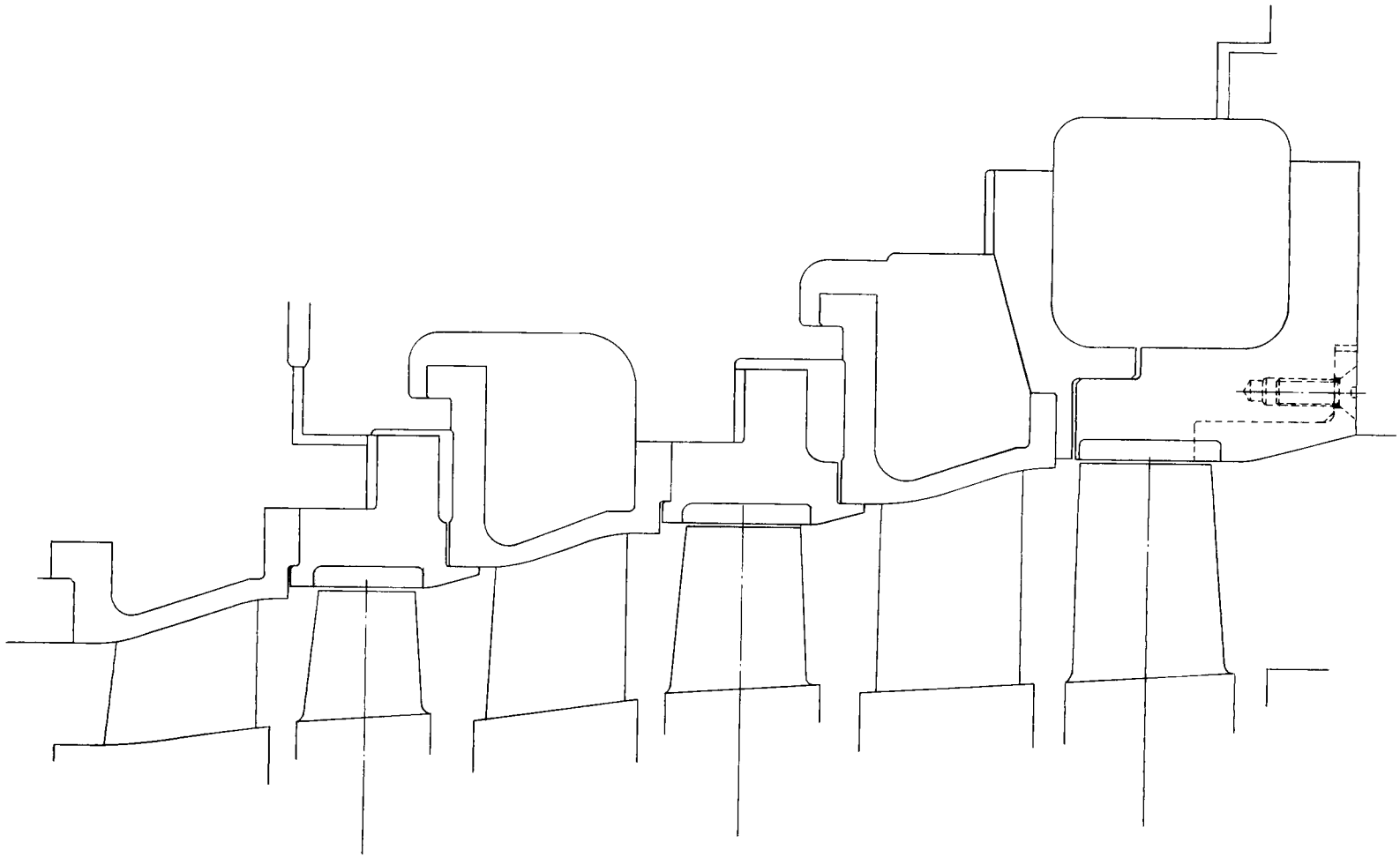

Figure 17. Turbine Fluid-Dynamic Region. (Phase II, Non-Shrouded Design)

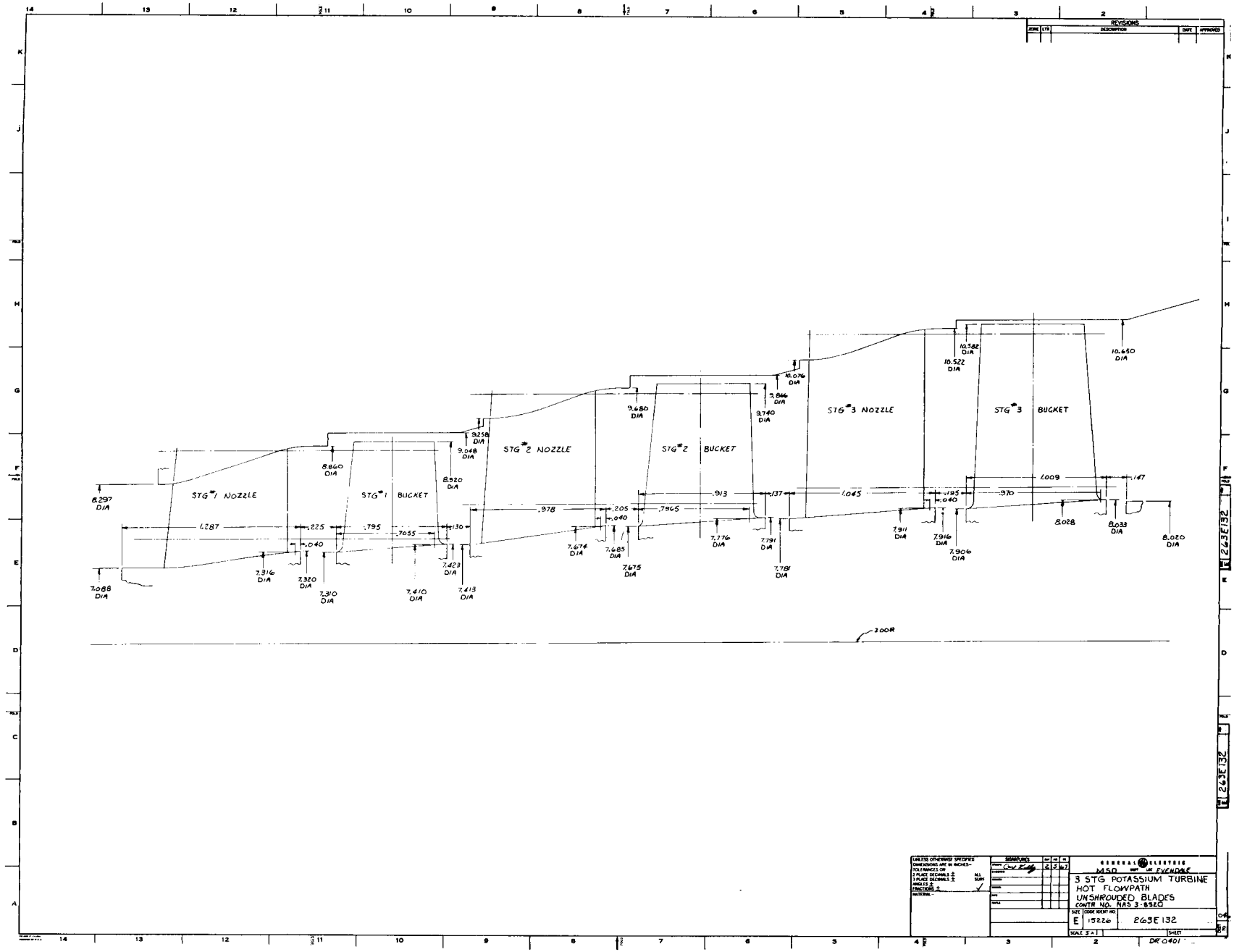

Figure 20a. Hot Flowpath. (Phase II, Non-Shrouded Design)

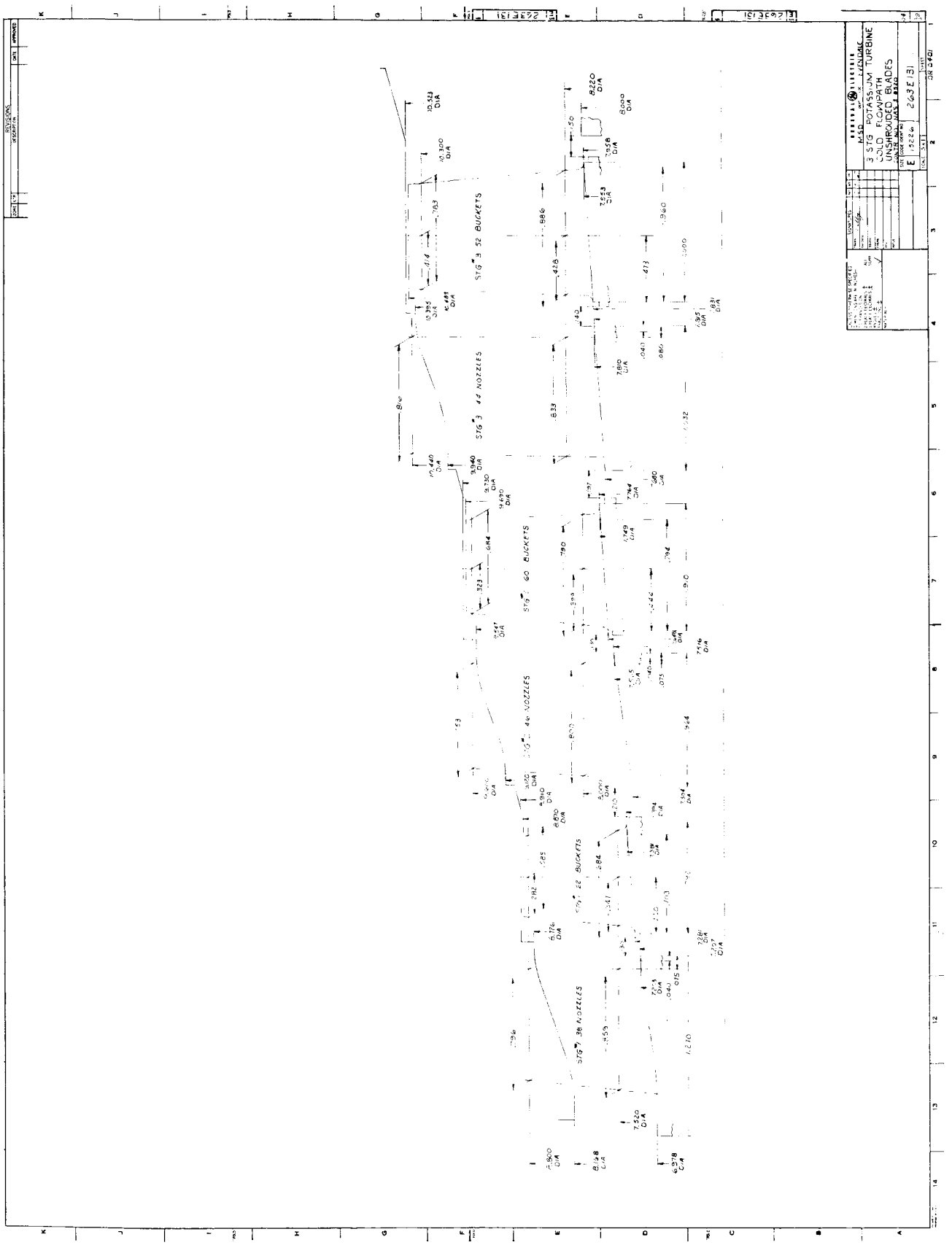

Figure 20b. Cold Flowpath. (Phase II, Non-Shrouded Design)

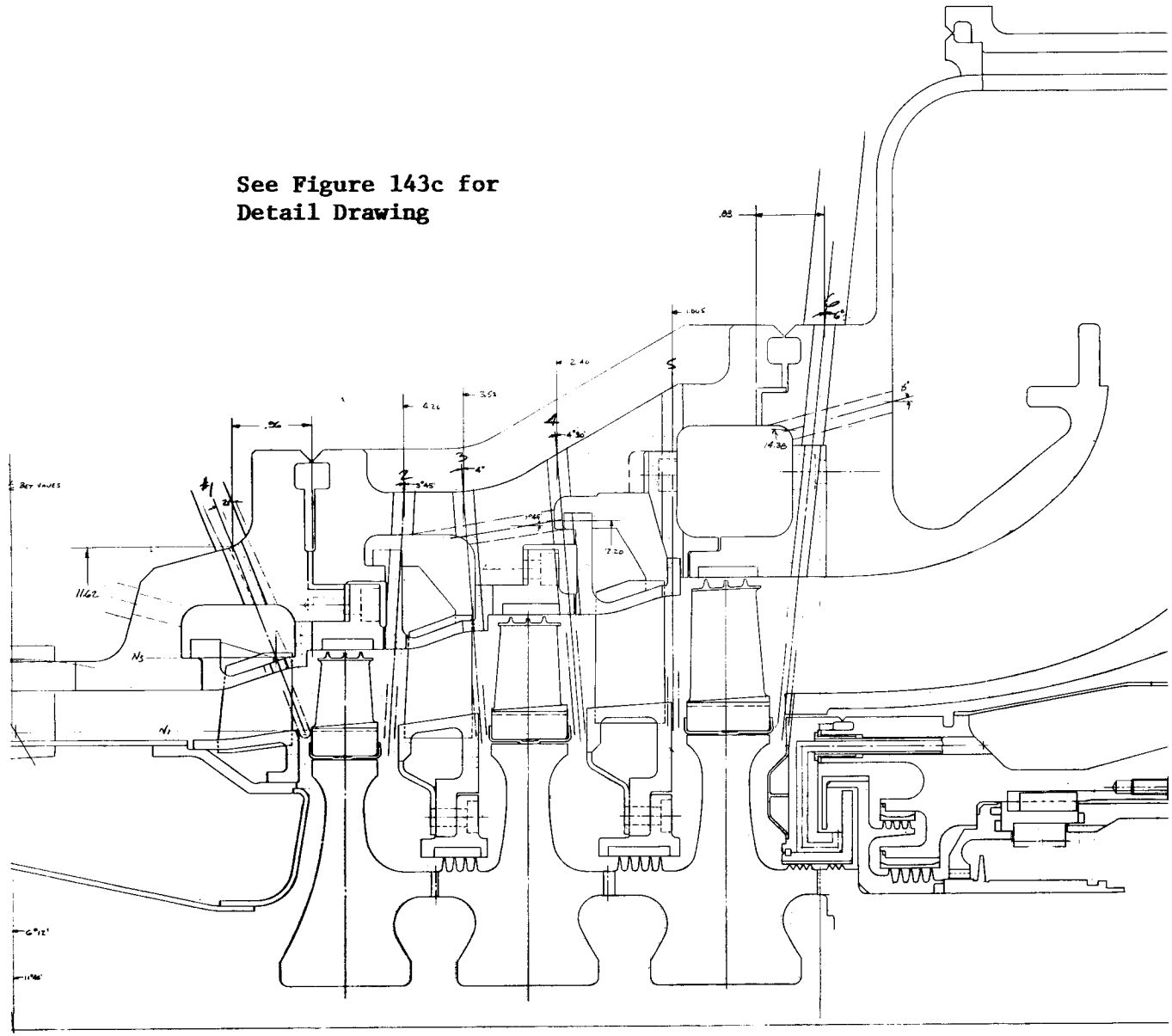

Figure 21. Installation of Borescope Inspection Ports in Turbine Casing.

STRESS DESIGN CRITERIA

Life Determination:

$$\text{Percent Life Used Up} = \frac{t1^1}{t1} + \frac{t2^1}{t2} + \text{- - - - - -}$$

Where $t1^1$ = Actual Operating Time

$t2$ = Maximum Allowable Operating Time

Stress - Temperature - Life Parameter

$$P = T\,(C+\log_{10} t) \times 10^{-3}$$

T = Temperature (°R)
C = Constant (Material and Available Data)
t = Required Operating Time (Hours)

Theory of Failure

Henky - von Mises

$$\sigma_e = \frac{\sqrt{2}}{2} \sqrt{(\sigma_x-\sigma_y)^2 + (\sigma_y-\sigma_z)^2 + (\sigma_z-\sigma_x)^2 \times 6\tau_{xy}^2 + 6\tau_{yz}^2 + 6\tau_{zx}^2}$$

σ = direct stress
τ = shear stress
x, y, z = rectangular coordinates

Steady State Loads

Use Lower Value Of:

(a) 100% of 0.2% Offset Yield Strength
(b) 100% of 2% Plastic Creep
(c) 80% (or 3 Sigma Deviations) of Rupture Strength.
On Localized Stresses, Use 90% of Rupture.
(d) Shear Stress = 0.57 of Ultimate Strength

Alternating Stress

Use Goodman Diagram

Gas Bending Loads = Full Application and Removal

Figure 22. Stress Design Criteria for the Three-Stage Turbine

ASSUMPTIONS FOR SUBSEQUENT TEMPERATURE DISTRIBUTION CHARTS AND CALCULATIONS USING THTC PROGRAM

1. Radiation used only between the rotor wheels, not including the curvic coupling torque tube, and the tie bolt. View factors were always 1.0.

2. Fluid film coefficients were entered as constant values unaffected by time and temperature.

3. Initial temperatures in the vapor stream areas were assumed to be 700°F and 200°F in all other areas, except for graduated temperatures in transitioning from the hot wheels to the shaft.

4. Fluid film coefficients (Btu/hr ft^2 °F) were generally assumed as follows: (also see Figure 26).

    a. 1000 on vapor condensing surfaces.
    b. 500 in areas radially inside the curvic torque tubes.
    c. 50 in all sump areas.
    d. 10 between insulation and ambient.

5. Contact coefficients were assumed as follows: (also see Figure 26).

    a. 800 between tip seals and the casing.
    b. 500 between the curvic couplings.
    c. 100 between the insulation and 316 S.S. components.
    d. 50 between the bearing housing and the pad bearing.
    e. 10 between instrumentation ring and bearing housing.

6. The argon-filled 0.020" radial space between the tie bolt and the shaft was assumed to have a contact coefficient which varied between 23 & 16.

7. The rotor and stator blades were not considered as material nodes, but instead were assumed to be fluid film coefficients acting on the inner and outer walls of the flow path.

8. The temperatures in the rotor blade locations were assumed to be at the equilibrium temperature of the vapor entering the blade row.

9. The temperature in the nozzle blades was assumed to be the average of the entering and leaving equilibrium vapor temperature.

10. The cavities between the tip seals and casing were assumed to be materials of potassium vapor.

11. The cavity between the heat shield and the bearing housing was assumed to be a material node of argon.

12. The material non-temperature dependent data were density and latent heat. The temperature-dependent data were thermal conductivity, specific heat, and emissivity.

Figure 23.

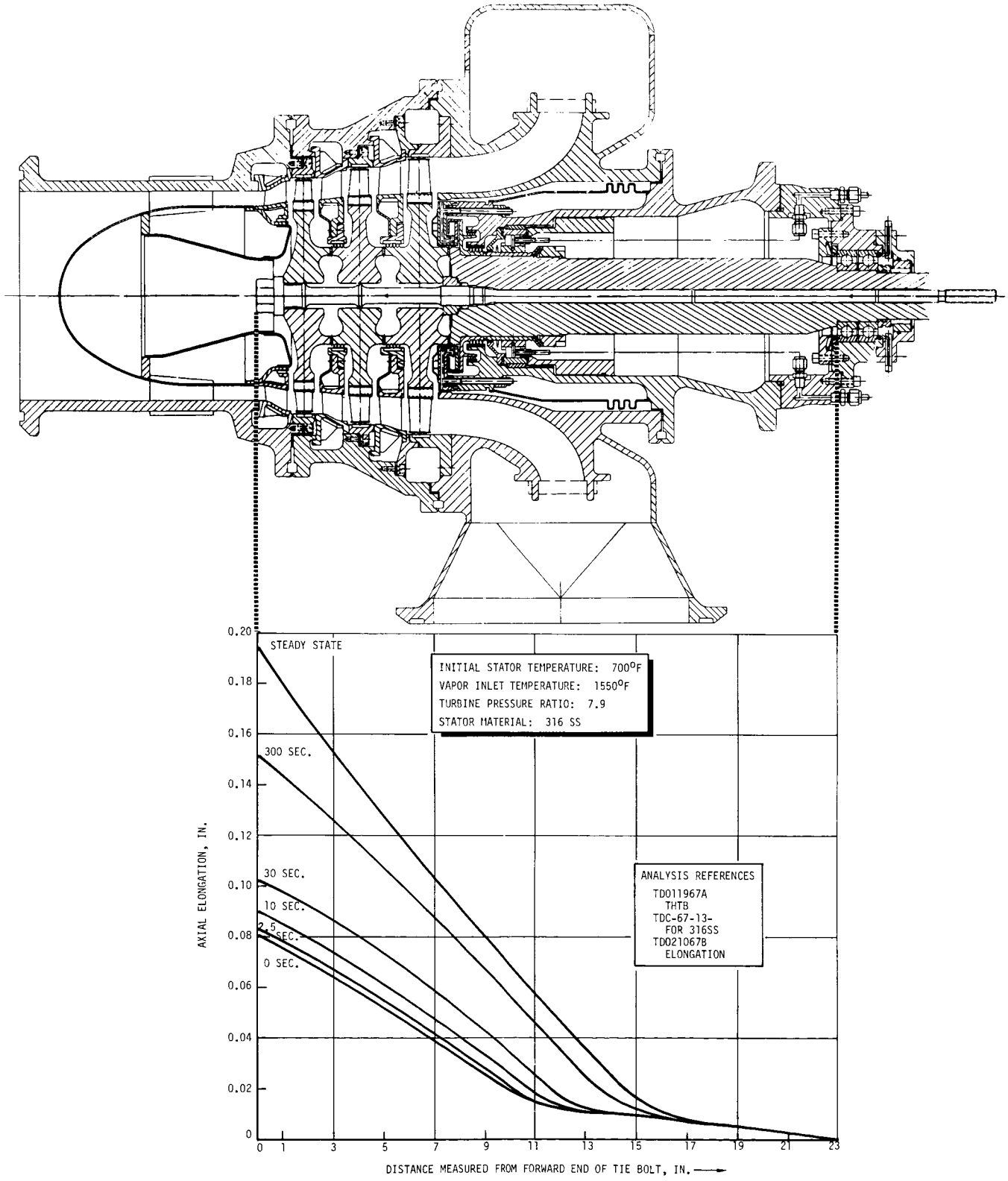

Figure 31. Stator Axial Growth as a Function of Time After Onset of Vapor Flow (Design Point Conditions).

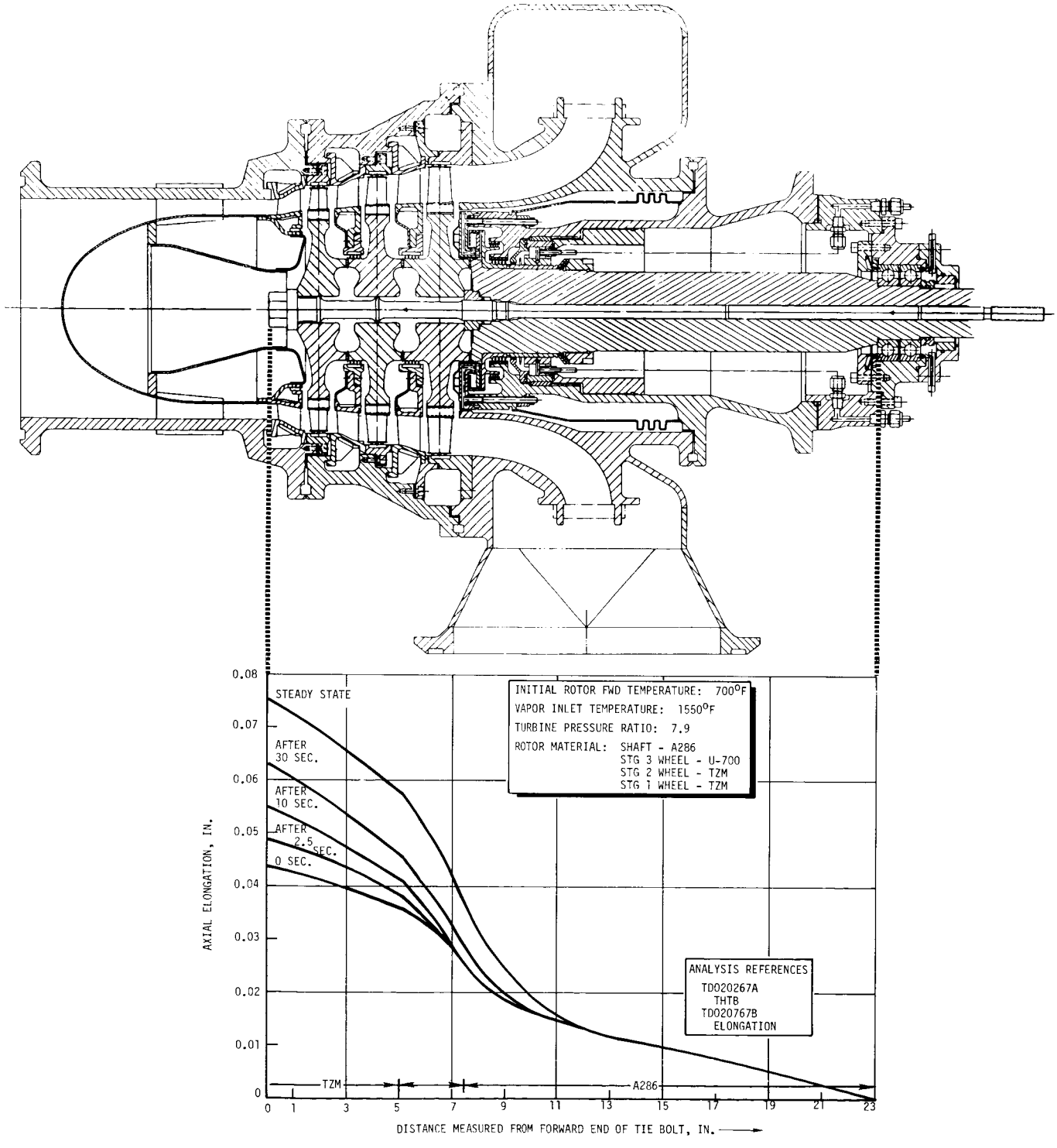

Figure 32. Rotor (Shaft & Wheels) Axial Growth as a Function of Time After Onset of Vapor Flow (Design Point Conditions).

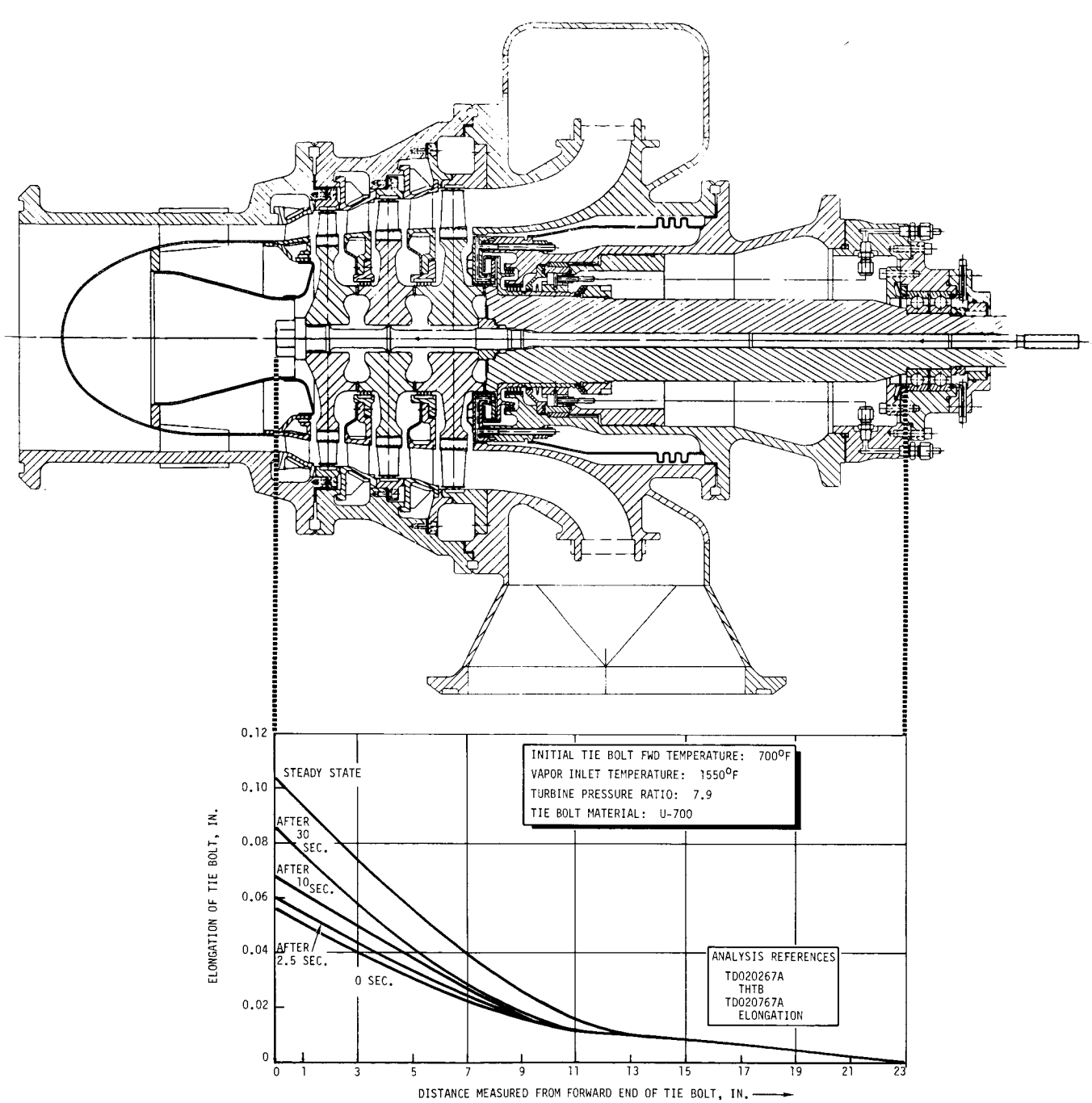

Figure 33. Tie Bolt Axial Growth as a Function of Time After Onset of Vapor Flow (Design Point Conditions).

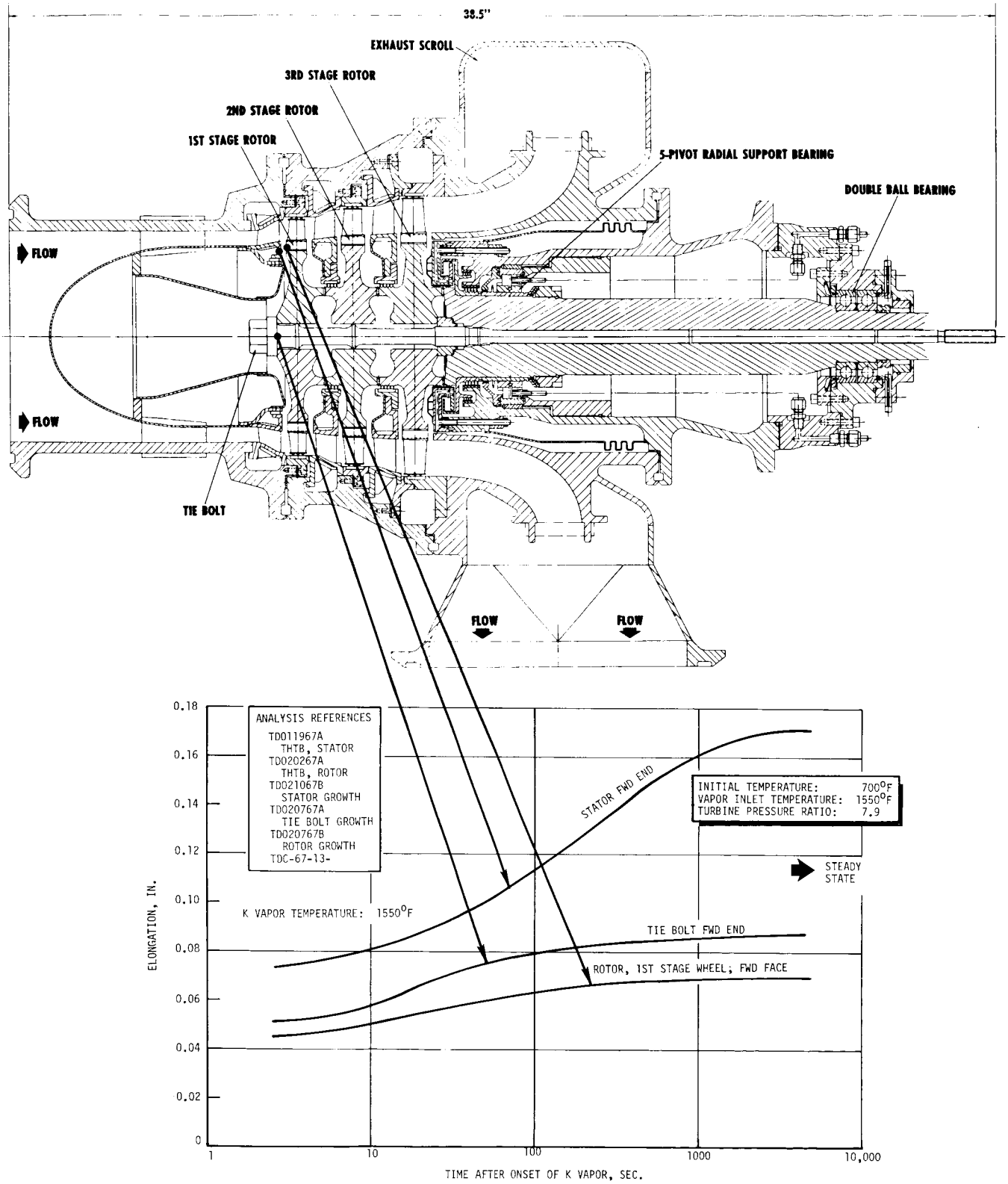

Figure 34. Thermal Growth of Forward End of Turbine as a Function of Time After Onset of Vapor Flow.

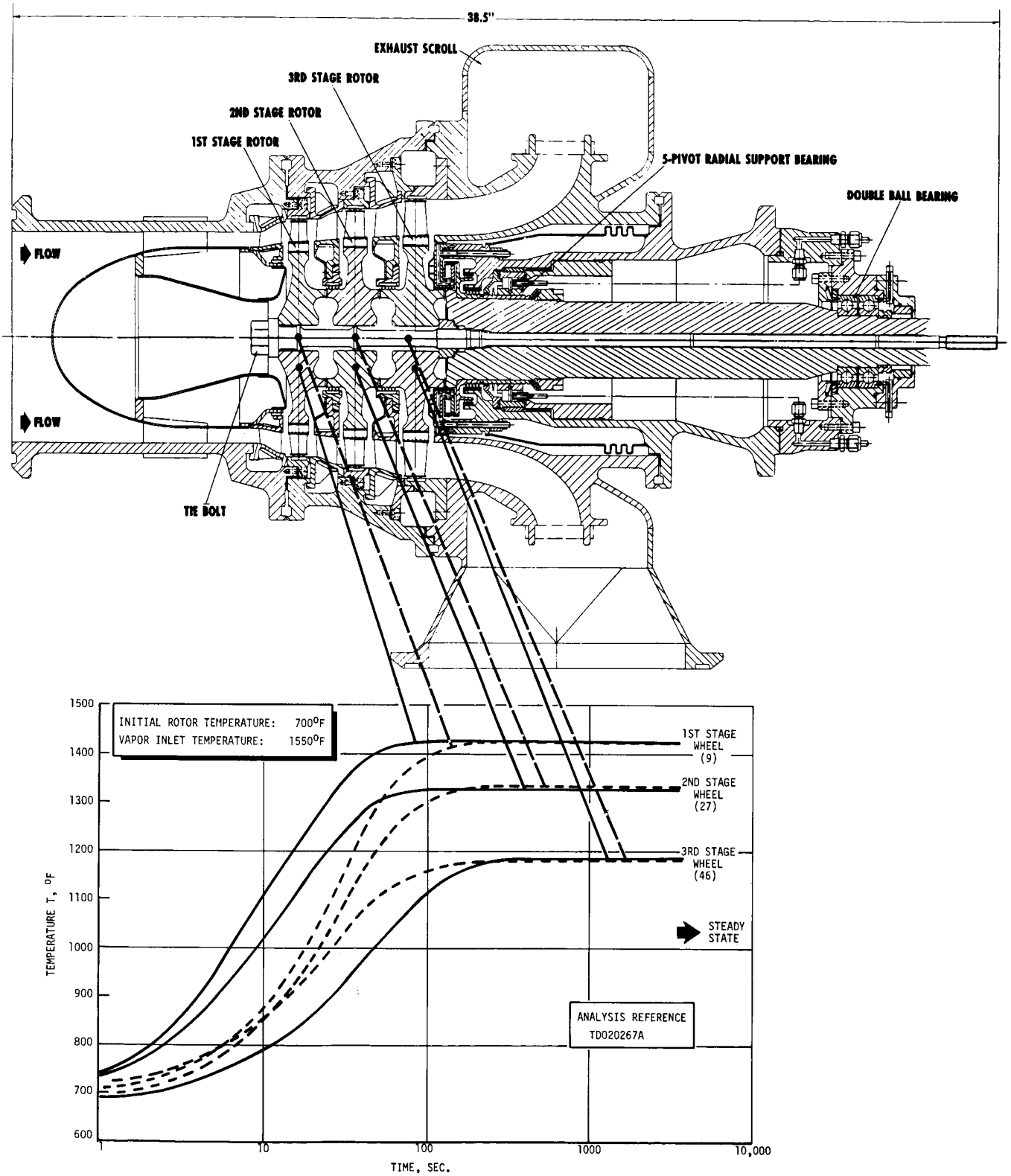

Figure 35. Change of Wheel Hub Temperature as a Function of Time After Onset of Vapor Flow.

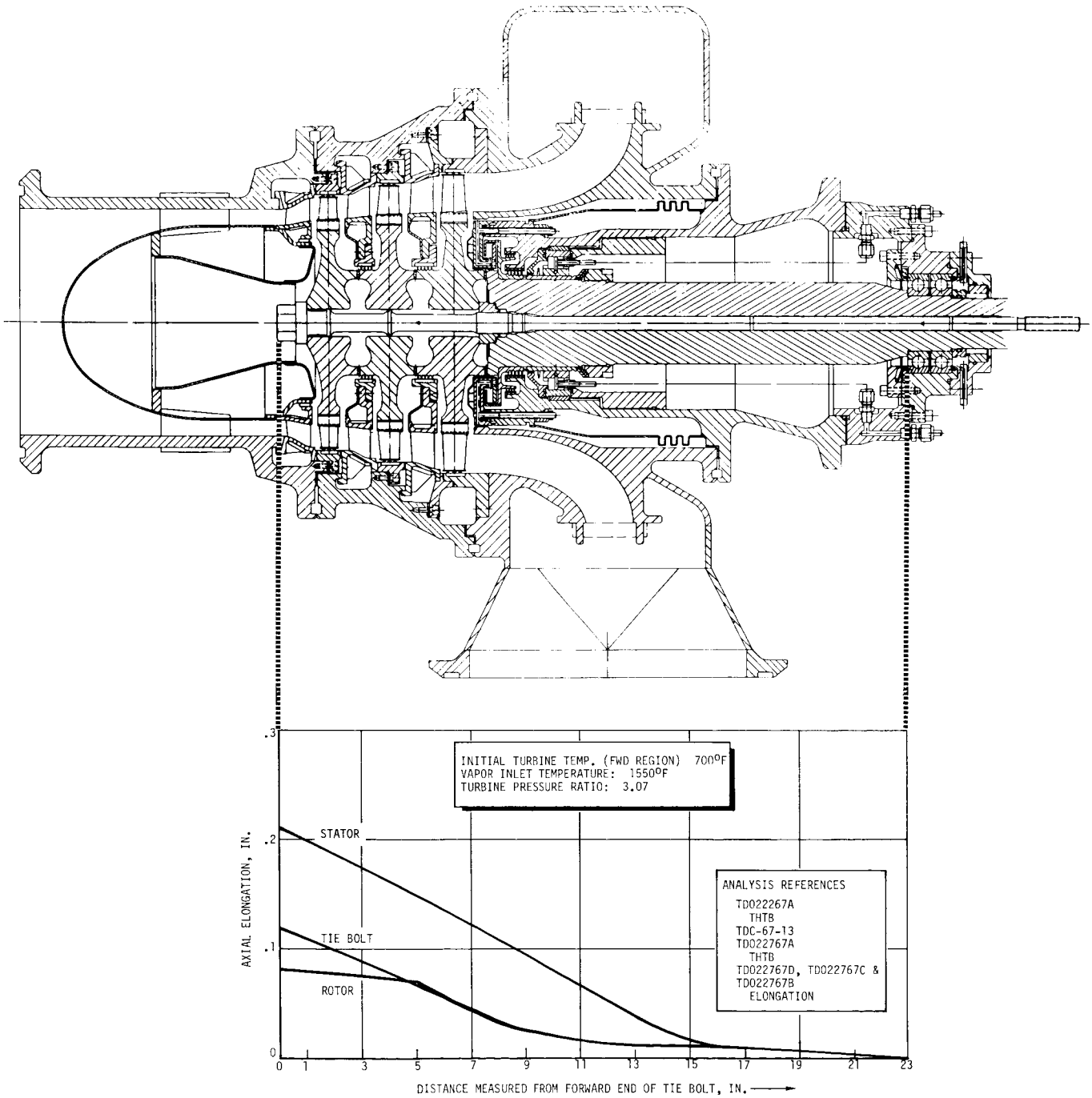

Figure 36. Steady-State Axial Growth of Key Components for Off-Design Conditions of 1550°F Inlet and T-S Pressure Ratio of 3.07.

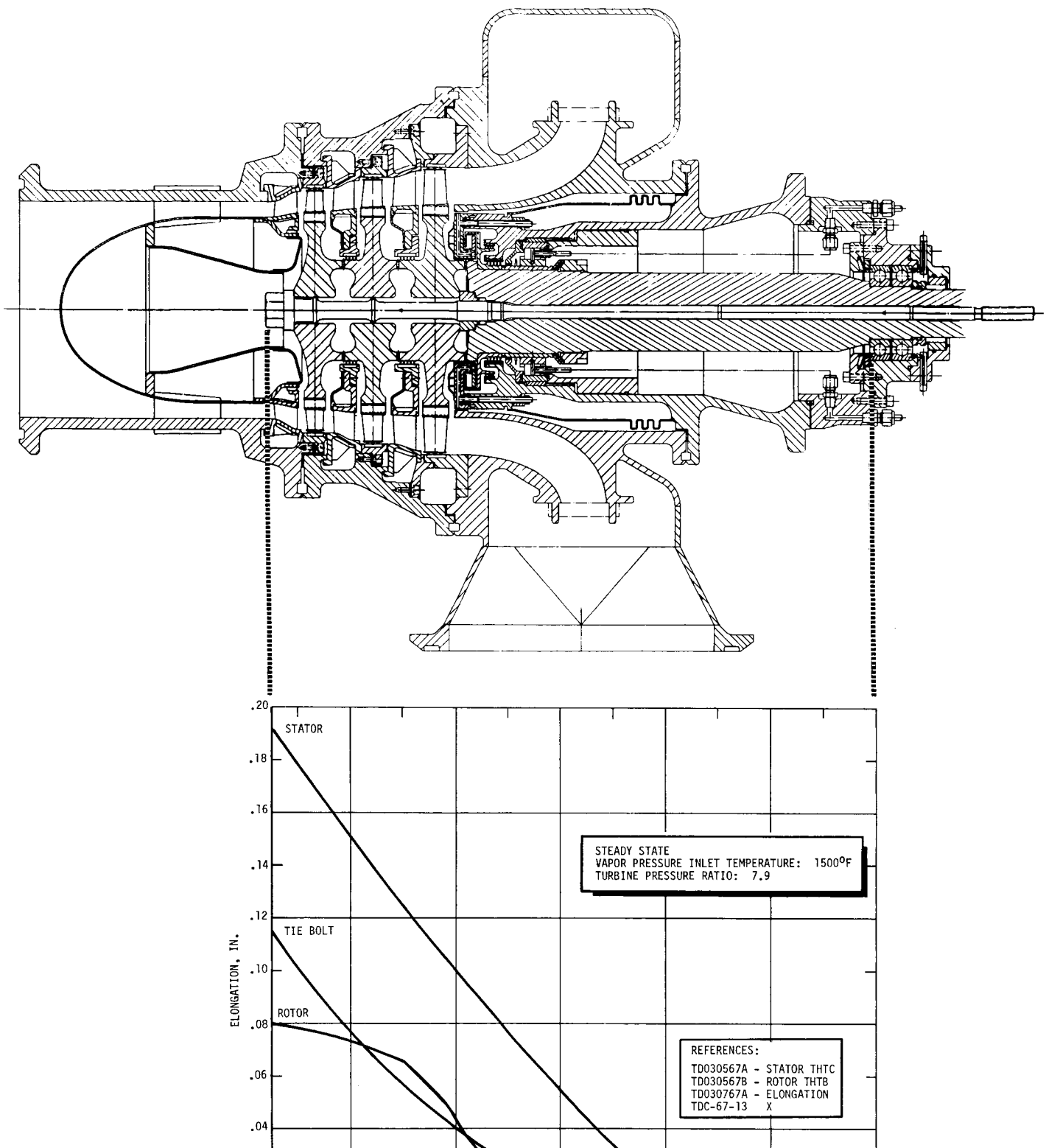

Figure 37. Steady State Axial Growth of Key Components as a Function of Time After Onset of Vapor Flow (Off-Design).

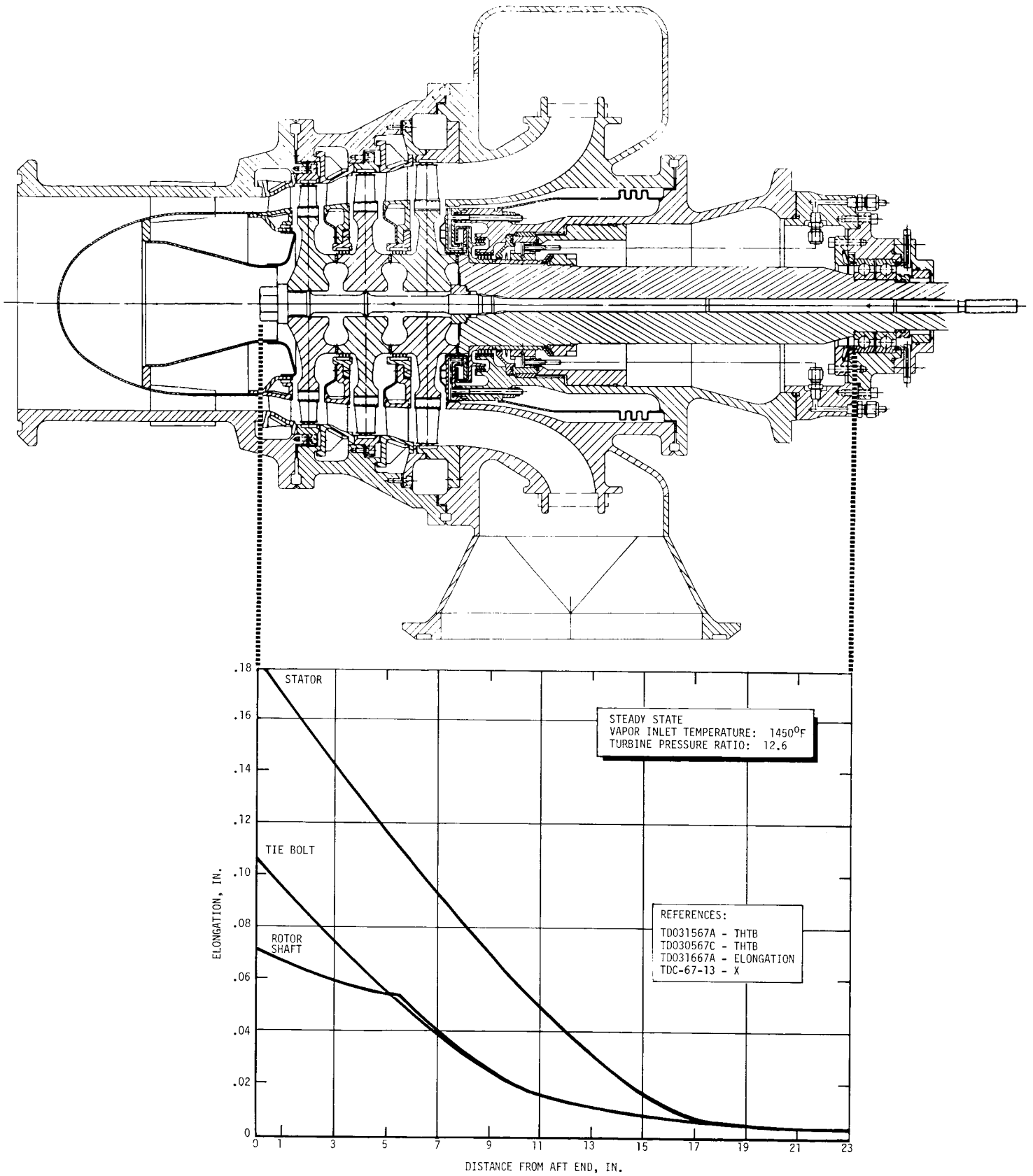

Figure 38. Steady State Axial Growth of Key Components as a Function of Time After Onset of Vapor Flow (Off-Design).

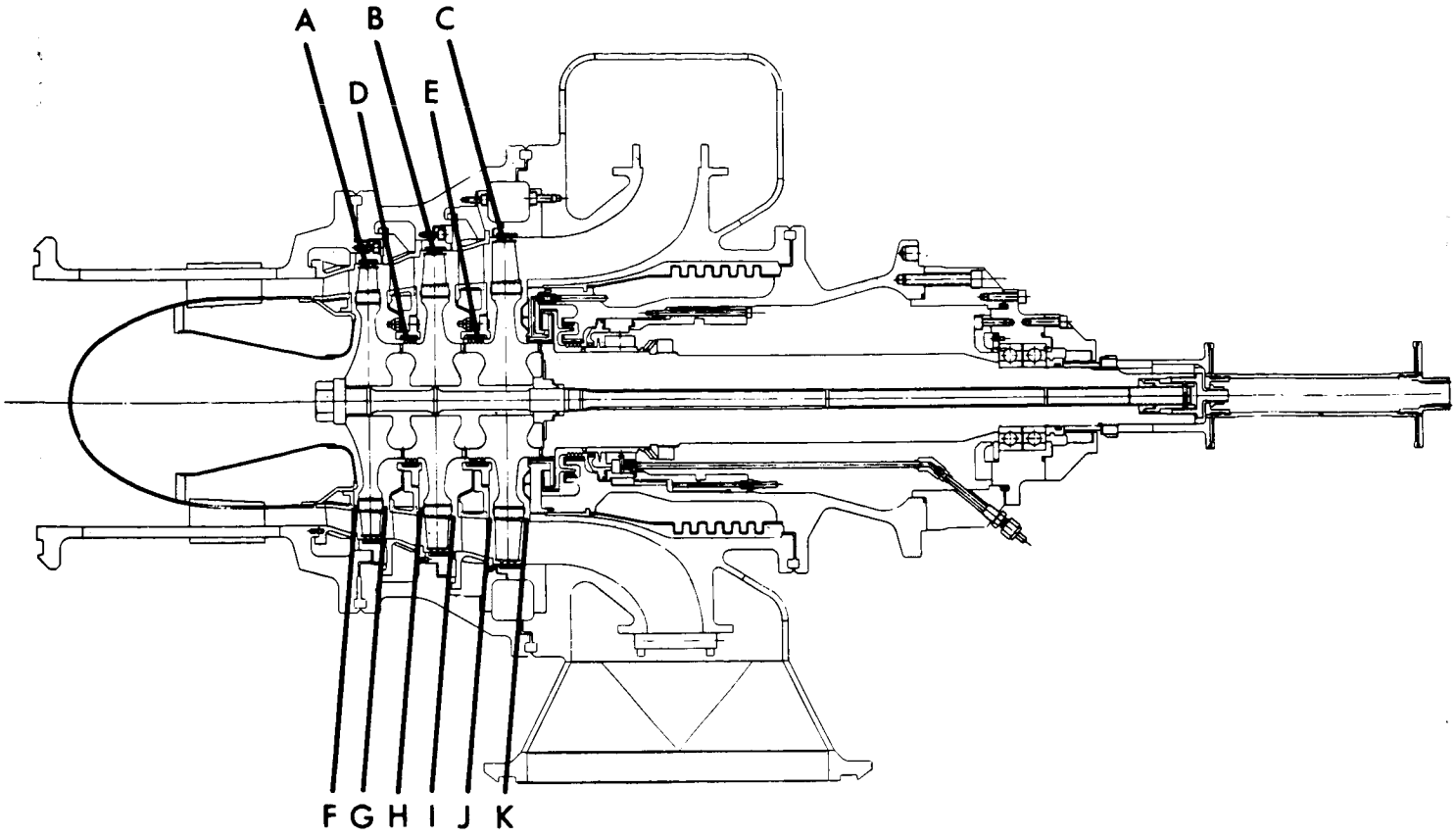

Turbine Radial Clearances

	Cold	Differential	Hot
A	.020	.043	.063
B	.020	.042	.062
C	.020	.014	.034
D	.010	.021	.031
E	.010	.006	.016

Turbine Axial Clearances

	Cold	Differential	Hot
F	.131	+.106	.237
G	.210	-.093	.117
H	.131	+.082	.213
I	.196	-.068	.126
J	.141	+.064	.205
K	.150	-.001	.149

HOT CLEARANCES ARE FOR DESIGN-POINT OPERATION

INLET TEMPERATURE: 1550°F
T-S PRESSURE RATIO: 7.9
ROTATIONAL SPEED: 18,250 rpm

Figure 39a. Turbine Stator-To-Rotor Hot and Cold Nominal Clearances.

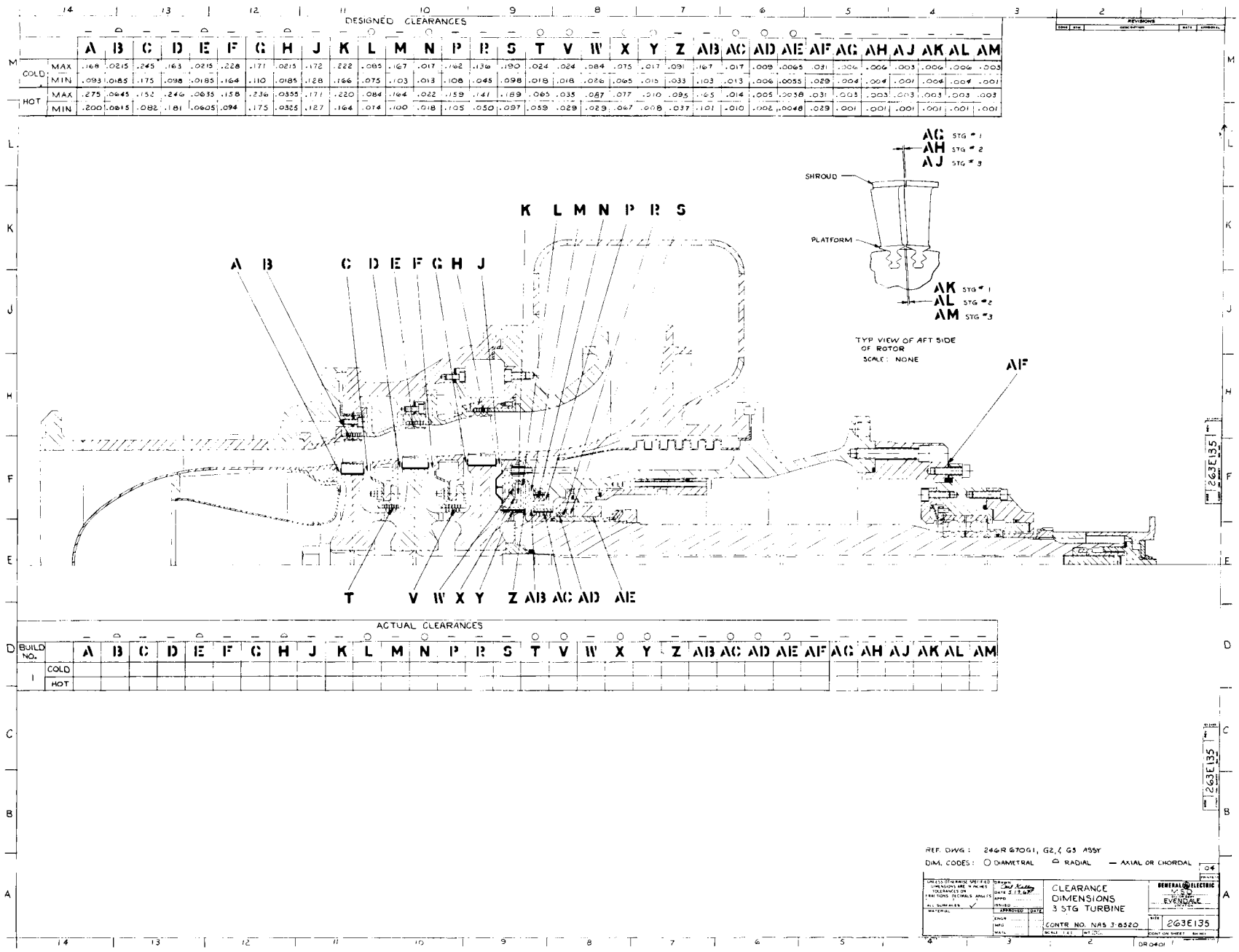

		A	B	C	D	E	F	G	H	J	K	L	M	N	P	R	S	T	V	W	X	Y	Z	AB	AC	AD	AE	AF	AG	AH	AJ	AK	AL	AM
COLD	MAX	.168	.0215	.245	.163	.0215	.228	.171	.0213	.172	.222	.085	.167	.017	.162	.136	.190	.024	.024	.084	.075	.017	.091	.167	.017	.009	.0065	.031	.006	.006	.003	.006	.006	.003
	MIN	.093	.0185	.175	.098	.0185	.164	.110	.0185	.128	.166	.075	.103	.013	.108	.045	.098	.018	.018	.026	.065	.015	.033	.103	.013	.006	.0055	.029	.004	.004	.001	.004	.004	.001
HOT	MAX	.275	.0645	.152	.246	.0635	.158	.236	.0355	.171	.220	.084	.164	.022	.159	.141	.189	.065	.035	.087	.077	.010	.095	.165	.014	.005	.0038	.031	.003	.003	.003	.003	.003	.003
	MIN	.200	.0615	.082	.181	.0605	.094	.175	.0325	.127	.164	.074	.100	.018	.105	.050	.097	.059	.029	.029	.047	.008	.037	.101	.010	.002	.0048	.029	.001	.001	.001	.001	.001	.001

BUILD NO.		A	B	C	D	E	F	G	H	J	K	L	M	N	P	R	S	T	V	W	X	Y	Z	AB	AC	AD	AE	AF	AG	AH	AJ	AK	AL	AM
1	COLD																																	
	HOT																																	

Figure 39b. Turbine Clearance Drawing.

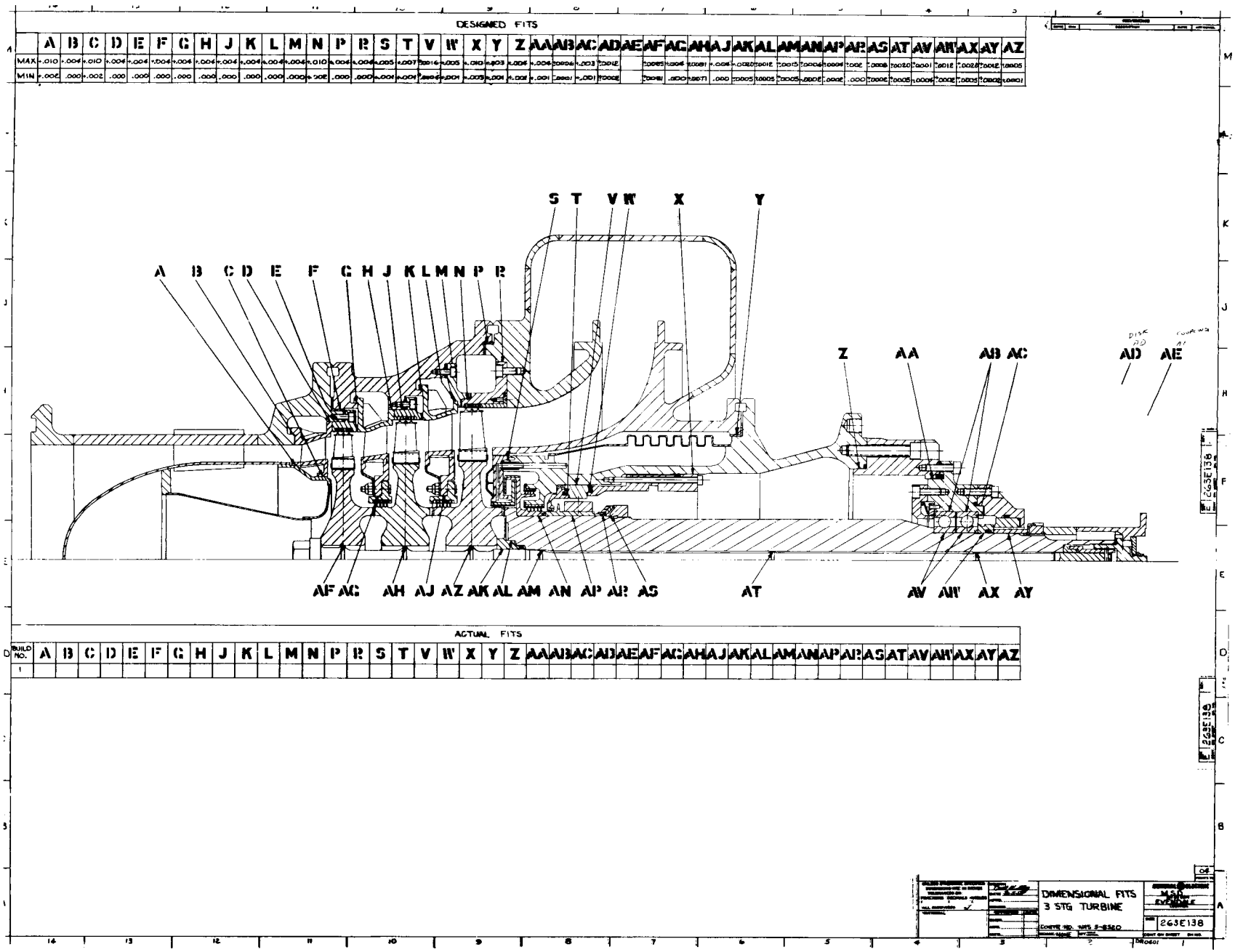

Figure 39c. Turbine Fits Drawing.

ASSUMPTIONS FOR CALCUALTION OF THREE-STAGE TURBINE CRITICAL SPEEDS USING "VAST" COMPUTER PROGRAM

1. The curvic coupling joints were treated as continuous structure with 25 percent reduced area moments of inertia.

2. The pivoted pad bearing spring constant is 500,000 #/in.

3. The condenser was assumed to be effective as a 6000# mass with a zero transverse moment of inertia acting at the scroll axial location.

4. The non-rotating structure consisted of the potassium turbine stator and bearing housing assembly attached to 12 feet of 8" ducting at the forward end and attached to the glove box dished head at the aft end.

5. The ultimate connections to ground were made at the three following locations: 1) fwd. end of the 8" duct (12 feet from turbine), 2) 2 feet forward of the turbine simulating a bellows connection between the 8" duct and the glove box, and 3) at the dished head connection to the glove box. (See Figure 43.)

6. The ball bearing (aft end of rotor) was assumed to have a spring constant of 1,000,000 lb/in.

7. The turbine rotor did not include the coupling between the K-turbine and the drive-train.

8. Torsional vibration was not analyzed.

9. The tie bolt was considered as being integral with the shaft.

10. Bolted connections were considered as continuous structure.

Figure 41.

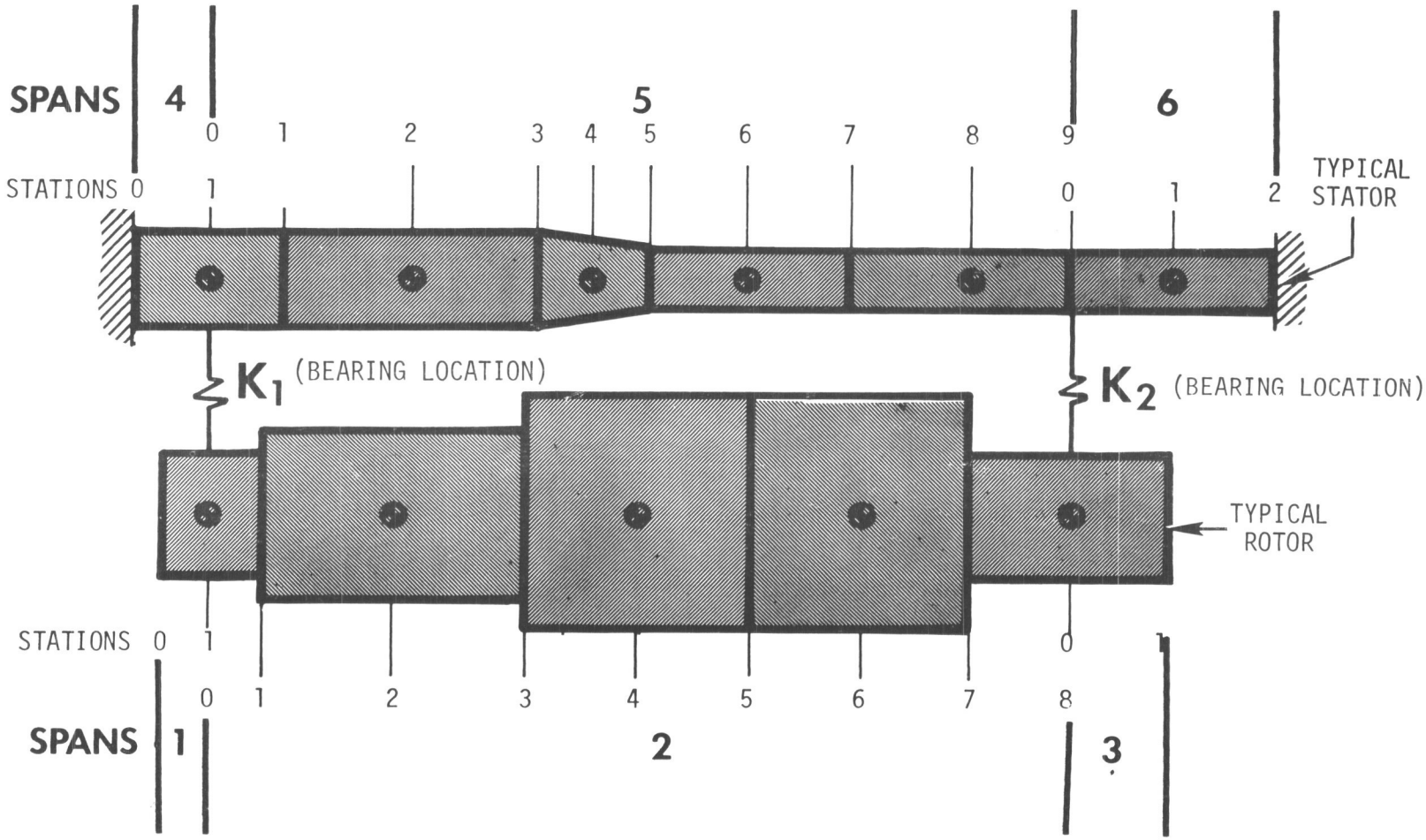

Figure 42. Computer Conceptual Model for System Critical Speed Analysis.

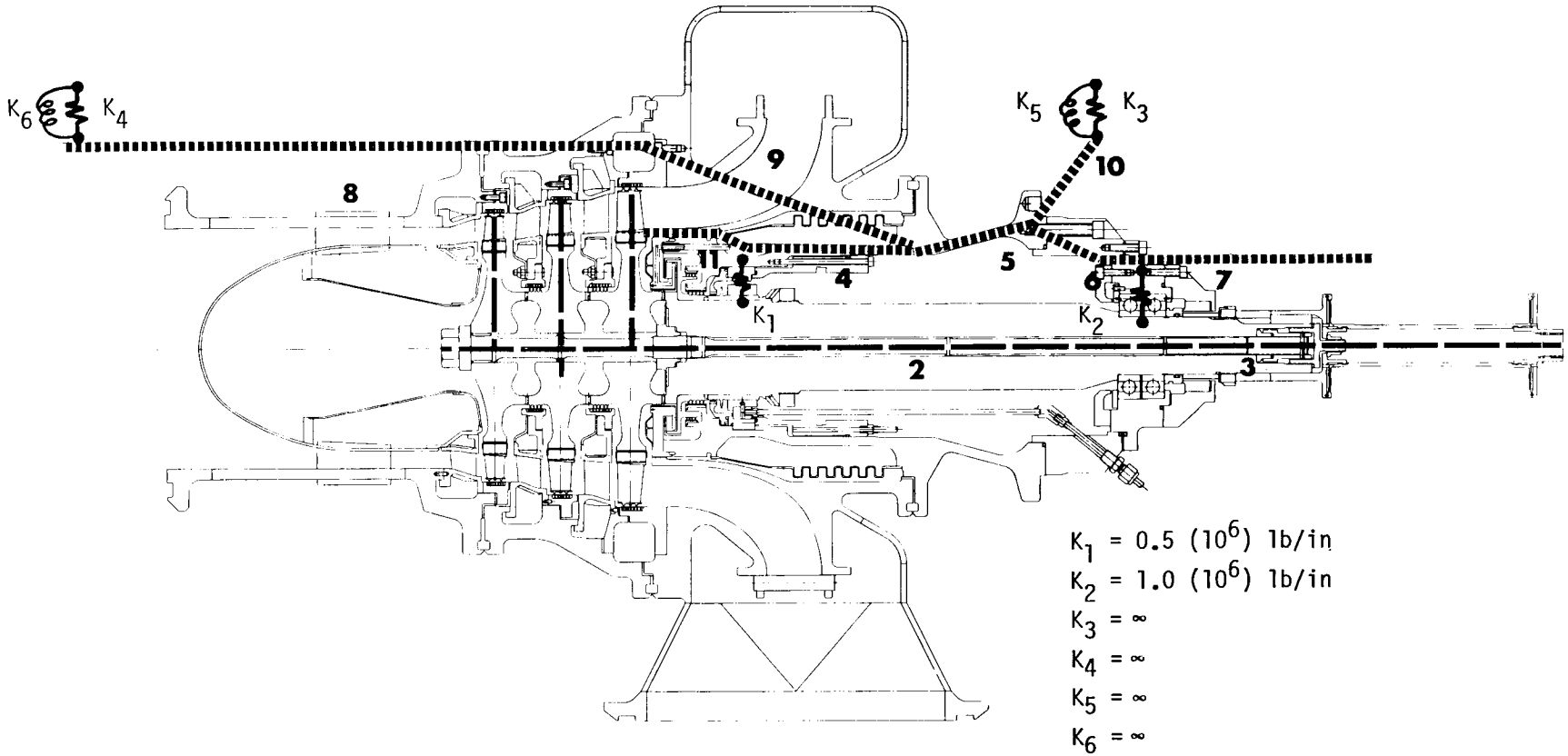

Figure 43. Three-Stage Turbine Critical Speed Model.

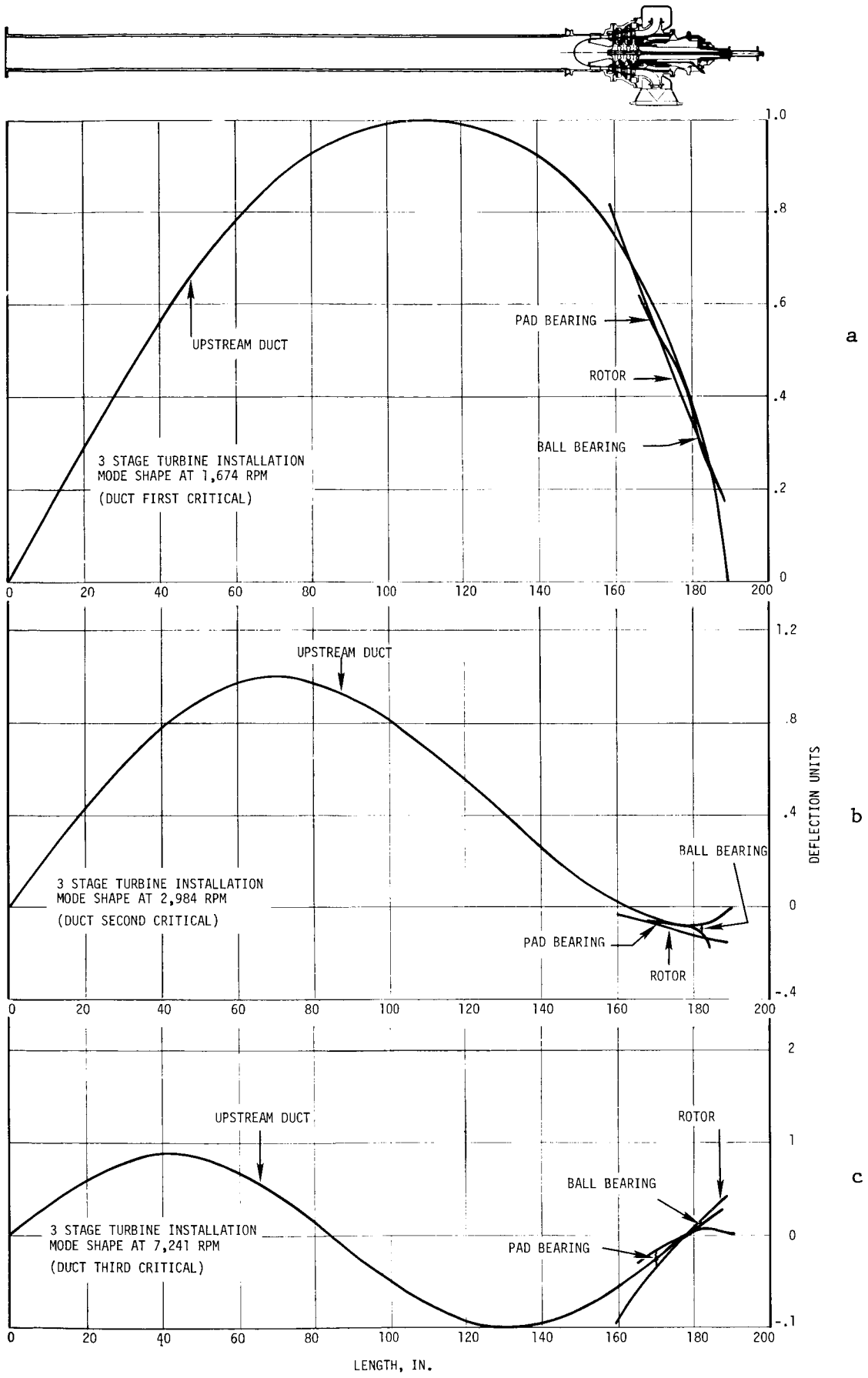

Figure 44a. Turbine Critical Speeds.

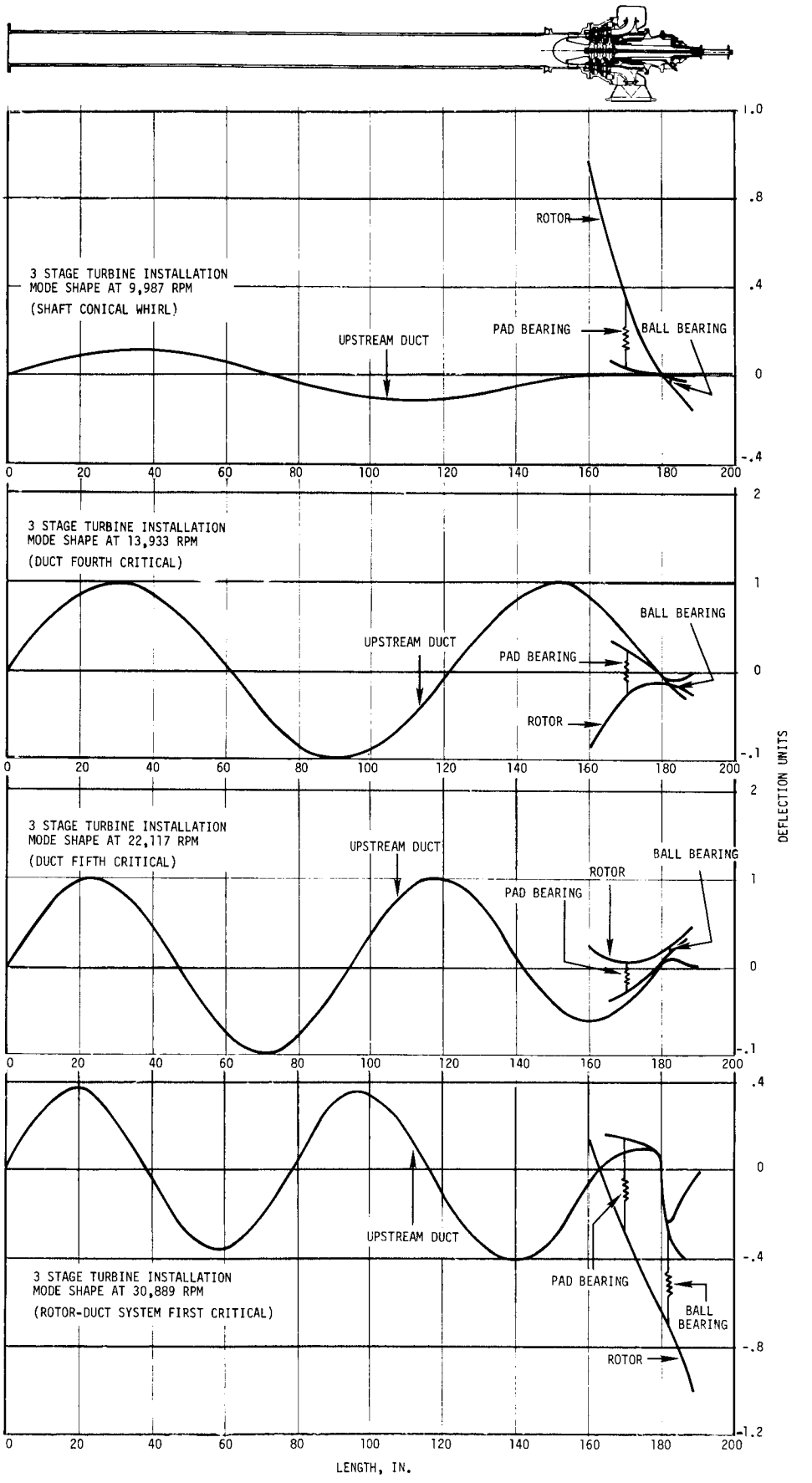

Figure 44b. Turbine Critical Speeds.

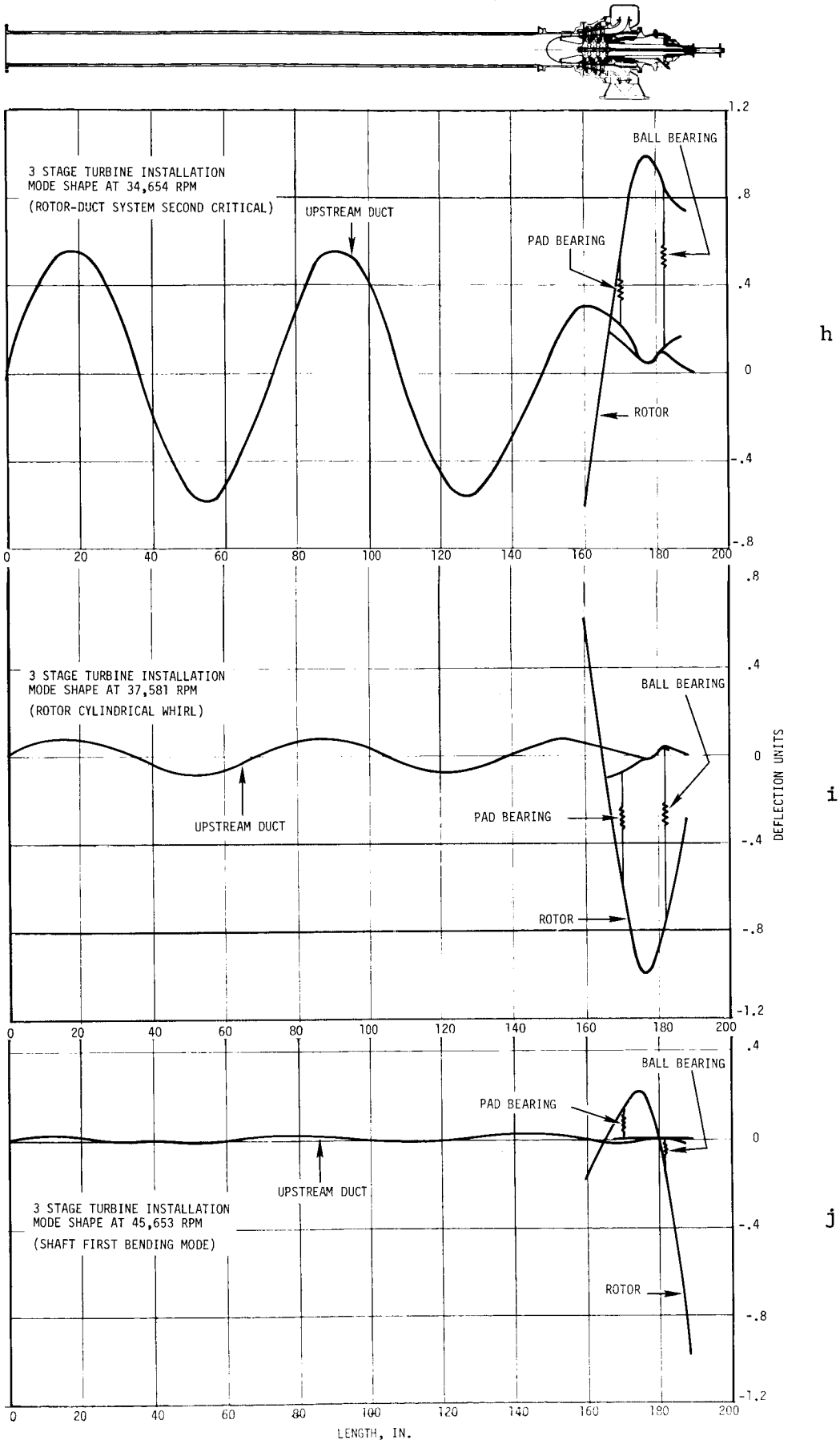

Figure 44c. Turbine Critical Speeds.

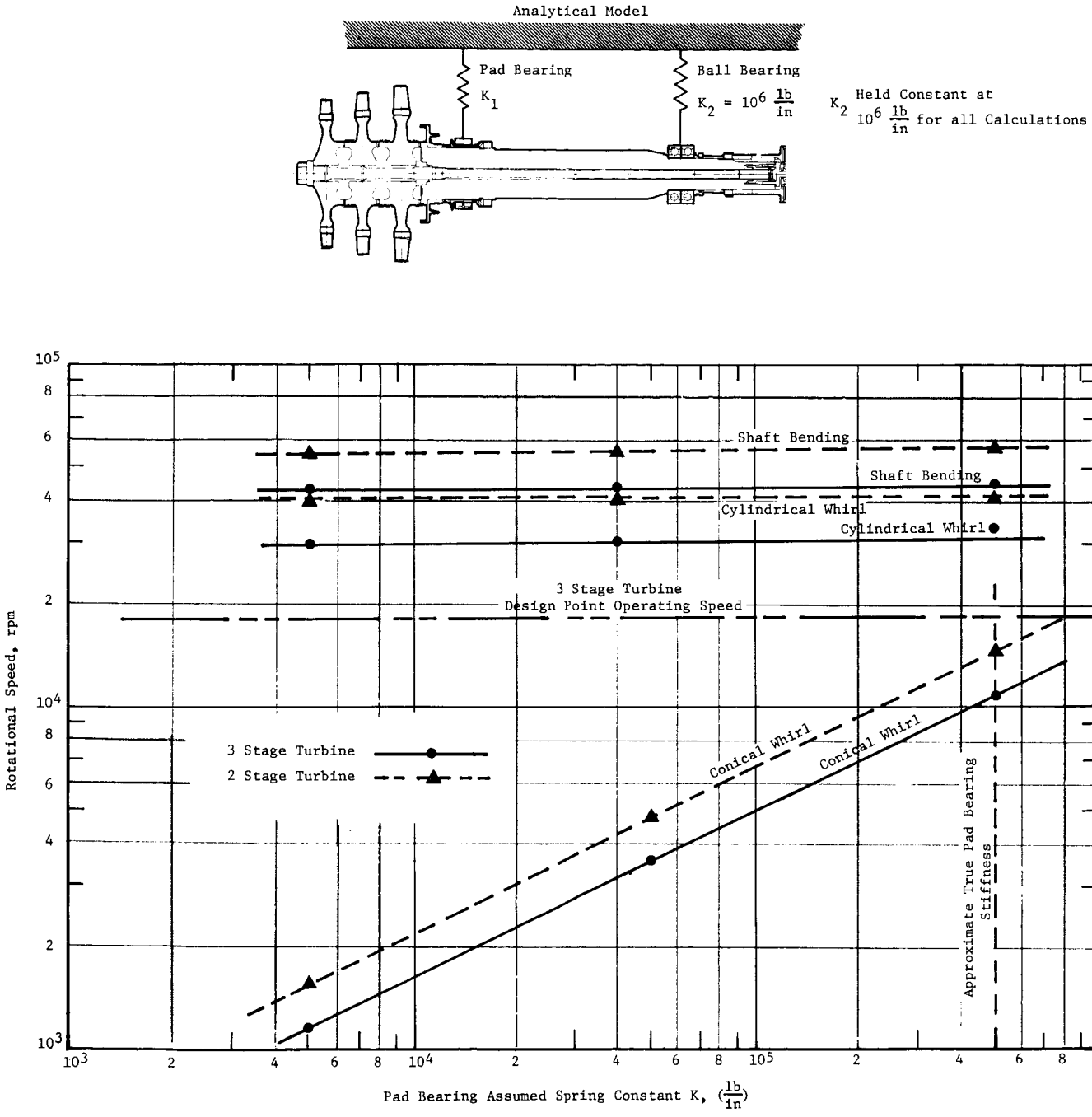

Figure 45. Comparison of Two-Stage and Three-Stage Turbine Rigid Body and Shaft Bending Critical Speeds as a Function of Stiffness of Pivoted Pad Bearing.

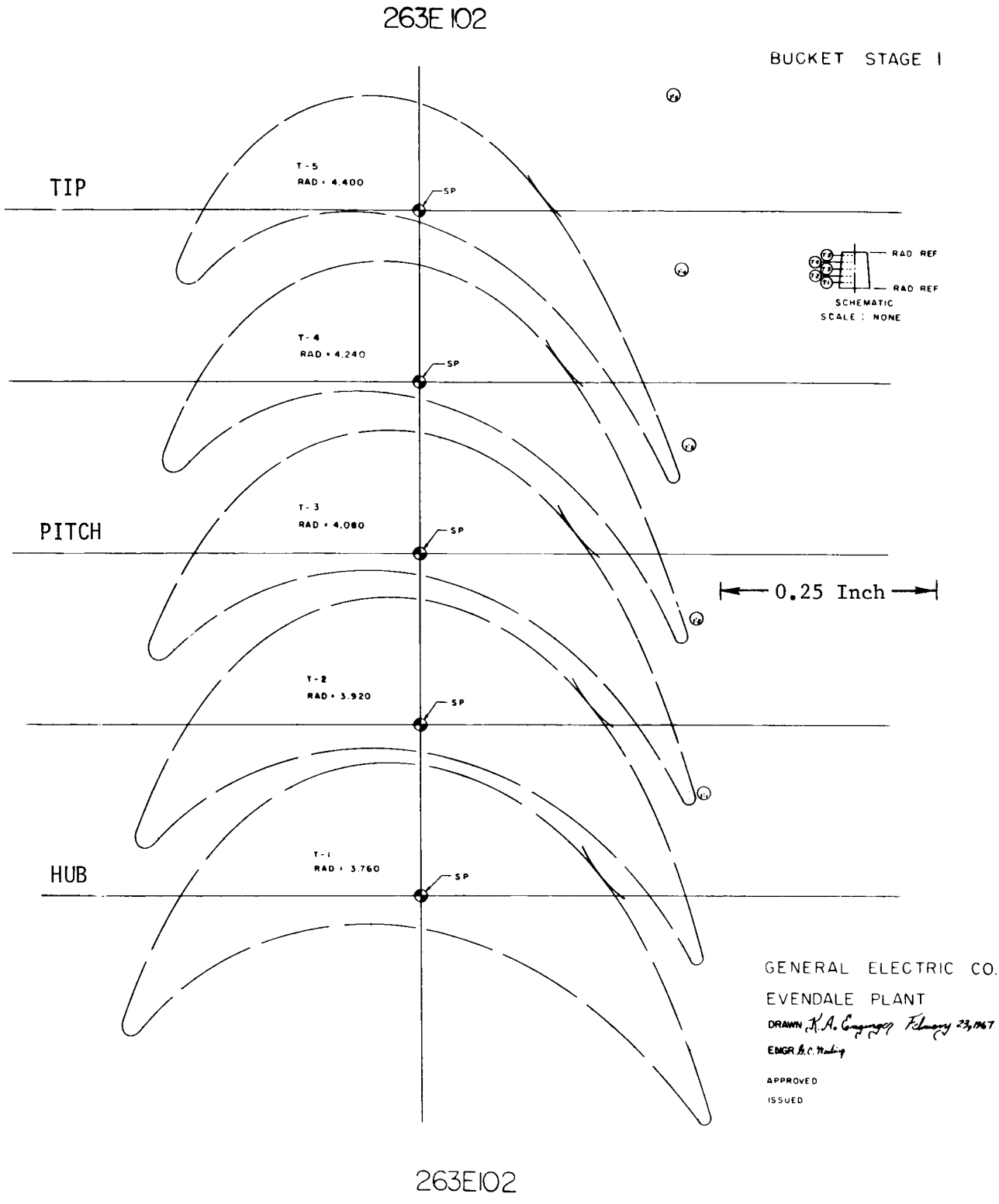

Figure 46. Stage 1 Rotor Blade Contour. (Glassine)

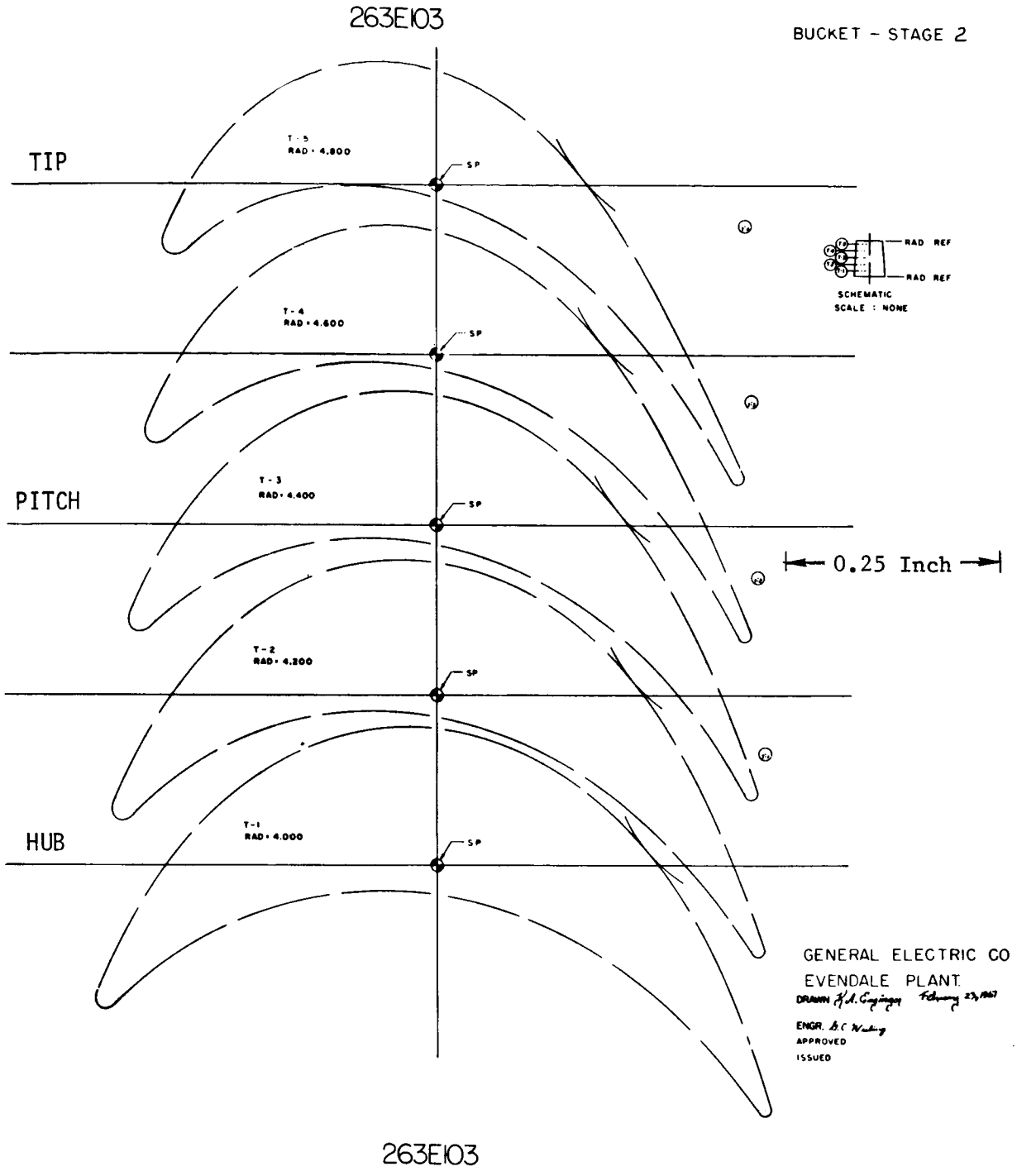

Figure 47. Stage 2 Rotor Blade Contour. (Glassine)

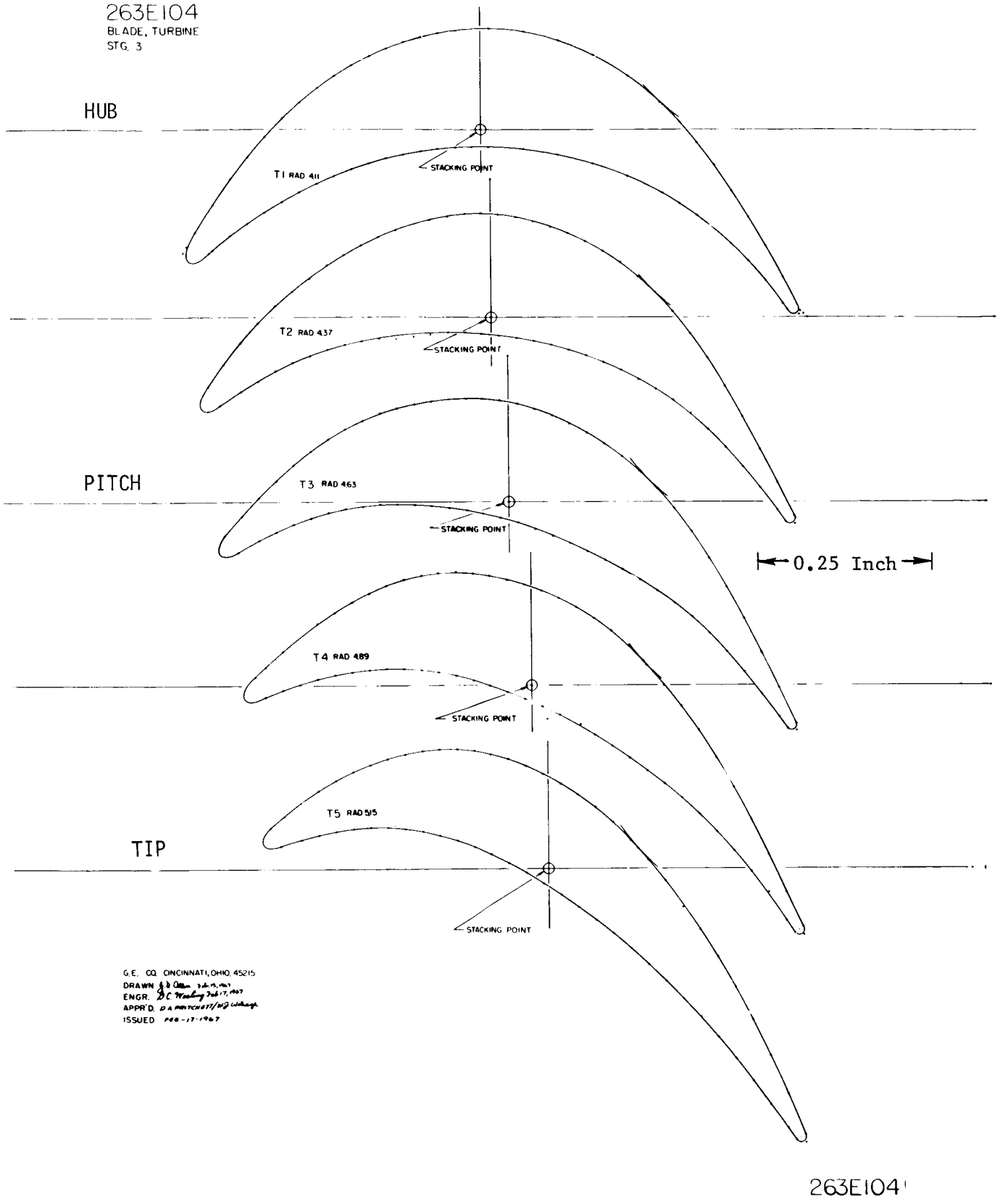

Figure 48. Stage 3 Rotor Blade Contour. (Glassine)

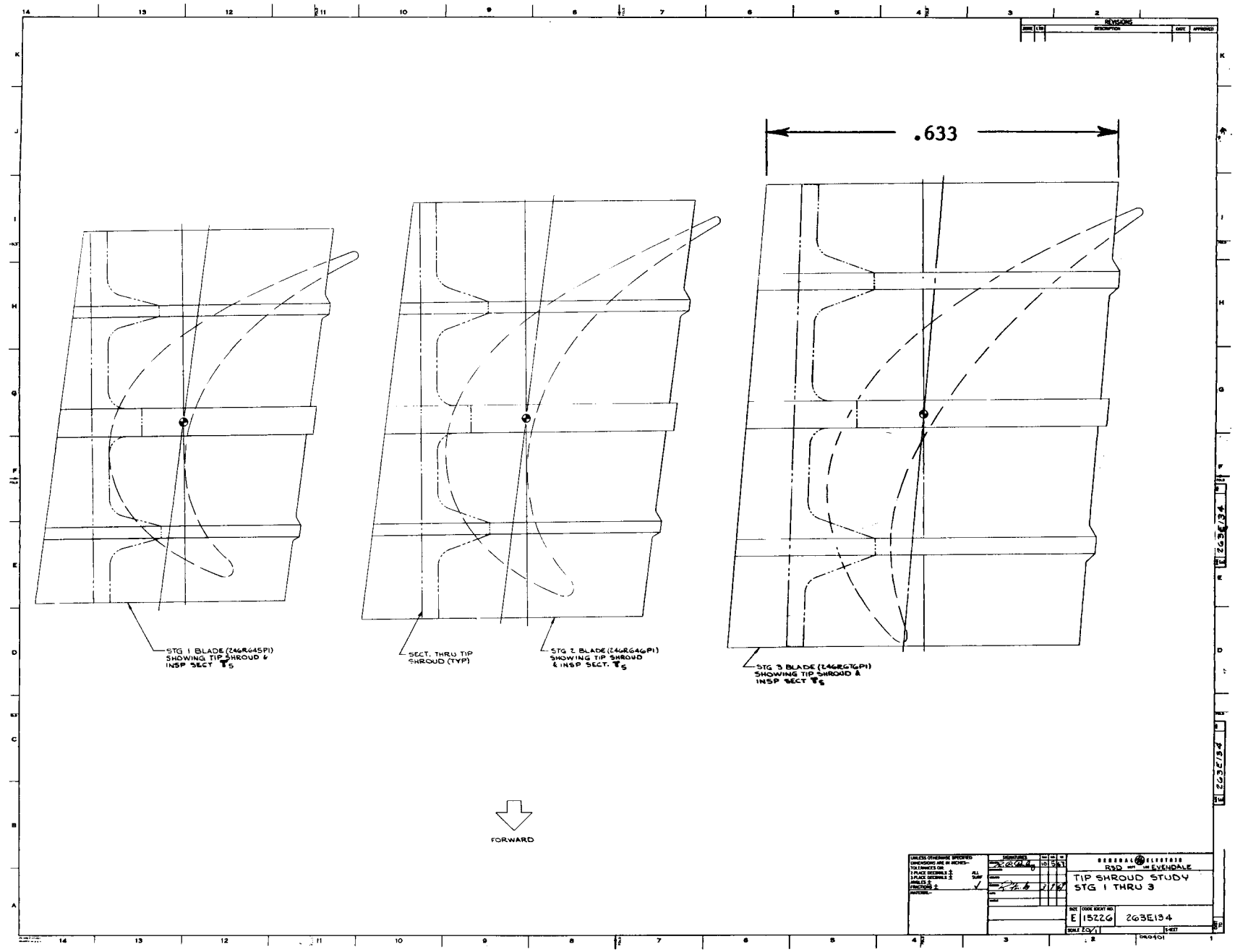

Figure 49. Superposition of Blade Shrouds on Airfoil True Tip Sections.

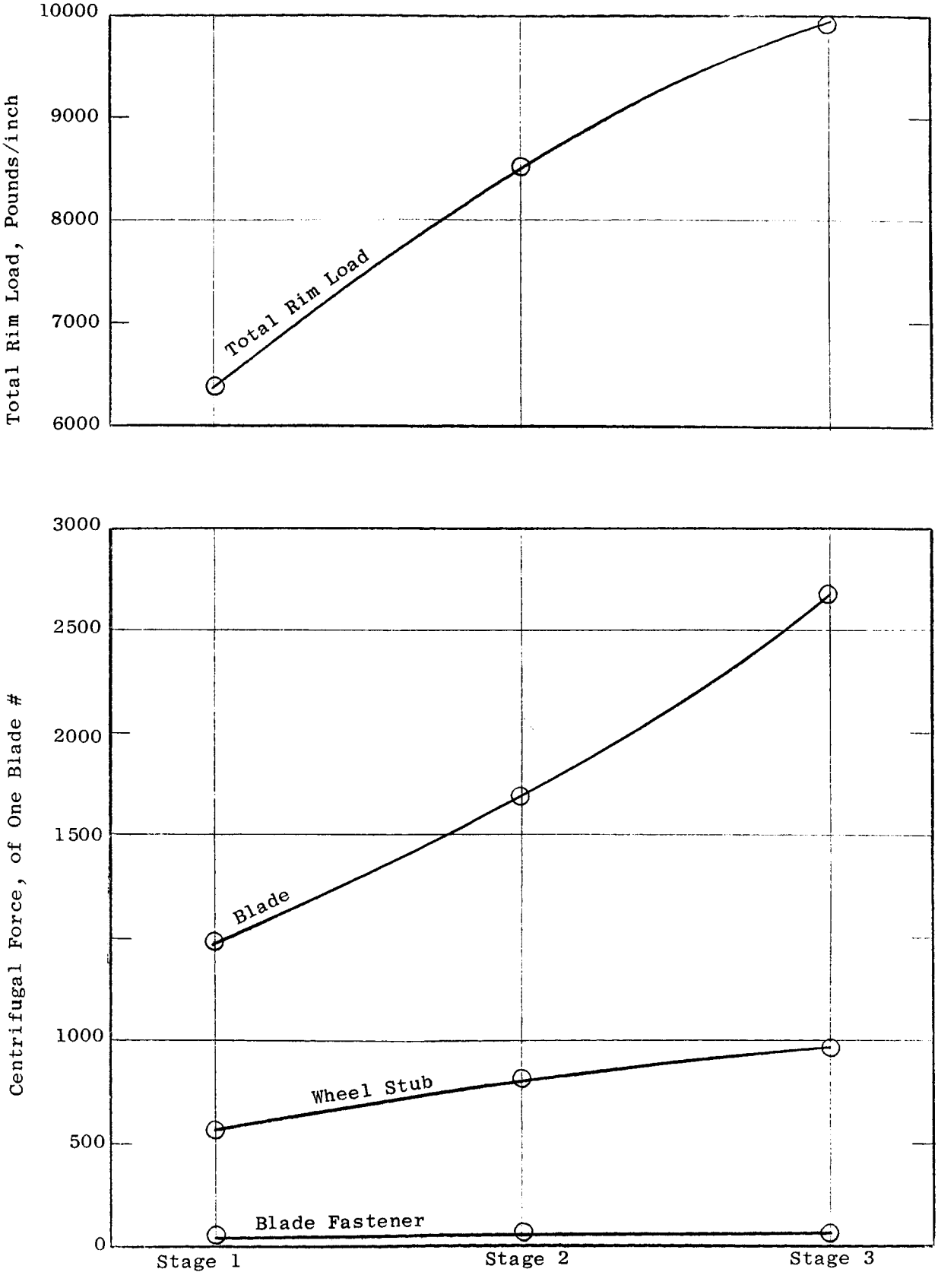

Figure 50a. Centrifugal Loading of Blades and Dovetail Sections for Three Stage Turbine. (Phase I, Tip-Shrouded Design)

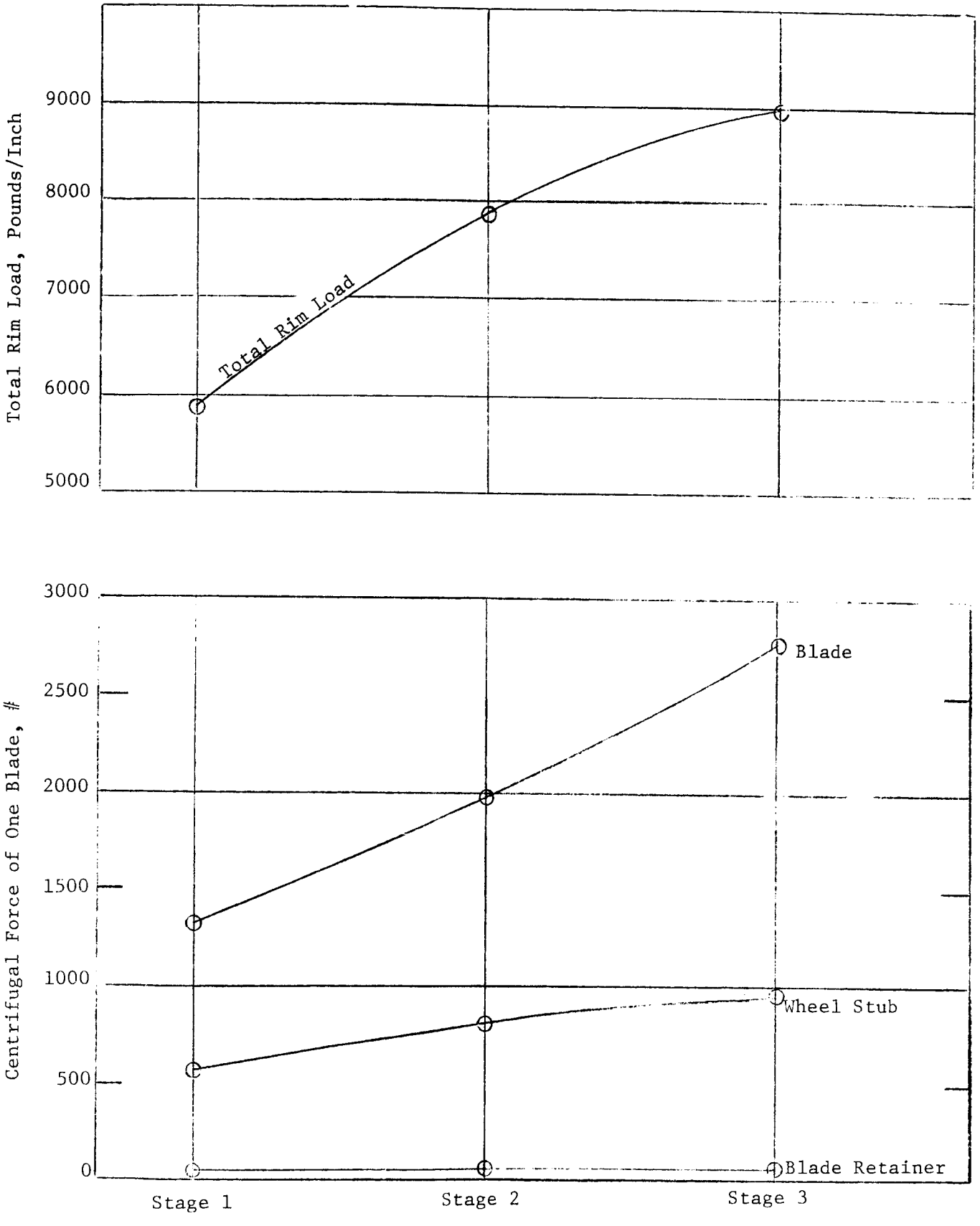

Figure 50b. Centrifugal Loading of Blades and Dovetail Sections for Three Stage Turbine, (Phase II, Non Tip-Shrouded Design)

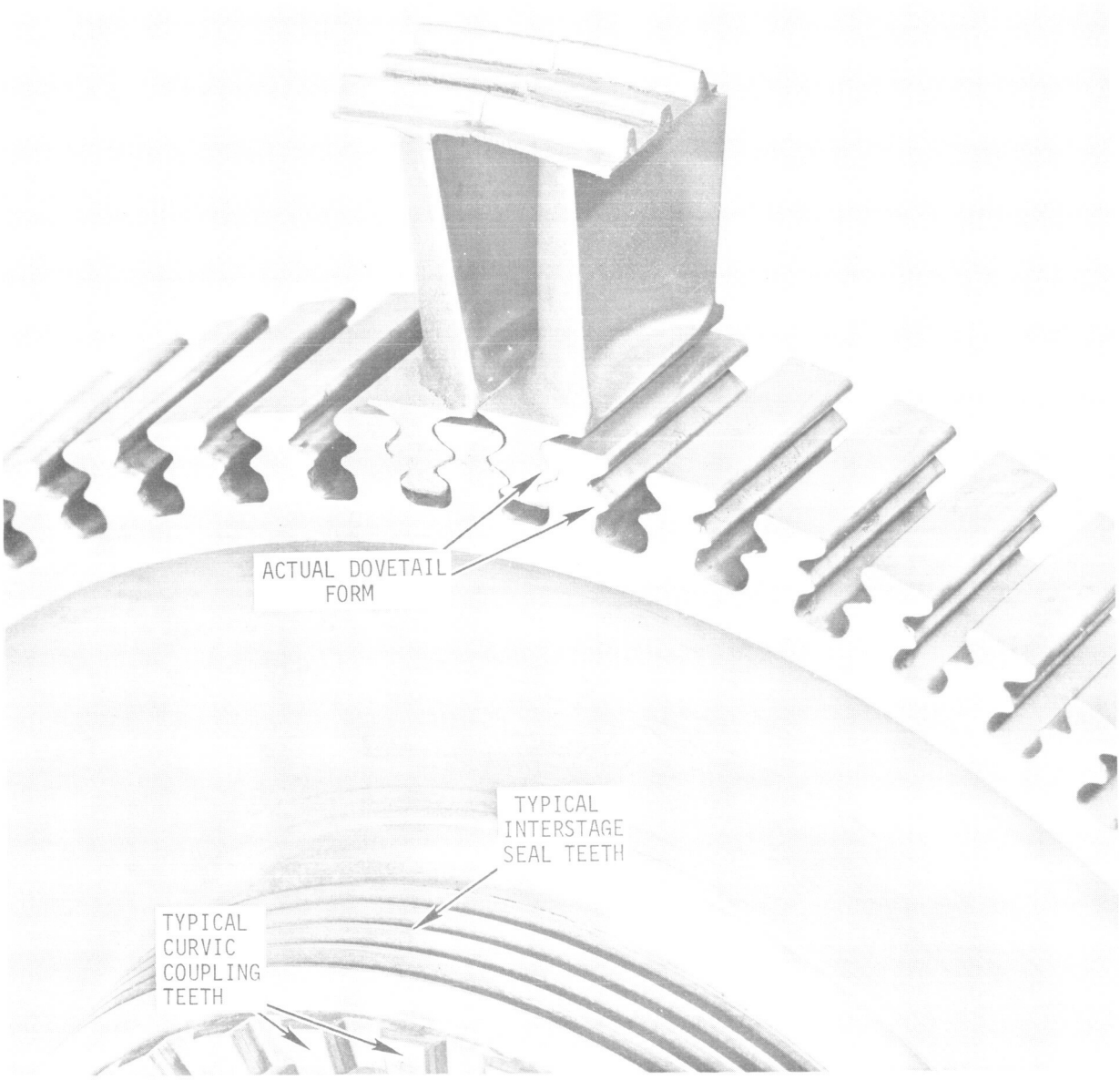

Figure 51. Mock-Up of Shrouded Rotor Blade. (C66111107)

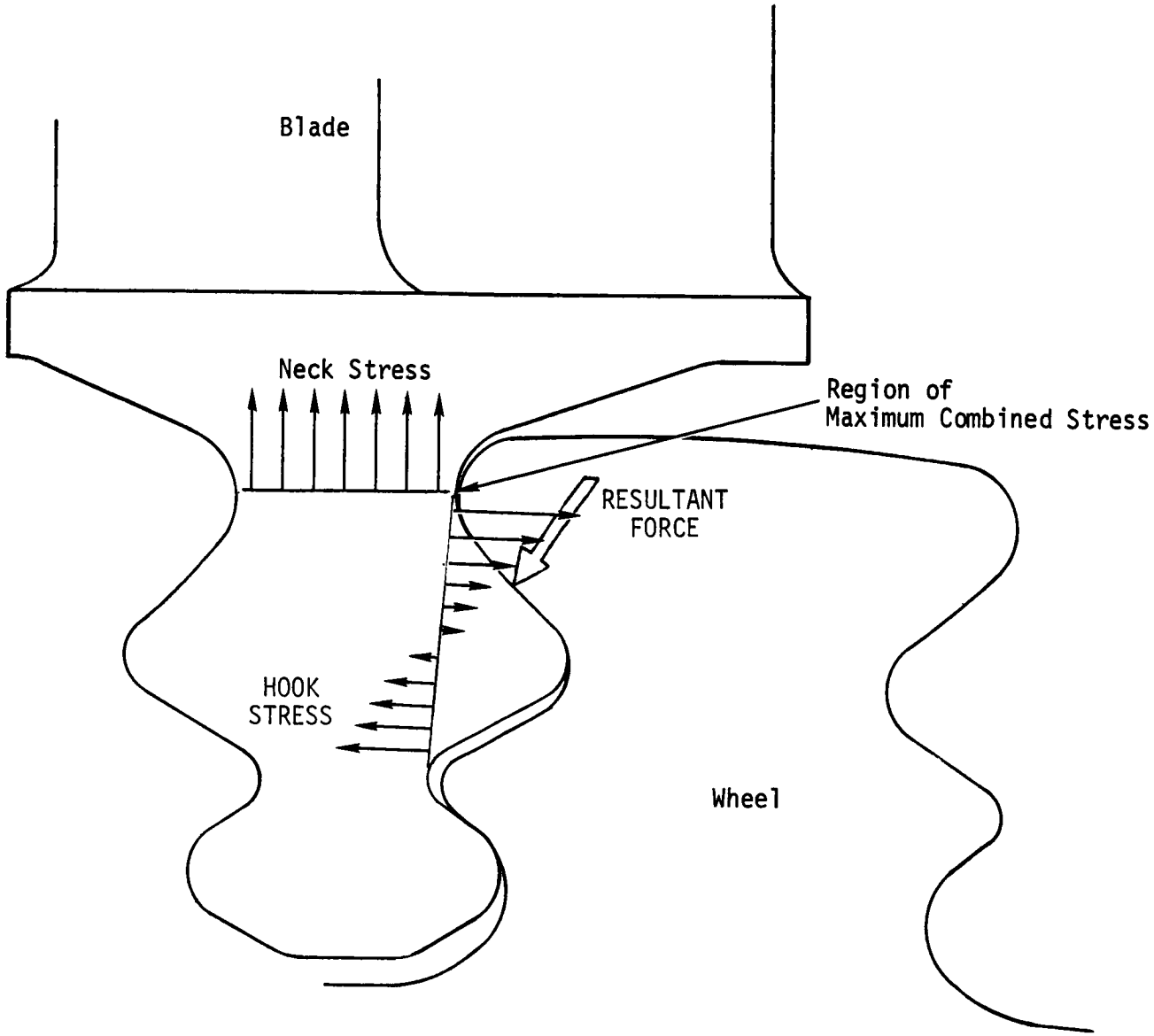

Figure 52. Typical Dovetail Stress Distribution.

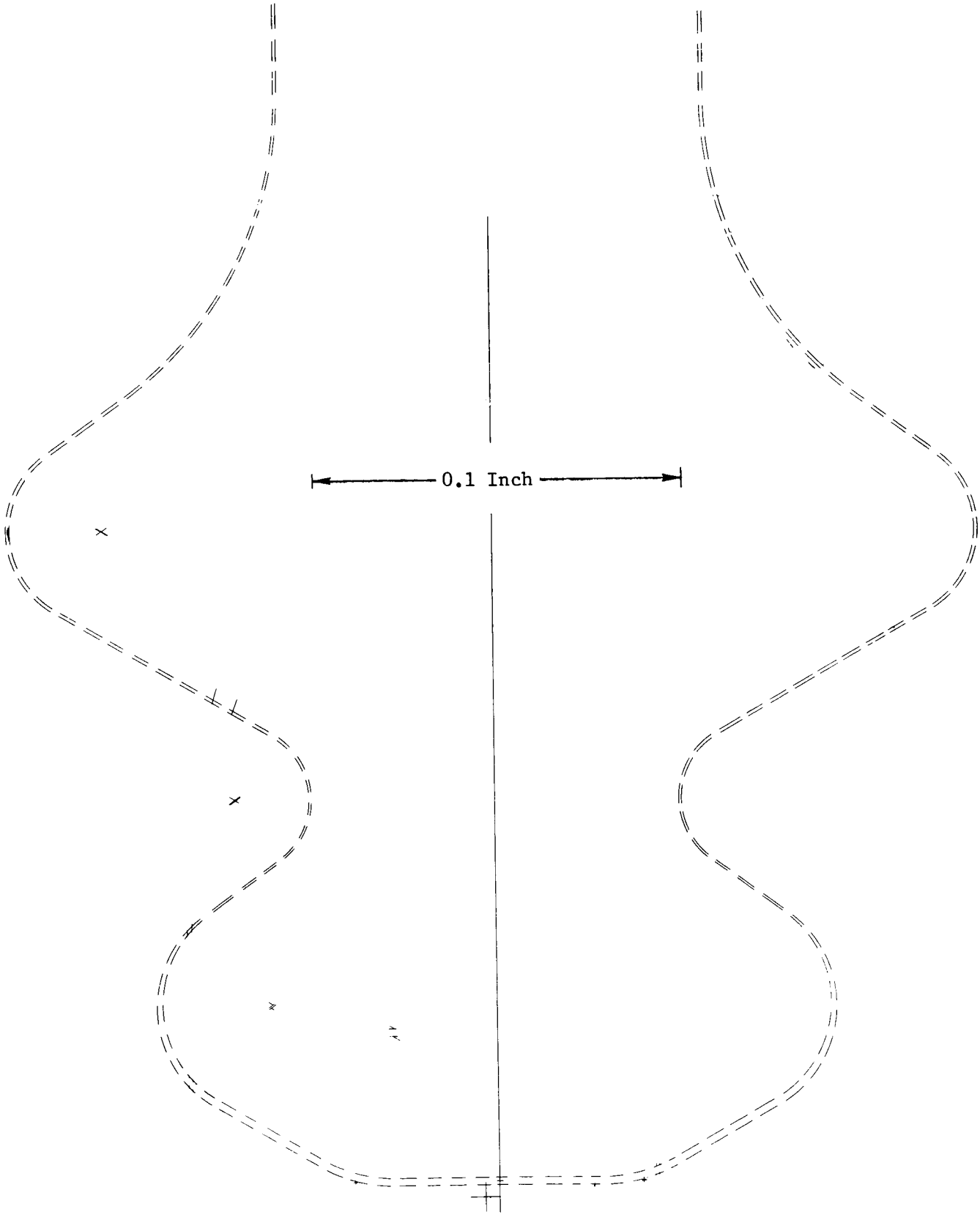

Figure 53. Blade Dovetail Form. (Glassine)- 646C570

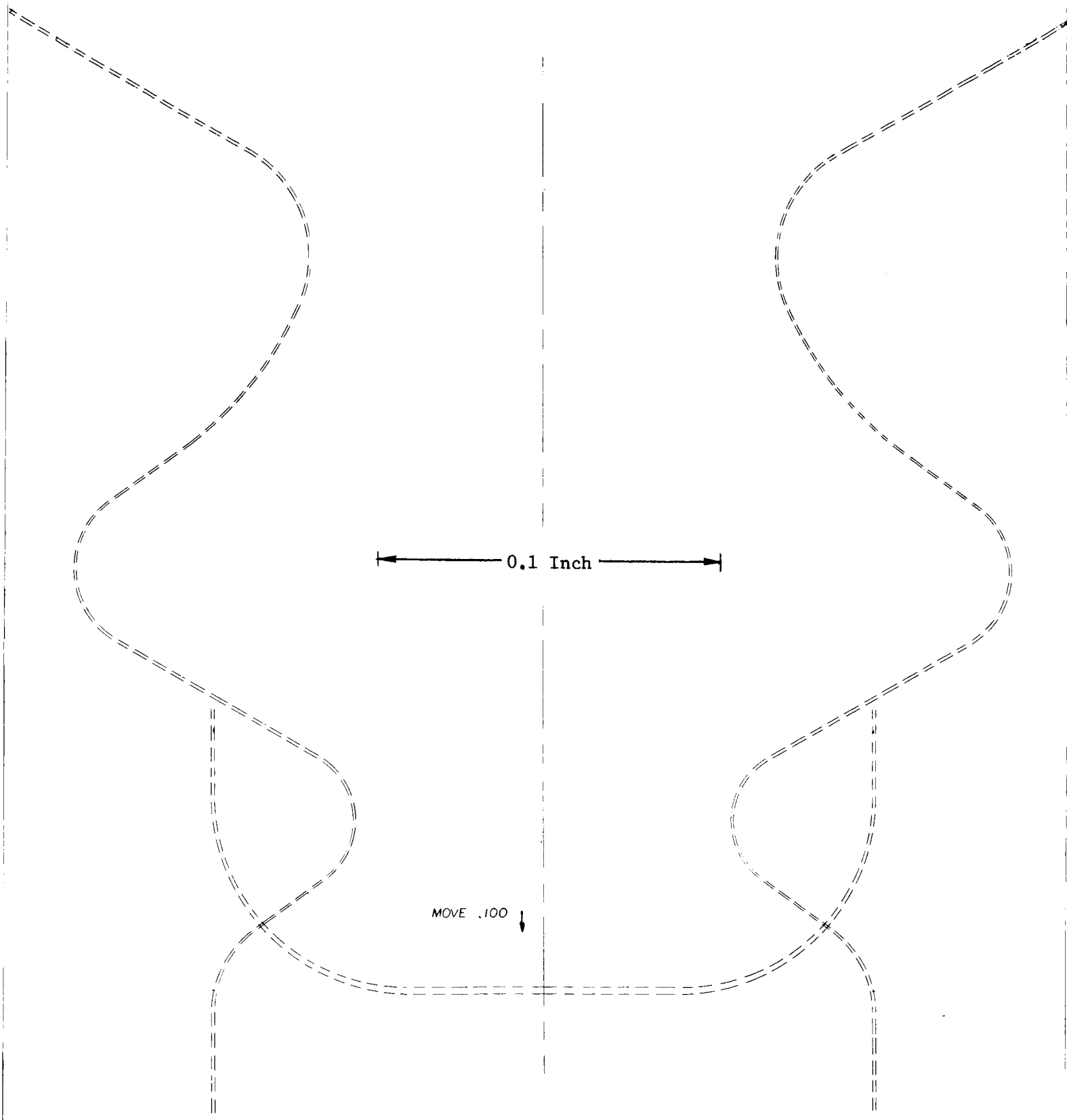

Figure 54. Wheel Slot Dovetail. (Glassine)- 299C198

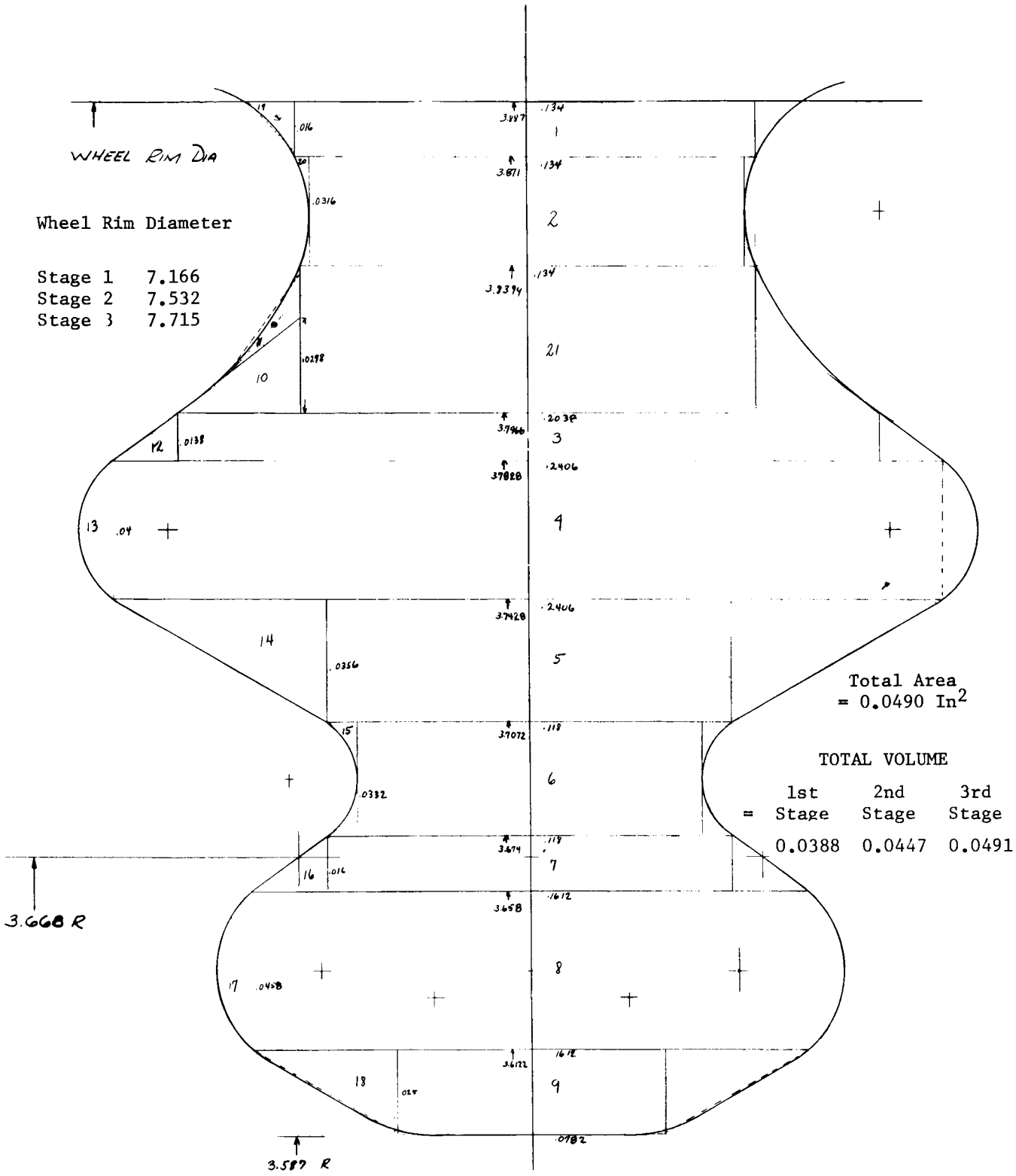

Figure 55. Dovetail Blade Weight Calculation. (941D151)

ANALYSIS REFERENCE DRAWINGS

Stage 1	263E884
Stage 2	263E885
Stage 3	263E116

	1st Stage	2nd Stage	3rd Stage
Total Area (In^2)	0.0709	0.0741	0.0964
Total Volume (In^3)	0.0561	0.0676	0.0968

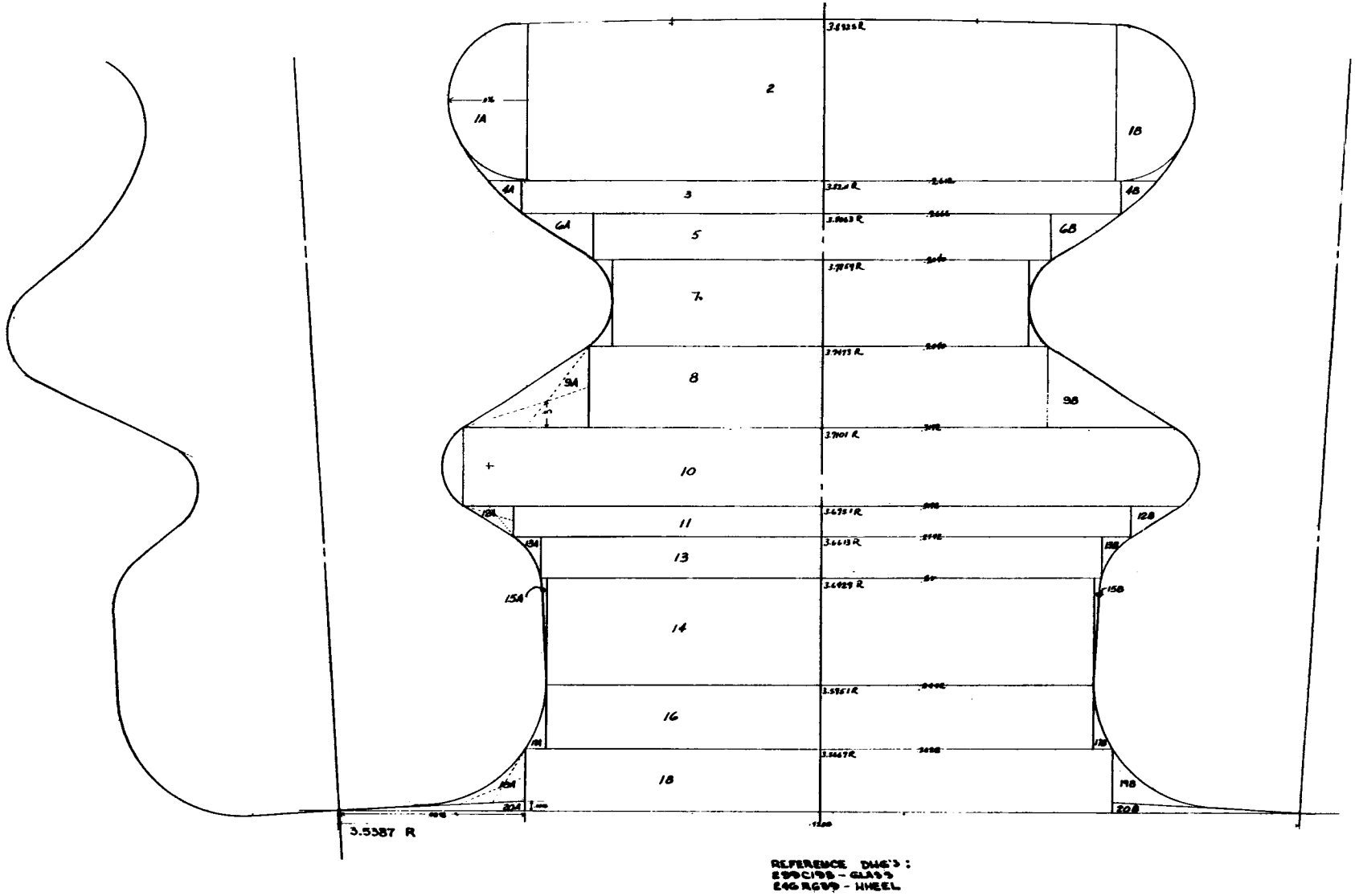

Figure 56. Typical Wheel Dovetail Weight Calculation. (Shown for Stage 3)

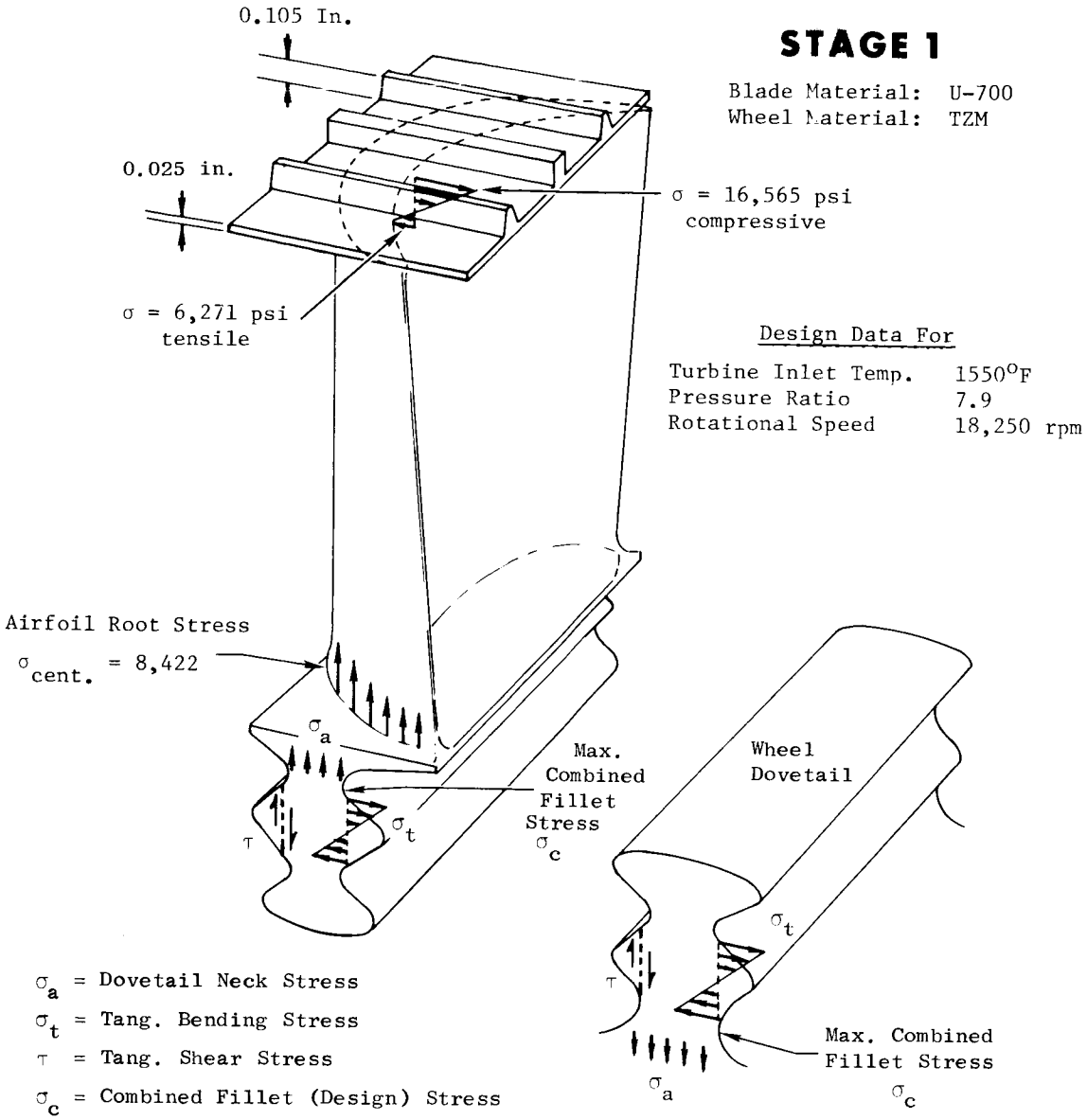

Blade Temp. 1445°F
Blade Life 32,690 hrs.

Wheel Temp. 1445°F
Wheel Life ∞ hrs.

BLADE DOVETAIL

Stress (psi)	Top Tang.	Bottom Tang.
σ_a	13,018	7,405
σ_t	17,278	12,791
τ	10,383	7,734
σ_c	25,373	17,197

WHEEL DOVETAIL

Stress (psi)	Top Tang.	Bottom Tang.
σ_a	19,232	17,236
σ_t	13,968	22,526
τ	6,018	6,369
σ_c	27,314	33,272

Figure 57. Stage 1 Blade and Dovetail Stress Summary. U700 Blades and TZM Wheel. (Phase I, Shrouded Design)

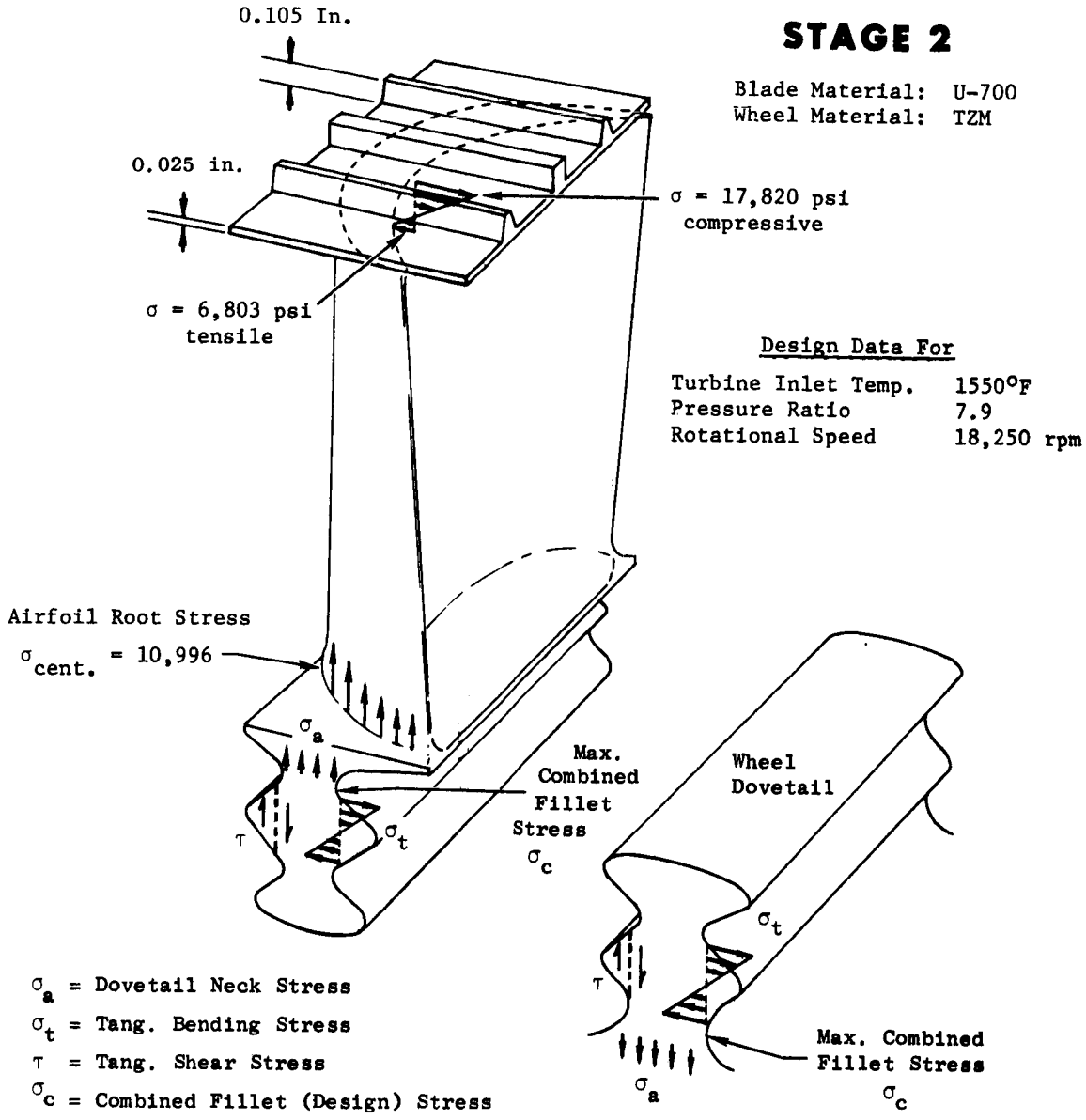

STAGE 2

Blade Material: U-700
Wheel Material: TZM

Design Data For

Turbine Inlet Temp.	1550°F
Pressure Ratio	7.9
Rotational Speed	18,250 rpm

Blade Temp. 1335°F
Blade Life 180,000 hrs.

BLADE DOVETAIL

Stress (psi)	Top Tang.	Bottom Tang.
σ_a	17,023	9,599
σ_t	21,580	16,078
τ	12,968	9,721
σ_c	32,250	21,818

Wheel Temp. 1335°F
Wheel Life ∞ hrs.

WHEEL DOVETAIL

Stress (psi)	Top Tang.	Bottom Tang.
σ_a	17,502	18,452
σ_t	17,445	28,315
τ	7,516	8,006
σ_c	28,899	39,509

Figure 58. Stage 2 Blade and Dovetail Stress Summary. U700 Blades and TZM Wheel. (Phase I, Shrouded Design)

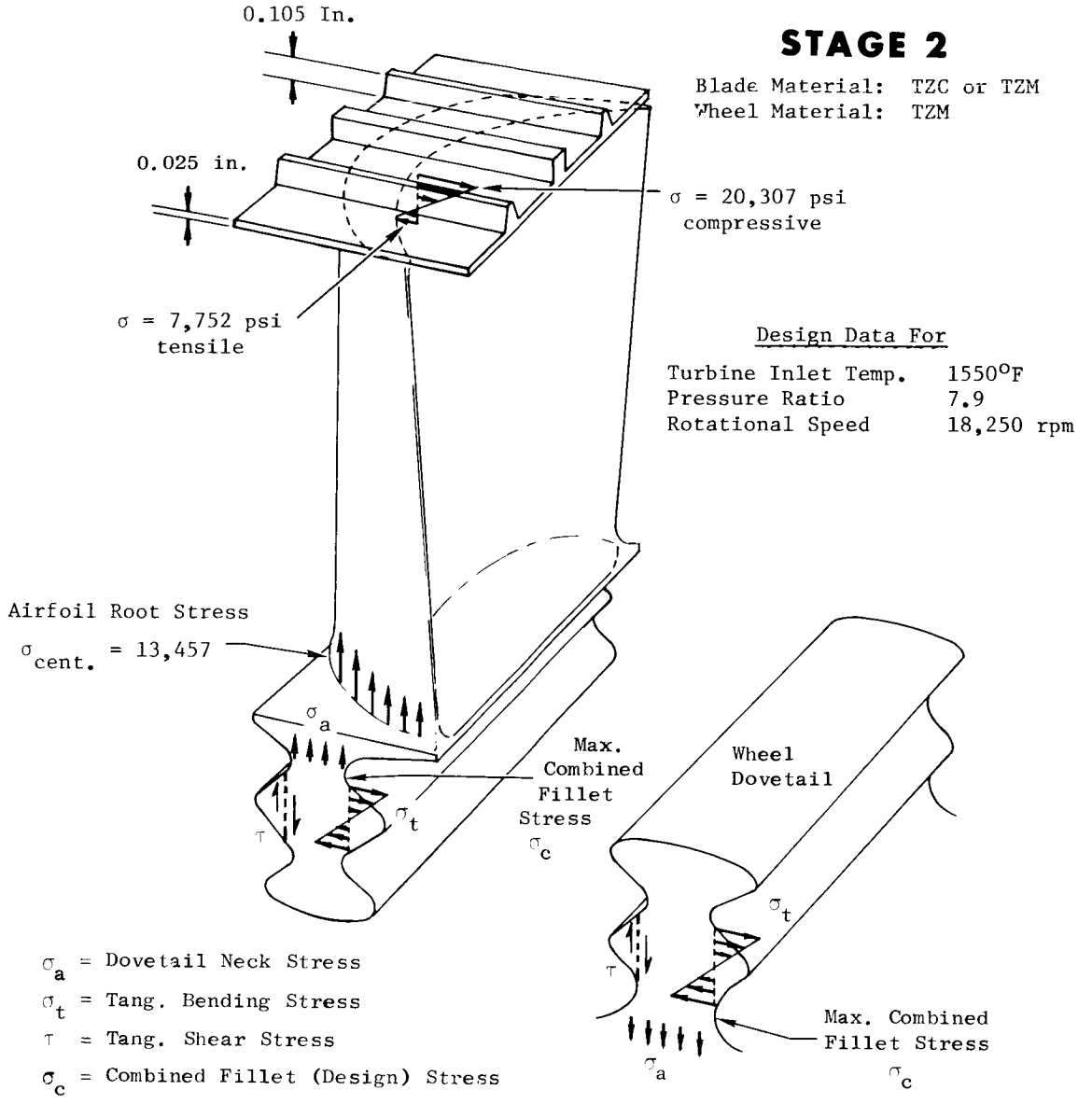

Blade Temp. 1335°F
Blade Life ∞ hrs.

BLADE DOVETAIL

Stress (psi)	Top Tang.	Bottom Tang.
σ_a	21,031	11,867
σ_t	26,867	20,013
τ	16,146	12,100
σ_c	40,031	27,102

Wheel Temp. 1335°F
Wheel Life ∞ hrs.

WHEEL DOVETAIL

Stress (psi)	Top Tang.	Bottom Tang.
σ_a	21,068	22,051
σ_t	21,720	35,245
τ	9,358	9,965
σ_c	35,423	48,533

Figure 59. Stage 2 Blade and Dovetail Stress Summary. TZC or TZM Blades and TZM Wheel. (Phase I, Shrouded Design)

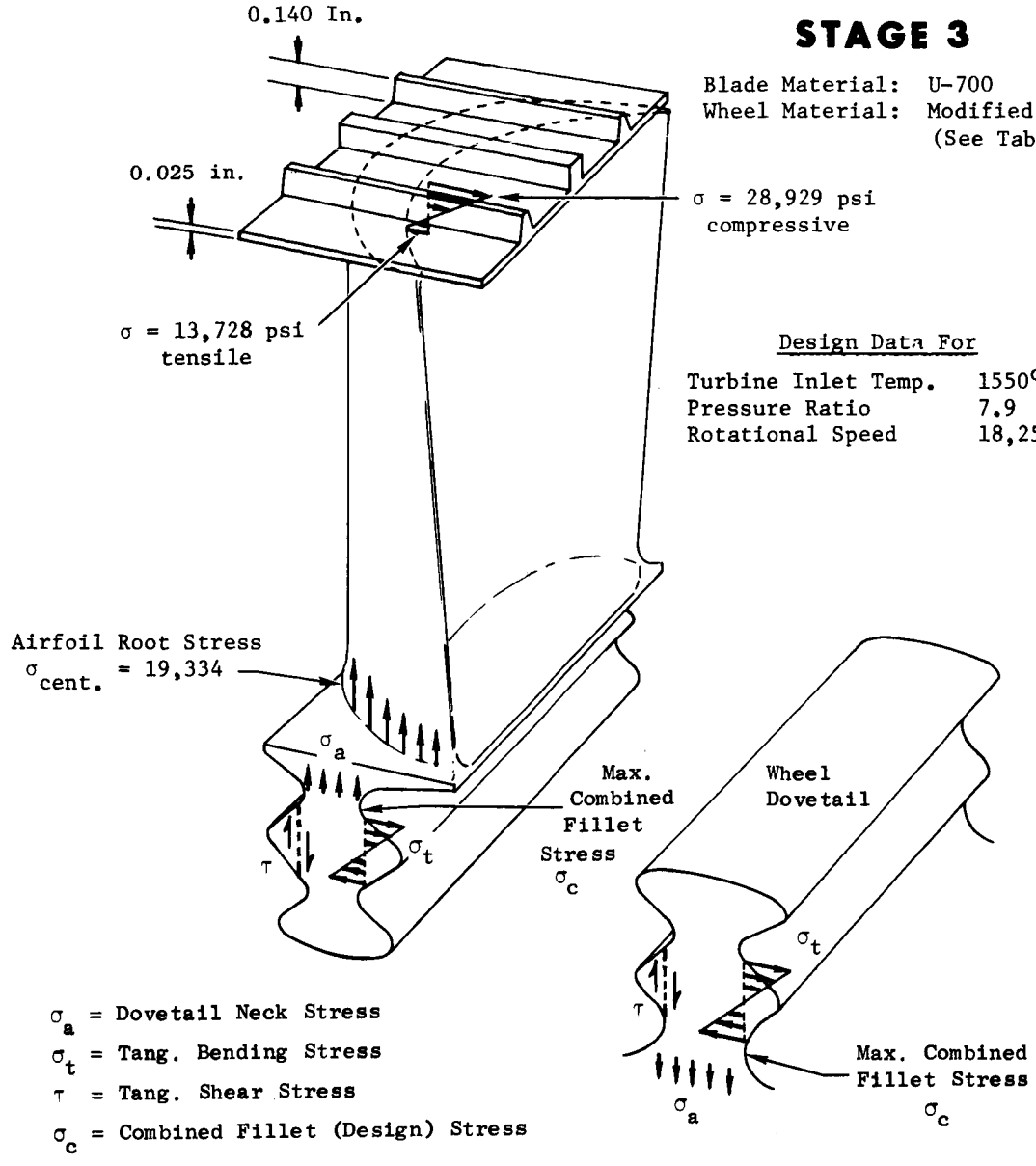

STAGE 3

Blade Material: U-700
Wheel Material: Modified Astroloy (See Table III)

Design Data For

Turbine Inlet Temp.	1550°F
Pressure Ratio	7.9
Rotational Speed	18,250 rpm

Blade Temp. 1230°F
Blade Life 250,000 hrs.

BLADE DOVETAIL

Stress (psi)	Top Tang.	Bottom Tang.
σ_a	22,794	12,704
σ_t	27,760	20,913
τ	16,681	12,645
σ_c	42,148	28,532

Wheel Temp. 1230°F
Wheel Life 150,000 hrs.

WHEEL DOVETAIL

Stress (psi)	Top Tang.	Bottom Tang.
σ_a	13,823	16,728
σ_t	22,441	36,829
τ	9,668	10,413
σ_c	30,749	46,423

Figure 60. Stage 3 Blade and Dovetail Stress Summary. U700 Blades and Modified Astroloy Wheel. (Phase I, Shrouded Design)

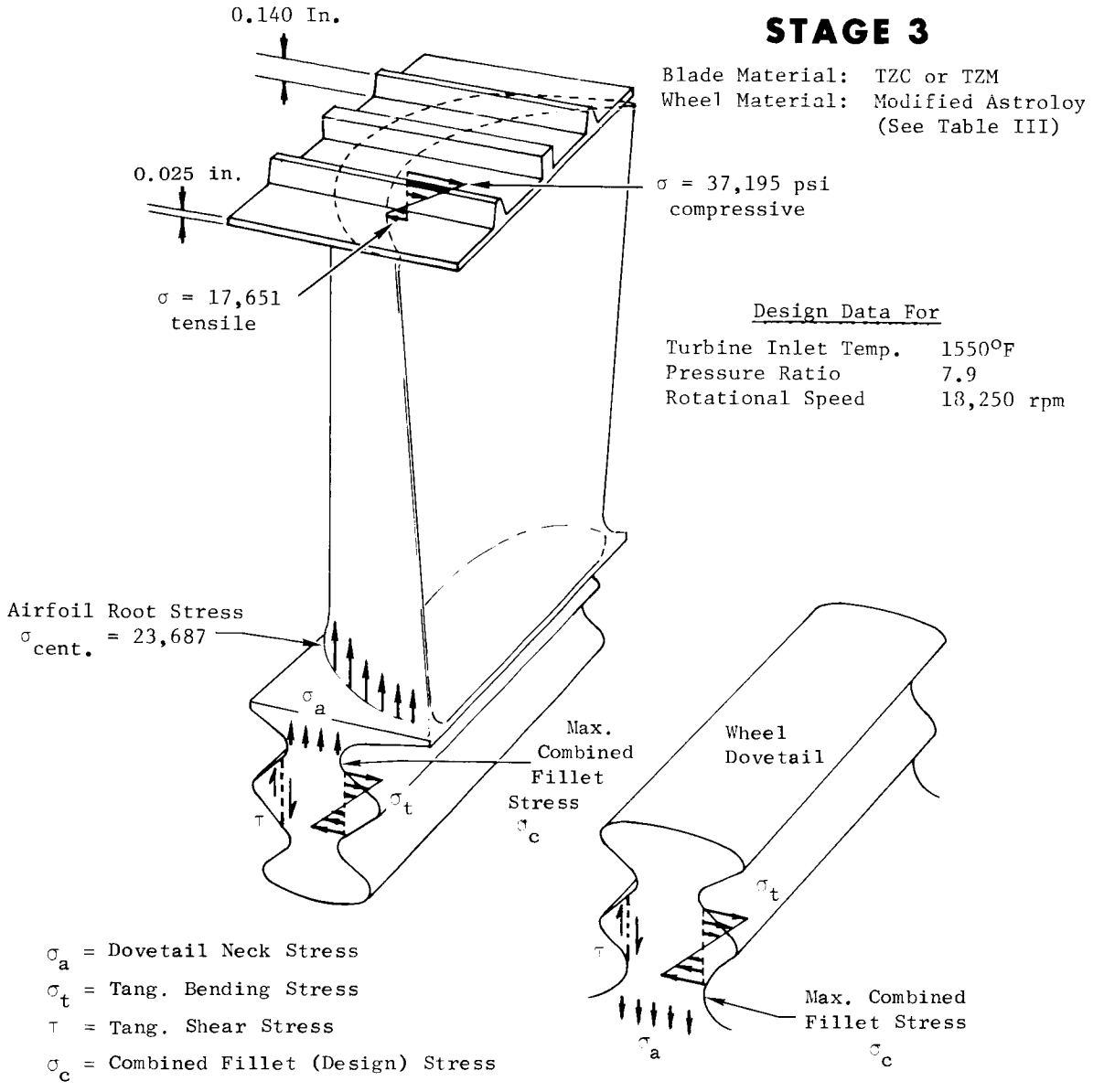

STAGE 3

Blade Material: TZC or TZM
Wheel Material: Modified Astroloy (See Table III)

Design Data For

Turbine Inlet Temp.	1550°F
Pressure Ratio	7.9
Rotational Speed	18,250 rpm

Blade Temp. 1230°F
Blade Life ∞ hrs.

BLADE DOVETAIL

Stress (psi)	Top Tang.	Bottom Tang.
σ_a	28,149	15,699
σ_t	34,499	25,987
τ	20,732	15,712
σ_c	52,248	35,393

Wheel Temp. 1230°F
Wheel Life 20,870 hrs.

WHEEL DOVETAIL

Stress (psi)	Top Tang.	Bottom Tang.
σ_a	16,654	20,060
σ_t	27,890	45,764
τ	12,016	12,940
σ_c	37,850	57,211

Figure 61. Stage 3 Blade and Dovetail Stress Summary. TZC or TZM Blades and Modified Astroloy Wheel. (Phase I, Shrouded Design)

STAGE 1

Blade Material: U-700
Wheel Material: TZM

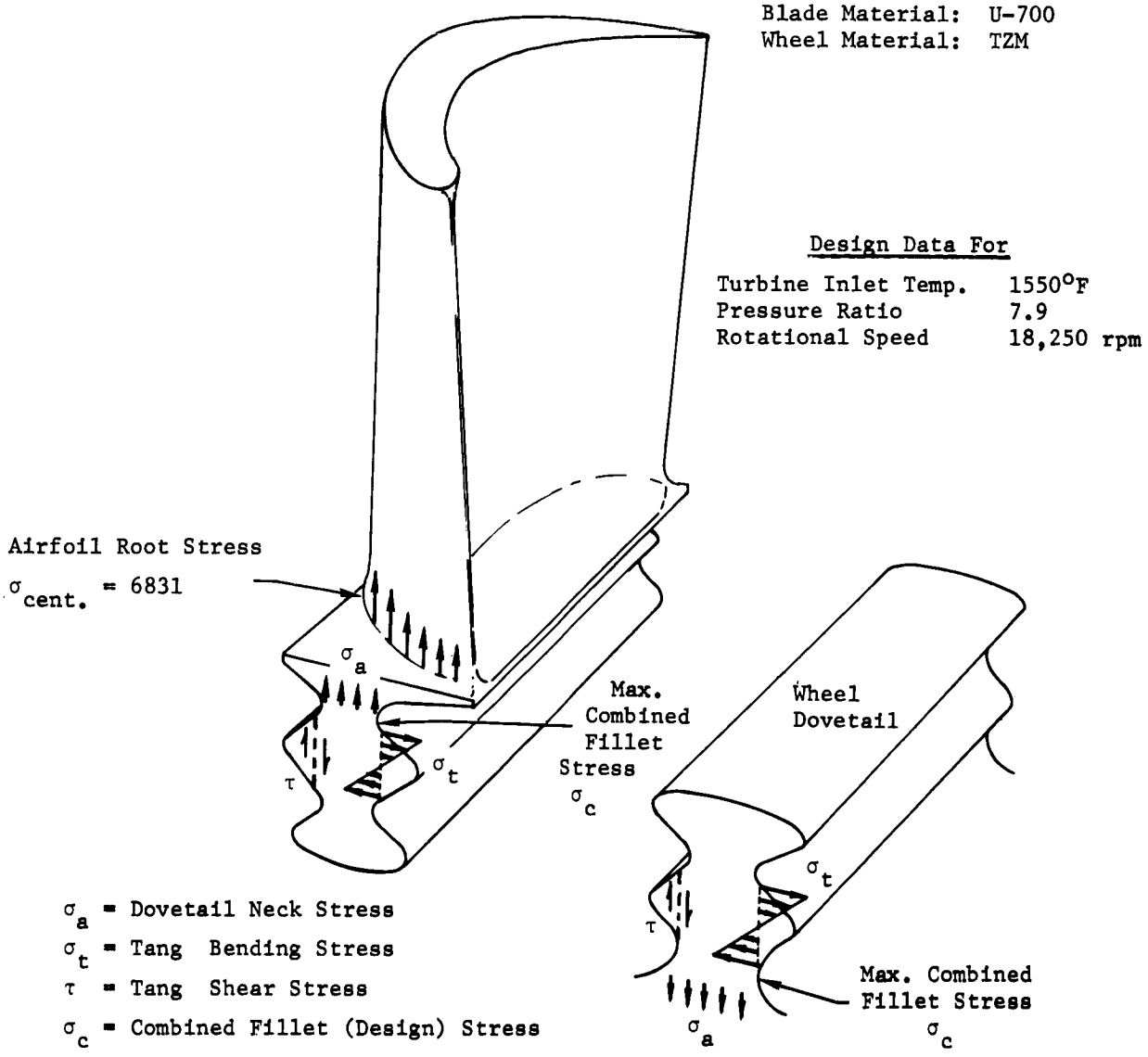

Blade Temp. 1445°F
Blade Life 30,000 hrs.

BLADE DOVETAIL

Stress (psi)	Top Tang.	Bottom Tang.
σ_a	11,112	6,338
σ_t	15,318	11,341
τ	9,205	6,857
σ_c	22,182	15,091

Wheel Temp. 1445°F
Wheel Life ∞ hrs.

WHEEL DOVETAIL

Stress (psi)	Top Tang.	Bottom Tang.
σ_a	17,417	15,682
σ_t	12,383	19,972
τ	5,325	5,647
σ_c	24,518	29,793

Figure 62. Stage 1 Blade and Dovetail Stress Summary. U700 Blades and TZM Wheel. (Phase II, Non-Shrouded Design)

STAGE 2

Blade Material: U-700
Wheel Material: TZM

Design Data For

Turbine Inlet Temp.	1550°F
Pressure Ratio	7.9
Rotational Speed	18,250 rpm

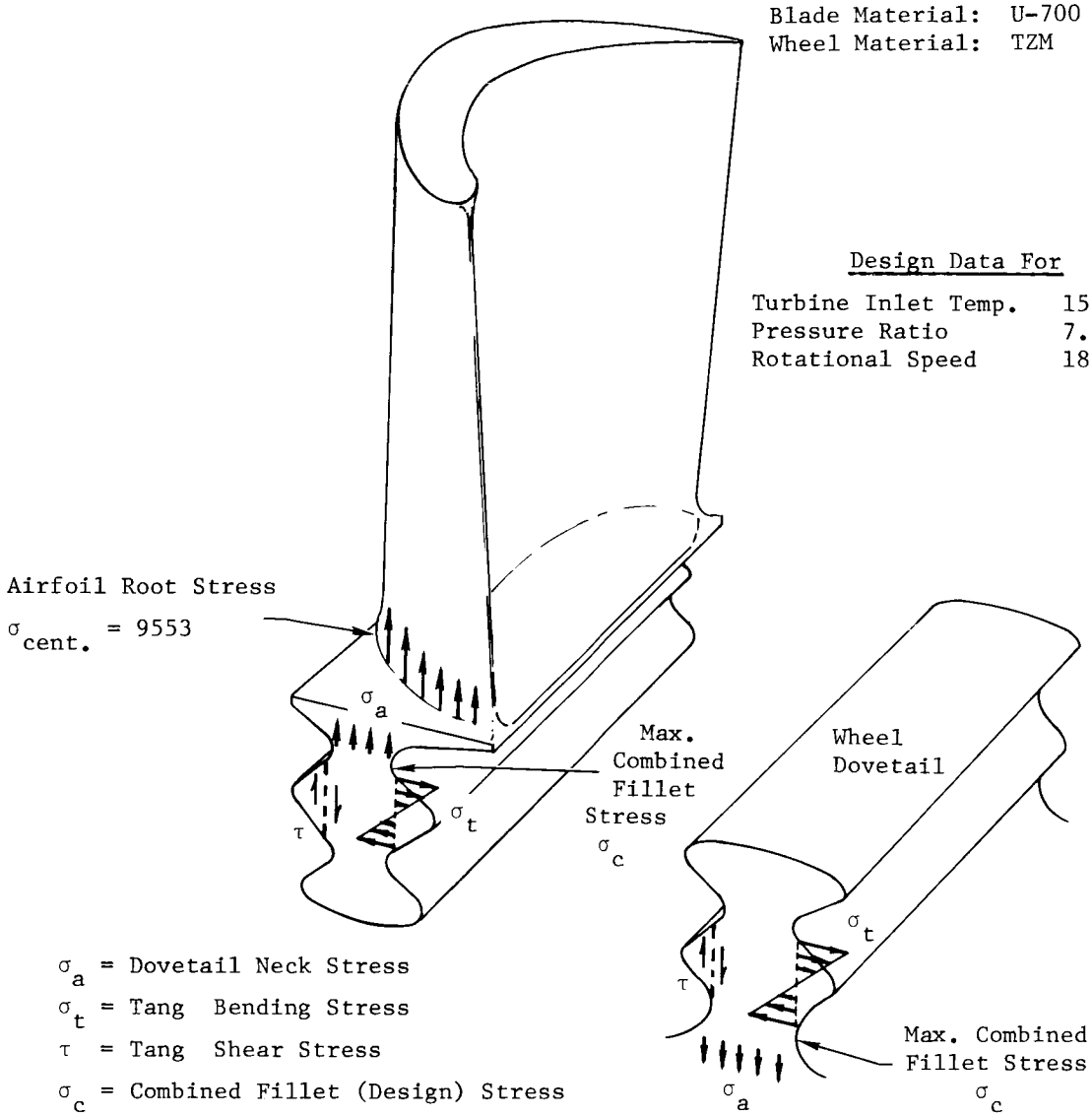

σ_a = Dovetail Neck Stress
σ_t = Tang Bending Stress
τ = Tang Shear Stress
σ_c = Combined Fillet (Design) Stress

Blade Temp. 1335°F
Blade Life 45,000 hrs.

BLADE DOVETAIL

Stress (psi)	Top Tang.	Bottom Tang.
σ_a	15,196	8,582
σ_t	19,704	14,678
τ	11,841	8,875
σ_c	34,900	19,793

Wheel Temp. 1335°F
Wheel Life ∞ hrs.

WHEEL DOVETAIL

Stress (psi)	Top Tang.	Bottom Tang.
σ_a	16,228	16,844
σ_t	15,929	25,849
τ	6,849	7,309
σ_c	26,579	36,067

Figure 63. Stage 2 Blade and Dovetail Stress Summary. U700 Blades and TZM Wheel. (Phase II, Non-Shrouded Design)

STAGE 2

Blade Material: TZM or TZC
Wheel Material: TZM

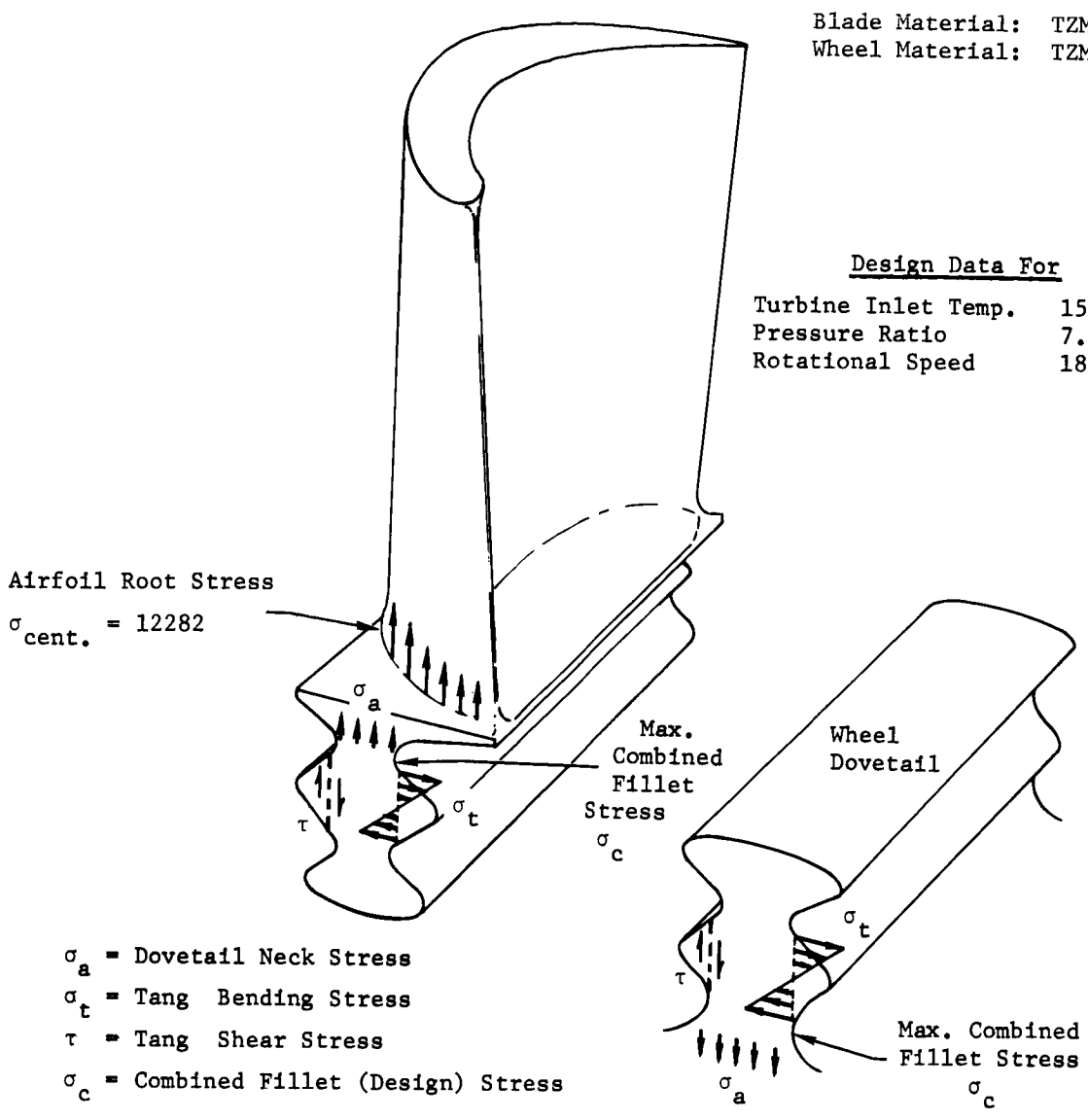

Blade Temp. 1335°F
Blade Life ∞ hrs.

BLADE DOVETAIL

Stress (psi)	Top Tang.	Bottom Tang.
σ_a	19,538	11,034
σ_t	25,331	18,872
τ	15,222	11,411
σ_c	37,529	25,448

Wheel Temp. 1335°F
Wheel Life ∞ hrs.

WHEEL DOVETAIL

Stress (psi)	Top Tang.	Bottom Tang.
σ_a	20,022	20,605
σ_t	20,478	33,235
τ	8,805	9,397
σ_c	33,520	45,633

Figure 64. Stage 2 Blade and Dovetail Stress Summary. TZM or TZC Blades and TZM Wheel. (Phase II, Non-Shrouded Design)

STAGE 3

Blade Material: U-700
Wheel Material: Modified Astroloy
(See Table III)

Design Data For

Turbine Inlet Temp.	1550°F
Pressure Ratio	7.9
Rotational Speed	18,250 rpm

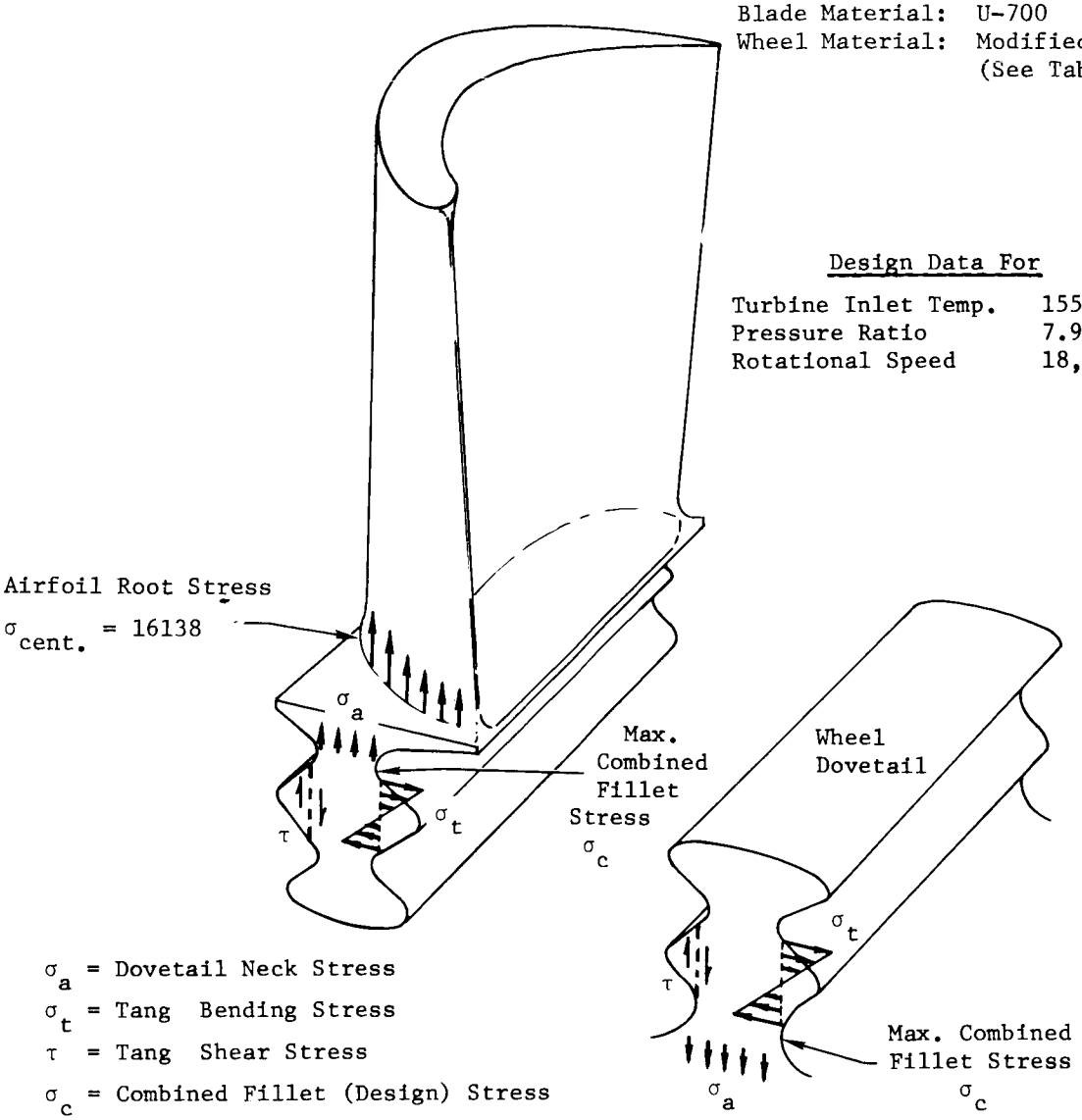

σ_a = Dovetail Neck Stress
σ_t = Tang Bending Stress
τ = Tang Shear Stress
σ_c = Combined Fillet (Design) Stress

Blade Temp. 1230°F
Blade Life 800,000 hrs

BLADE DOVETAIL

Stress (psi)	Top Tang.	Bottom Tang.
σ_a	19,625	10,962
σ_t	24,502	18,456
τ	14,724	11,159
σ_c	36,836	25,006

Wheel Temp. 1230°F
Wheel Life 350,000 hrs.

WHEEL DOVETAIL

Stress (psi)	Top Tang.	Bottom Tang.
σ_a	12,455	15,117
σ_t	19,807	32,502
τ	8,517	9,190
σ_c	27,318	41,202

Figure 65. Stage 3 Blade and Dovetail Stress Summary. U700 Blades and Modified Astroloy Wheel. (Phase II, Non-Shrouded Design)

STAGE 3

Blade Material: TZM or TZC
Wheel Material: Modified Astroloy
(See Table III)

Design Data For

Turbine Inlet Temp.	1550°F
Pressure Ratio	7.9
Rotational Speed	18,250 rpm

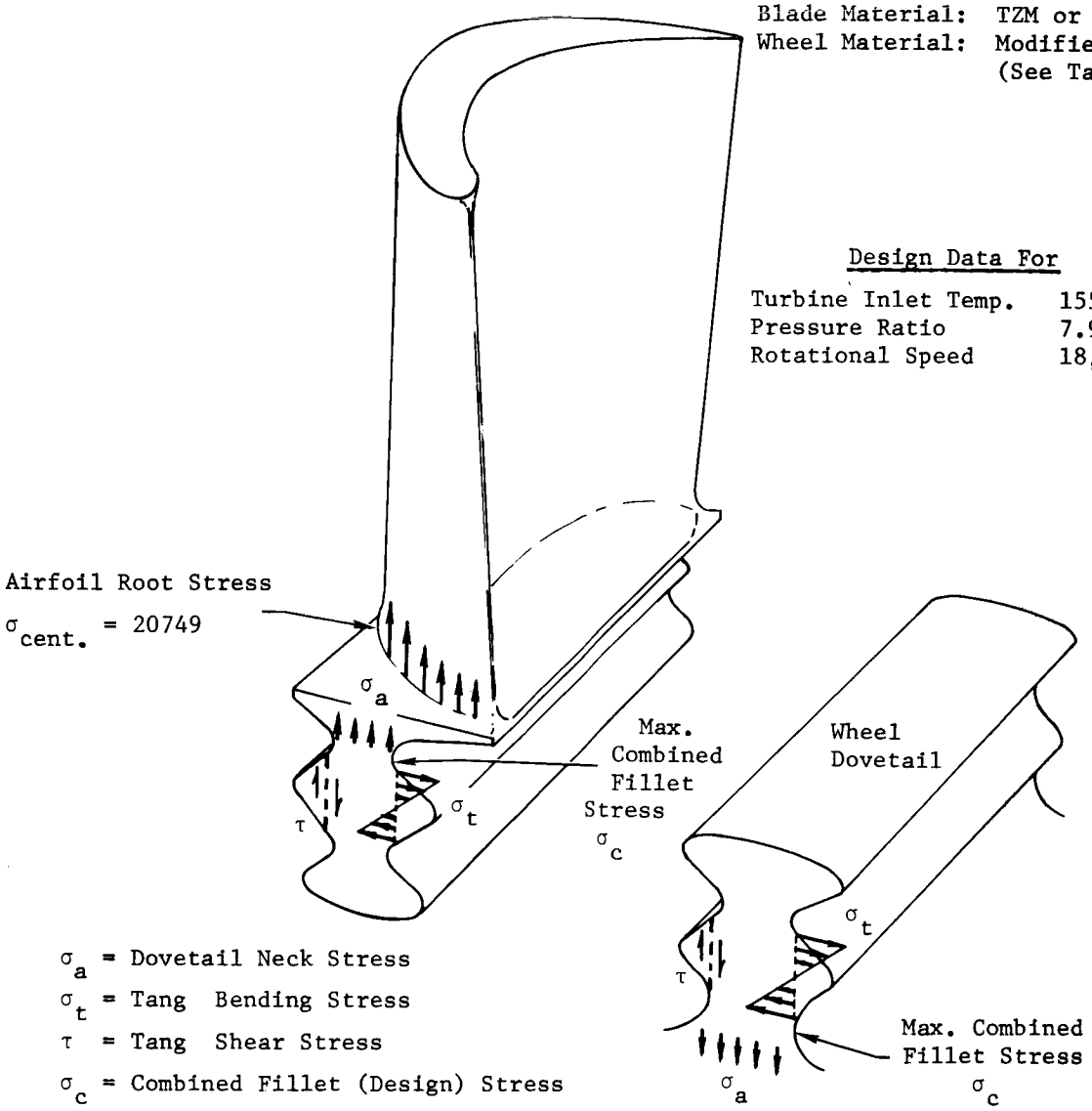

σ_a = Dovetail Neck Stress
σ_t = Tang Bending Stress
τ = Tang Shear Stress
σ_c = Combined Fillet (Design) Stress

Blade Temp. 1230°F
Blade Life ∞ hrs

BLADE DOVETAIL

Stress (psi)	Top Tang.	Bottom Tang.
σ_a	25,232	14,094
σ_t	31,502	23,731
τ	18,931	14,348
σ_c	47,360	32,152

Wheel Temp. 1230°F
Wheel Life 50,000 hrs

WHEEL DOVETAIL

Stress (psi)	Top Tang.	Bottom Tang.
σ_a	15,395	18,578
σ_t	25,466	41,790
τ	10,950	11,816
σ_c	40,861	52,412

Figure 66. Stage 3 Blade and Dovetail Stress Summary. TZM or TZC Blades and Modified Astroloy Wheel. (Phase II, Non-Shrouded Design)

THREE-STAGE POTASSIUM TURBINE BLADES -

ASSUMPTIONS USED IN VIBRATION ANALYSES 2/8/67 - 4/17/67

1. Blade contours are defined by coordinates having issue dates as listed in Table IX on "Synopsis of General Blade Program Section Properties of 3-Stage Turbine".

2. Airfoil section properties are calculated at root, pitch, and tip sections by the General Blade program, and interpolated at intermediate points by second-order equations.

3. Section properties of tip shrouds are applied at the C.G. of the section, with locations between the tip of the blade and the C.G. of the shrouds having 0 properties. The area at the shroud C.G. is chosen so that the volume of the shroud is reproduced by the integration of the tip and C.G. areas over the distance separating them. A similar procedure is followed for assigning values to the polar moment of inertia. Shroud chord = thickness = St. Venant torsional stiffness T_{SV}=1 are satisfactory. An X-direction load of 10 lb/in and a Y-direction load of -10 lb/in are applied to the shroud to load the structure, with a distributed torque load of 10 lb. All other functions are 0 for the shroud C.G. section, and all functions except E, G, and T_S/T_{SV} are 0 for sections between the shroud C.G. and the blade tip. Spanwise force at the tip = 0. T_S/T_{SV} = 10 at all shroud sections. See Figure 67(b) for explanation of nomenclature.

4. Section properties of the dovetail are calculated using actual dovetail dimensions from the airfoil to the upper tang pressure contact point, which is 0.12574 above plane AG of existing blade drawings. T_S/T_{SV} = 10 is assumed for the dovetail blade intersection, and T_S/T_{SV} = 1 for all other dovetail sections. Zero values are assigned to all induced tensile stress functions, bending stress functions for the max. M.I. axis, and third moments.

5. The wheel radius for computation purposes is considered to be that of the upper tang contact point. THE BLADE IS ANALYZED AS THOUGH THE DOVETAIL BELOW THE CONTACT POINT WERE INTEGRAL WITH THE WHEEL, AND ALL OF THE BLADE AND DOVETAIL ABOVE THE CONTACT POINT WERE FREE. True geometry is used except that only 68 percent of the blade platform width is used as discussed in the text. The shroud is considered free from blade-to-blade.

6. Material properties were assigned on the basis of calculated blade temperatures.

7. Tip boundary conditions are: Moments $M_x = M_y = M_z = 0$; Shear forces $V_x = V_y = 0$.

Figure 67a.

8. Root boundary conditions are: Displacements u = v = 0; torsional rigidity $\frac{M_y}{\theta_x} = 3.062 \times 10^4$ (calculated as torsional rigidity of a rectangular shaft having the dimensions of the dovetail at about 0.1765 in. above the tang contact point); $\theta_y = \phi = 0$.

9. For all shroud, airfoil, and dovetail sections, zero value is assigned to torque coefficients M_x and M_y, offsets and tilts in the X and Y directions, distributed loads and torques (except at shroud C.G.), local elastic axis X and Y coordinates, and M_x Eq θ_y and M_y Eq θ_x coefficients. No computer entry is made to produce discontinuous increments of centrifugal force.

10. Blades are analyzed at 0 and 20,000 RPM, it having been found that linear interpolations and extrapolations based upon them are sufficiently accurate for most practical purposes.

11. For unshrouded blades, the stations which described the shrouds are assigned height increments of 0.0001 in. above the true blade tip and the properties of the tip airfoil section are assigned.

Figure 67a. (Cont'd)

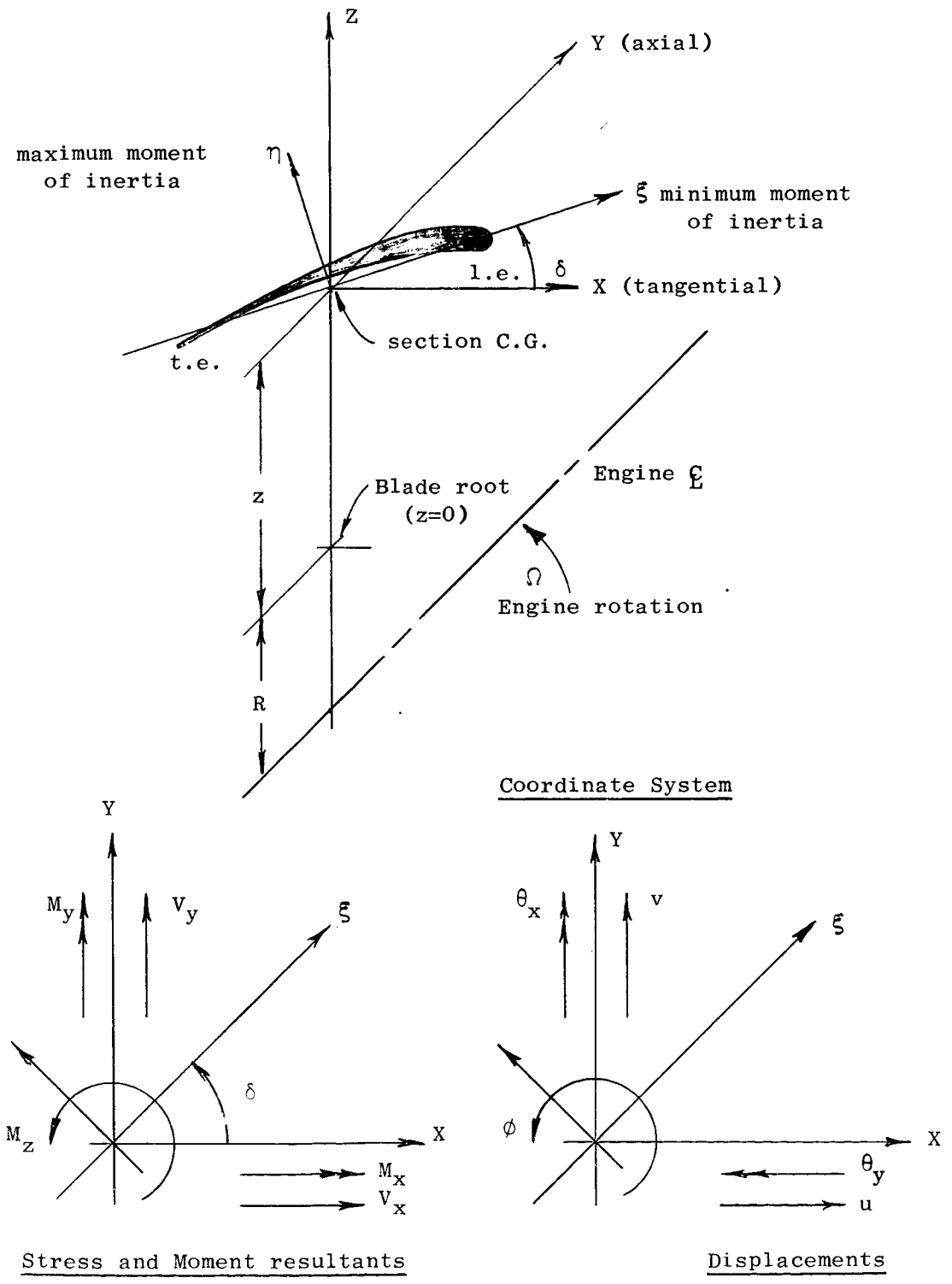

Figure 67b. Rotor Blade Orientation Nomenclature.

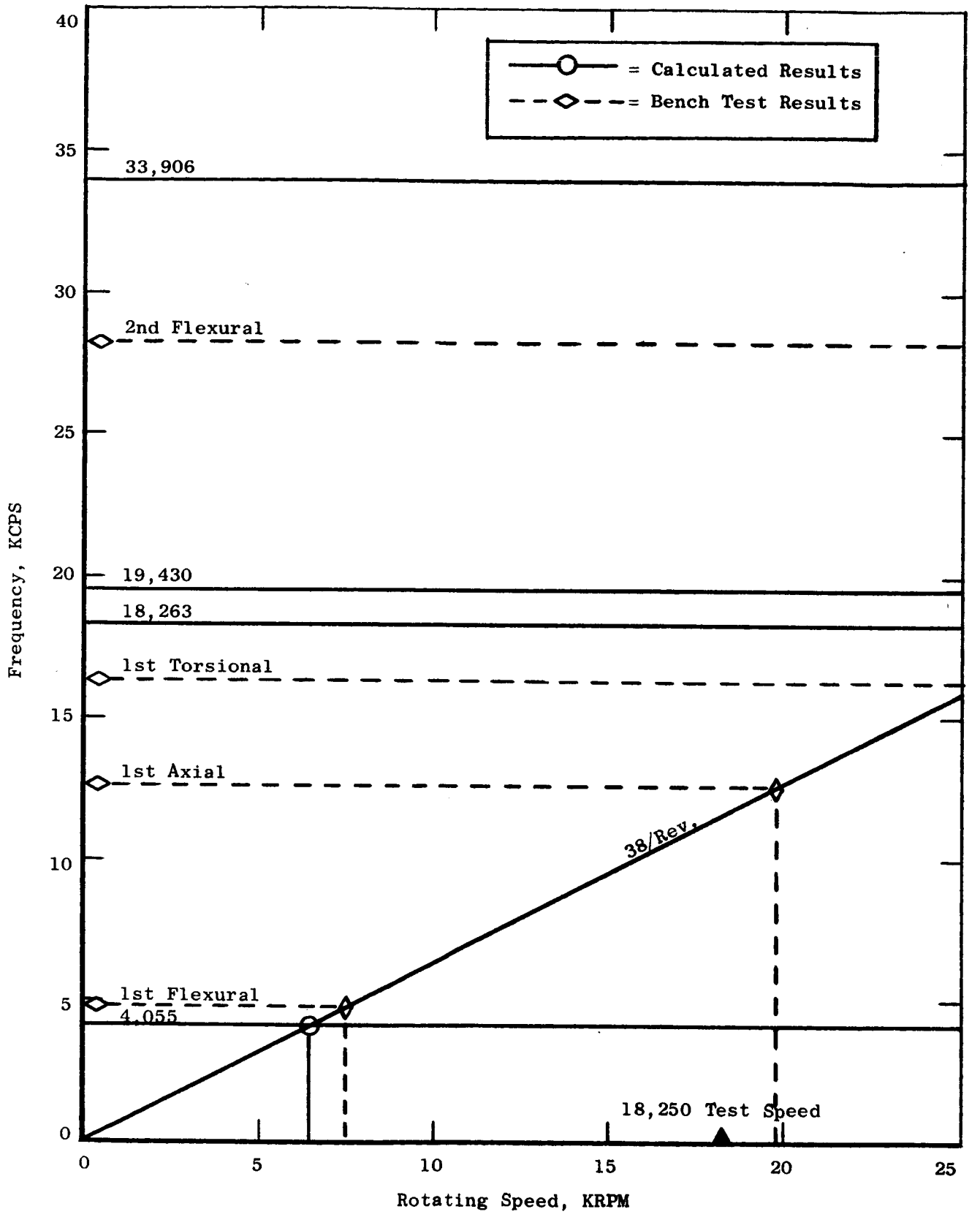

Figure 68. Campbell Diagram for Stage 1 of Three-Stage Potassium Turbine. (Phase I, Tip Shrouded Design)

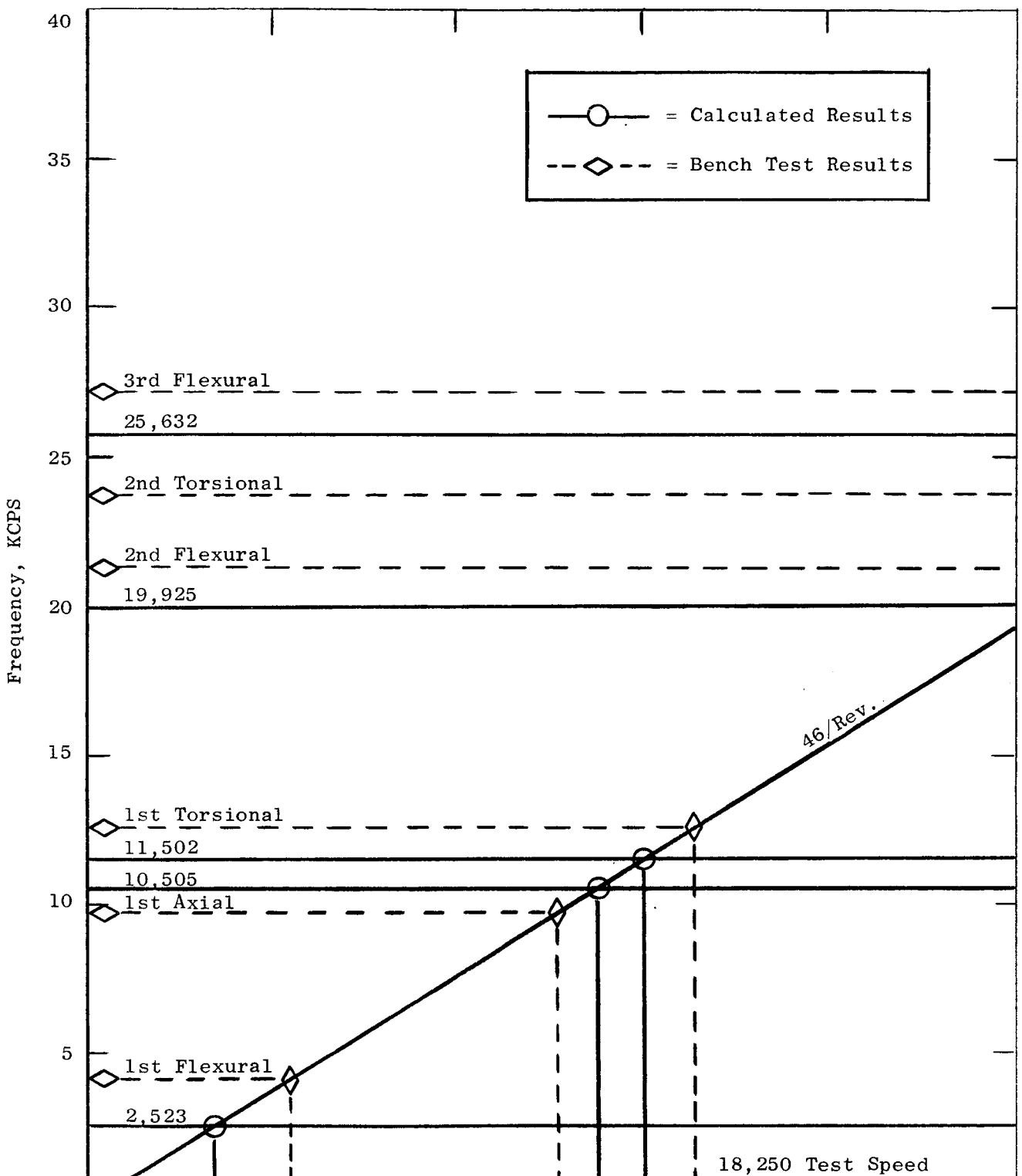

Figure 69. Campbell Diagram for Stage 2 of Three-Stage Potassium Turbine. (Phase I, Tip Shrouded Design)

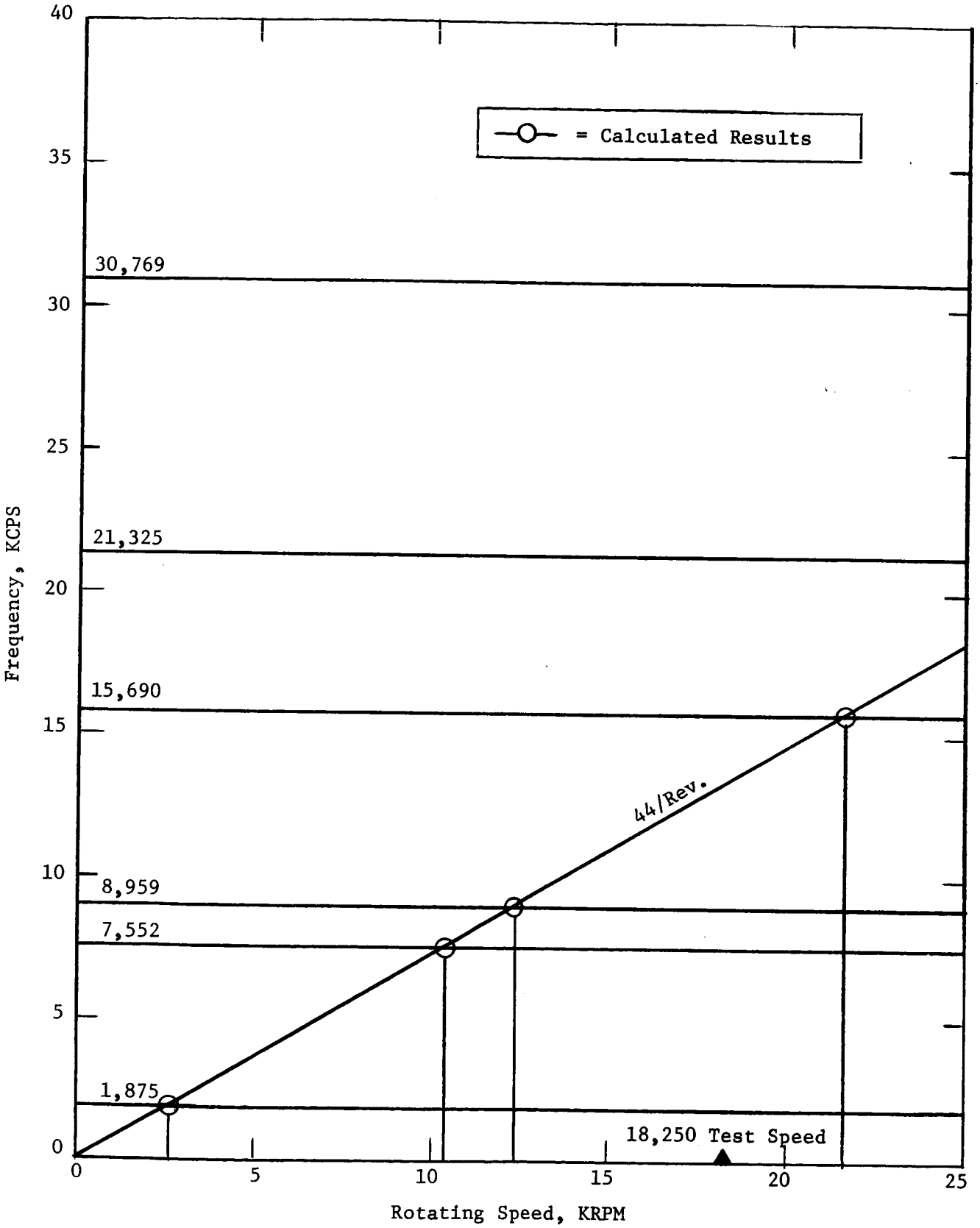

Figure 70. Campbell Diagram for Stage 3 of Three-Stage Potassium Turbine. (Phase I, Tip Shrouded Design) (TDC-67-39)

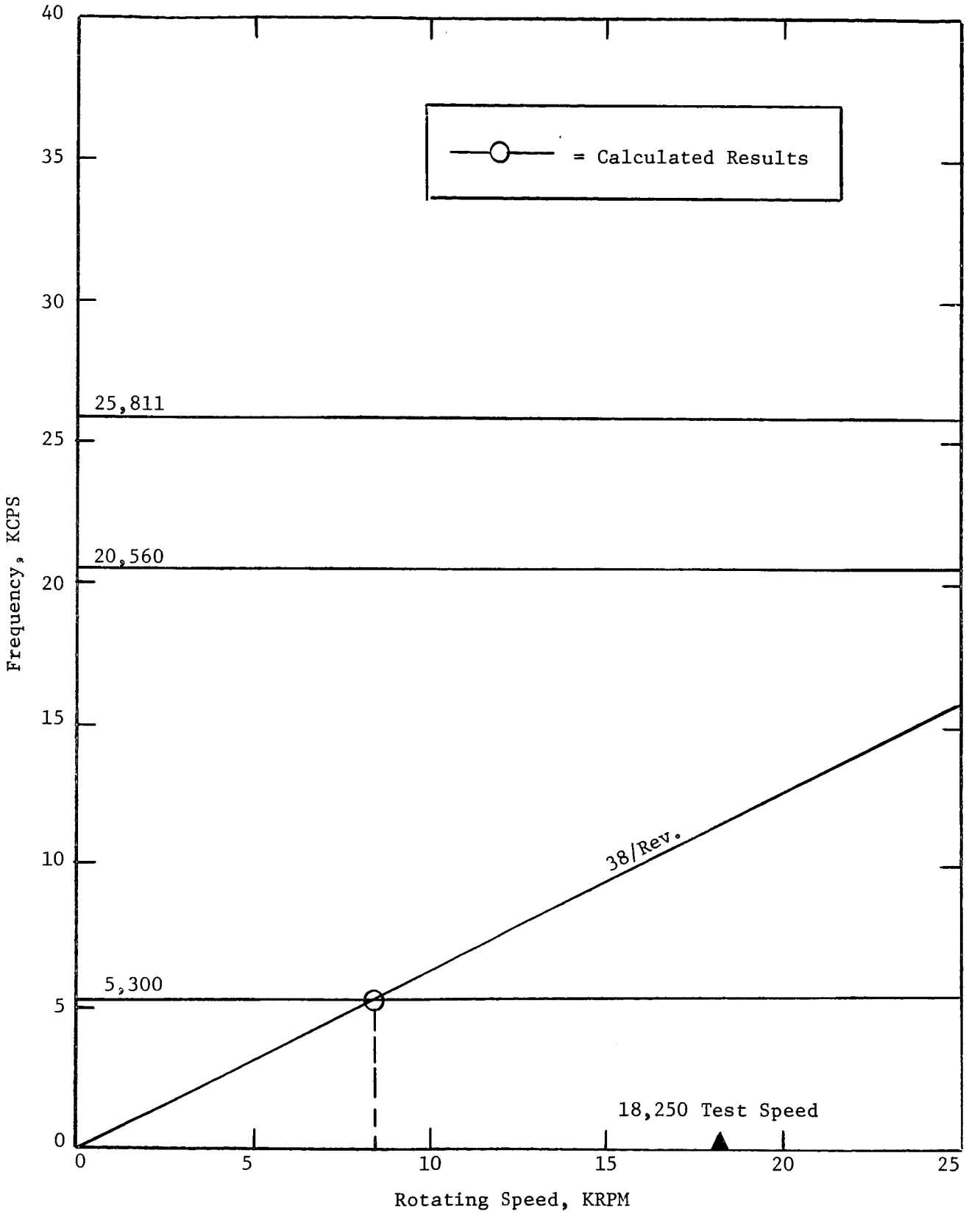

Figure 71. Campbell Diagram for Stage 1 of Three-Stage Potassium Turbine. (Phase II, Non-Shrouded Design) (TDC-67-106)

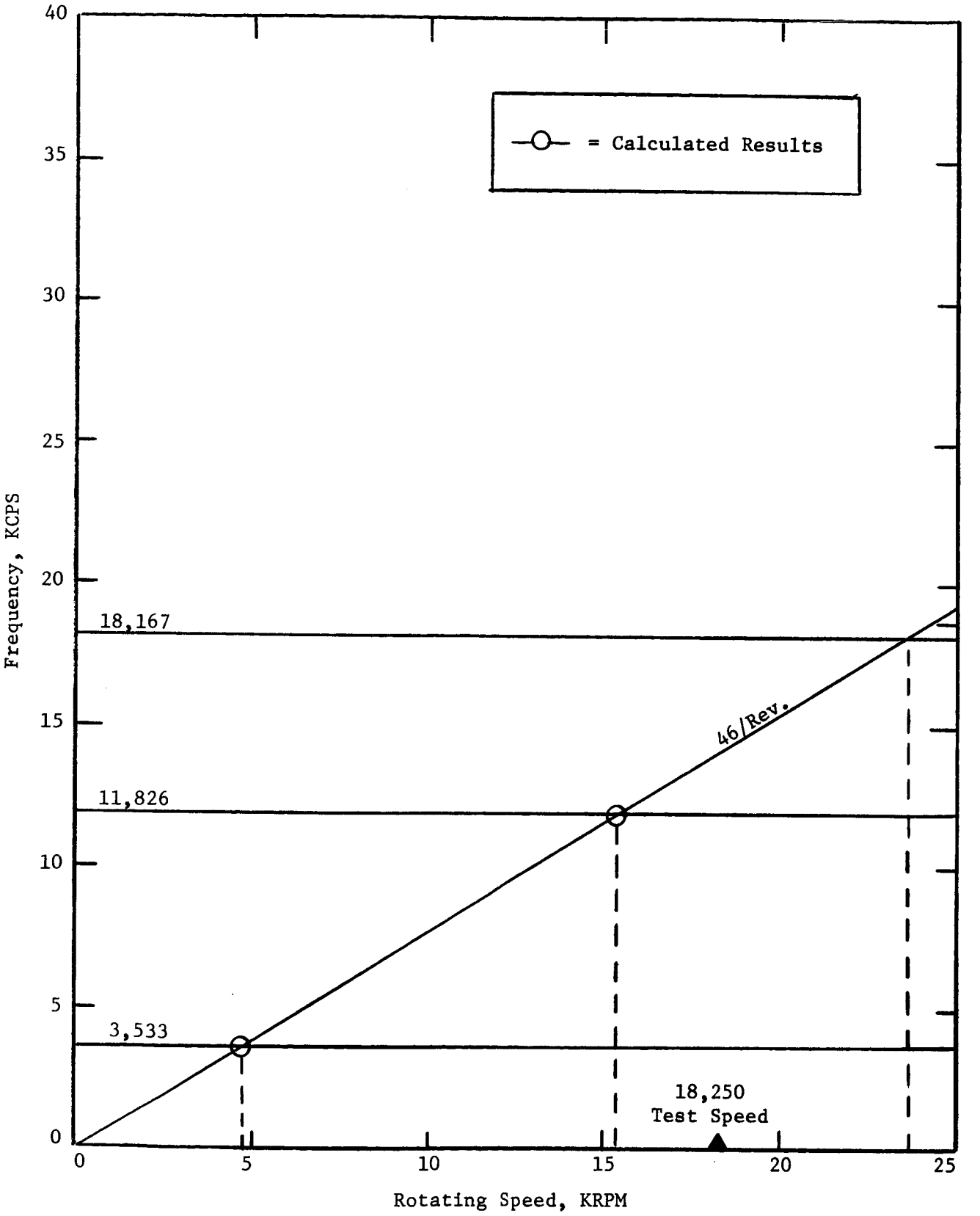

Figure 72. Campbell Diagram for Stage 2 of Three-Stage Potassium Turbine. (Phase II, Non-Shrouded Design) (TDC-67-107)

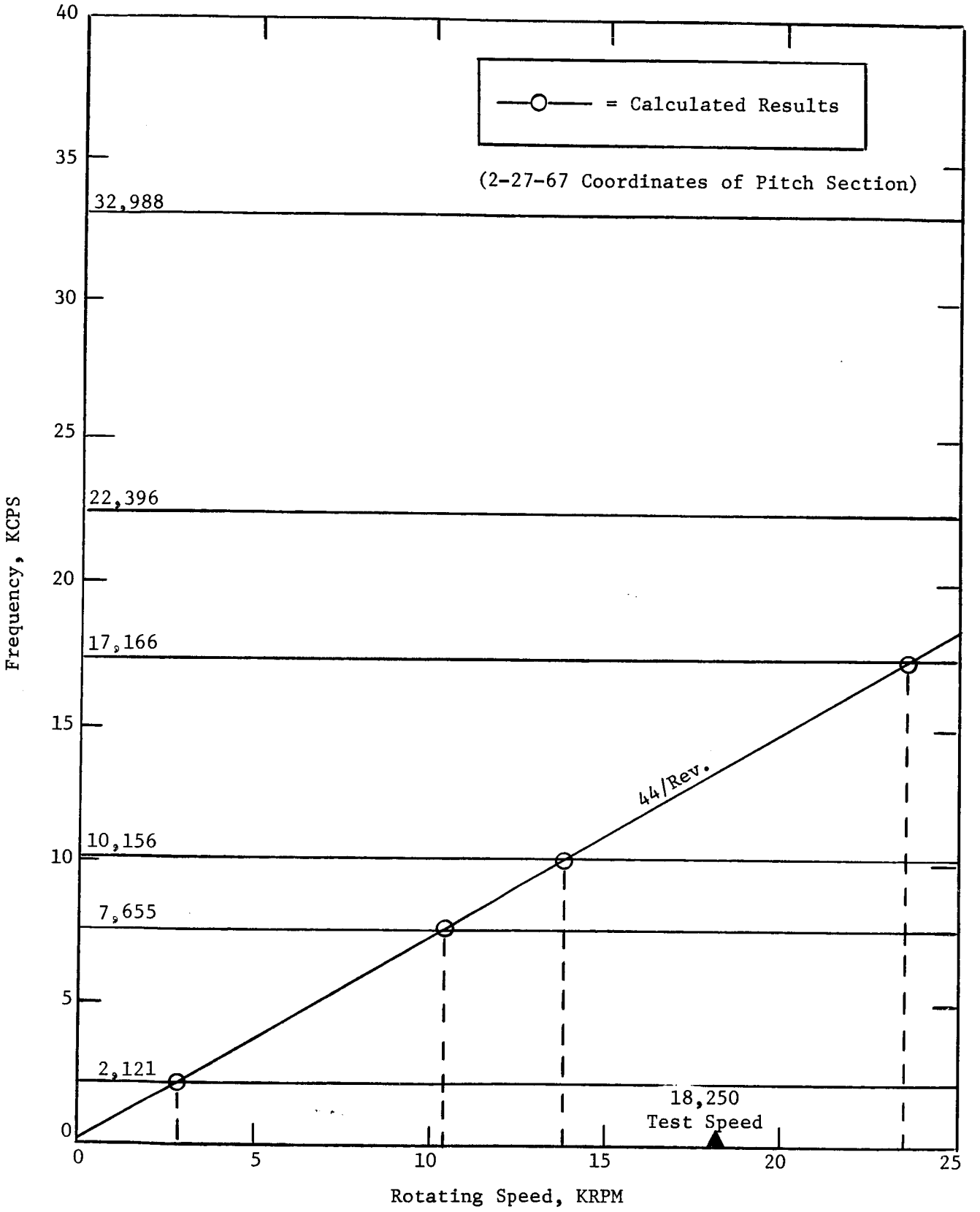

Figure 73. Campbell Diagram for Stage 3 of Three-Stage Potassium Turbine. (Phase II, Non-Shrouded Design) (TDC-67-108)

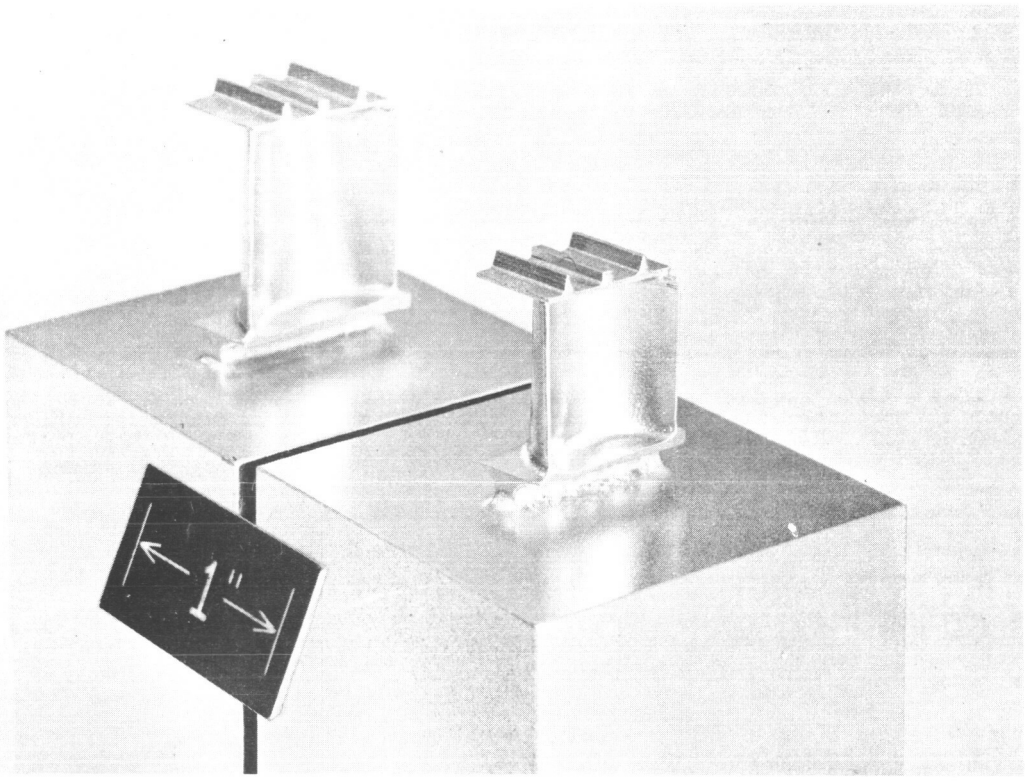

Figure 74a. View Toward Trailing Edge of Shrouded Turbine Blade Vibration Test Mockups - Stage 1 (R) and Stage 2 (L).

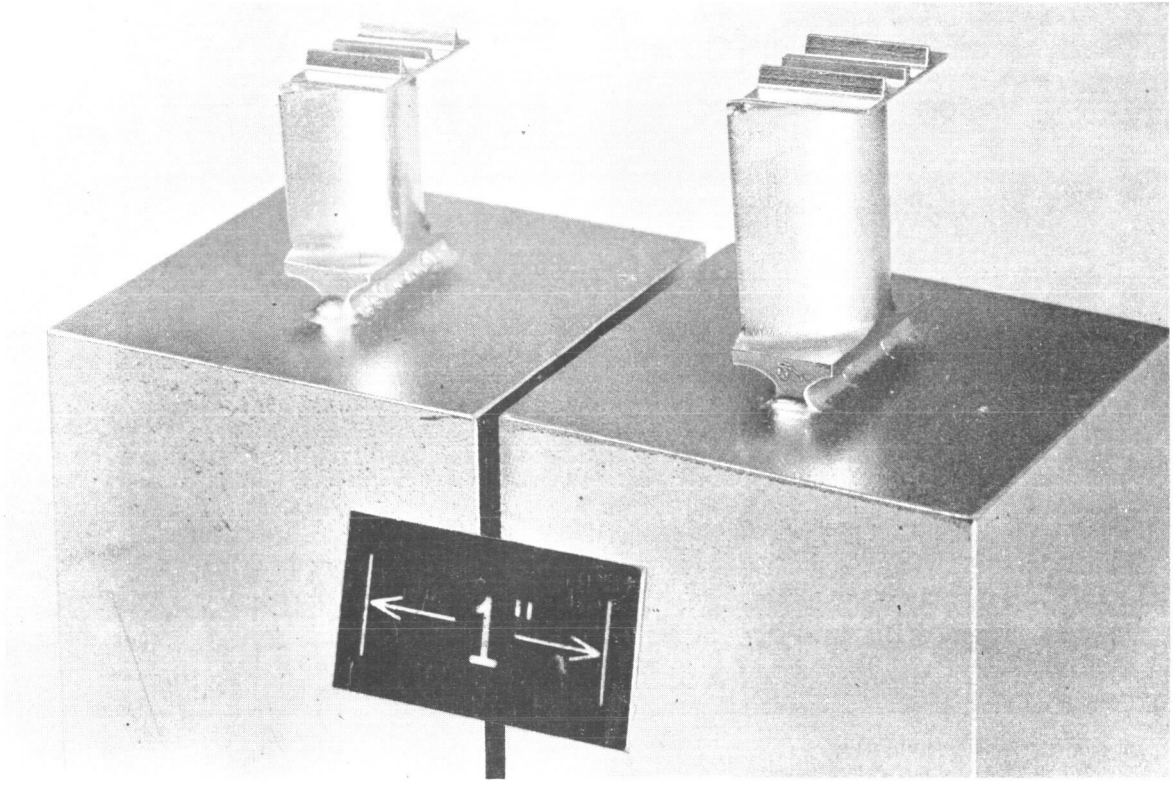

Figure 74b. View Toward Leading Edge of Shrouded Turbine Blade Vibration Test Mockups - Stage 2 (R) and Stage 1 (L).

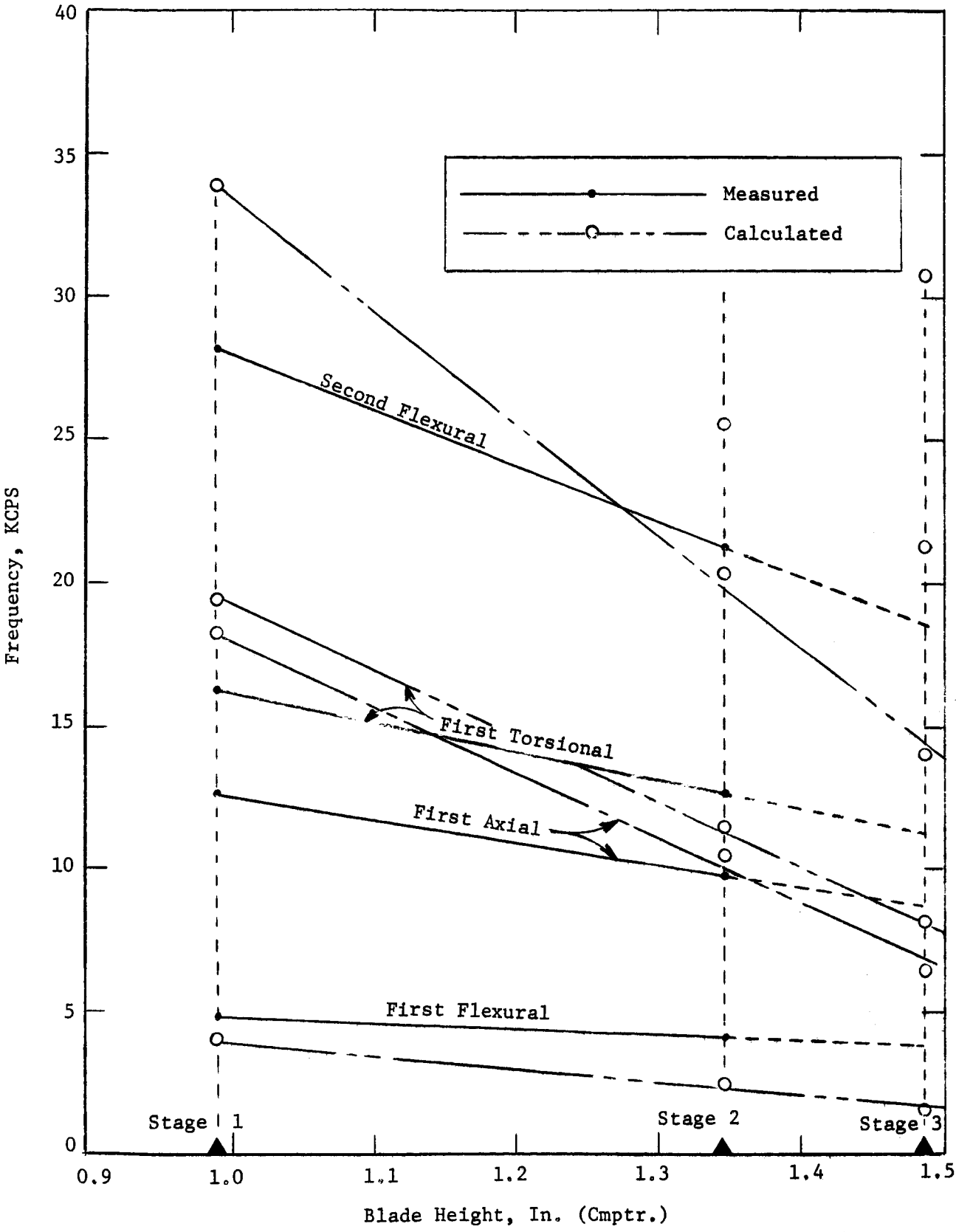

Figure 74c. Measured Versus Calculated Critical Frequencies for Shrouded Turbine Blades of Three-Stage Potassium Turbine. (TDC-67-109)

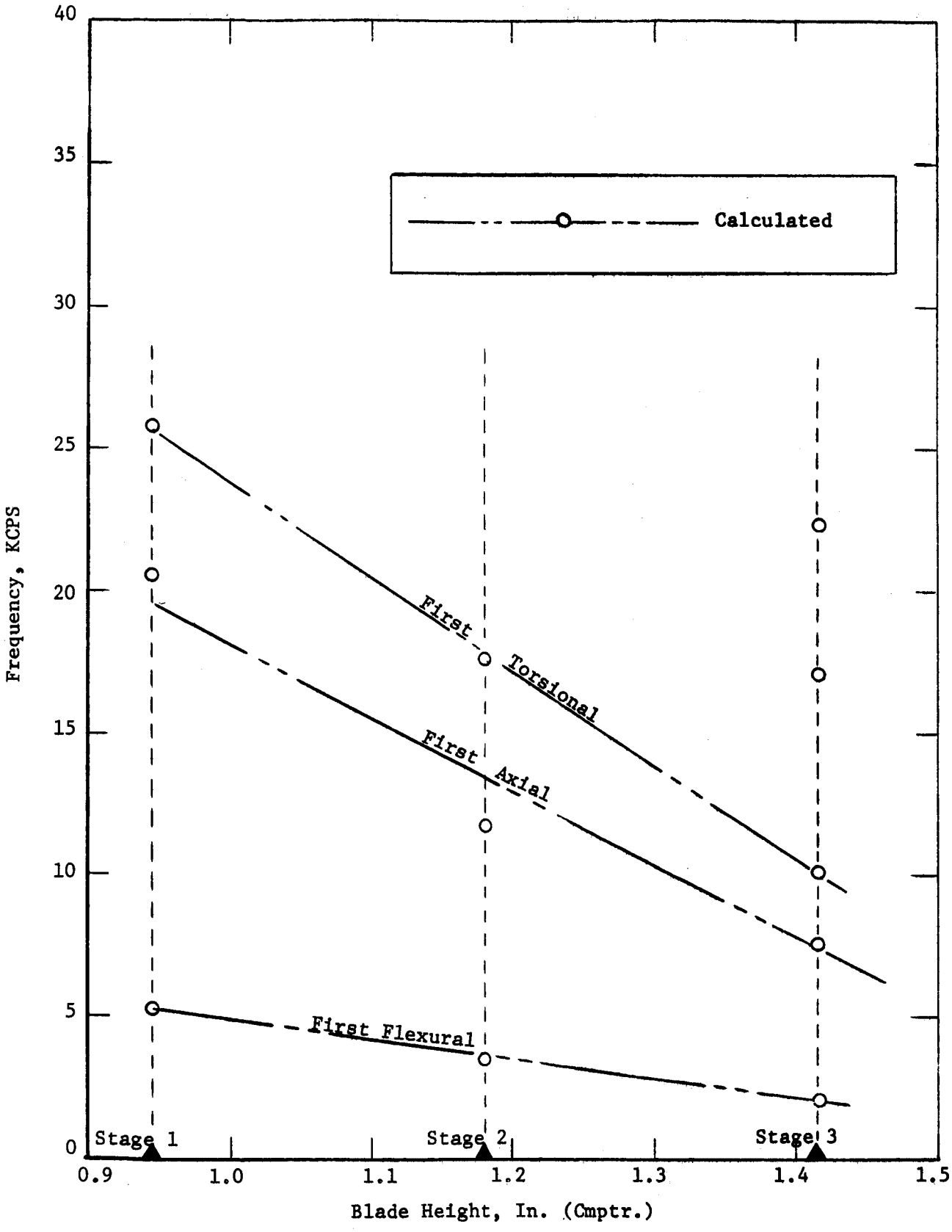

Figure 74d. Measured Versus Calculated Critical Frequencies for Unshrouded Turbine Blades of Three-Stage Potassium Turbine. (TDC-67-110)

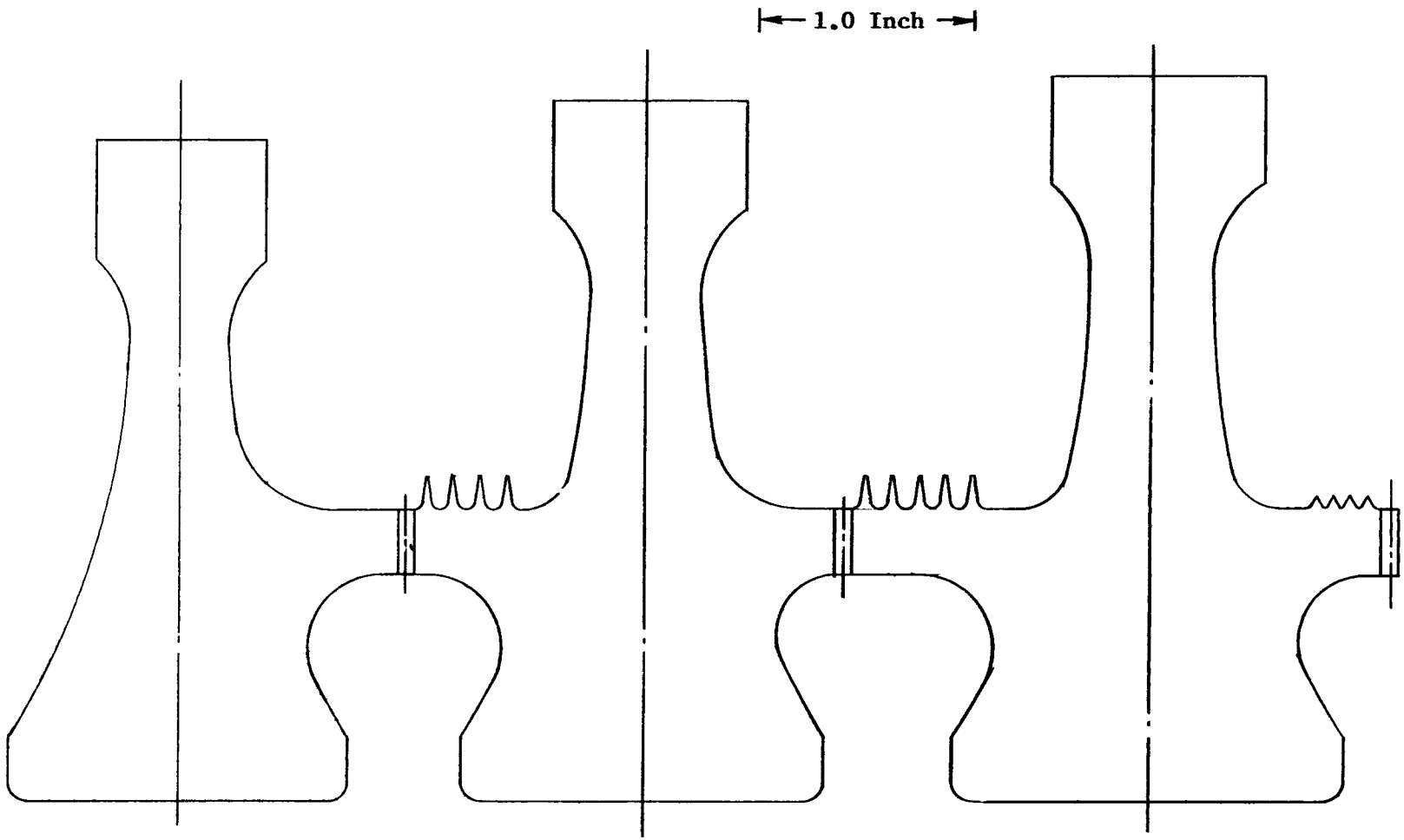

Figure 75. Turbine Wheel Assemblage.

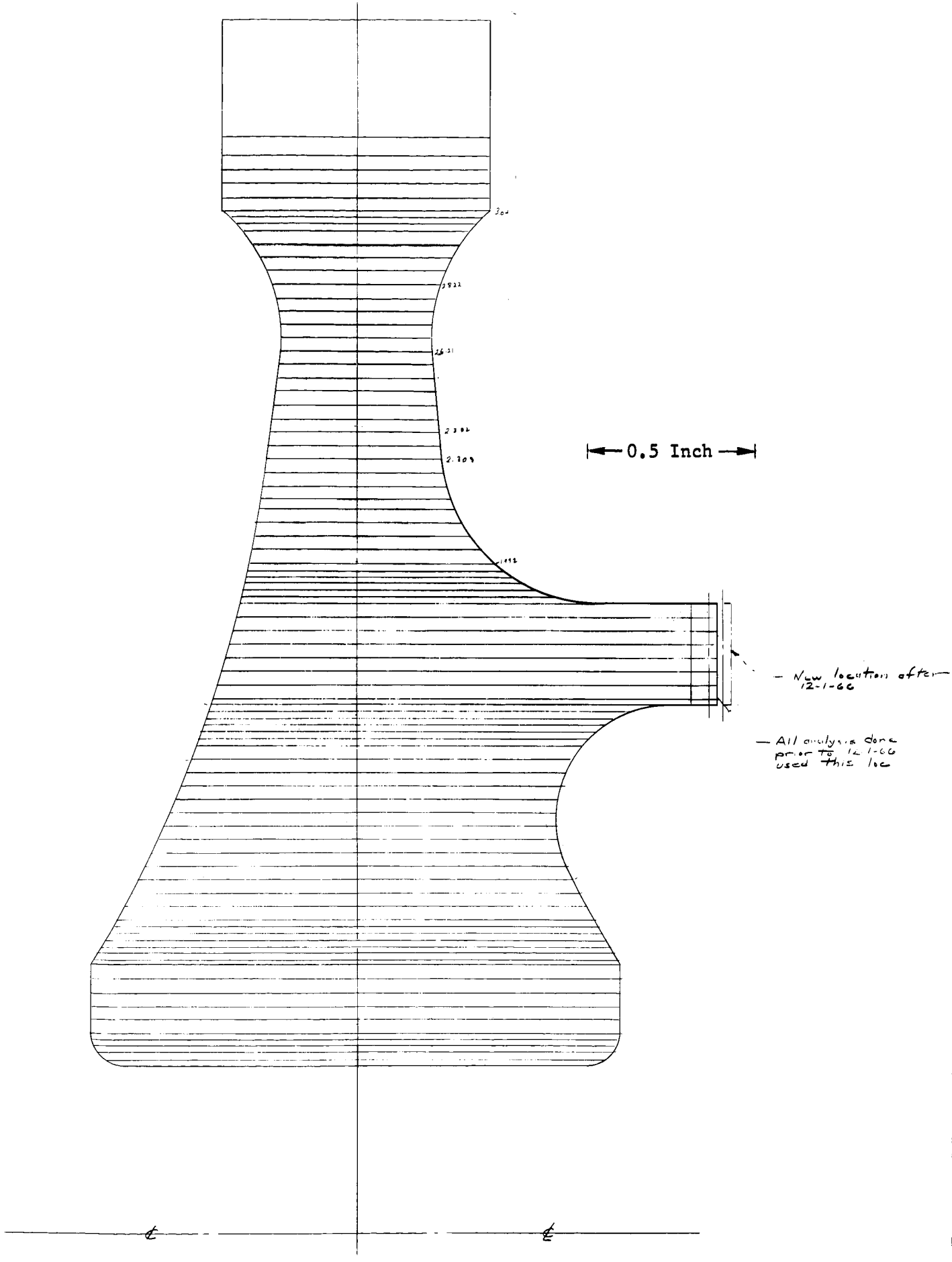

Figure 76. Stage 1 Wheel Stress Calculation Model. (941D160)

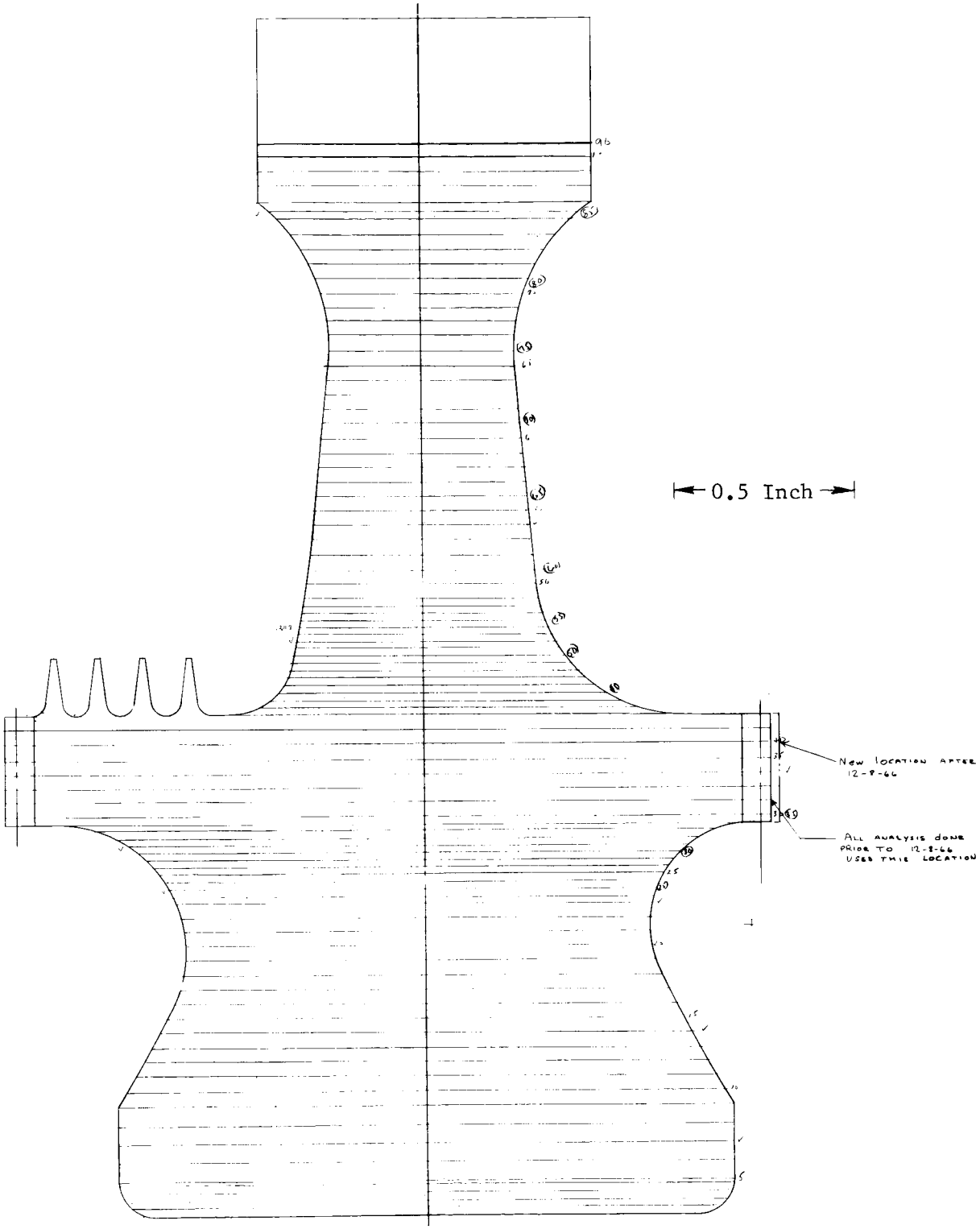

Figure 77. Stage 2 Wheel Stress Calculation Model. (941D161)

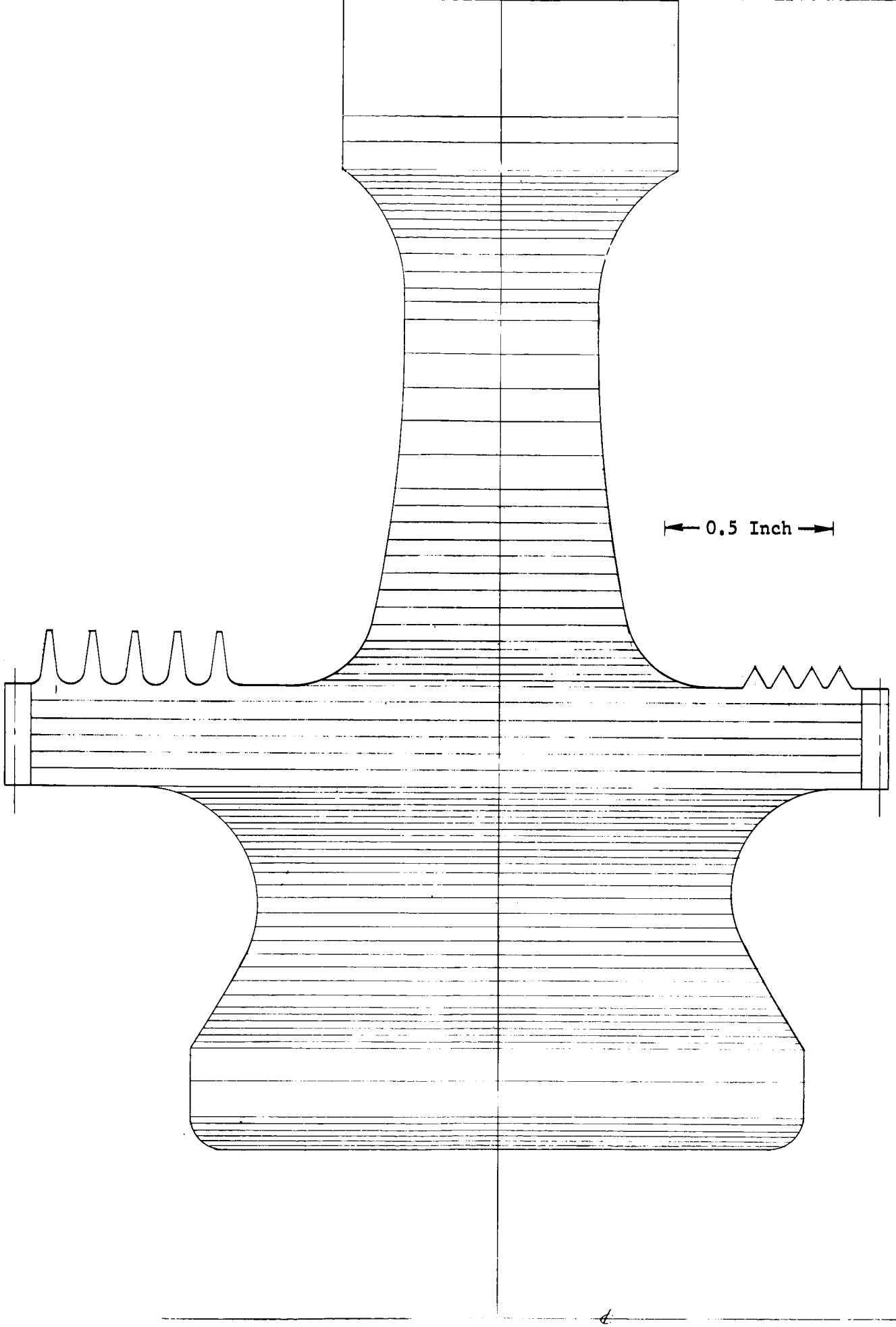

Figure 78. Stage 3 Wheel Stress Calculation Model. (941D162)

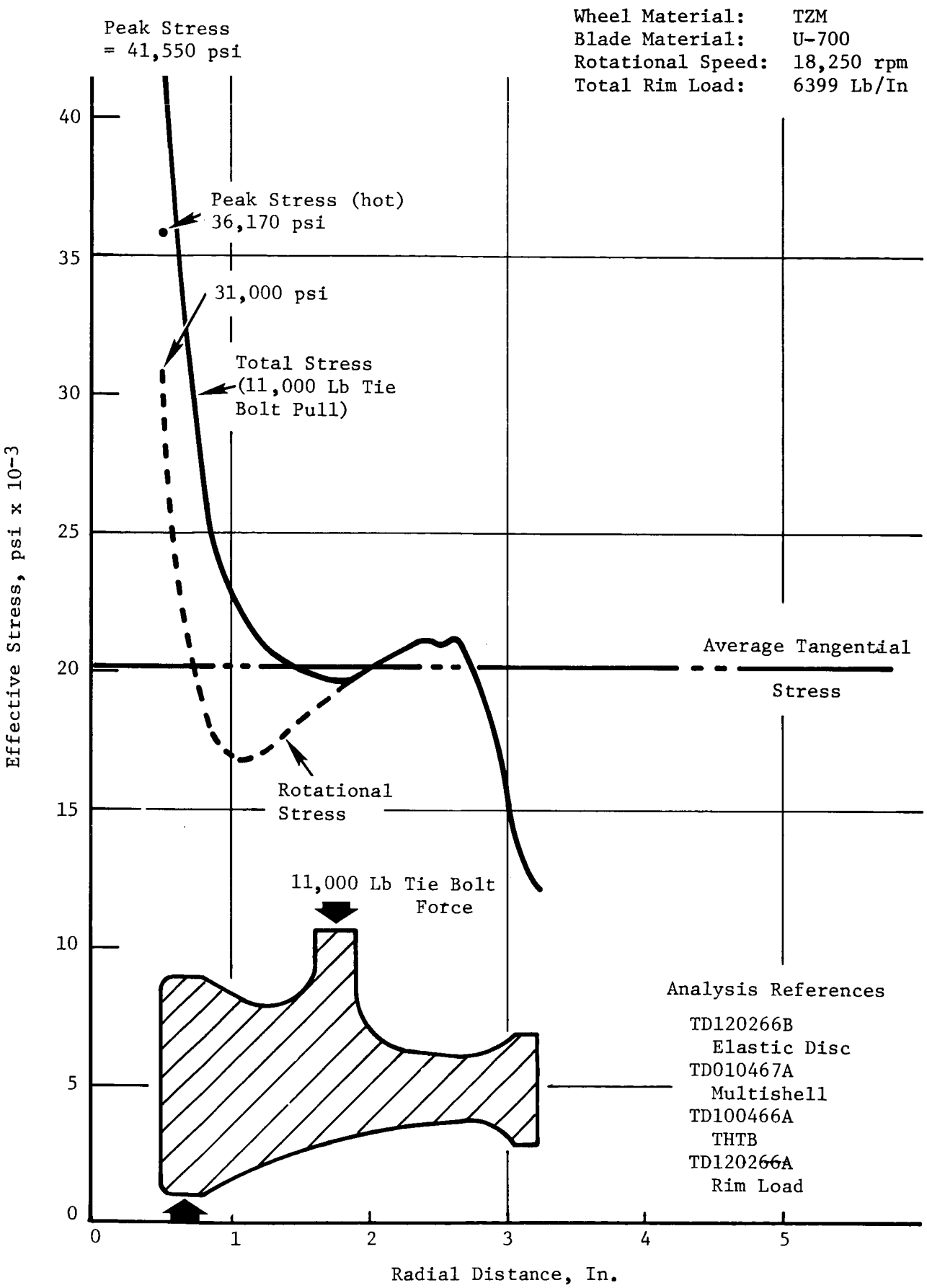

Figure 79. Stage One Wheel Stress. (With Tip-Shrouded Blades)

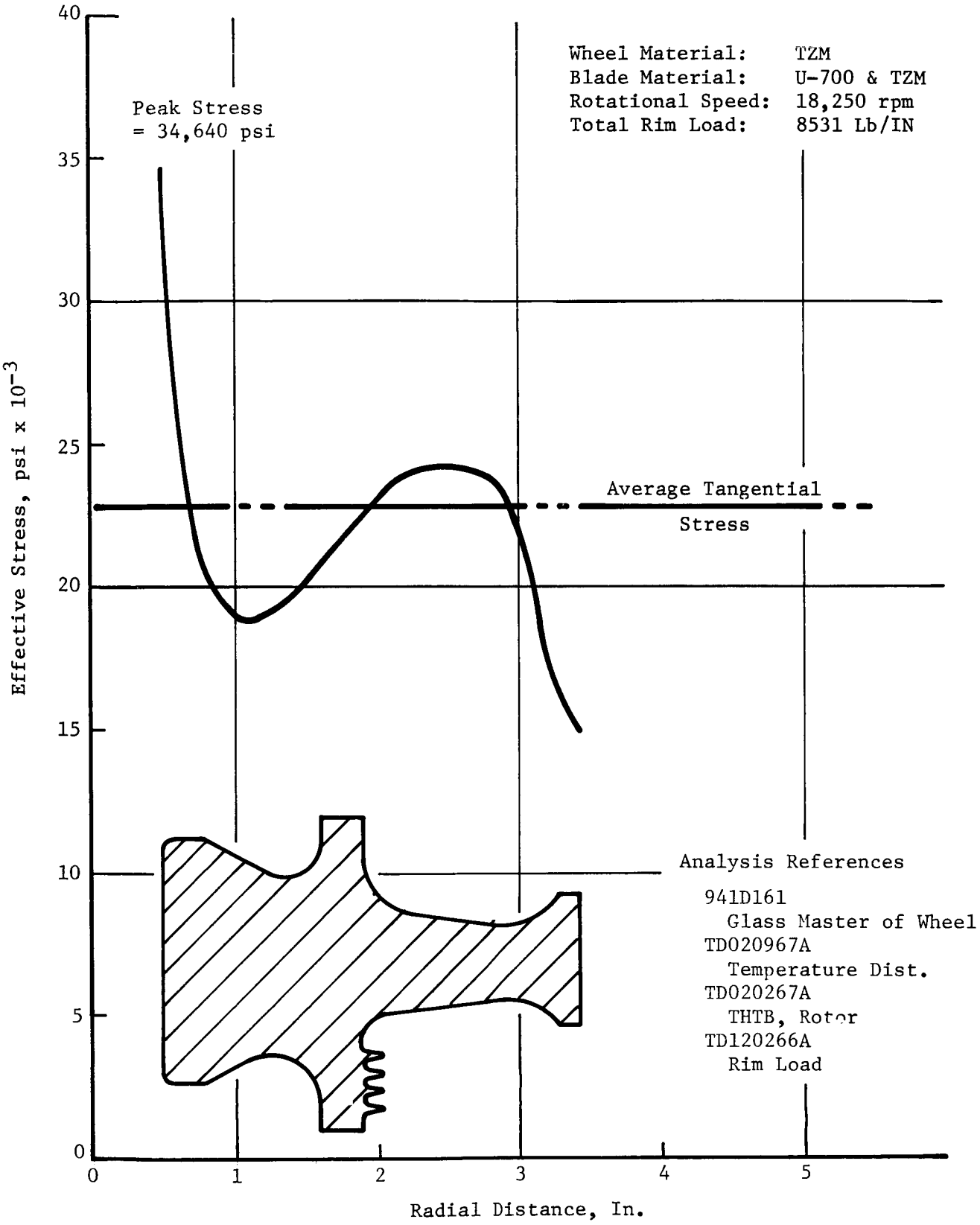

Figure 80. Stage 2 Wheel Stress. (With Tip-Shrouded Blades)

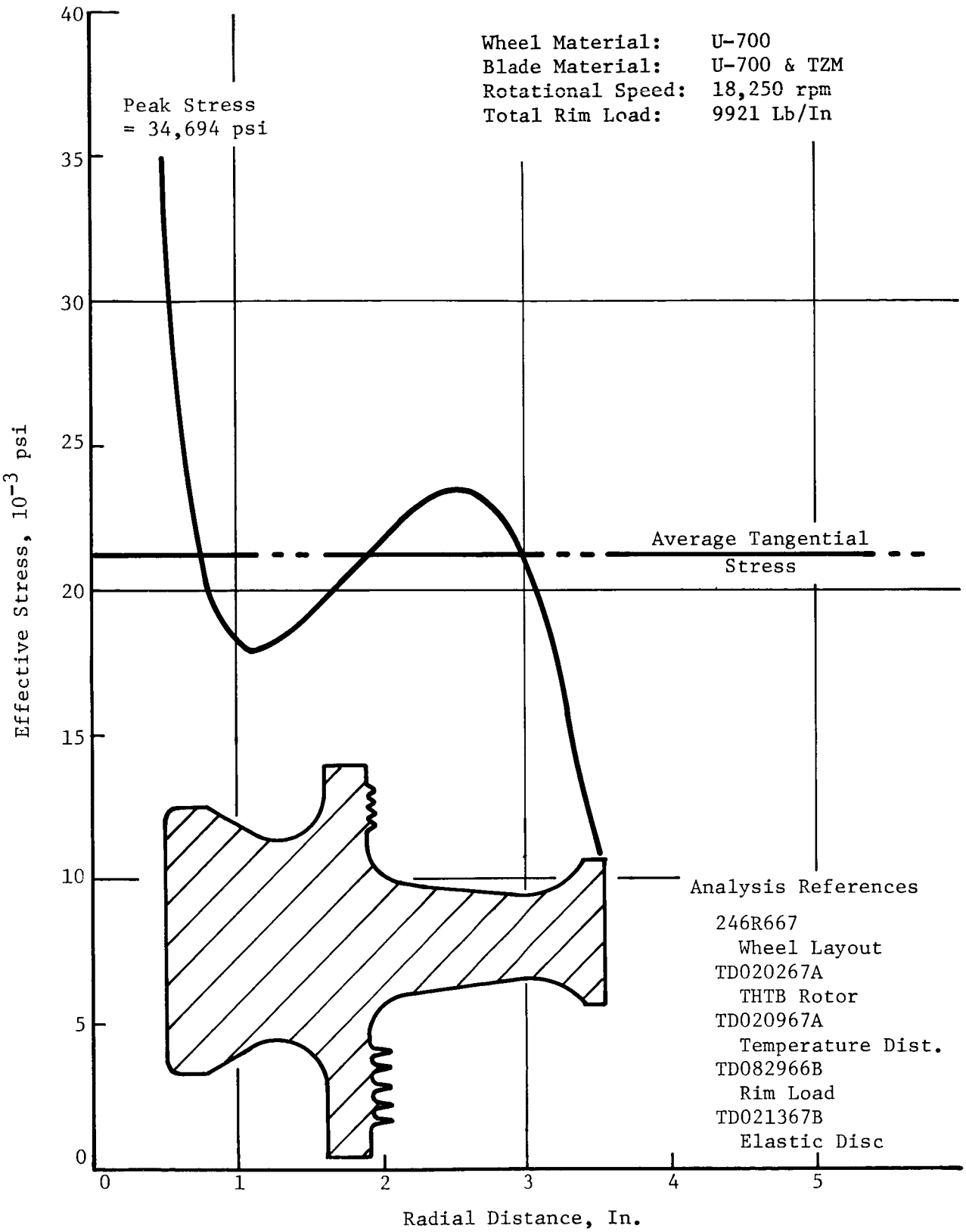

Figure 81. Stage 3 Wheel Stress. (With Tip-Shrouded Blades)

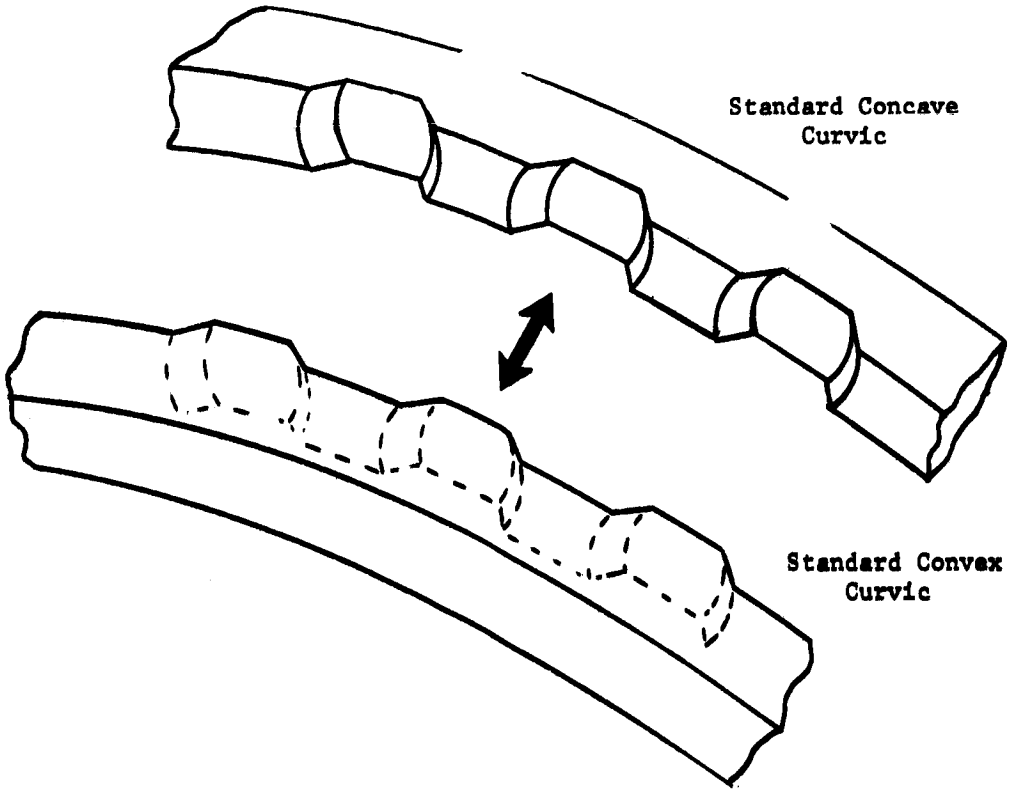

Figure 82a. Standard Curvic Coupling Geometry.

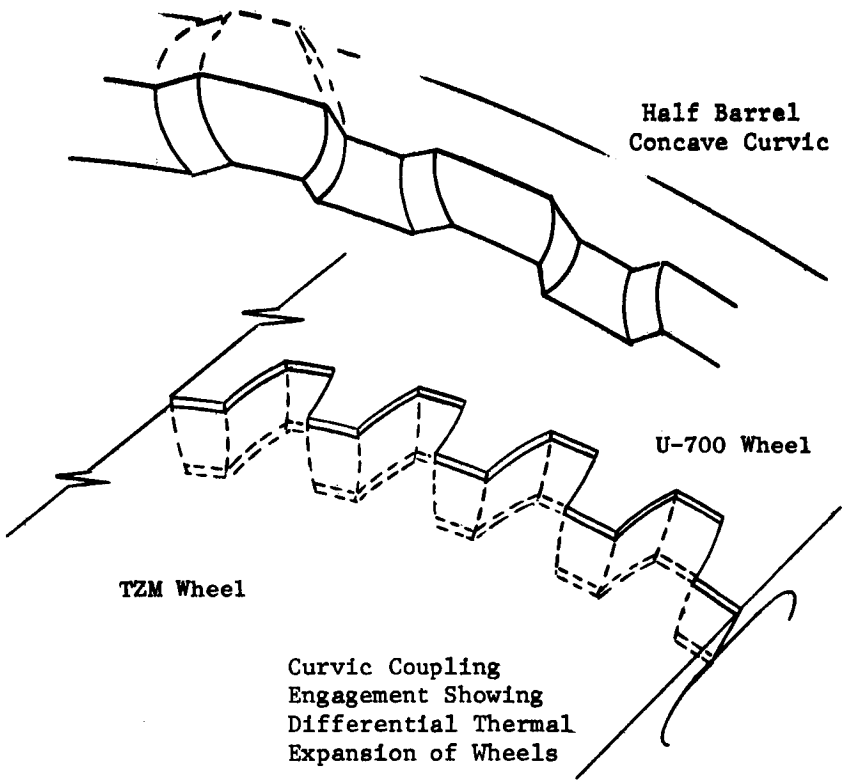

Figure 82b. Half-Barrel Curvic Coupling Geometry.

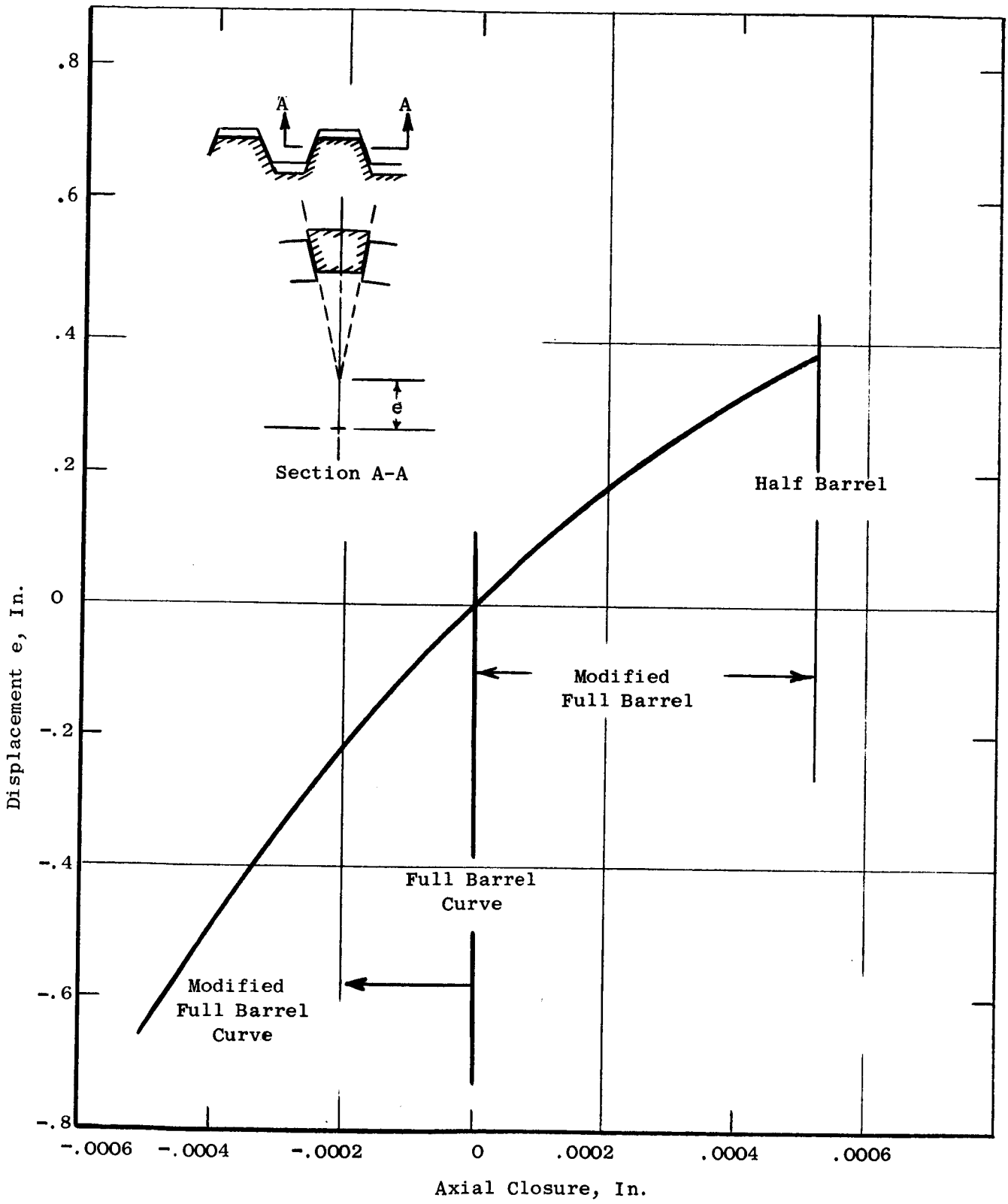

Figure 83. Axial Clearance of 16 Tooth Curvic Coupling.

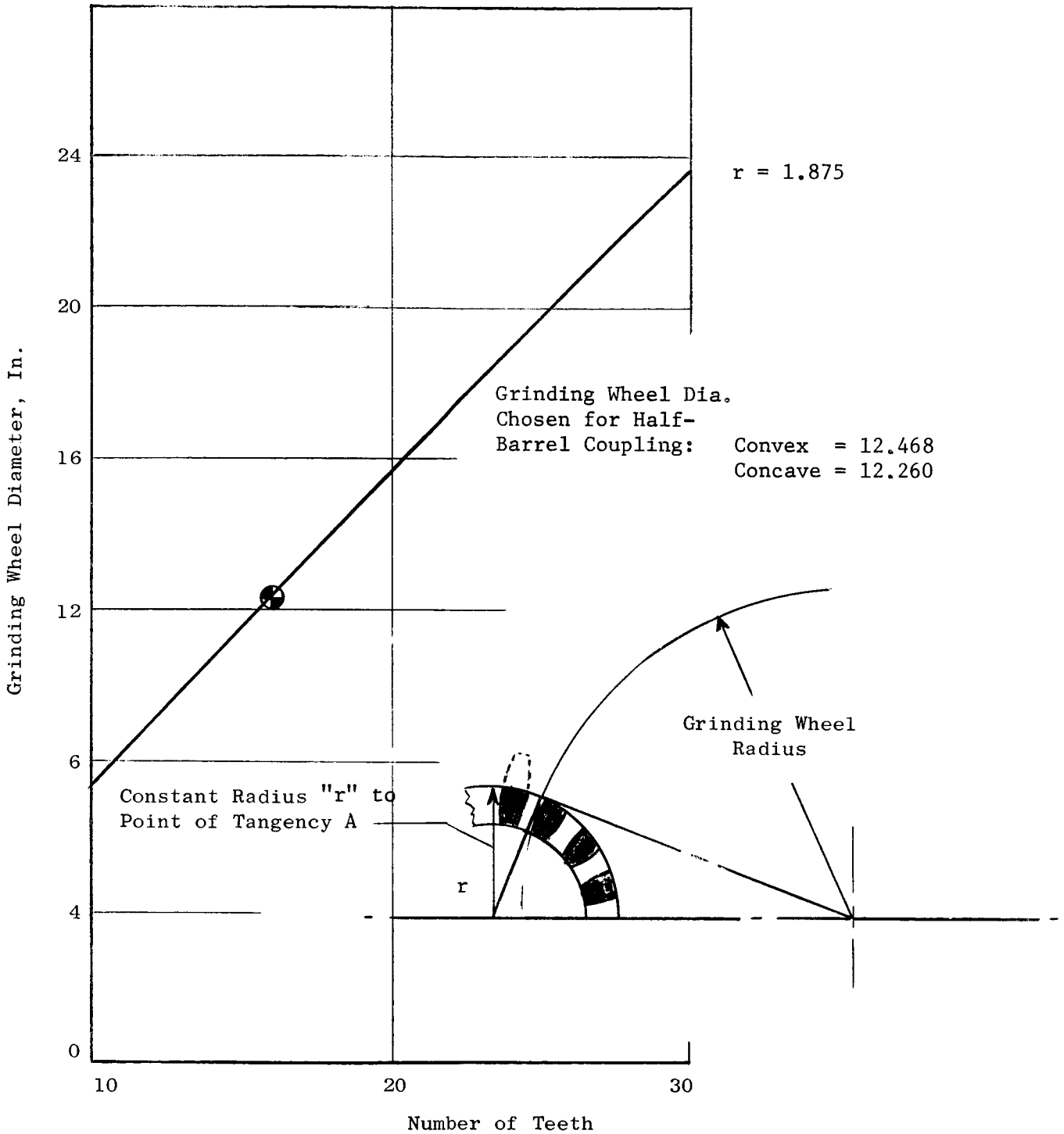

Figure 84. Effect of Number of Teeth on Grinding Wheel Diameter.

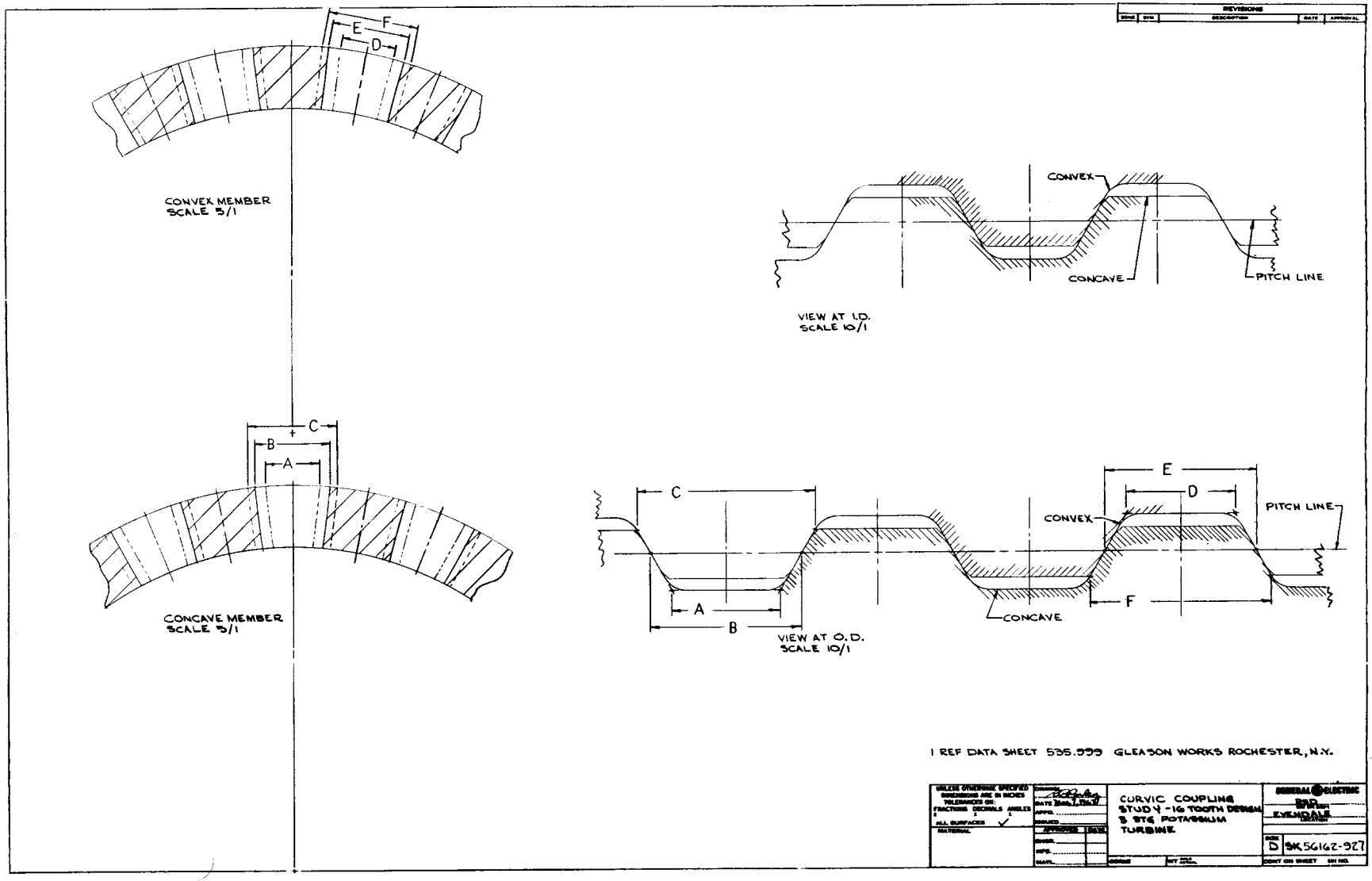

Figure 85. Curvic Coupling Design. (Half-Barrel)

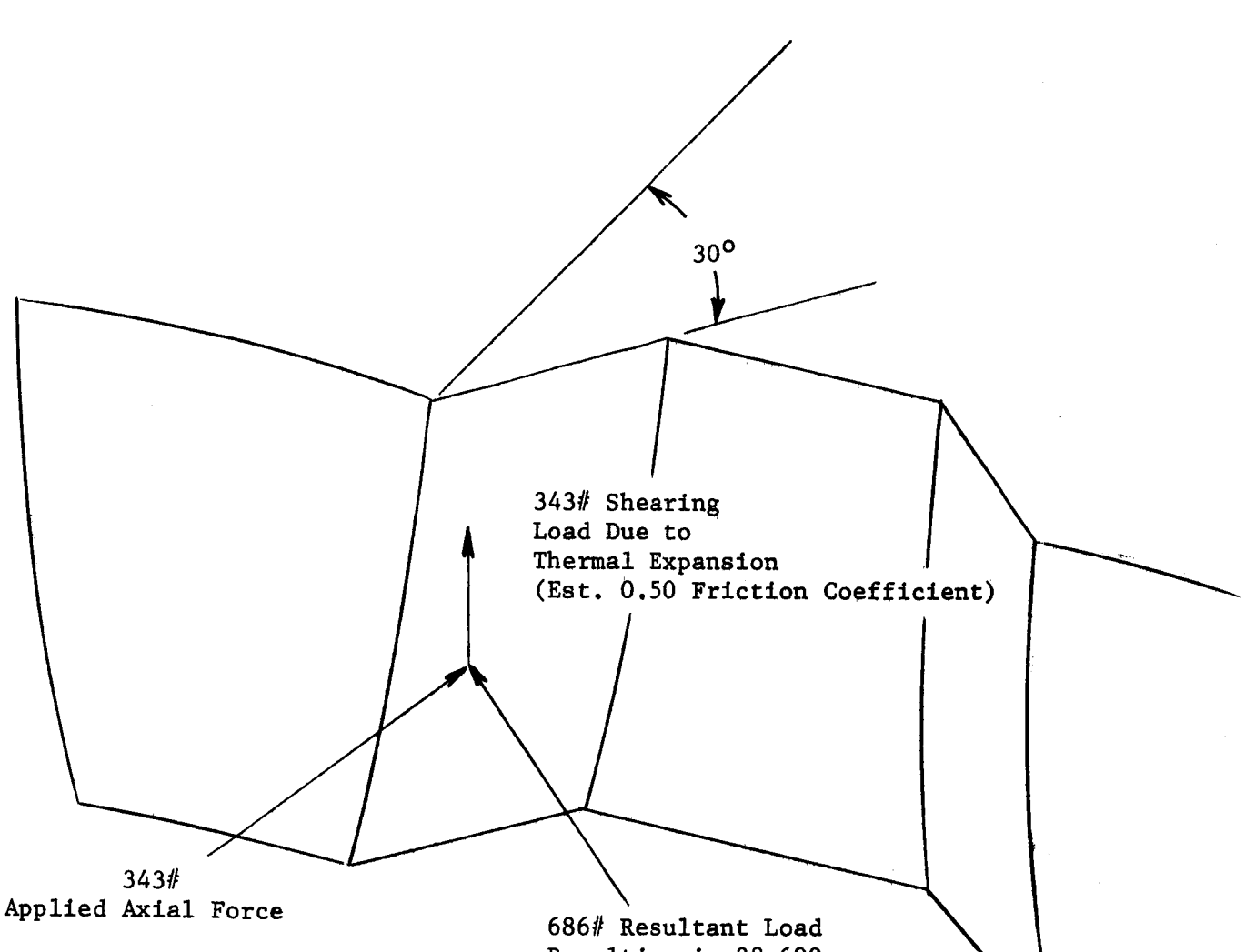

Figure 86. Curvic Coupling Forces.

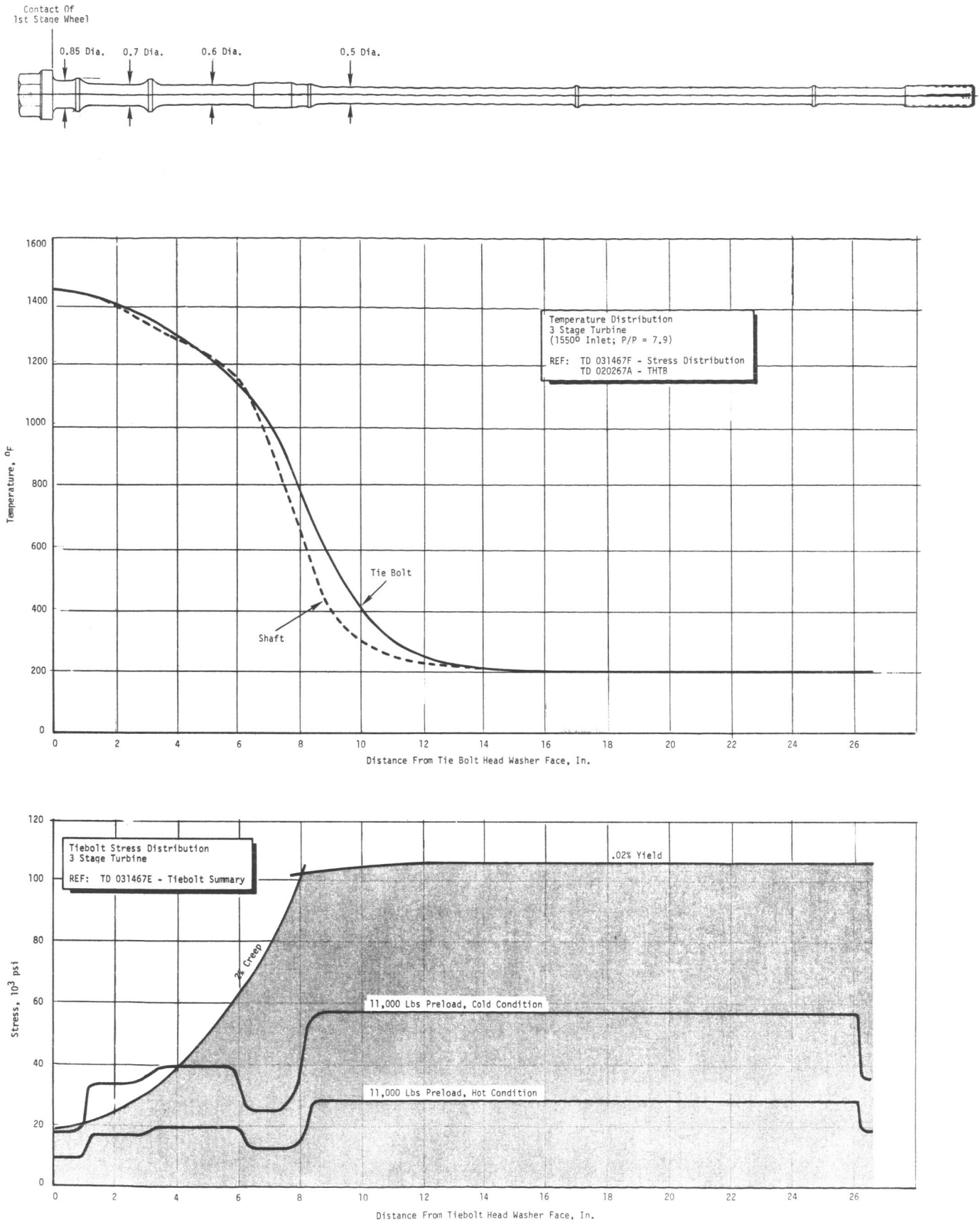

Figure 87. Tie Bolt and Shaft Stress Distribution.

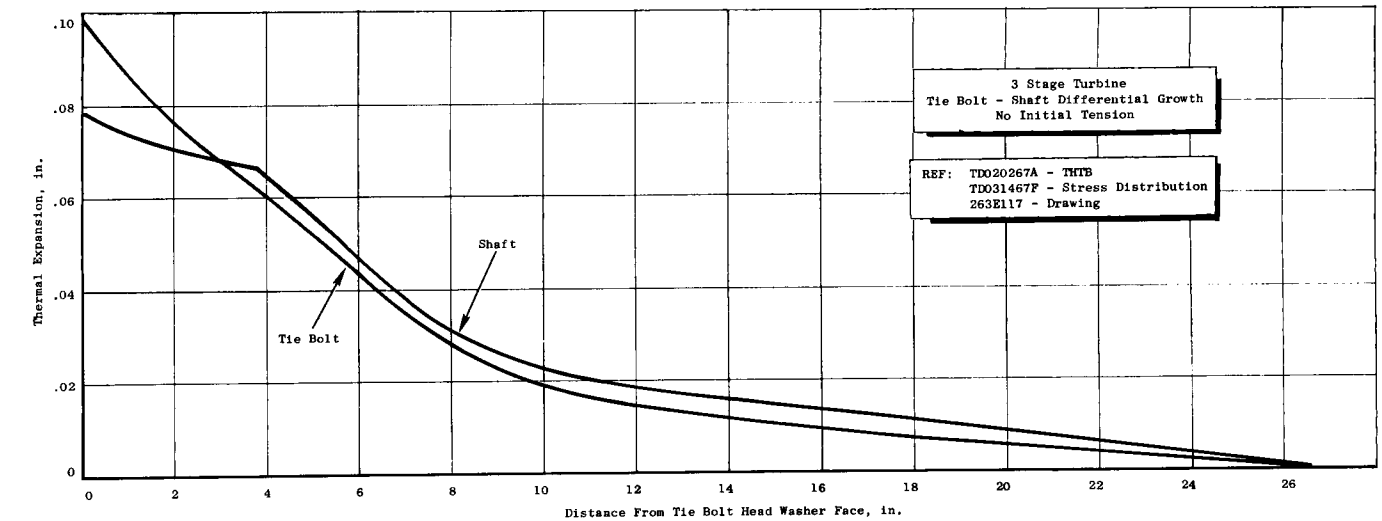

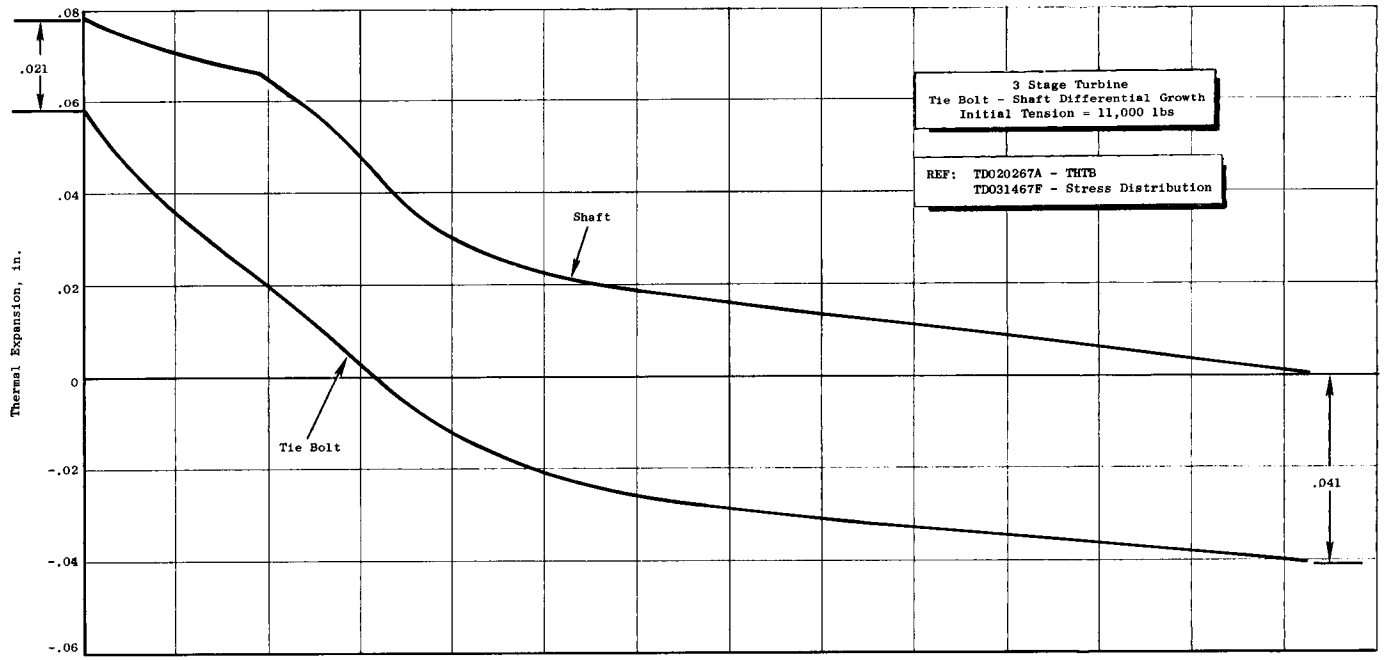

Figure 88. Tie Bolt to Shaft Differential Growth.

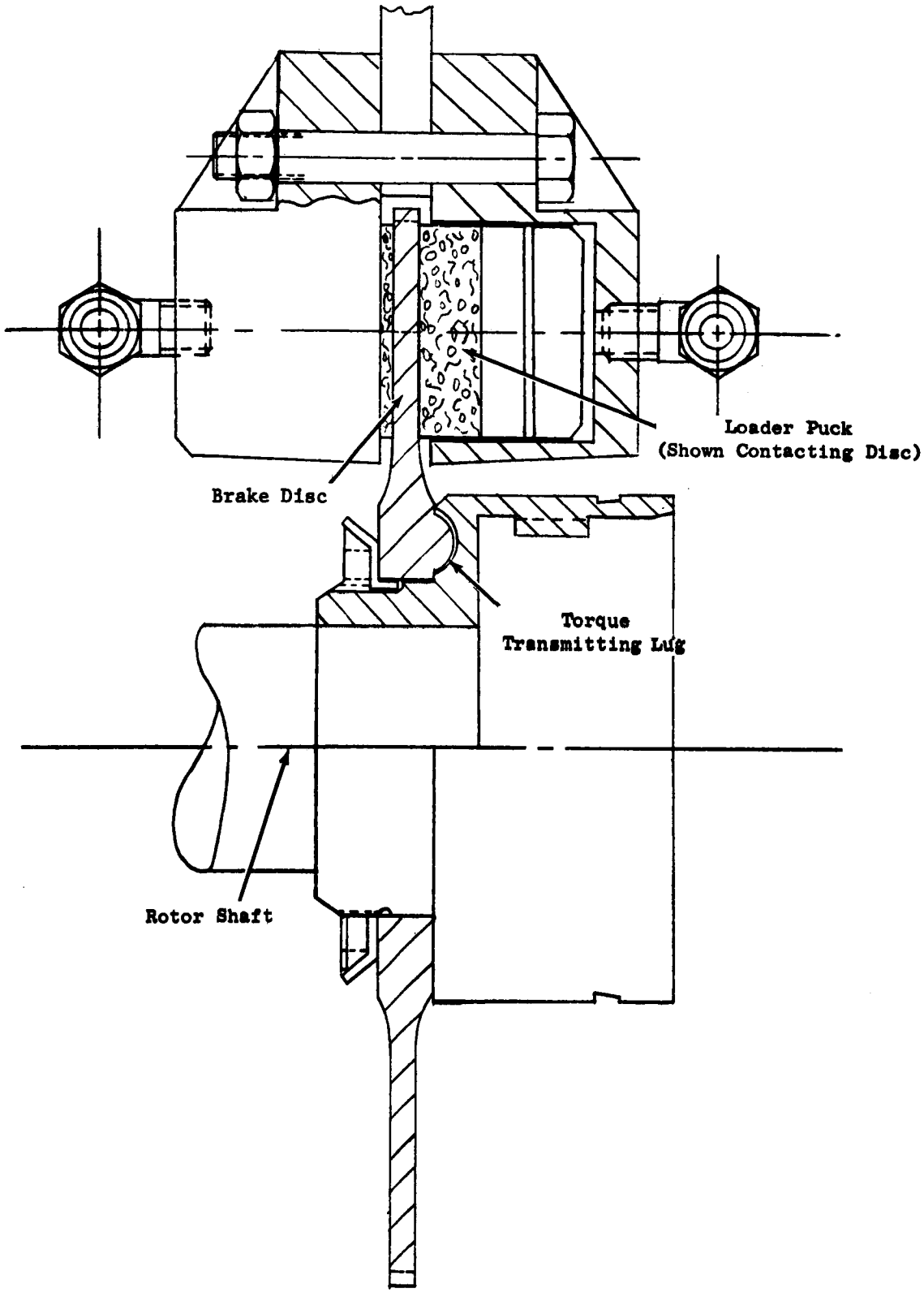

Figure 89. Disc Brake Assembly.

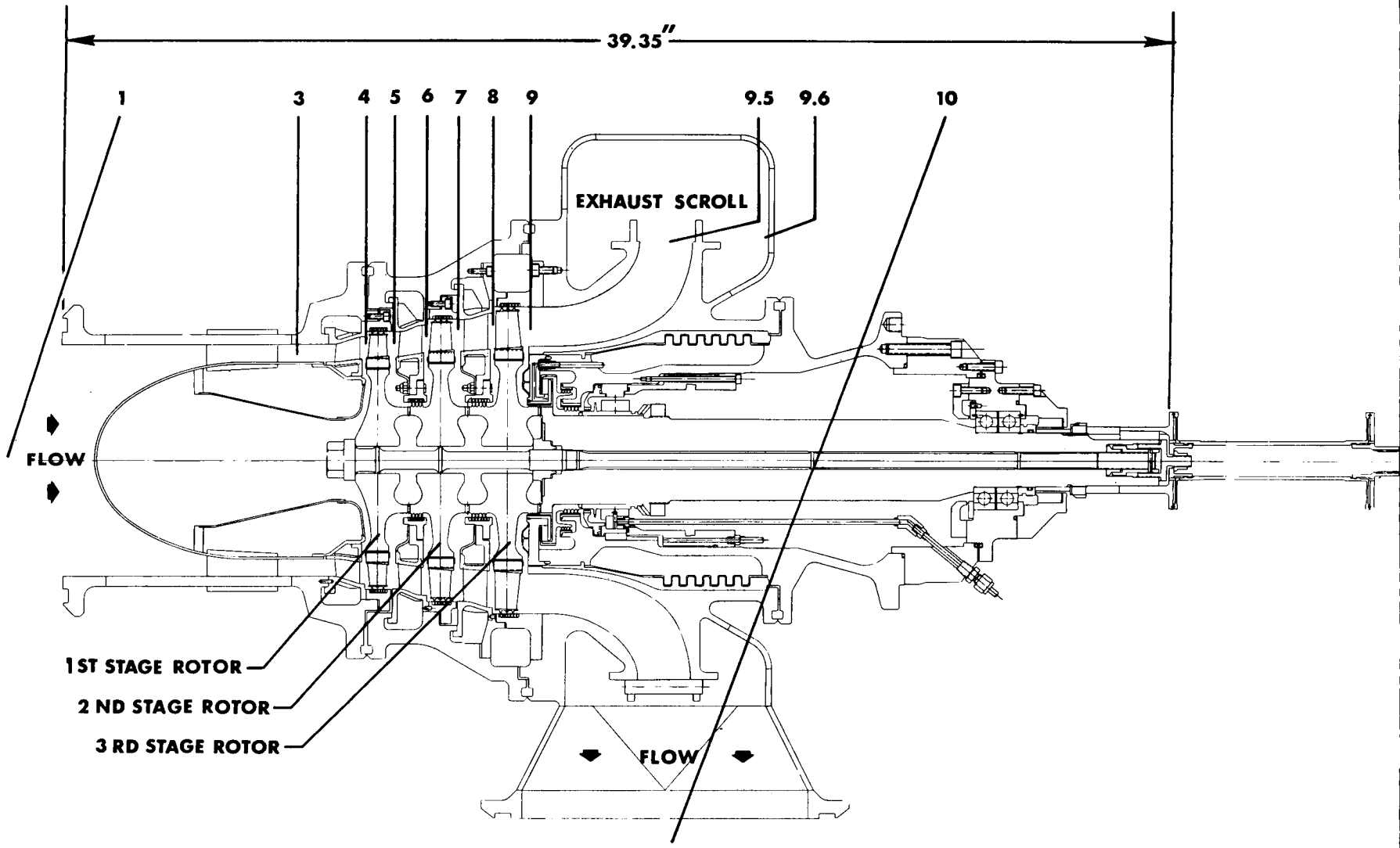

Figure 90a. Instrumentation Stations.

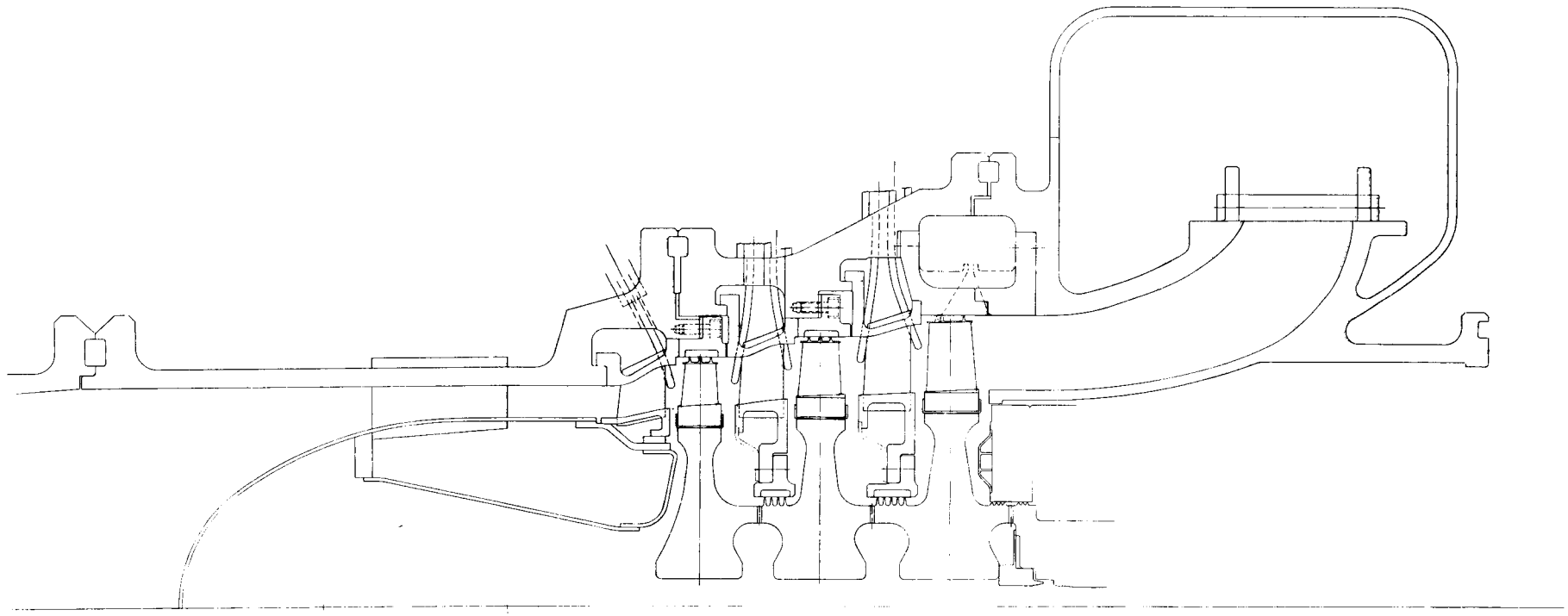

Figure 90b. Turbine Instrumentation.

941D183

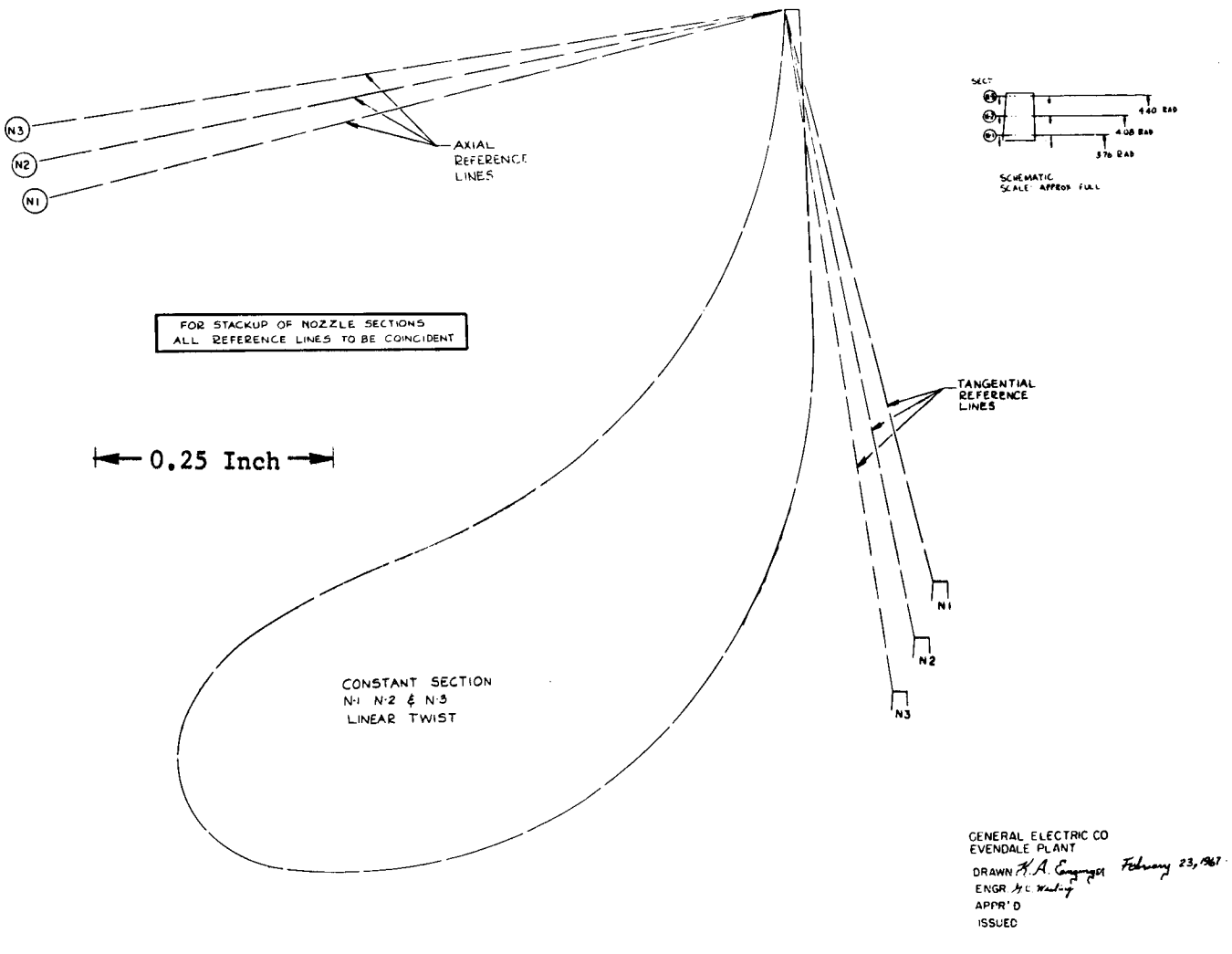

941D183

Figure 92. Stage 1 Nozzle Vane Contour. (Glassine)

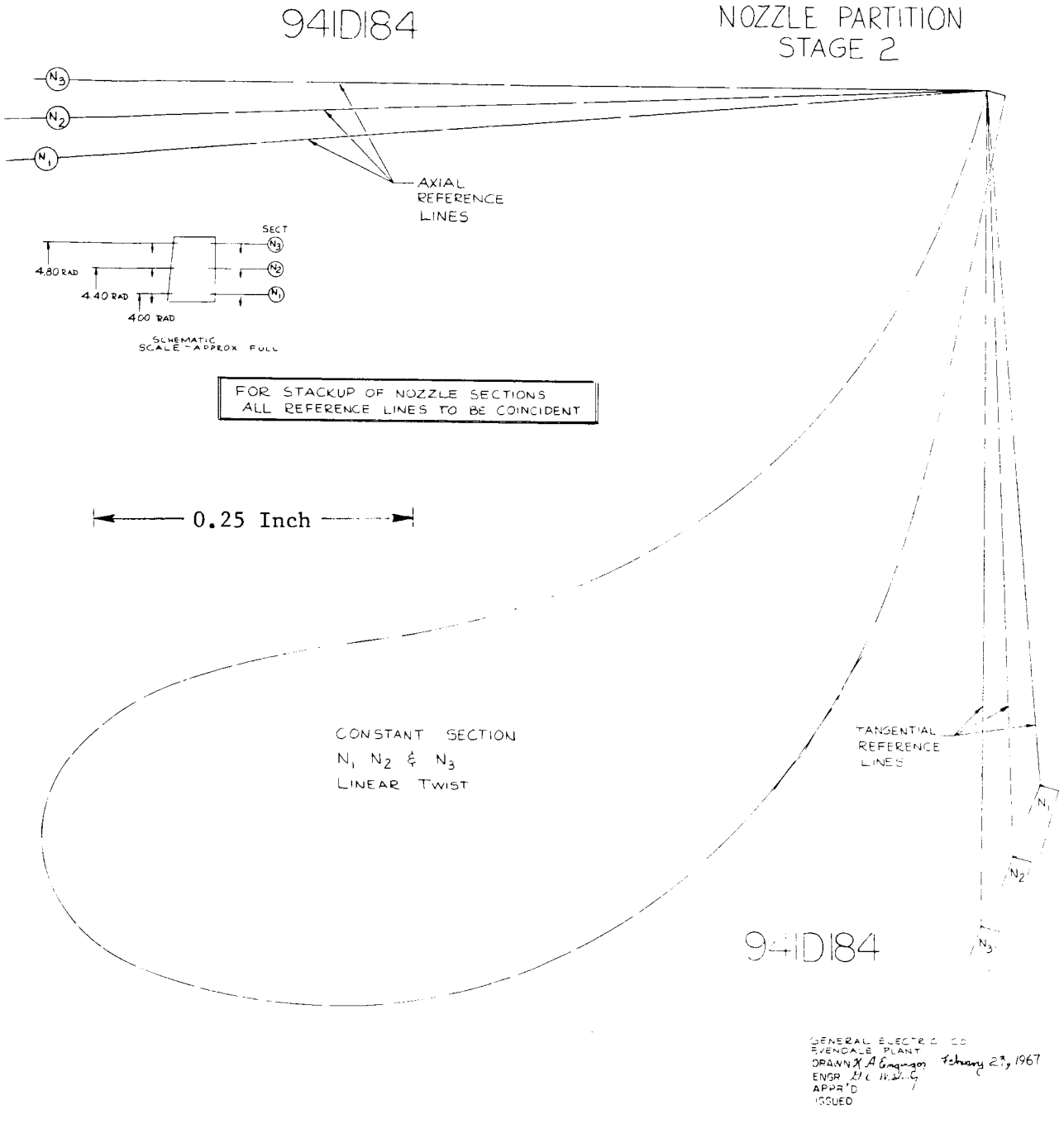

Figure 93. Stage 2 Nozzle Vane Contour. (Glassine)

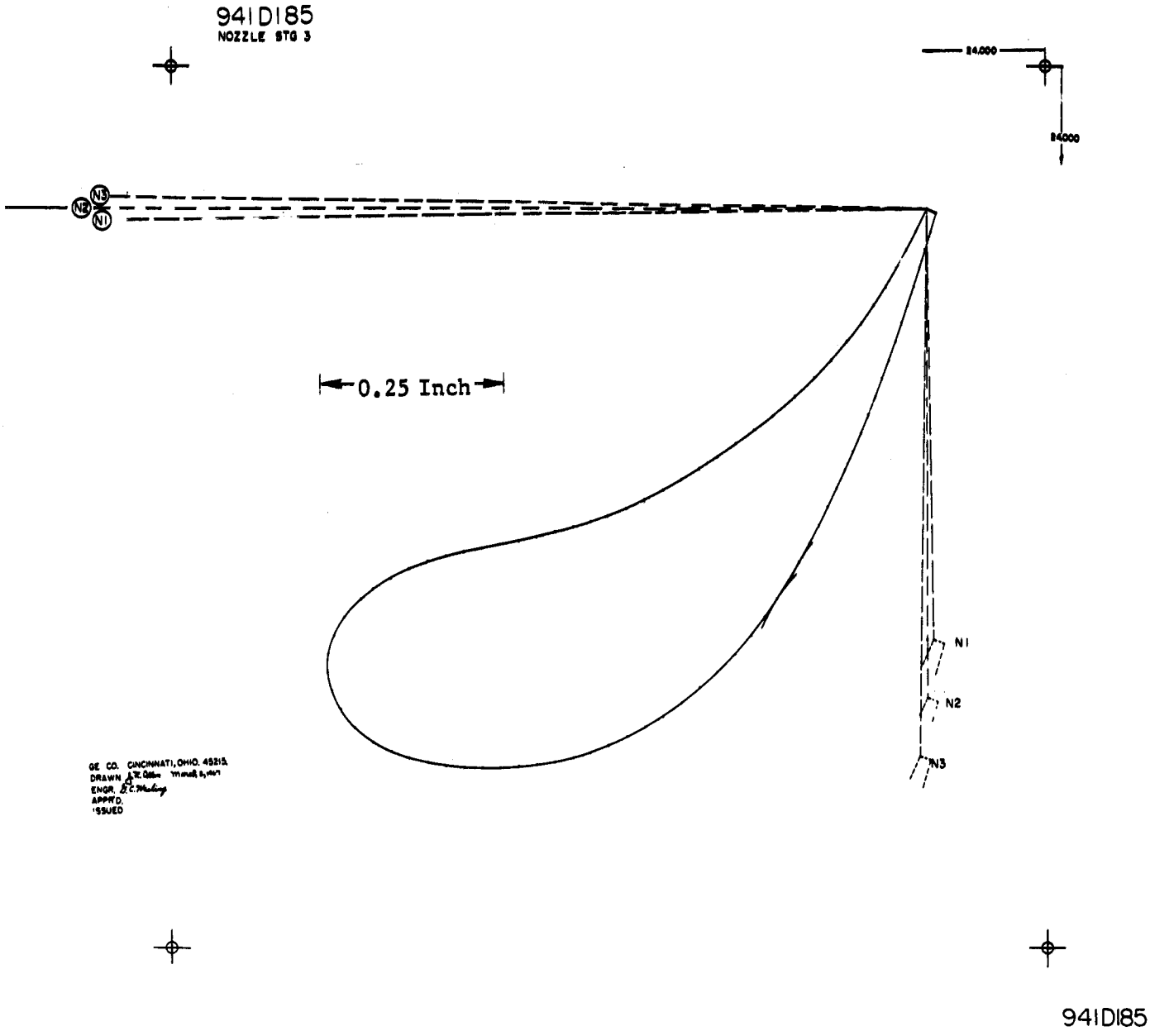

Figure 94. Stage 3 Nozzle Vane Contour. (Glassine)

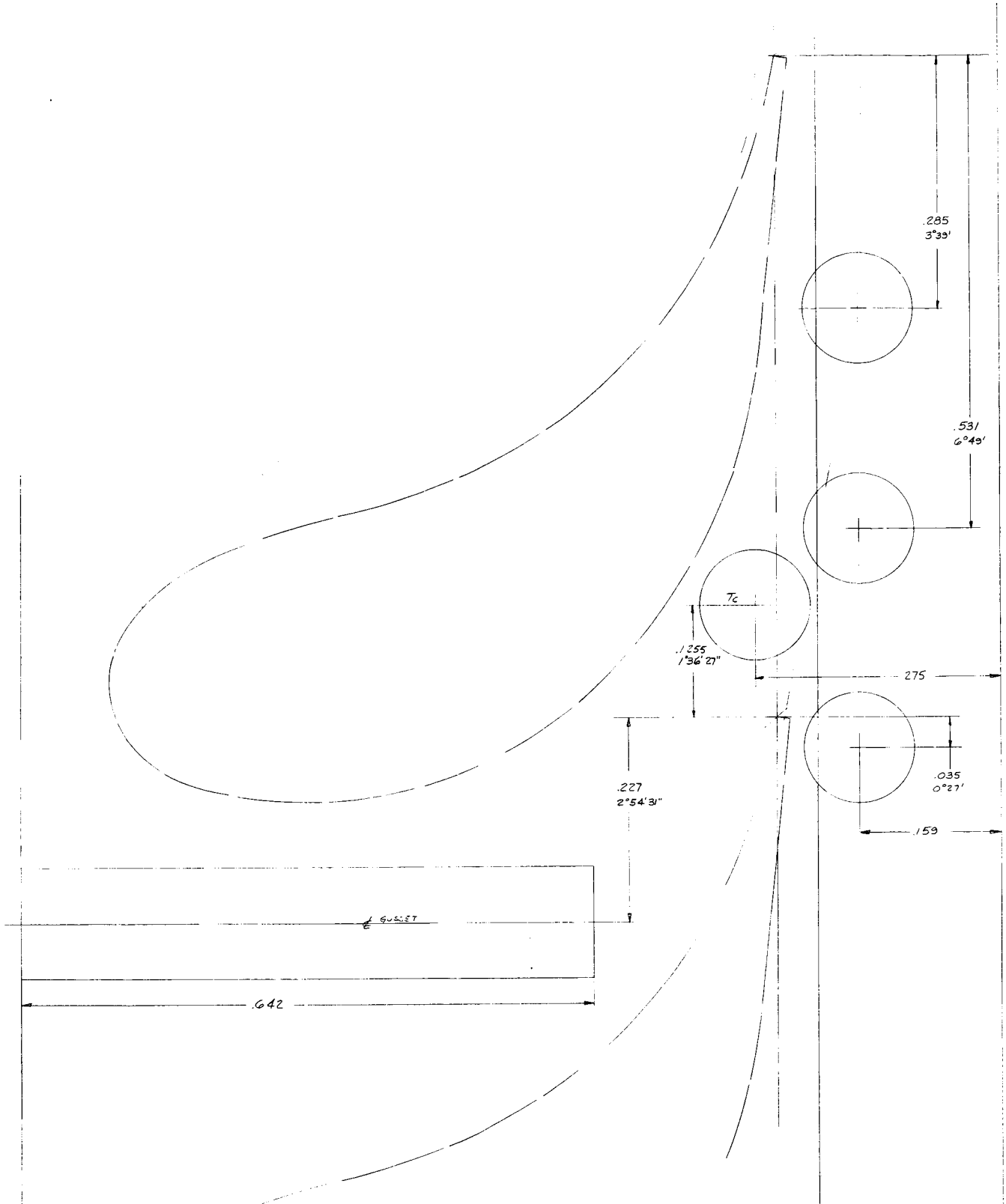

Figure 95. Placement of Pressure - Temperature Instrumentation - Typical (Shown for Stage 1)

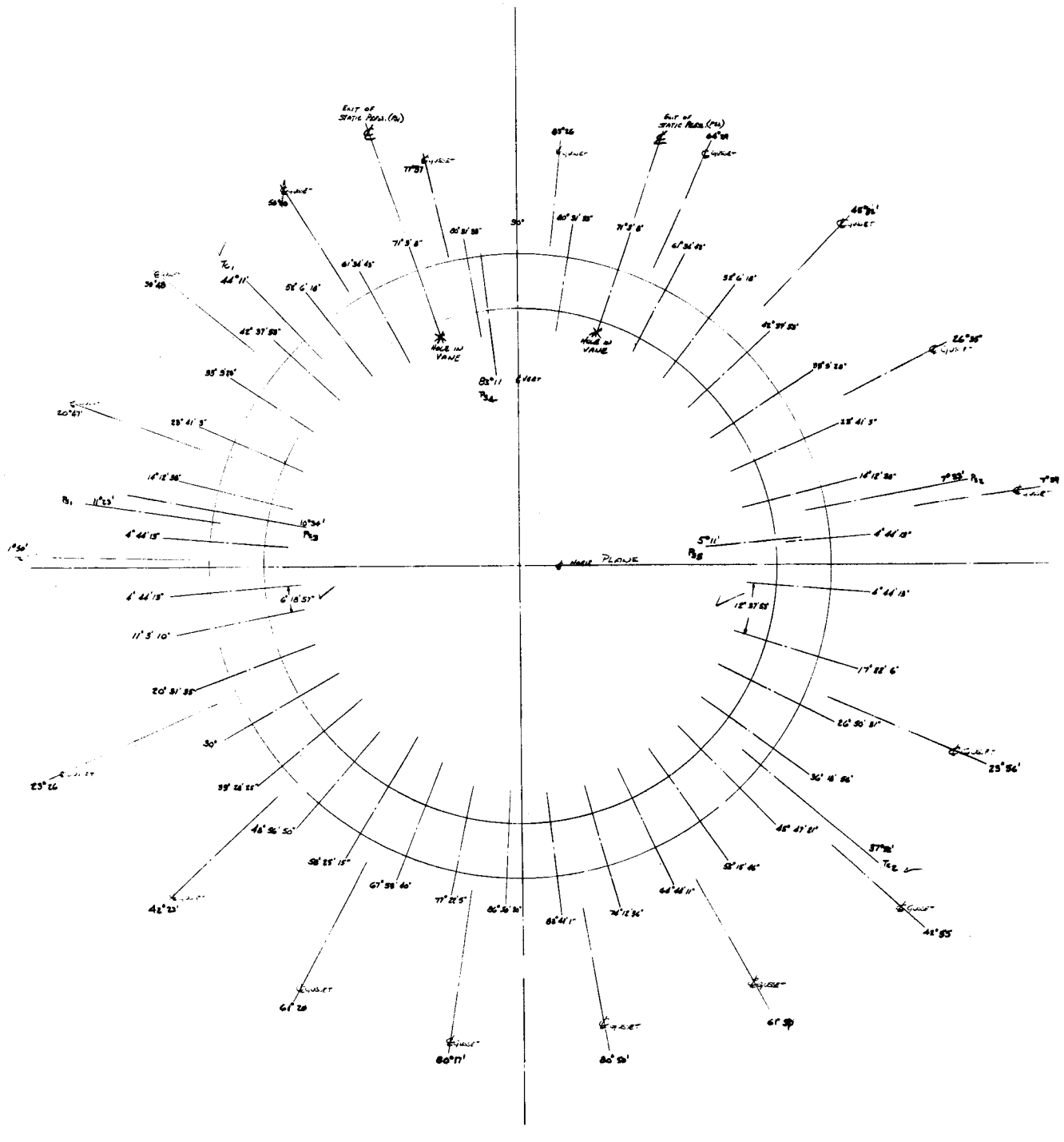

Figure 96. Stage 1 Nozzle Vane Placement.

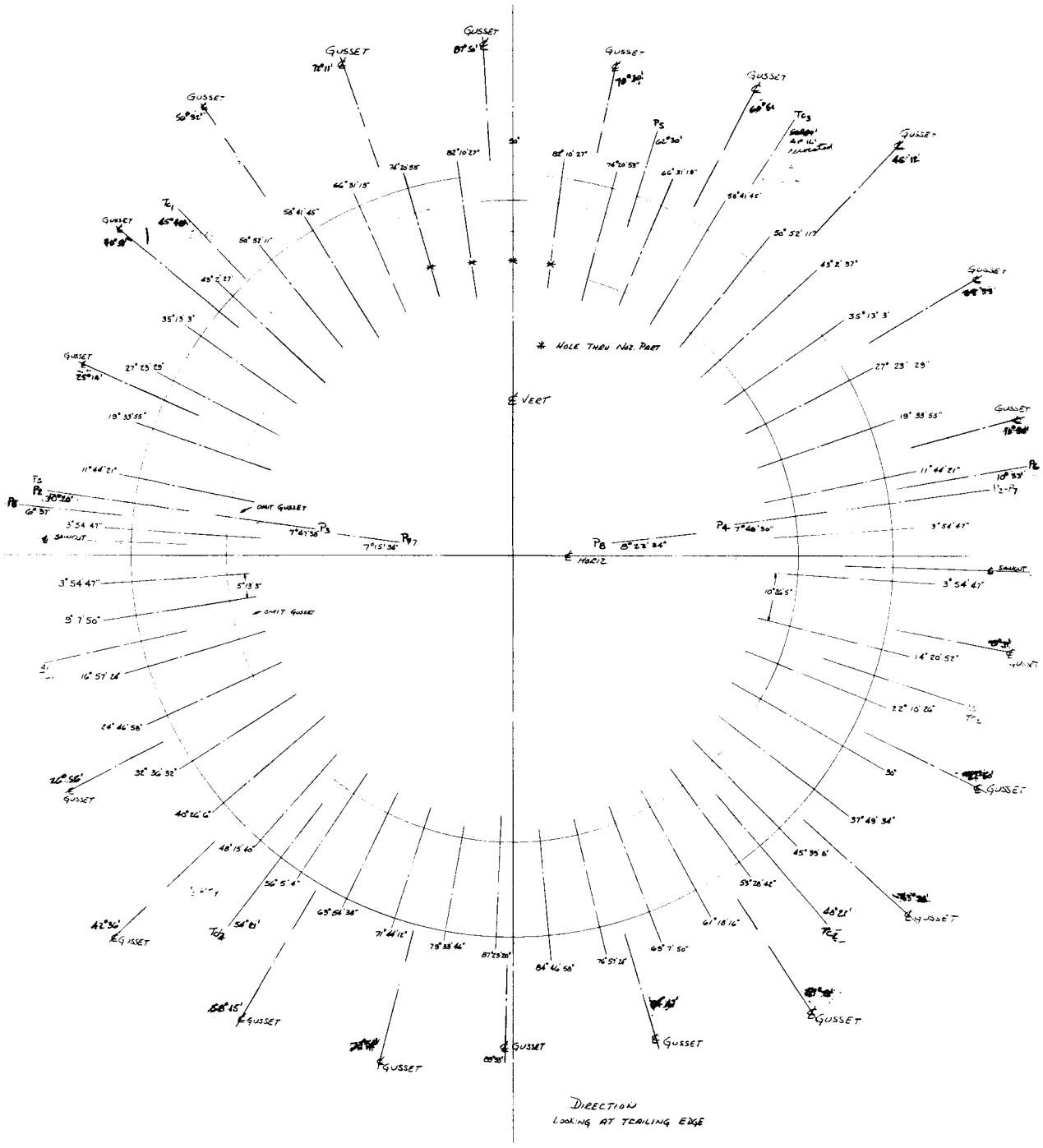

Figure 97. Stage 2 Nozzle Vane Placement.

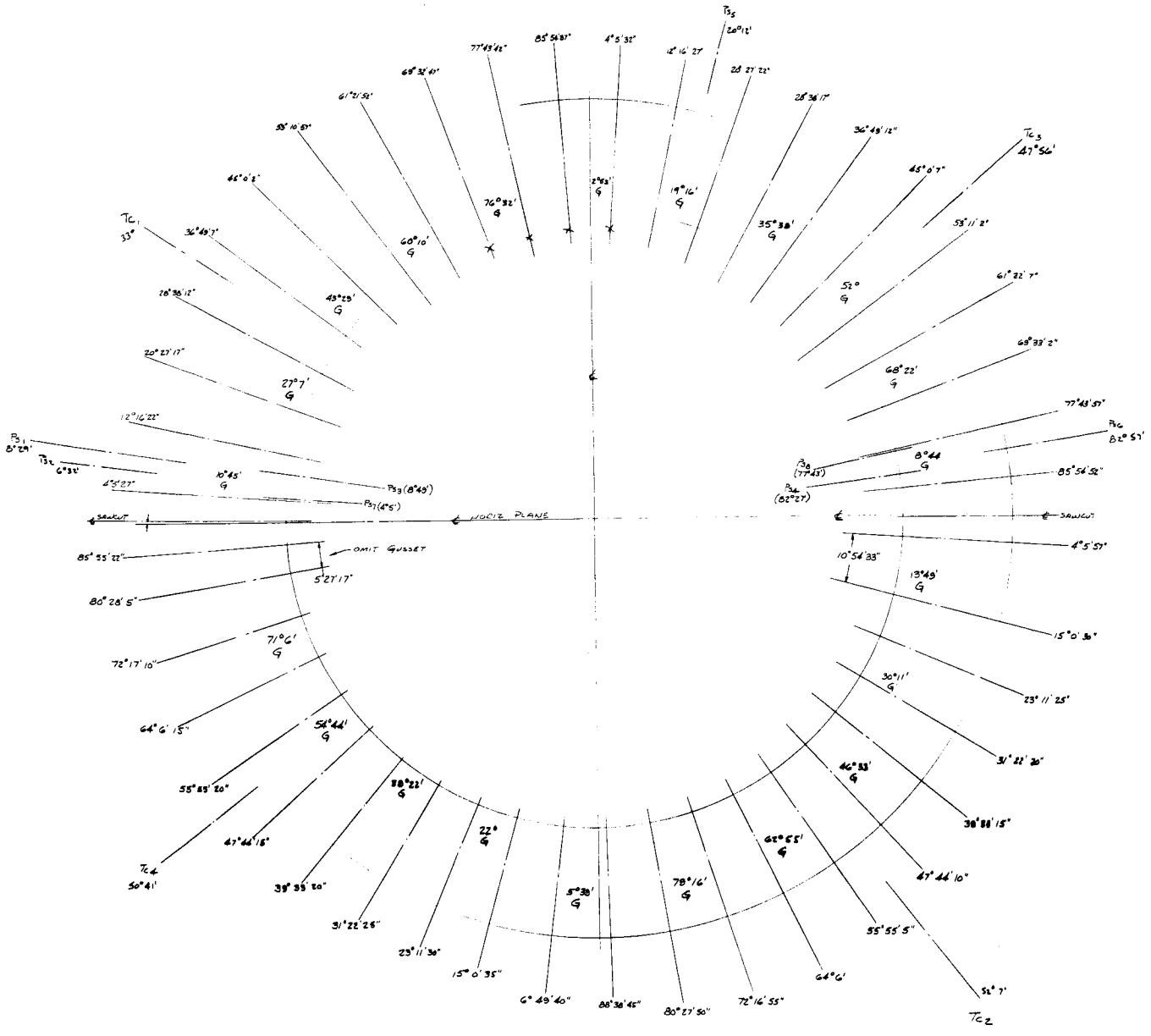

Figure 98. Stage 3 Nozzle Vane Placement.

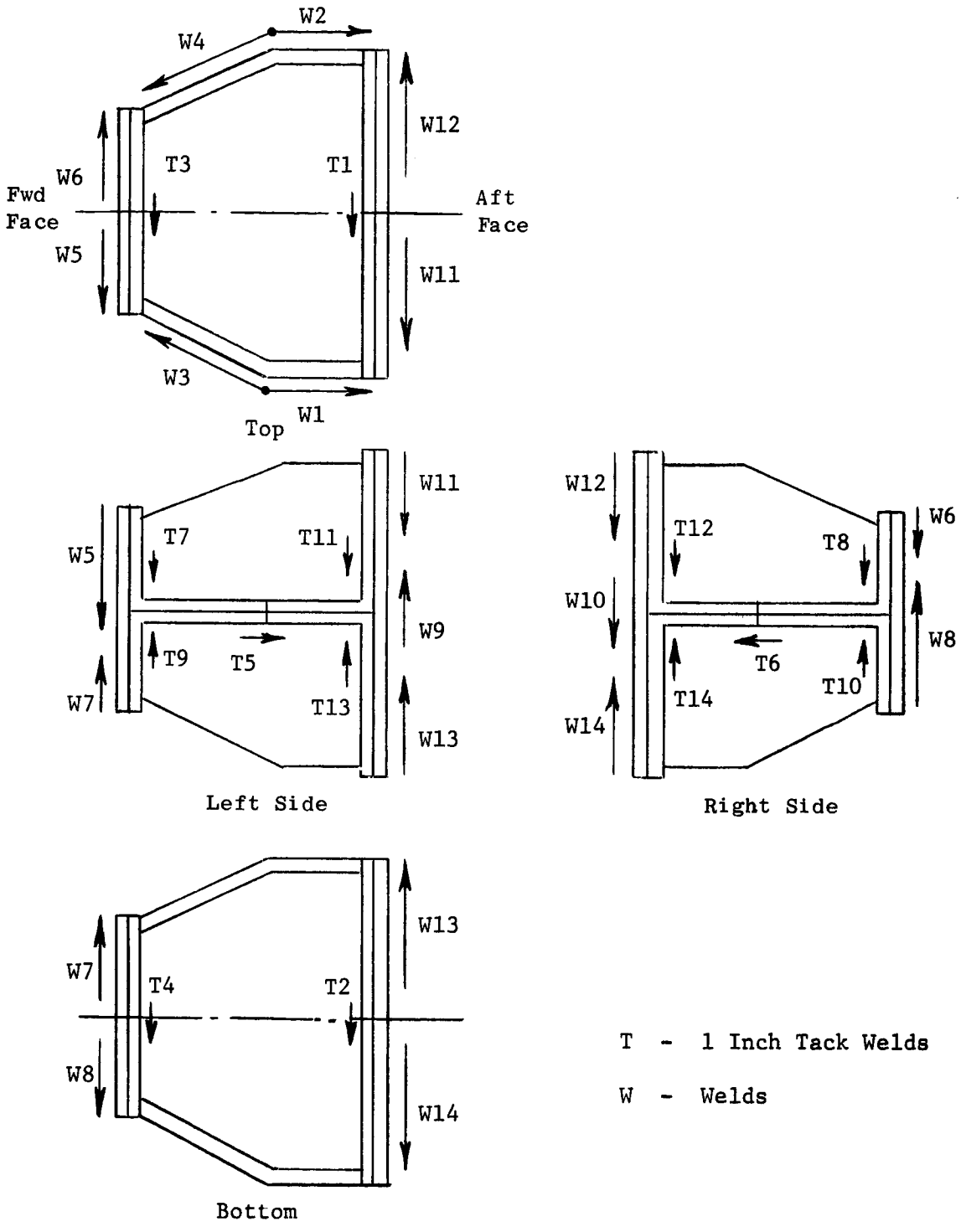

Figure 99a. Turbine Casing, Welding Sequence.

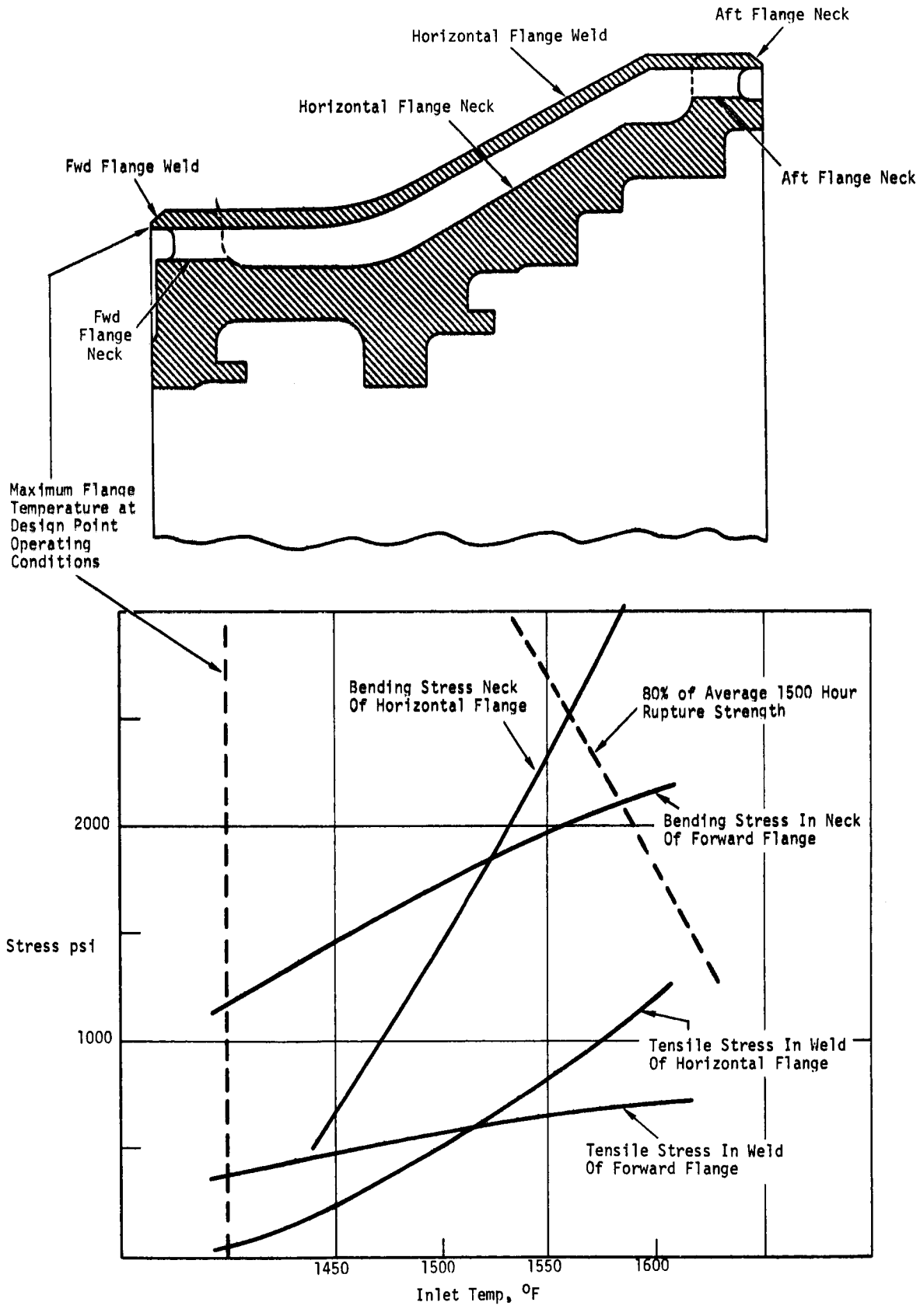

Figure 99b. Stresses in Turbine Casing Flanges.

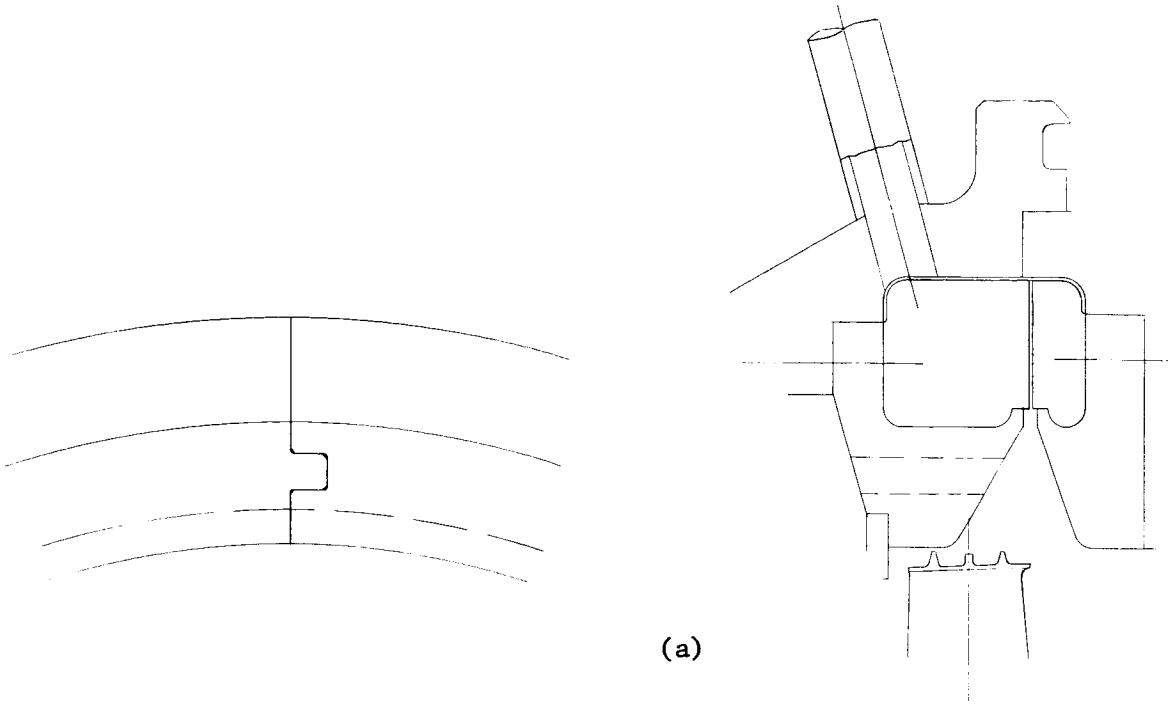

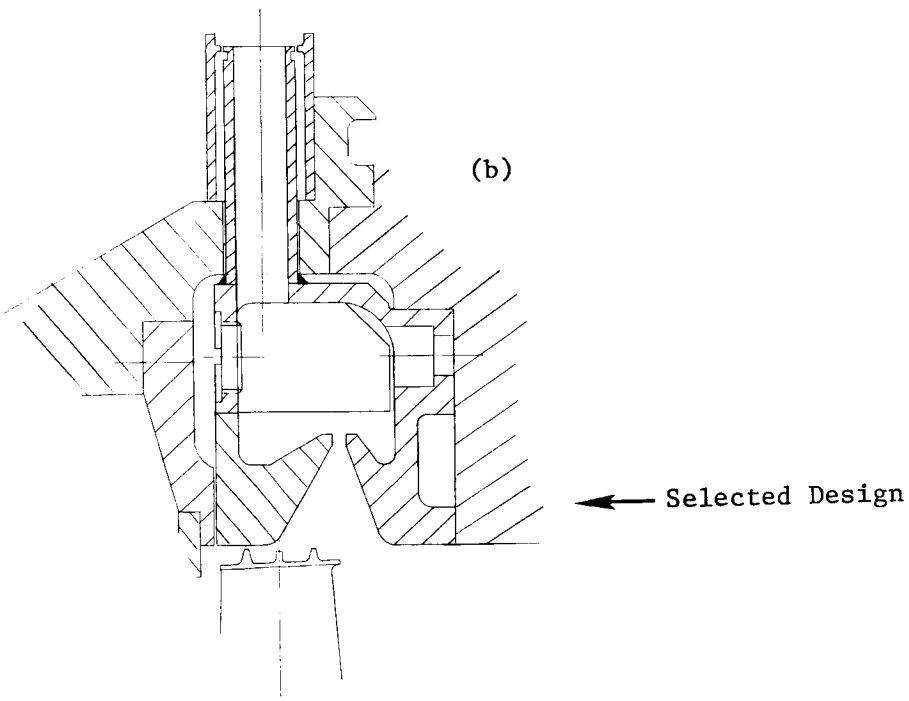

Figure 100. Stage 3 Moisture Extraction Designs. (941D310)

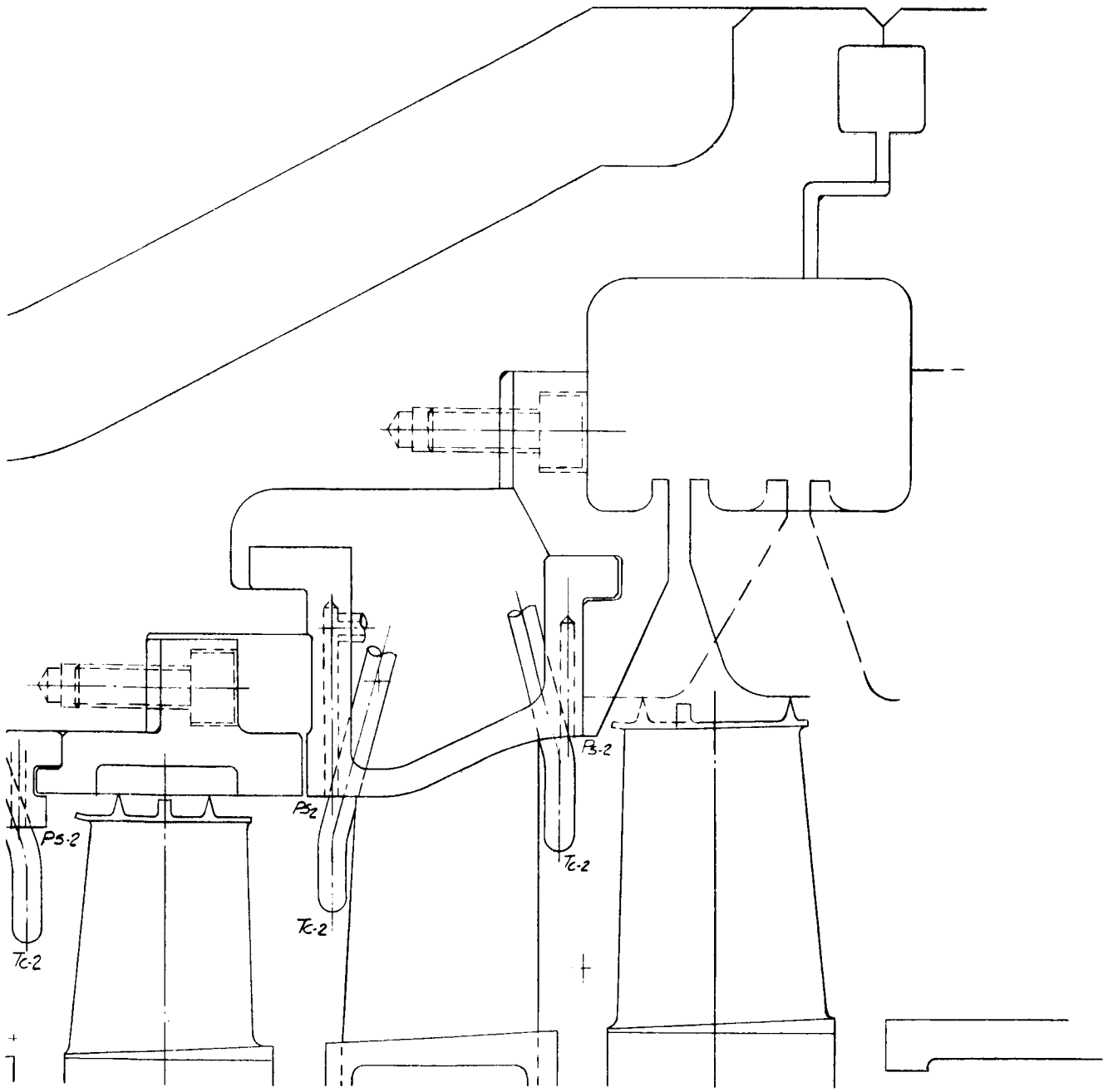

Figure 101. Alternate Design for Extracting Moisture From Leading Edge of Stage 3 Rotor Blades.

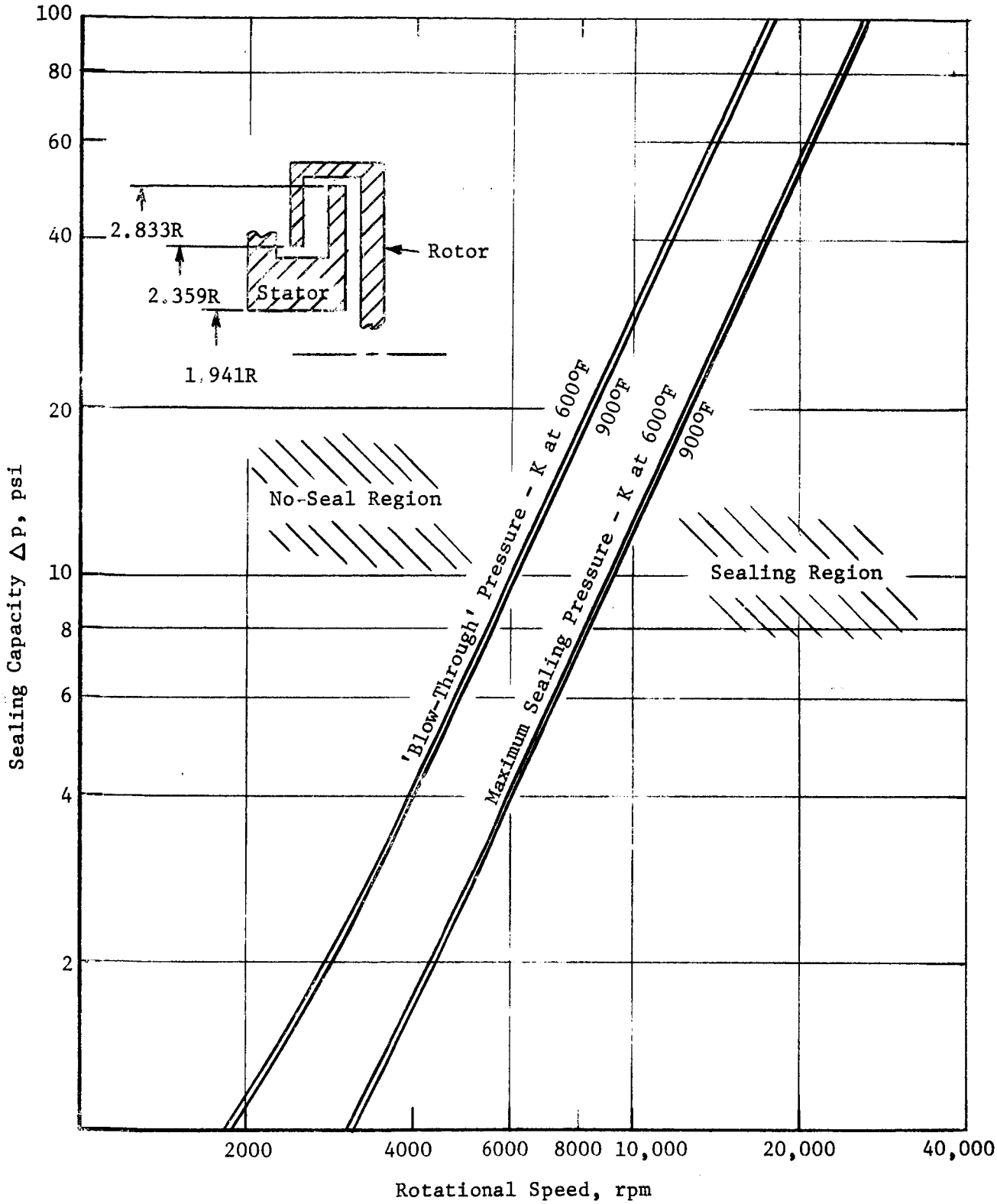

Figure 102. Sealing Capability of 3-Stage Potassium Turbine Hydrodynamic Seal

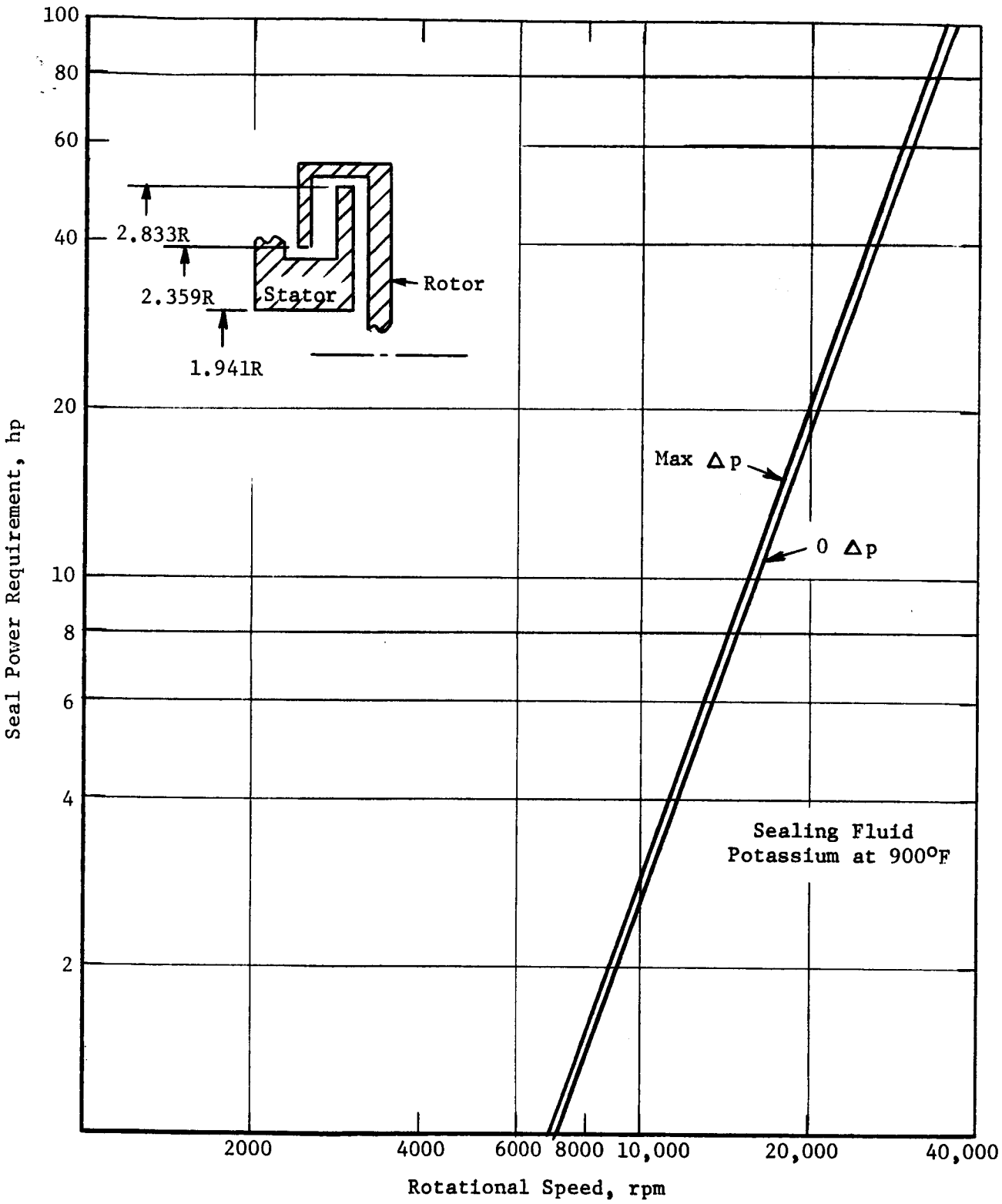

Figure 103. Power Requirements of 3-Stage Potassium Turbine Hydrodynamic Seal.

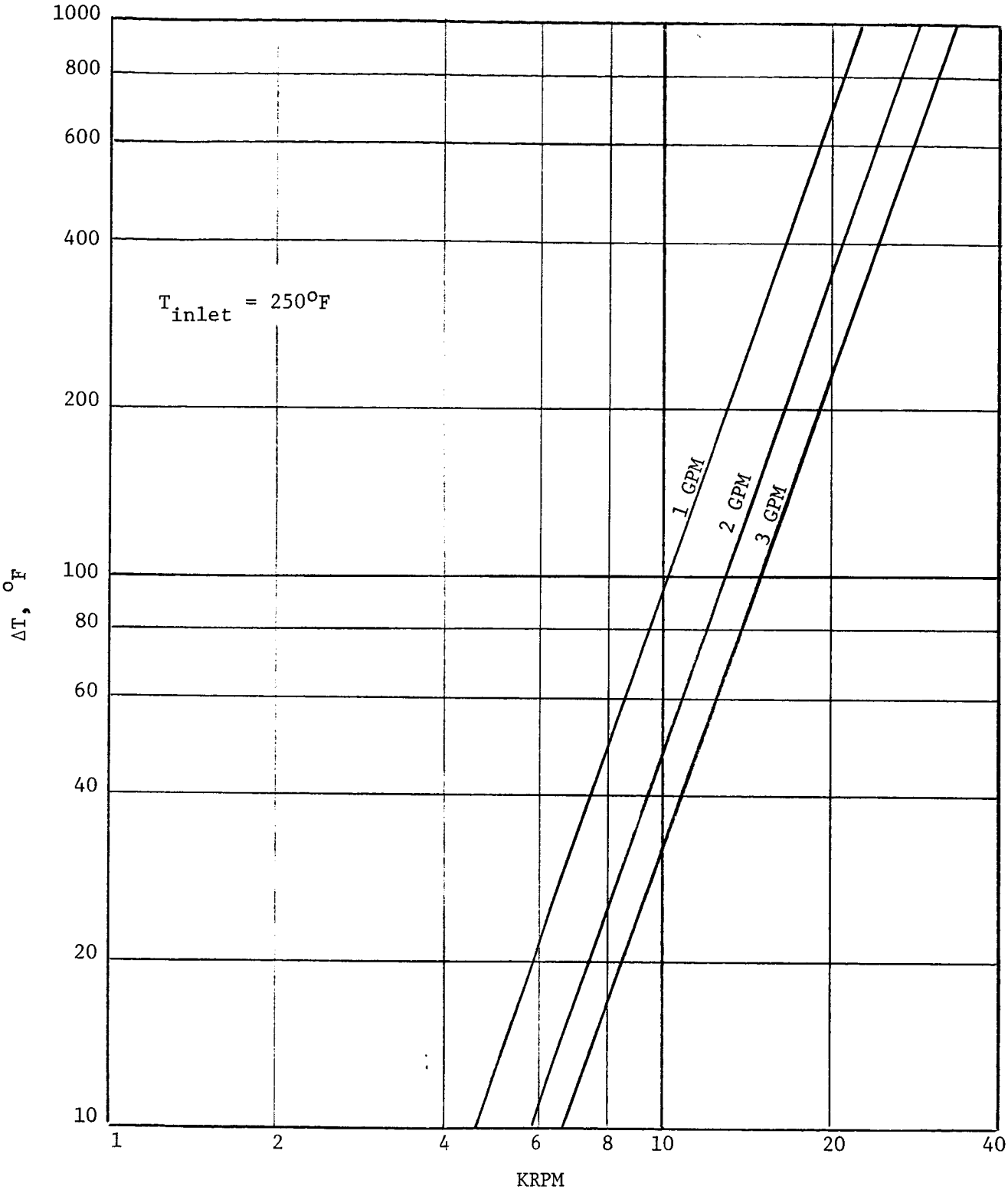

Figure 104. Potassium Temperature Rise for Various Hydrodynamic Seal Flow Rate for 3 Stage Turbine. (See Figure 103) Only Power Absorption for Maximum ΔP Considered.

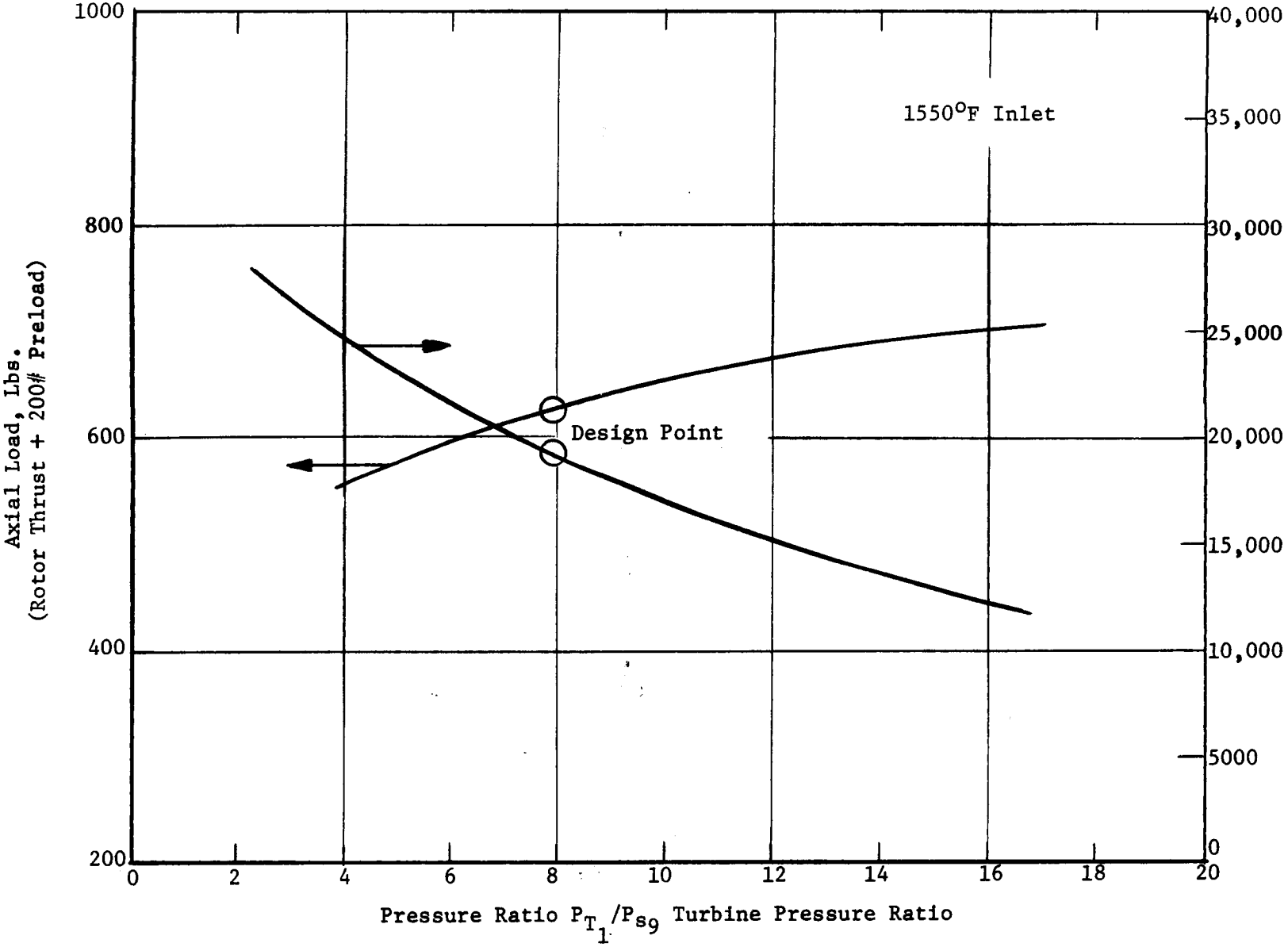

Figure 105. Bearing Axial Load and Life.

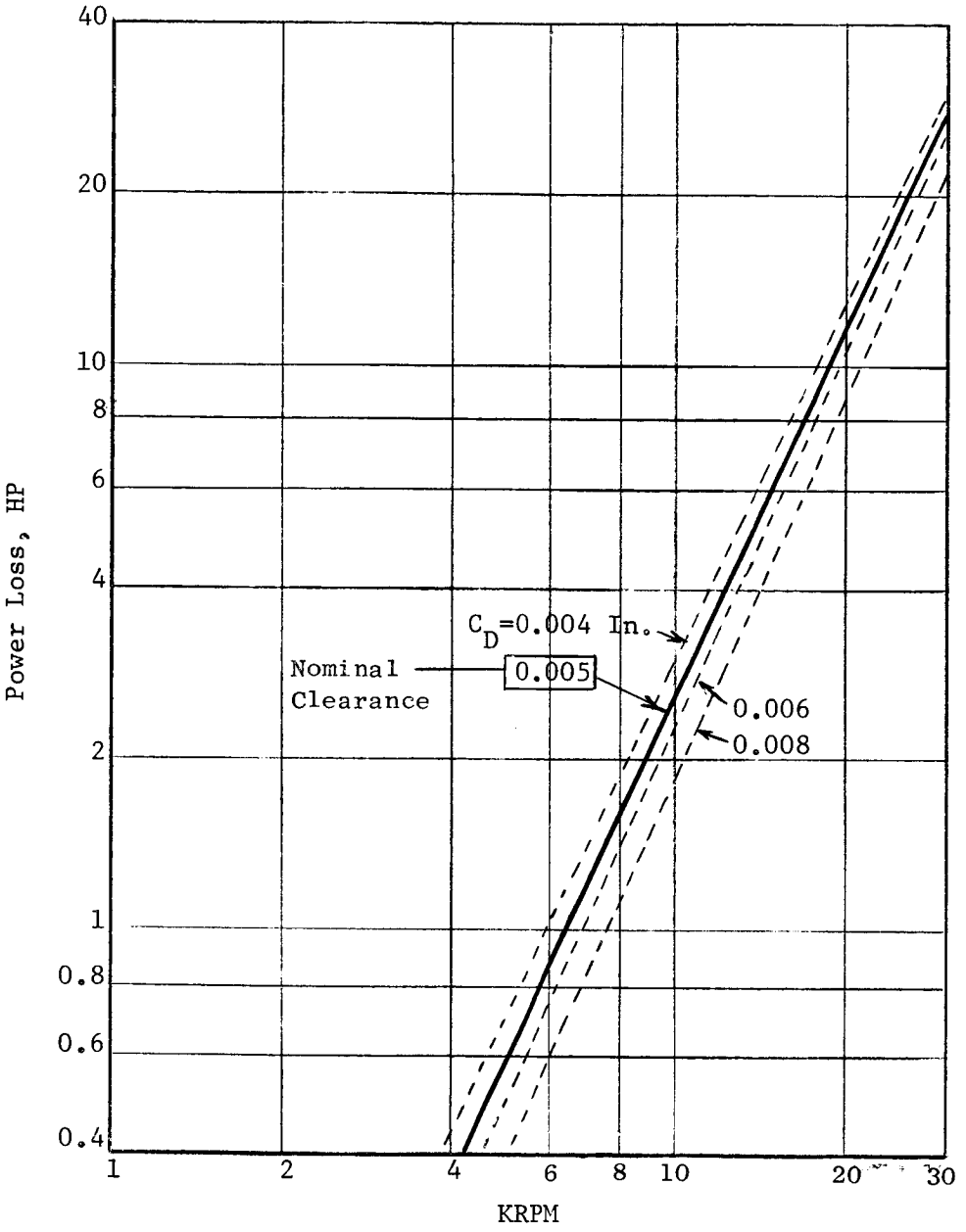

Figure 106. Power Loss of Three-Stage Turbine Pivoted Pad Bearing With Four Diametral Clearance and DTE 797 Oil at 200°F. 0.7 Gm.-In. Unbalance Assumed. (TDC-67-94)

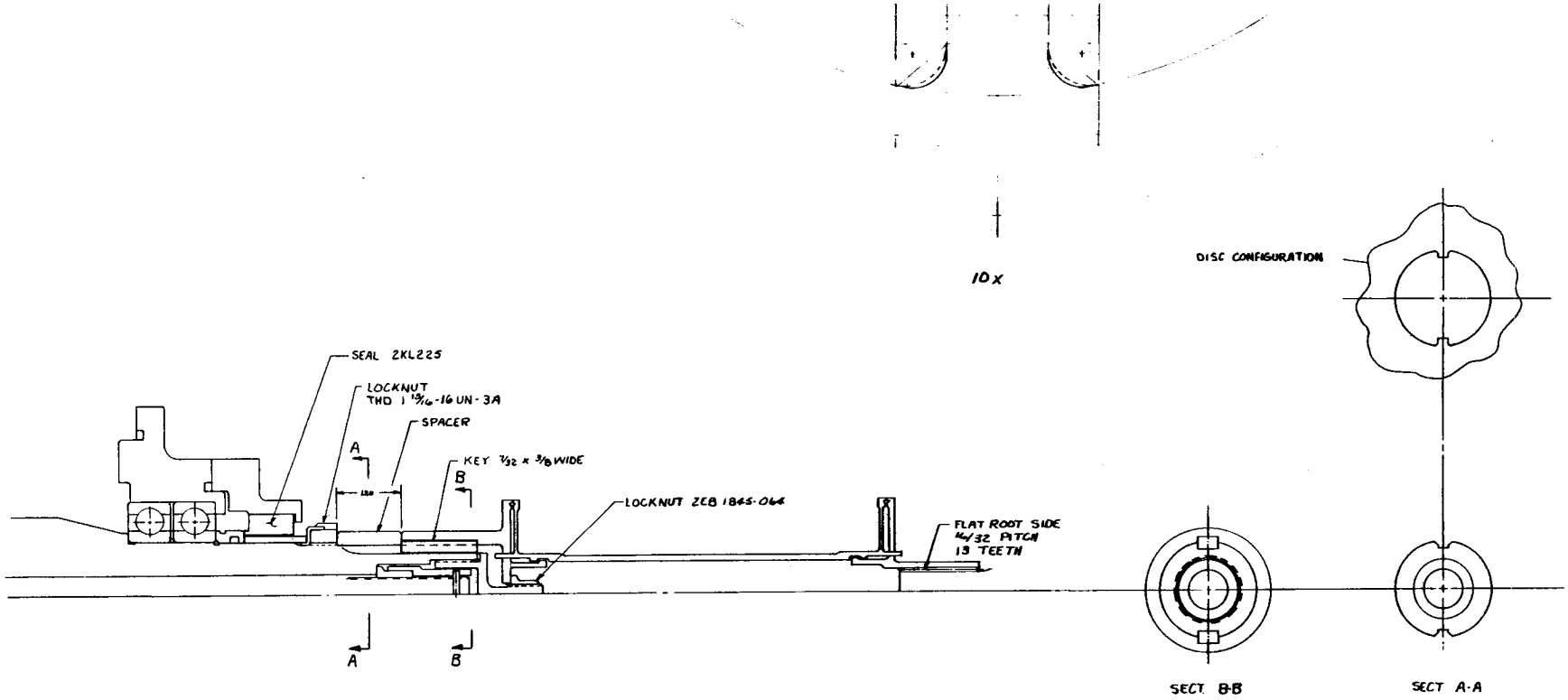

L/O FLEXIBLE COUPLING, 3 STG TURBINE TO WATER BRAKE

GENERAL ELECTRIC
R.S.D.
EVENDALE

941D196

Figure 107. Flexible Membrane Coupling. (941D196)

PAGE 1 OF 4

GENERAL ELECTRIC — SPACE POWER & PROPULSION SECTION, CINCINNATI, OHIO 45215

PARTS LIST (SEE SPPS DRAFTING STANDARD NO. 5703-19)

(A) PARTS LIST NO. 246R670

(B) CODE IDENT. NO. 15226

(C) TITLE 3 STG POTASSIUM TURBINE ASSY

(D) ITEM NO.	(E) ZONE	(F) DWG CODE	(G) IDENTIFICATION NO.	(H) DESCRIPTION/NOMENCLATURE	(I) QTY	(J) SHEET NO.	(K) REV CODE	(L) INTRO REF.
1				ASSY	X			
2	G13		246R657	INLET DUCT	1			
3	G12		246R652	NOZ. DIAH. ASSY	1			
4	G12		246R650	WHEEL	1			
5	G12		246R645	BLADE	62			
6	G12		941D192P1	RETAINER	62			
7	G12		941D191	TIP SEAL	1			
8	G12		47C141464	SHIM	1			
9	G12		941D300P1	BOLT	1			
10	G12		246R653	NOZ. DIAH ASSY	1			
11	G12		941D194P1	INTERSTG. SEAL	1			
12	G12		941D300P5	BOLT	1			
13	B12		246R647	WHEEL	1			
14	B12		246R646	BLADE	52			
15	B12		941D192P2	RETAINER	60			
16	G11		263E112	TIP SEAL	1			
17	G12		941D198	SHIM	1			
18	G11		941D300P2	BOLT	1			
19	G11		246R654	NOZ. DIAH. ASSY	1			
20	G11		941D194P2	INTERSTG SEAL	1			
21	G11		941D300P6	BOLT	1			
22	B11		246R667	WHEEL	1			
23	B11		246R673	BLADE	44			
24	B11		941D192P3	RETAINER	52			
25	G11		941D305	TIP SEAL ASSY	1			
26	G11		941D300P4	BOLT	1			
27	G11		263E114	CLAMPING RING	1			
28	G11		941D199	SHIM	1			

(M) DRAWING CODES
1. VENDOR ITEM - SPEC CONT DWG
2. VENDOR ITEM - SOURCE CONT DWG
3. ALTERED PART
4. CUSTOMER FURNISHED PART
5. CATALOG ITEM

(N) REVISION CODES
1. ITEM ADDED
2. ITEM DELETED
3. QTY CHGD
4. IDENT. NO. CHGD.
5. IDENT NO. & QTY CHGD
6. EDIT CORRECTION

(O) CONTRACT NO.

(P) PREPARED BY W. A. Huddleston

(Q) ISSUED BY

(R) DATE ISSUED

(S) REVISION AUTHORITY

(T) DISTRIBUTION CODE

PAGE 2 OF 4

GENERAL ELECTRIC — SPACE POWER & PROPULSION SECTION, CINCINNATI, OHIO 45215

PARTS LIST (SEE SPPS DRAFTING STANDARD NO. 5703-19)

(A) PARTS LIST NO. 246R670

(B) CODE IDENT. NO. 15226

(C) TITLE

(D) ITEM NO.	(E) ZONE	(F) DWG CODE	(G) IDENTIFICATION NO.	(H) DESCRIPTION/NOMENCLATURE	(I) QTY	(J) SHEET NO.	(K) REV CODE	(L) INTRO REF.
29	G11	5	941D300P3	BOLT	1			
30	G12	5	LH3830-02	NUT	16			
31	B12		246R671	CASING	1			
32	F9		246R651	SCROLL	1			
33	F9		263E105	BRG. HSG ASSY	1			
34	B7		263E118	SHAFT	1			
35	B11		941D170	SLEEVE	1			
36	B11		47C141474G1	SEAL-CHEVRON	1			
37	B11		47C141465P1	O-RING	1			
38	B11		47C140248	PAD BRG ASSY	1			
39	B11		941D168	FWD BRG RETAINER	1			
40	B11		47C141465P2	O-RING	1			
41	F9		263E892	AFT BRG RETAINER	1			
42	F9		47C141465P3	O-RING	2			
43	F9		941D300P7	BOLT	1			
44	B9	1 THRU 3	142B1487G1	TUBE ASSY	2			
45	B9		142B1487G2	TUBE ASSY	2			
46	B9		142B1487G3	TUBE ASSY	1			
47	B9		47C141473P1	FEEDTHRU	4			
48	B9		47C141465P4	O-RING	4			
49	F9		142B1489	BELLEV. WASHER	2			
50	F9		941D175	LOCKNUT	1			
51	F8		263E127	SUMP HSG	1			
52	F8		941D300P8	BOLT	1			
53	B9		47C141465P5	O-RING	1			
54	B8		47C141465P6	O-RING	1			
55	F8		142B1491P1	SHIM	1			

(M) DRAWING CODES
1. VENDOR ITEM - SPEC CONT DWG
2. VENDOR ITEM - SOURCE CONT DWG
3. ALTERED PART
4. CUSTOMER FURNISHED PART
5. CATALOG ITEM

(N) REVISION CODES
1. ITEM ADDED
2. ITEM DELETED
3. QTY CHGD
4. IDENT. NO. CHGD.
5. IDENT NO. & QTY CHGD
6. EDIT CORRECTION

(O) CONTRACT NO.

(P) PREPARED BY W. A. Huddleston

(Q) ISSUED BY

(R) DATE ISSUED

(S) REVISION AUTHORITY

(T) DISTRIBUTION CODE

Figure 108. Three Stage Turbine Parts List.

PAGE 3 OF 4

GENERAL ELECTRIC
SPACE POWER & PROPULSION SECTION
CINCINNATI, OHIO 45215

PARTS LIST
SEE GPPS DRAFTING STANDARD NO. GTSD-140

(A) PARTS LIST NO. 246R670

(B) CODE IDENT. NO. 15226

(C) TITLE

(D) ITEM NO.	(E) ZONE	(F) DRG CODE	(G) IDENTIFICATION NO.	(H) DESCRIPTION/NOMENCLATURE	(I) QTY	(J) SHEET NO.	(K) REV CODE	(L) INTRO REF.
56	F8		263E107	THRUST BRG. HSG	1			
57	F8		941D300P9	BOLT	1			
58	F8		47C141461	RETAINER	1			
59	F8		941D300P11	BOLT	1			
60	B8		142B1481P1	SHIM	1			
61	B8		142B1490	BELLEV. WASHER	1			
62	B8		47C141454	BRG RETAINER	1			
63	B8		142B1940	BALL BRG	2			
64	B8		142B1481P3	SHIM	1			
65	F8		941D187	SEAL HSG	1			
66	F8		941D300P10	BOLT	1			
67	B8		47C141465P7	O-RING	1			
68	B7		47C141465P8	O-RING	1			
69	B7		142B1481P2	SHIM	1			
70	B7	5	47B116003-P1	FACE SEAL	1			
71	B8		142B1483P1	DOWEL PIN	2			
72	B8		142B1484	ROT. SEAL FACE	1			
73	B8		47C141465P9	O-RING	1			
74	F8		142B1493	RET. SEAL RING	1			
75	F8		47C141468	LOCKNUT	1			
76	F8	5	142B1497	LOCKWASHER	1			
77	F7		142B1494	SPACER	1			
78	B7			COUPLING	1			
79	F7		142B1495	KEY	2			
80	G13		263E117	TIE-BOLT	1			
81	B12	5	142B1499	BAR X-SEAL	1			
82	F7	5	142B1496	NUT	1			
83			47C141471	LOCK-TIEBOLT	1			

(N) DRAWING CODES
1. VENDOR ITEM - SPEC CONT DWG
2. VENDOR ITEM - SOURCE CONT DWG
3. ALTERED PART
4. CUSTOMER FURNISHED PART
5. CATALOG ITEM

(O) REVISION CODES
1. ITEM ADDED
2. ITEM DELETED
3. QTY CHGD
4. IDENT. NO. CHGD.
5. IDENT NO. & QTY CHGD
6. EDIT CORRECTION

(P) CONTRACT NO.

(Q) PREPARED BY W.A. Headlick

(R) ISSUED BY

(S) DATE ISSUED

(T) REVISION AUTHORITY

(U) DISTRIBUTION CODE

PAGE 4 OF 4

GENERAL ELECTRIC
SPACE POWER & PROPULSION SECTION
CINCINNATI, OHIO 45215

PARTS LIST
SEE GPPS DRAFTING STANDARD NO. GTSD-140

(A) PARTS LIST NO. 246R670

(B) CODE IDENT. NO. 15226

(C) TITLE

(D) ITEM NO.	(E) ZONE	(F) DRG CODE	(G) IDENTIFICATION NO.	(H) DESCRIPTION/NOMENCLATURE	(I) QTY	(J) SHEET NO.	(K) REV CODE	(L) INTRO REF.
84	B7		47C141467	COUP. RETAINER	1			
85	B7	5	ZEB1845-064	SHAFT CAP	1			
86	B7		142B1492	GASKET	1			
87			246R675	BLADE	8			
88			246R676	BLADE	8			
89			246R681	BLADE		62		
90			246R682	BLADE		52		
91			246R686	BLADE		8		
92			246R683	BLADE		44		
93			246R687	BLADE		8		
94			941D307	TIP SEAL		1		
95			263E122	TIP SEAL		1		
96			941D306	TIP SEAL ASSY		1		
97			263E114P2	CLAMPING RING		1		
98			142B1488G1	TUBE-ABG. PURGE	1			
99			941D309G1	TUBE-ABG. PURGE	1			
100			47C140246P1	SEAL RET	1			
101			142B1471P1	KEY	6			
102			47B116002P1	PLUG			12	
103			263E129G1	MOIST. EX. RING			1	
104			263E128P1	CLAMPING RING			1	

(N) DRAWING CODES
1. VENDOR ITEM - SPEC CONT DWG
2. VENDOR ITEM - SOURCE CONT DWG
3. ALTERED PART
4. CUSTOMER FURNISHED PART
5. CATALOG ITEM

(O) REVISION CODES
1. ITEM ADDED
2. ITEM DELETED
3. QTY CHGD
4. IDENT. NO. CHGD.
5. IDENT NO. & QTY CHGD
6. EDIT CORRECTION

(P) CONTRACT NO.

(Q) PREPARED BY

(R) ISSUED BY

(S) DATE ISSUED

(T) REVISION AUTHORITY

(U) DISTRIBUTION CODE

Figure 108 Cont'd. Three Stage Turbine Parts List.

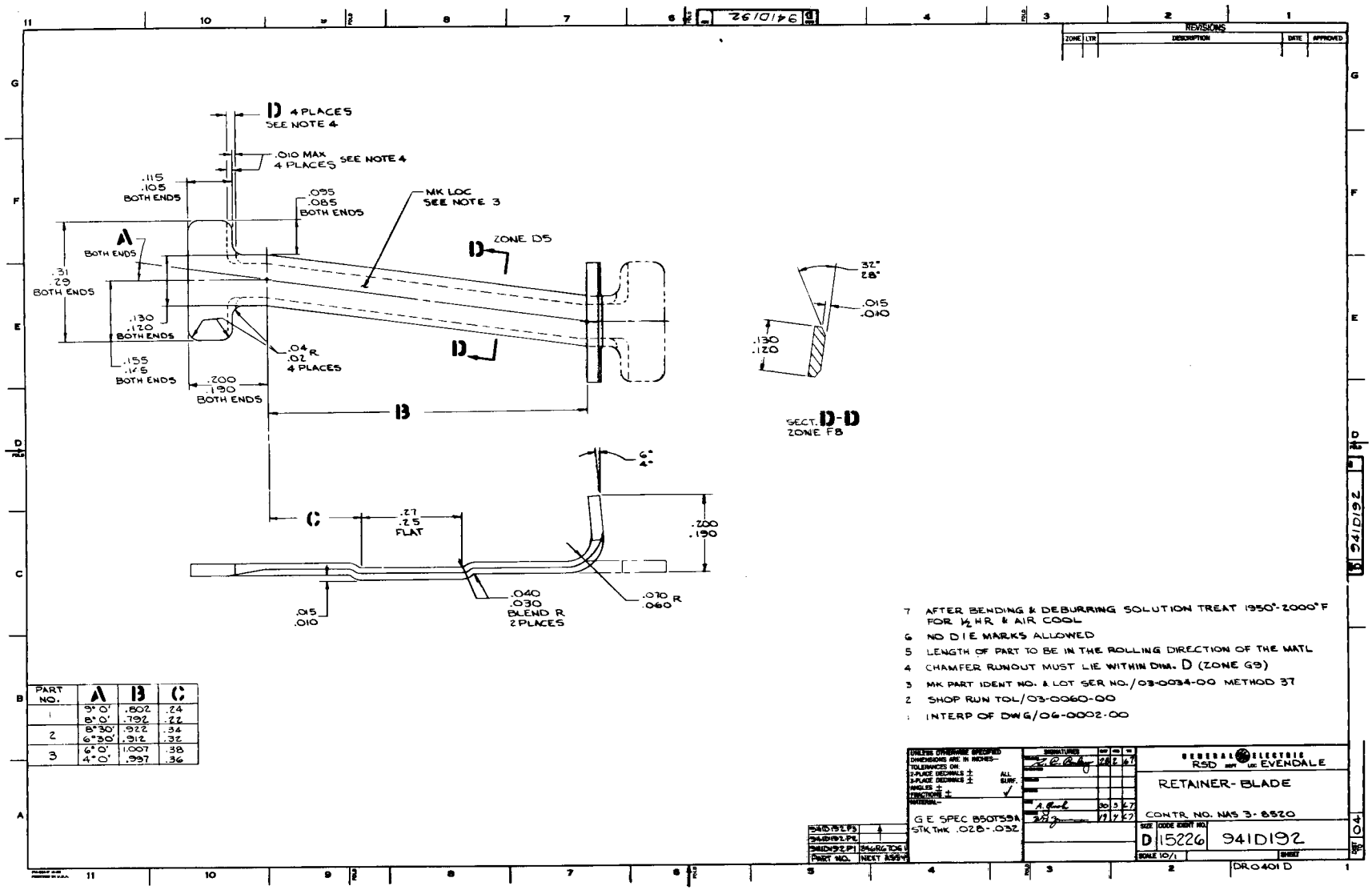

PART NO.	A	B	C
1	9° 0'	.802	.24
	8° 0'	.792	.22
2	8°30'	.922	.34
	6°30'	.912	.32
3	6° 0'	1.007	.38
	4° 0'	.997	.36

Figure 120. Turbine Blade Retaining Fasteners. (941D192)

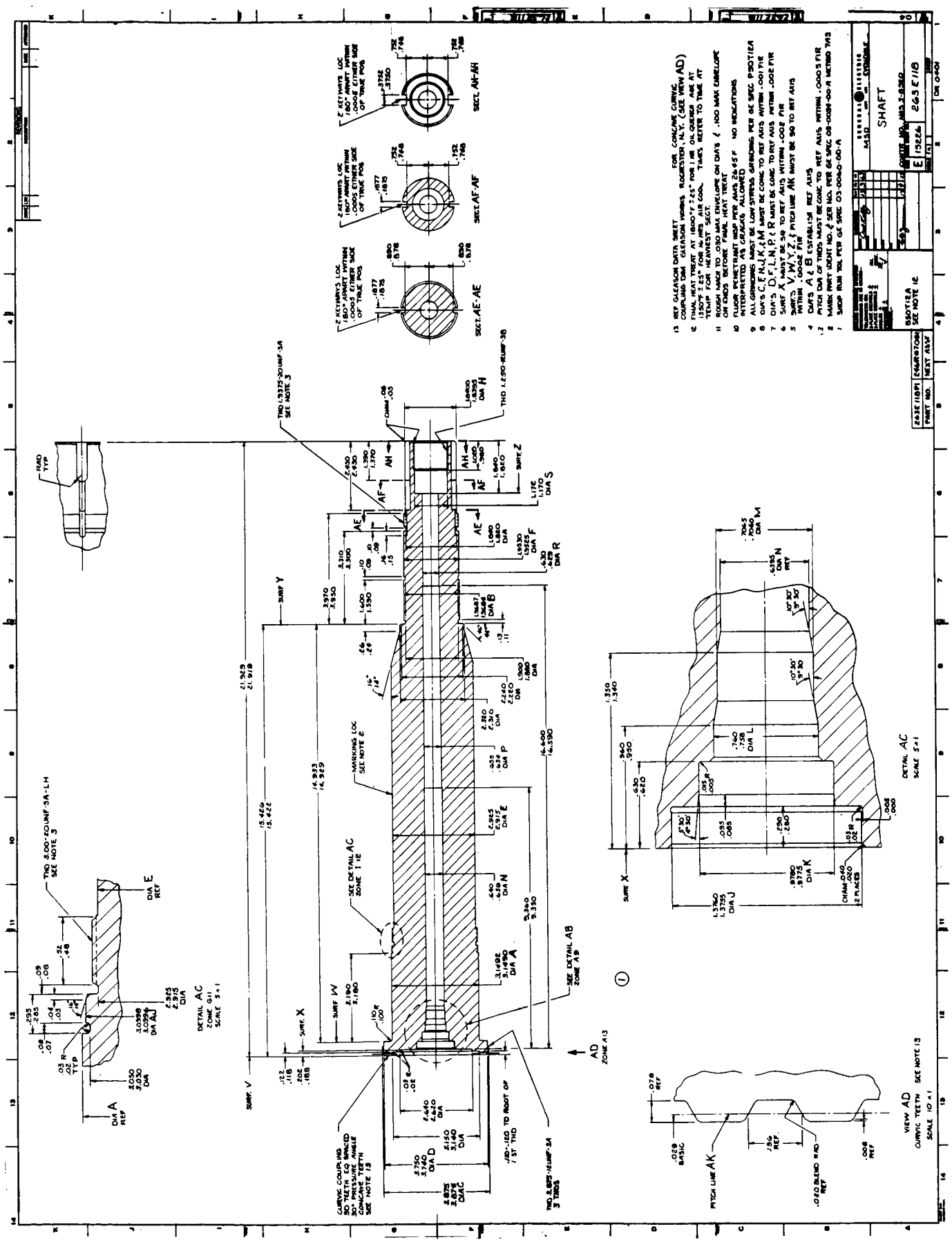

Figure 124. Turbine Shaft. (263E118)

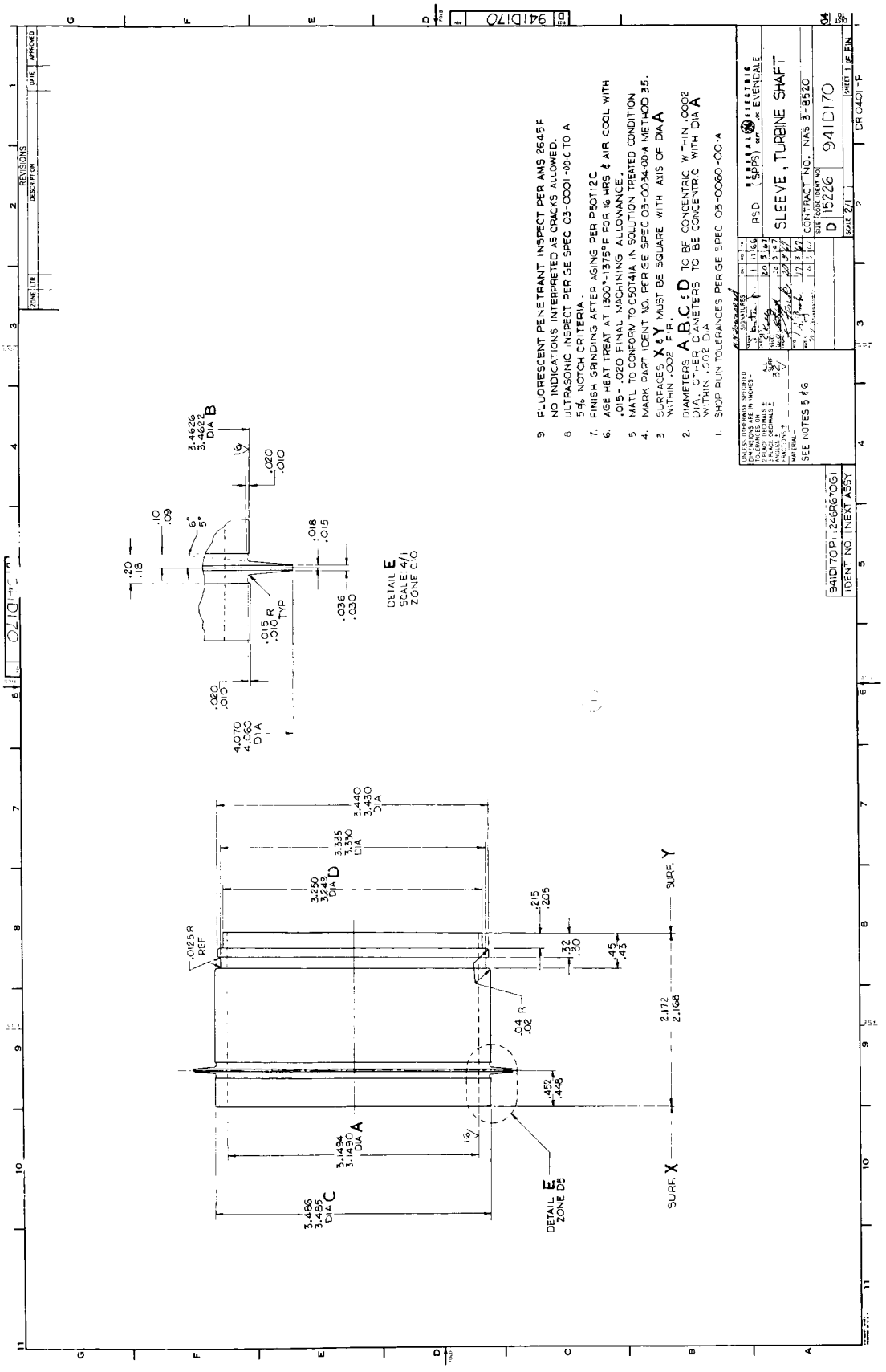

Figure 125. Shaft Sleeve (Pad Bearing Journal). (941D170)

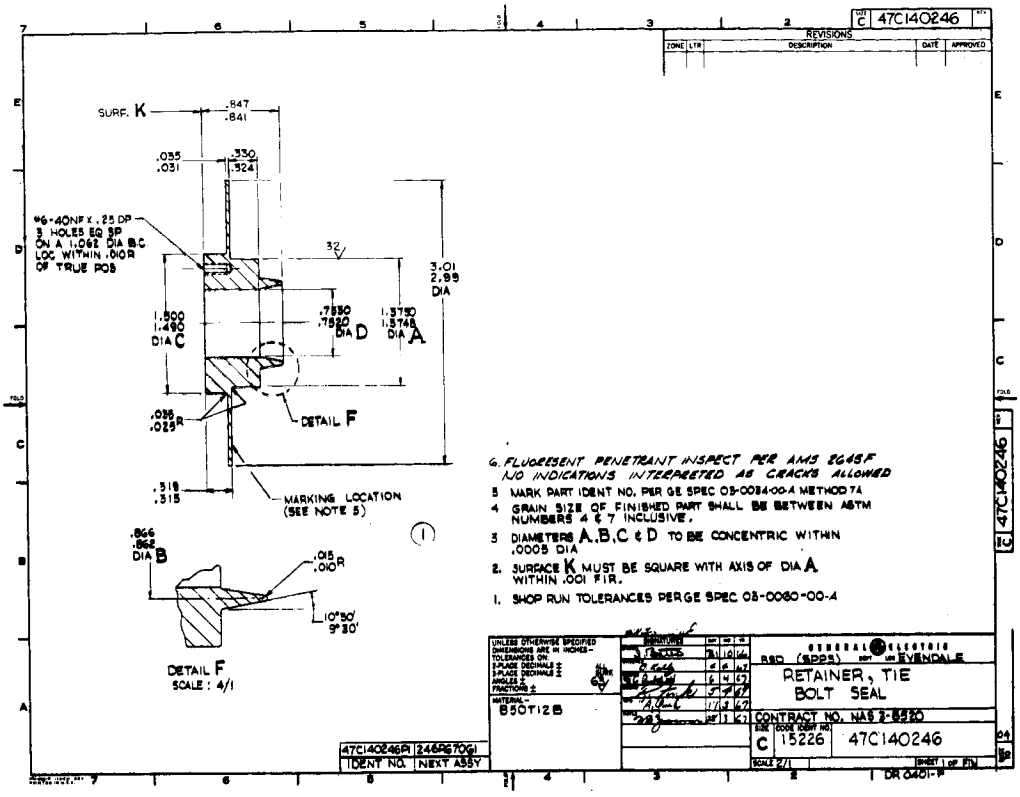

Figure 126. Tie Bolt Bar-X Seal Retainer. (47C140246)

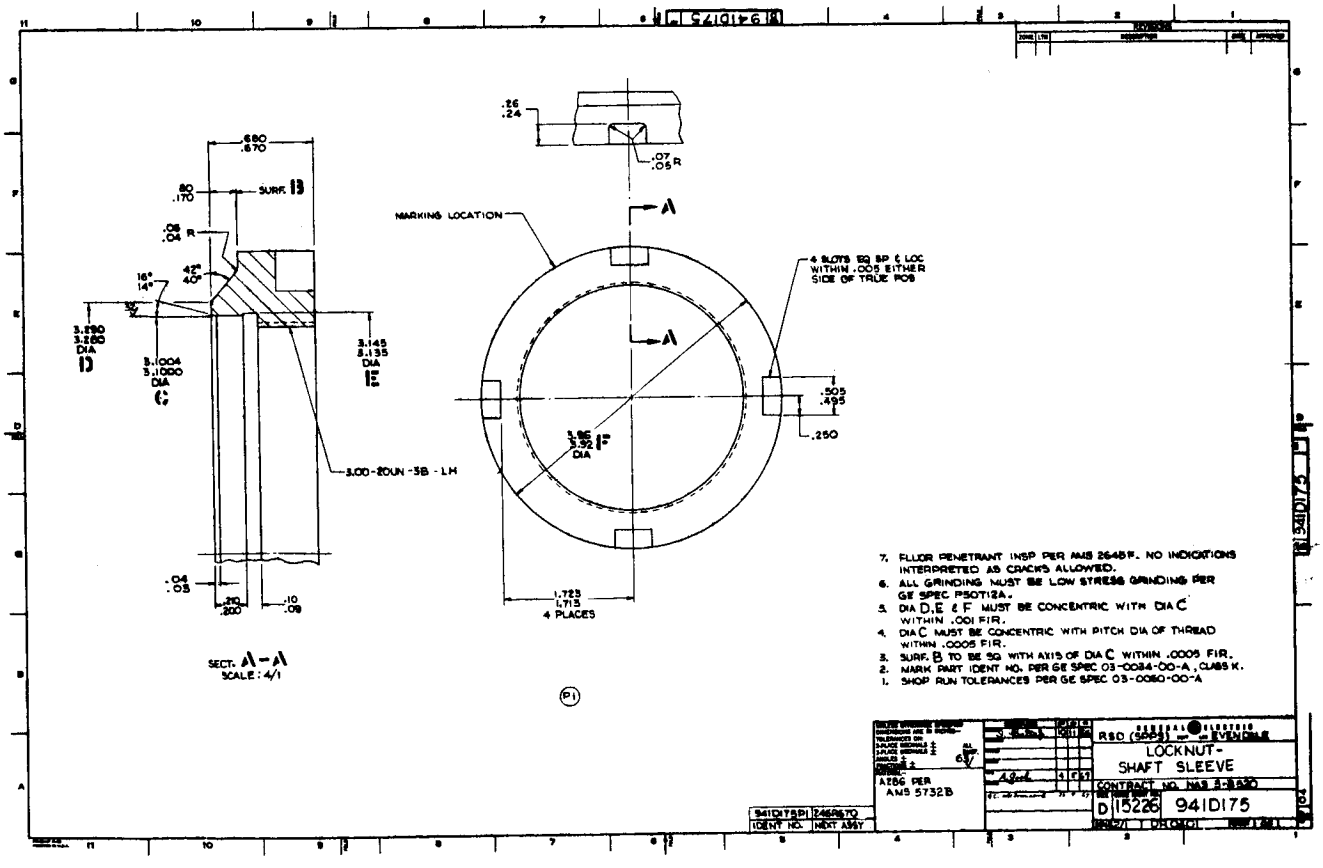

Figure 127. Shaft Main Bearing Sleeve Locknut. (941D175)

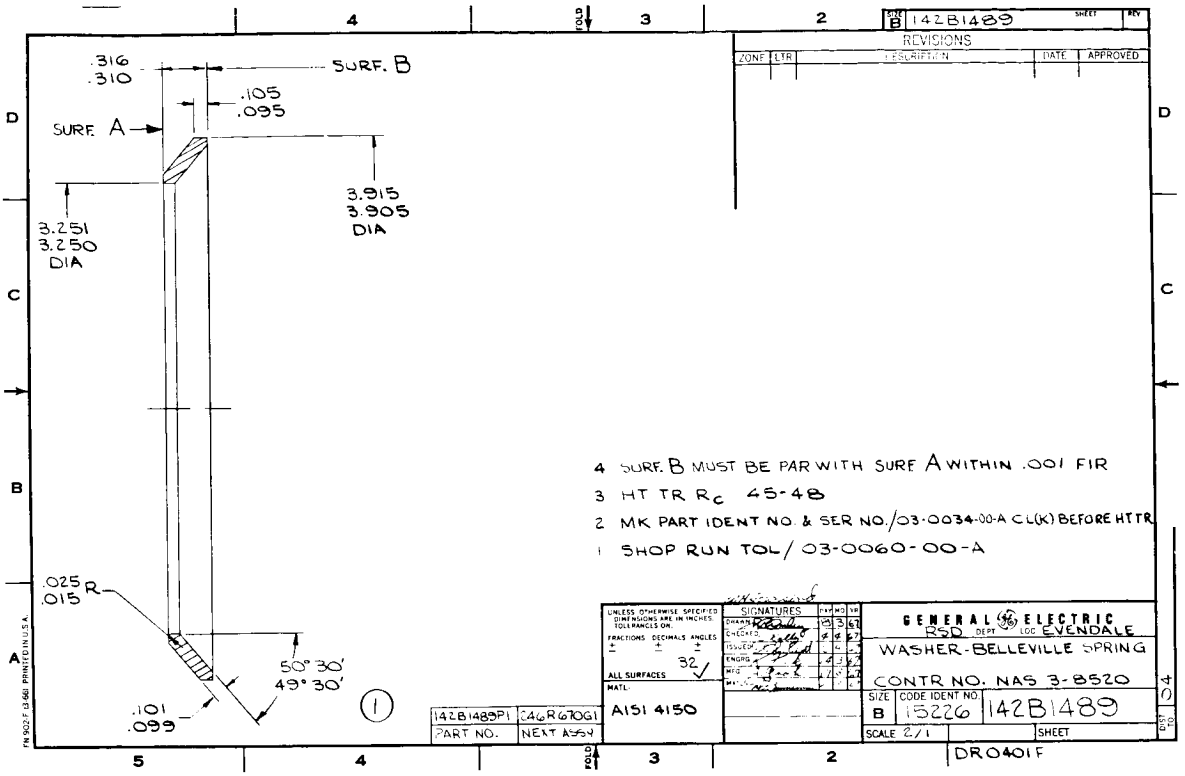

Figure 128. Main Shaft Pad Bearing Sleeve Loading Belleville Spring. (142B1489)

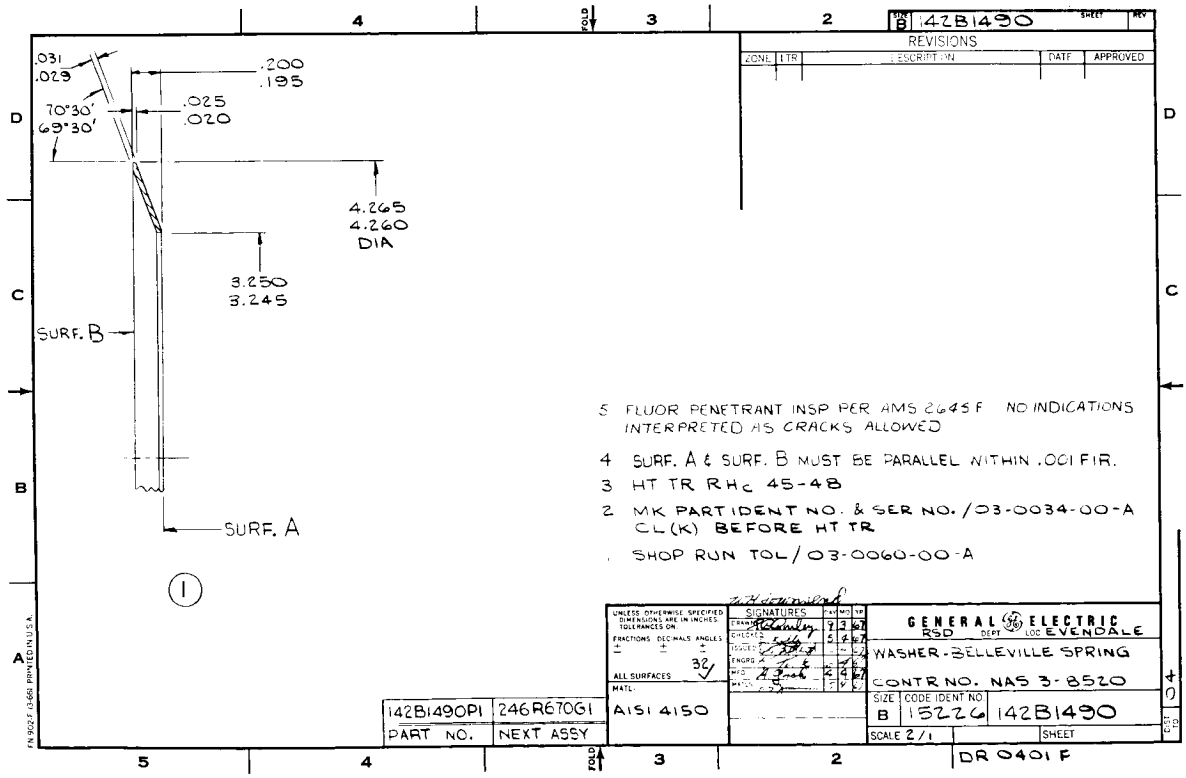

Figure 129. Ball Bearing Loading Belleville Spring. (142B1490)

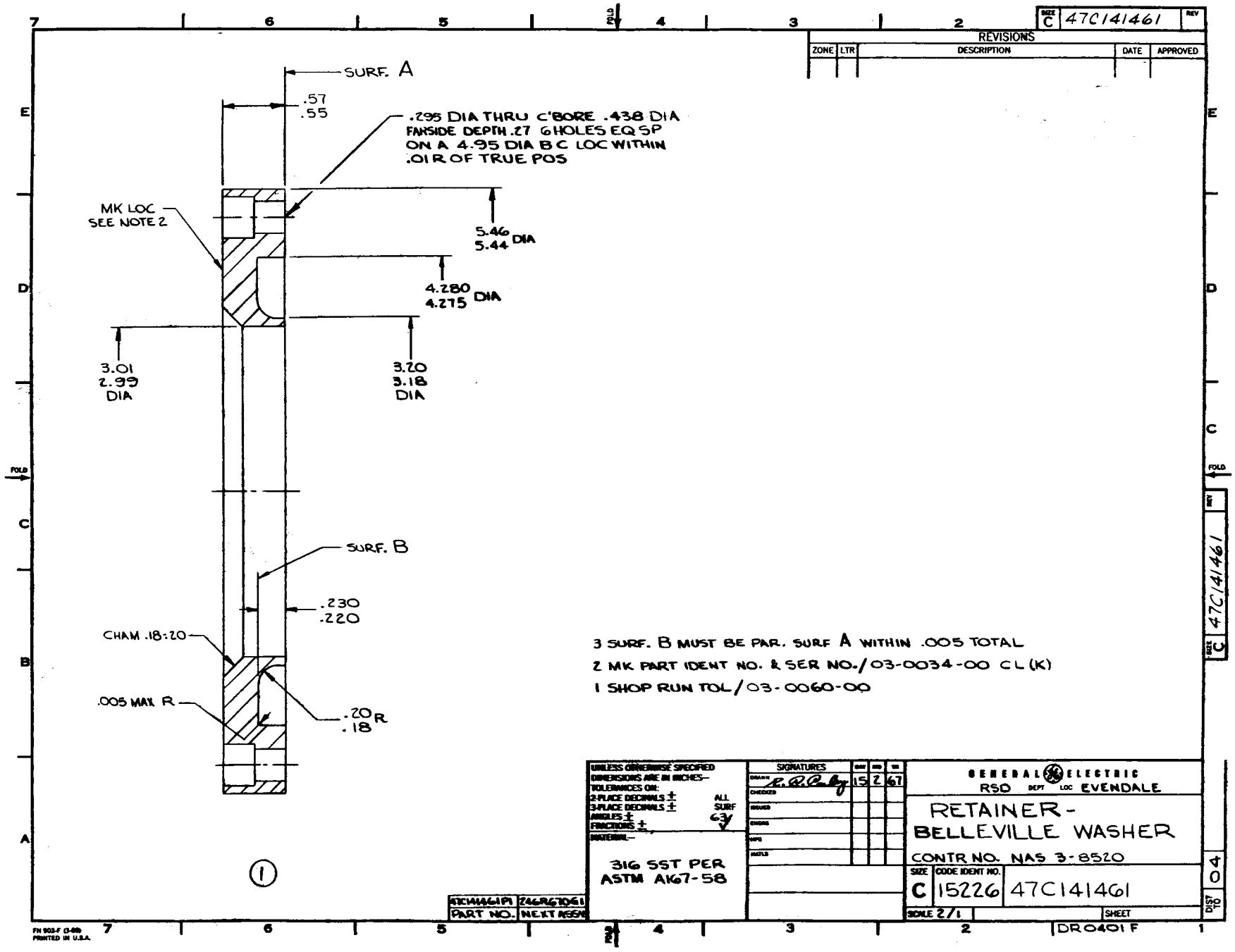

Figure 130. Thrust Bearing Belleville Spring Retainer. (47C141461)

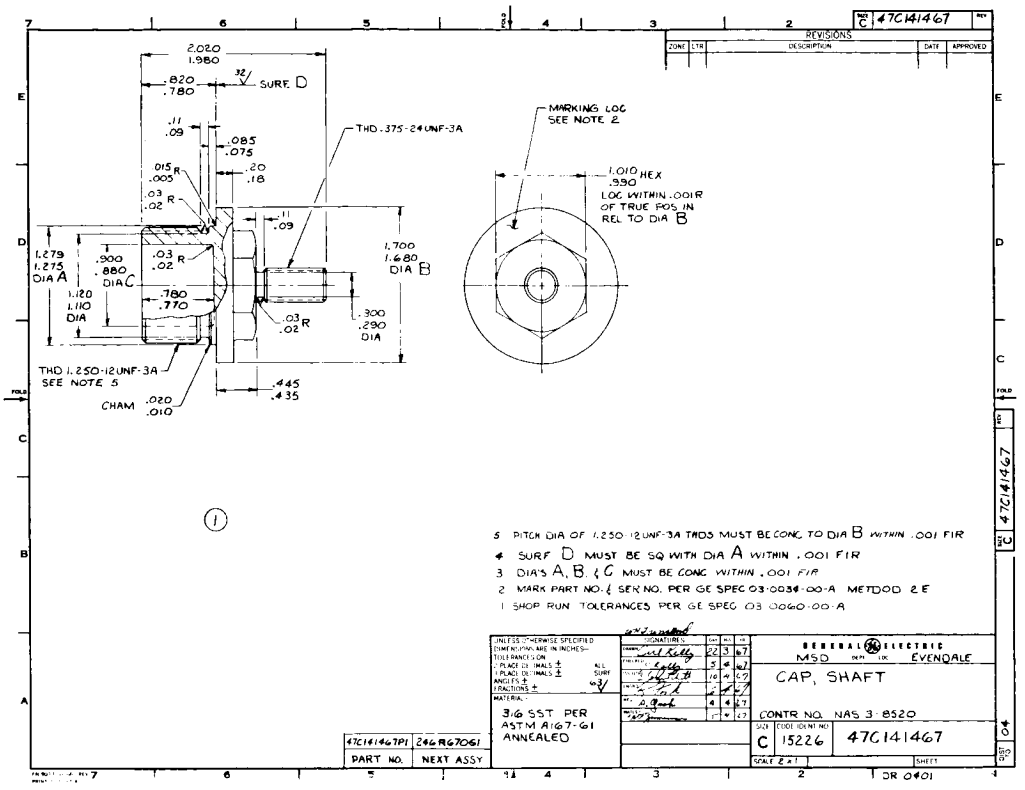

Figure 131. Shaft End Cap. (47C141467)

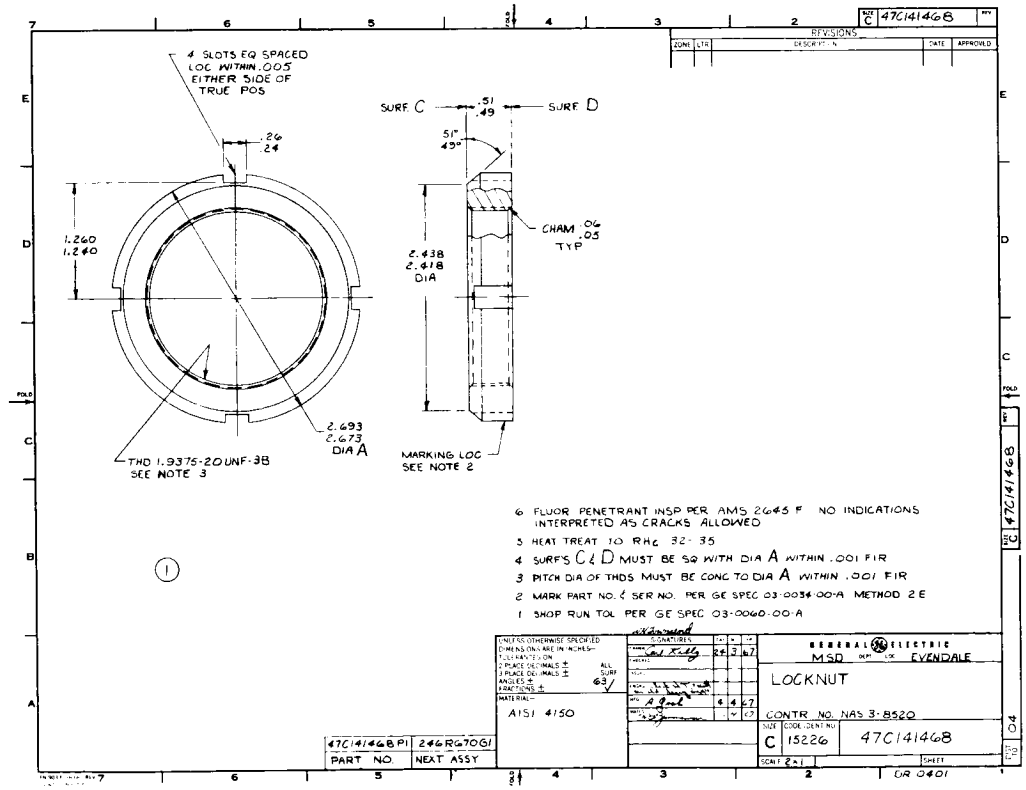

Figure 132. Thrust Bearing Retaining Locknut. (47C141468)

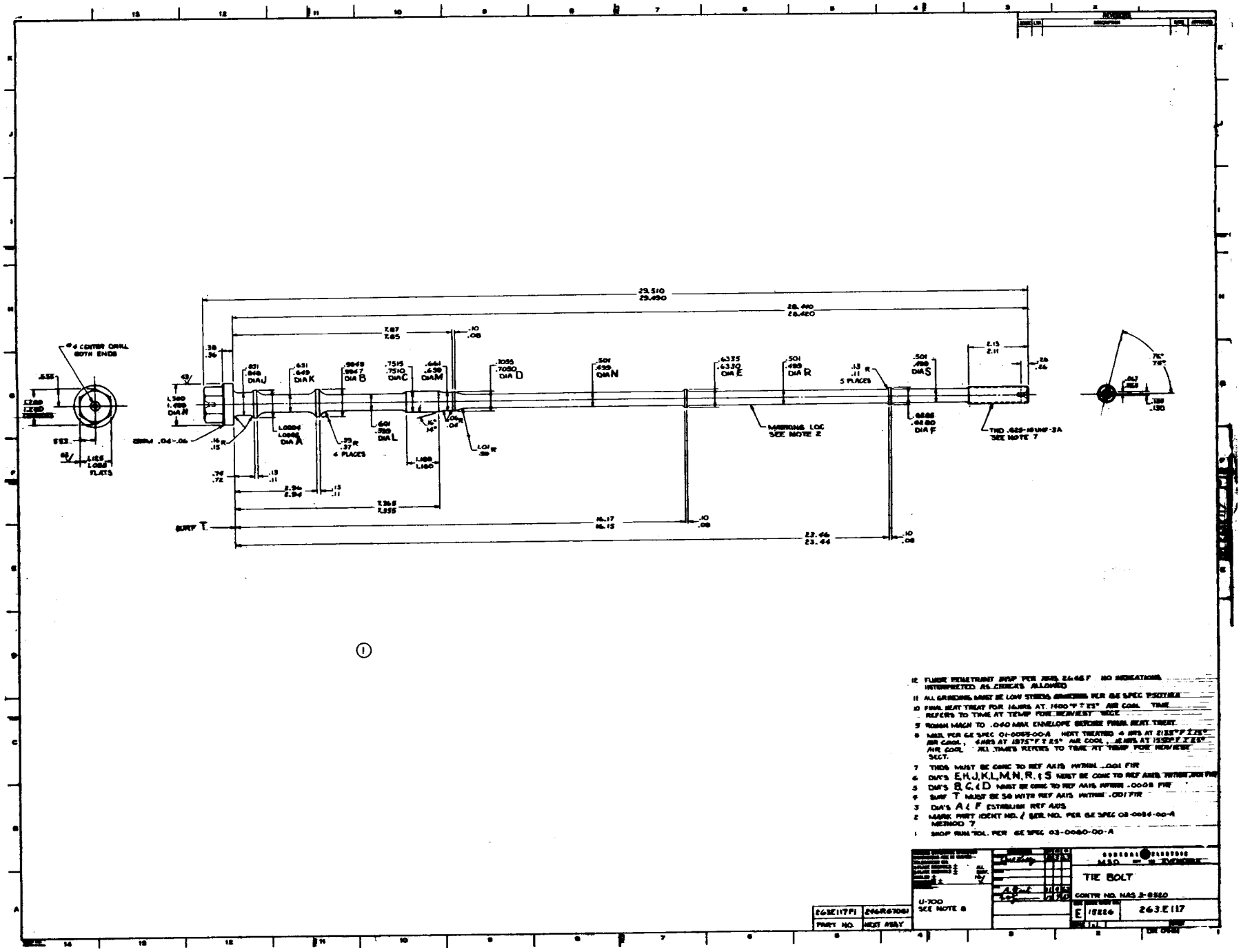

Figure 133. Main Tie-Bolt. (263E117)

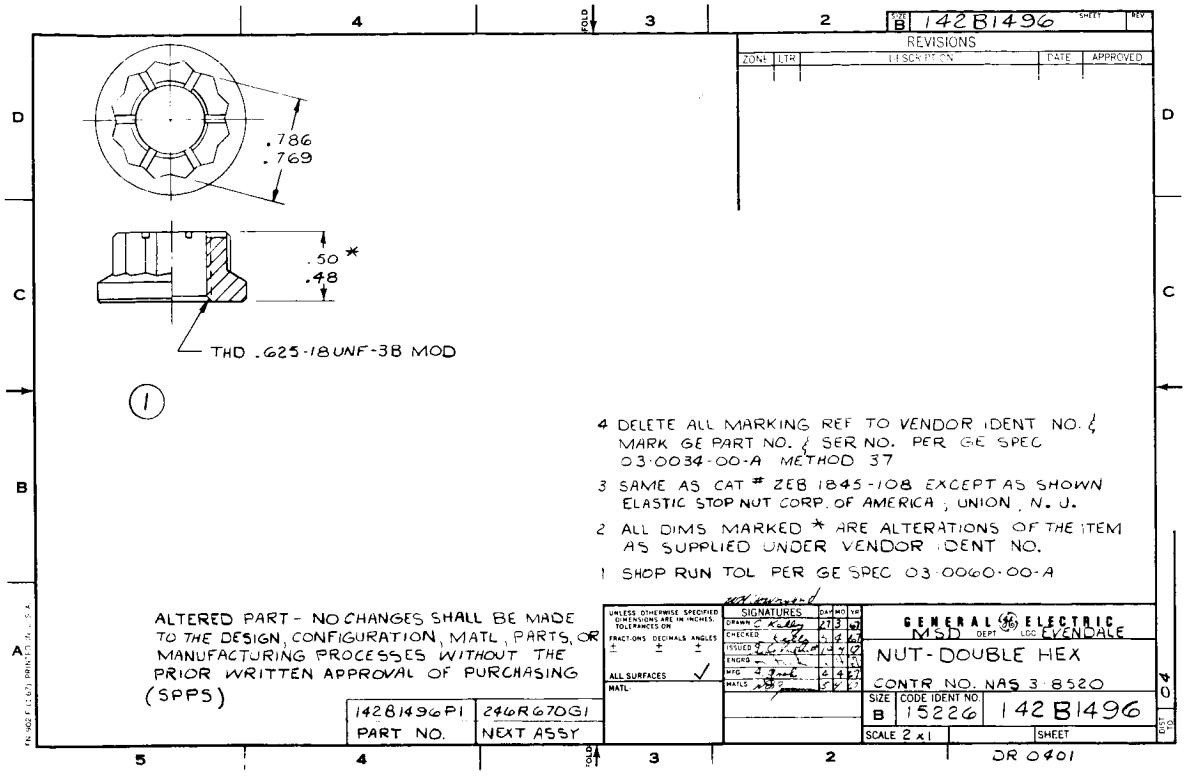

Figure 134. Tie-Bolt Locknut. (142B1496)

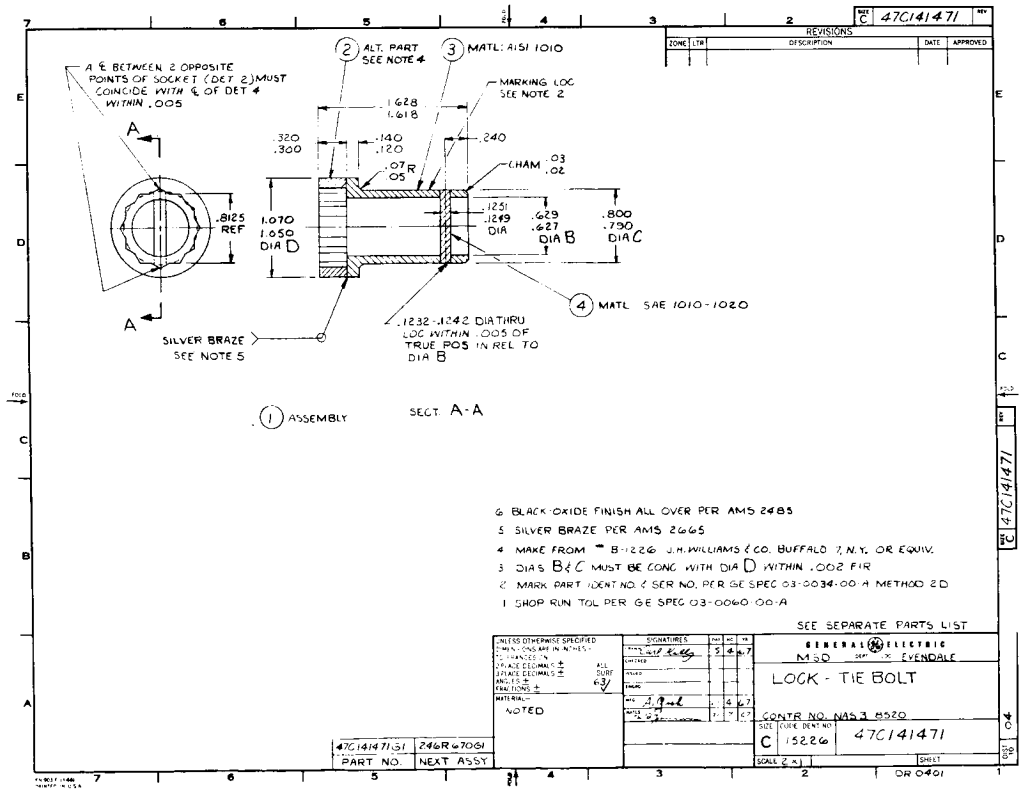

Figure 135. Tie-Bolt Nut Anti-Rotation Device. (47C141471)

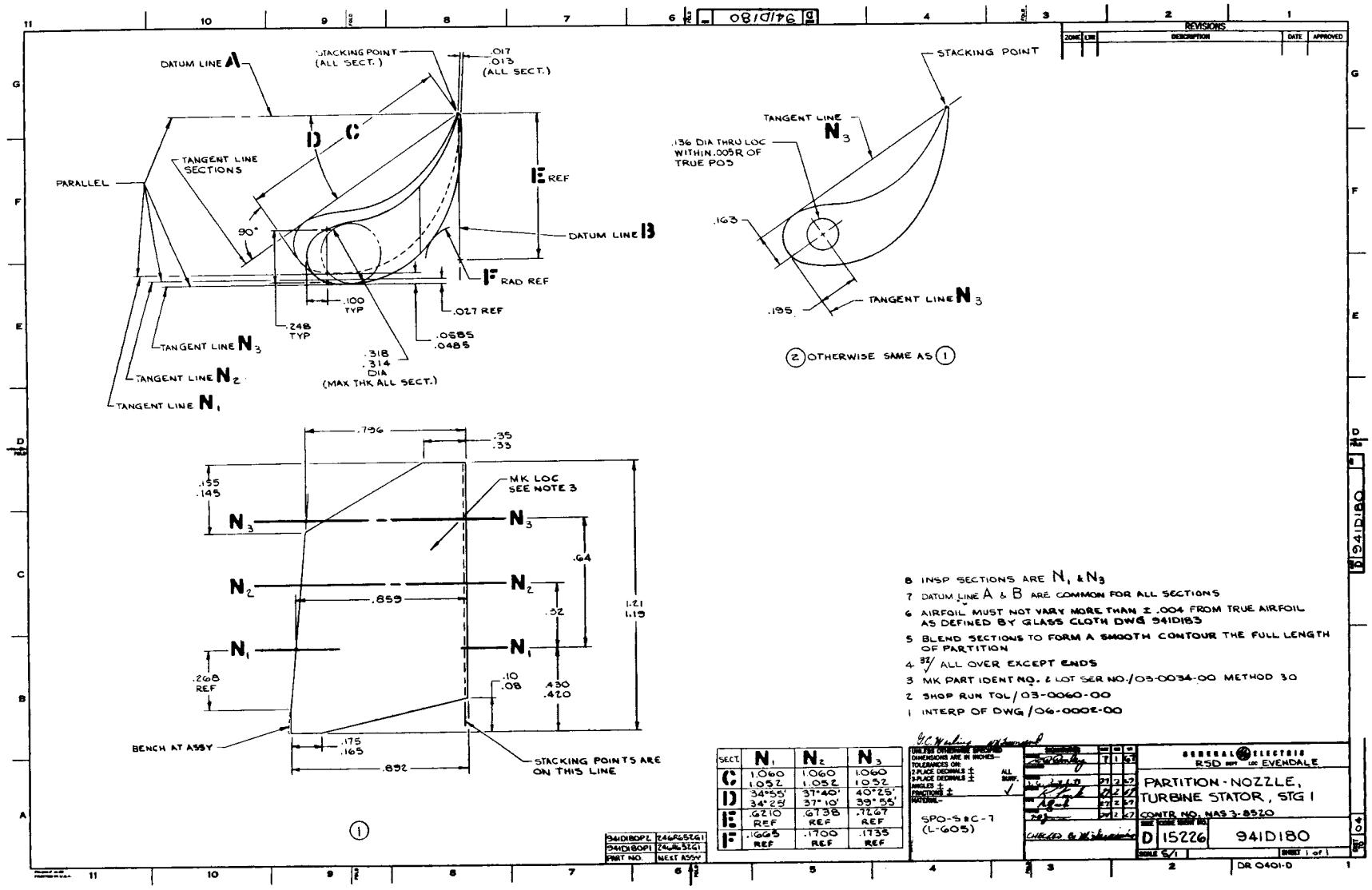

Figure 136. Stage 1 Nozzle Vane. (941D180)

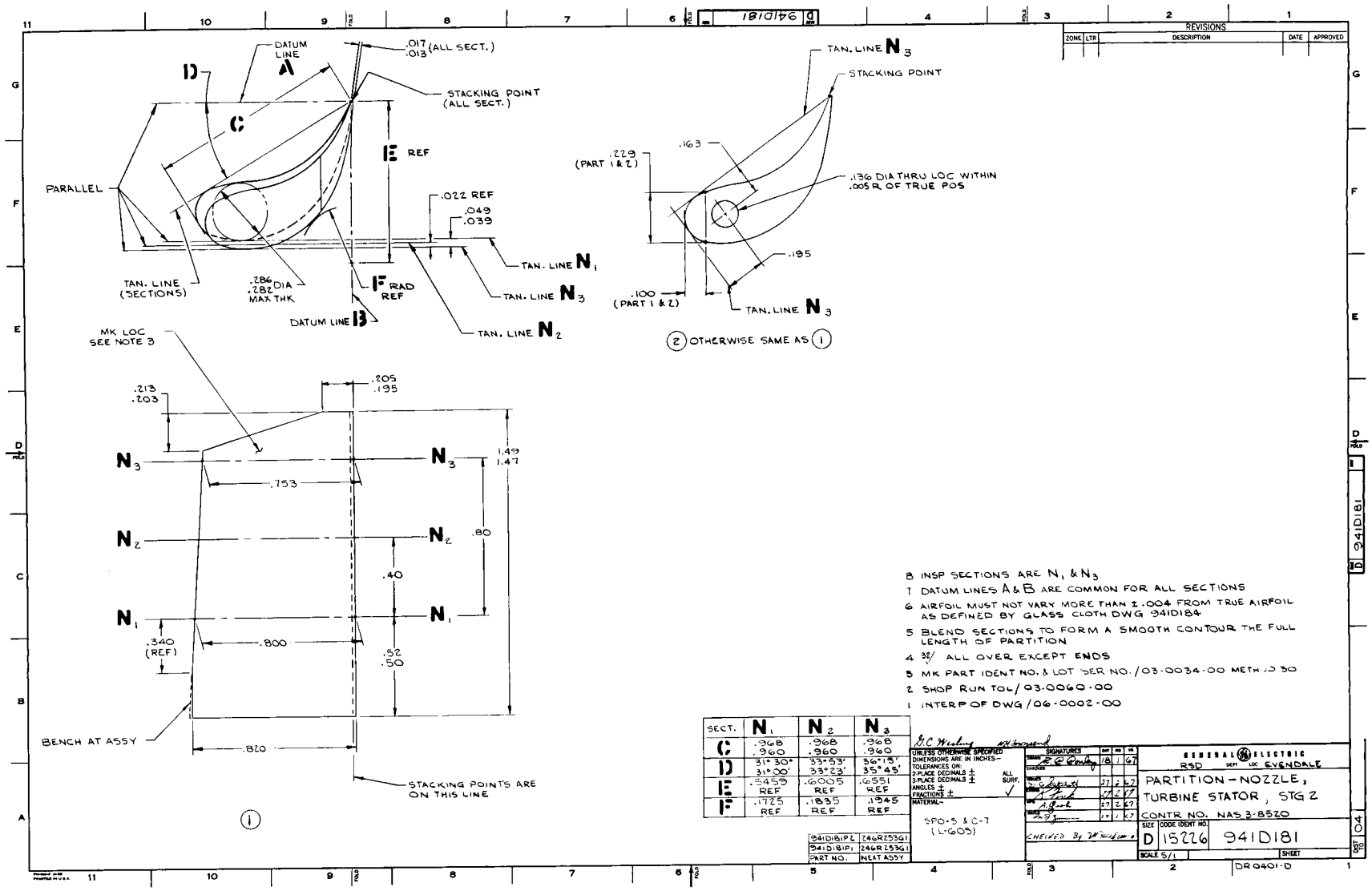

Figure 137. Stage 2 Nozzle Vane. (941D181)

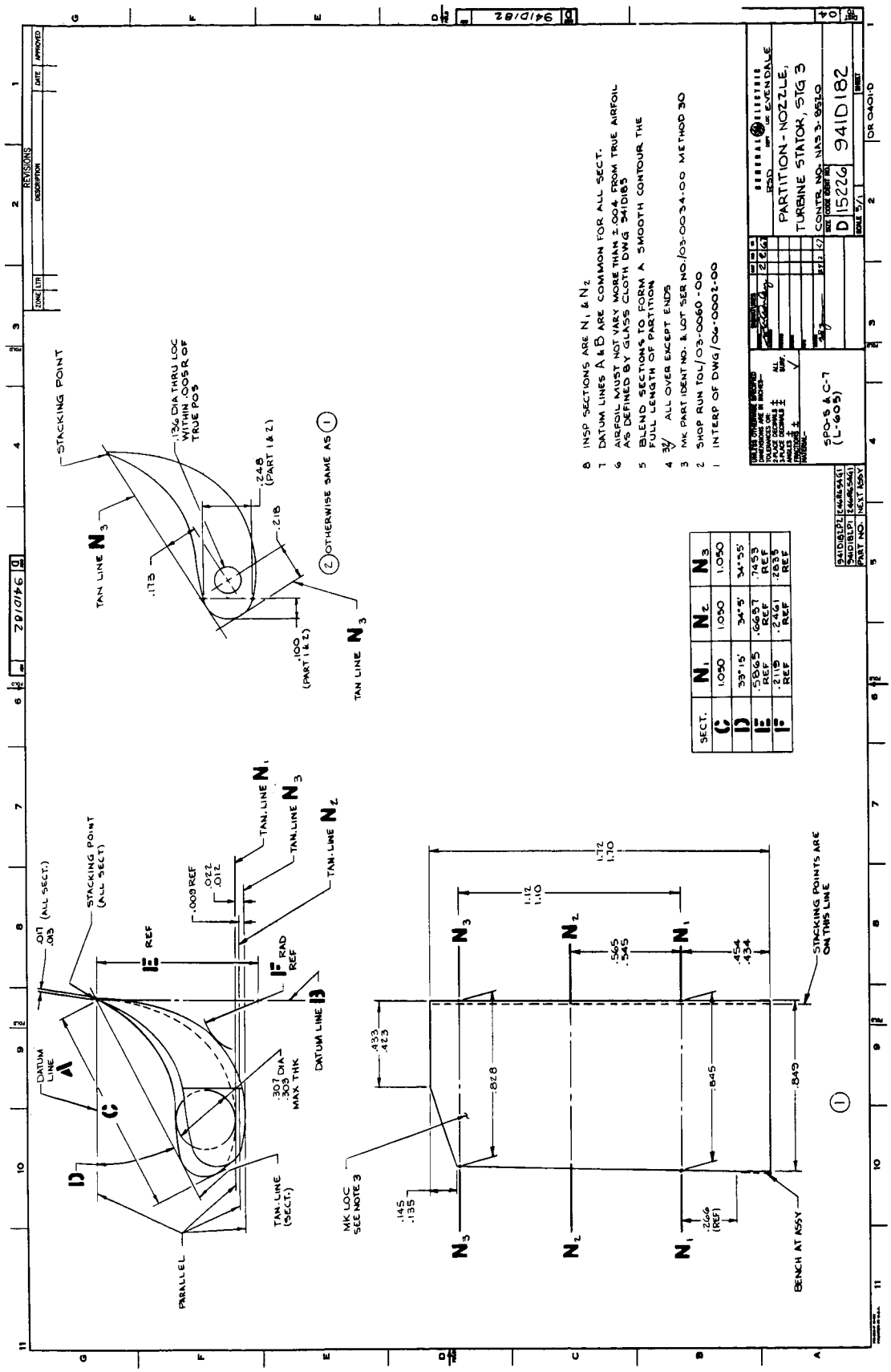

Figure 138. Stage 3 Nozzle Vane. (941D182)

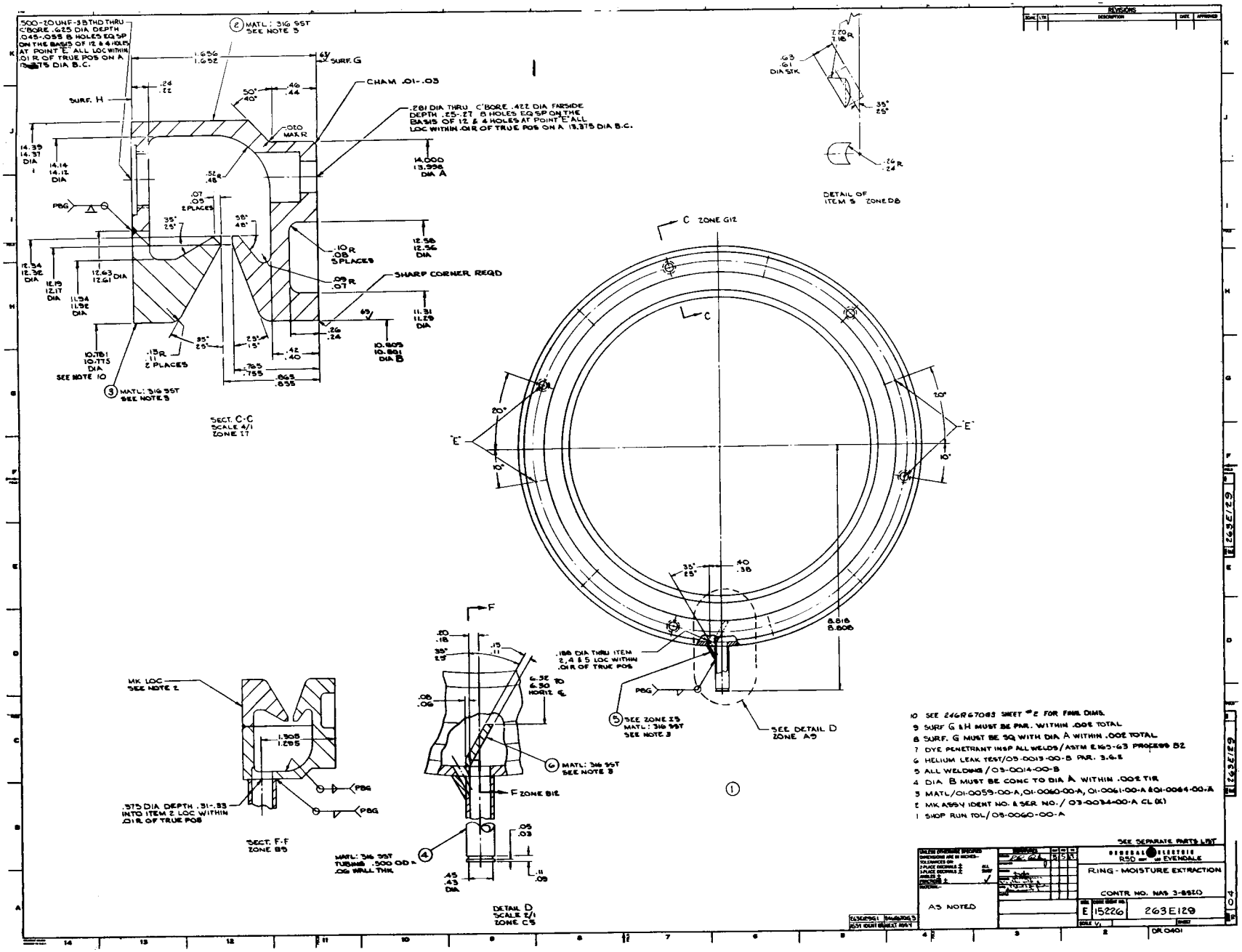

Figure 143b. Condensate Extraction Manifold. (263E129)

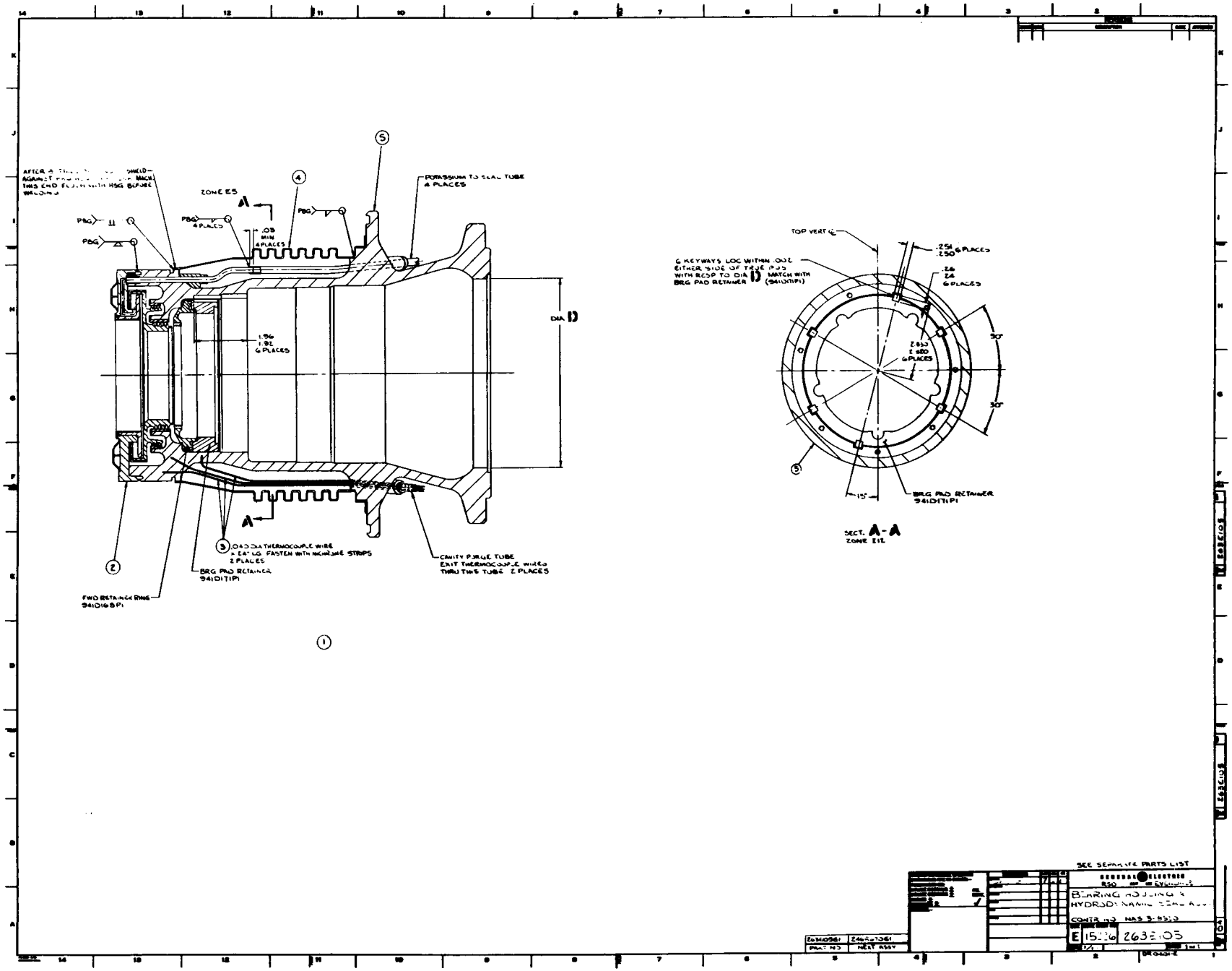

Figure 146. Bearing Housing Weldment Assembly. (263E105)

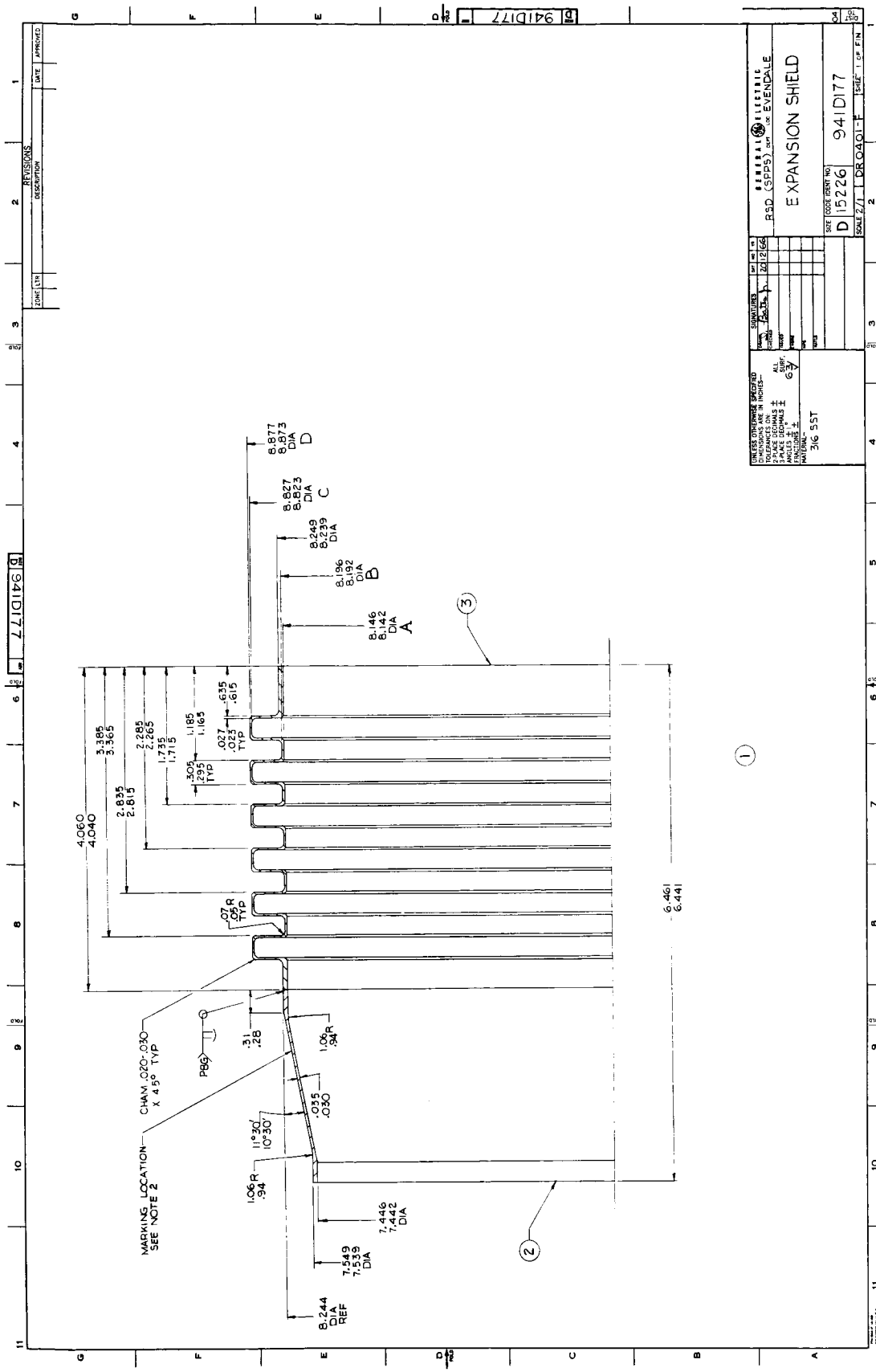

Figure 147. Bellows Expansion Shield. (941D177)

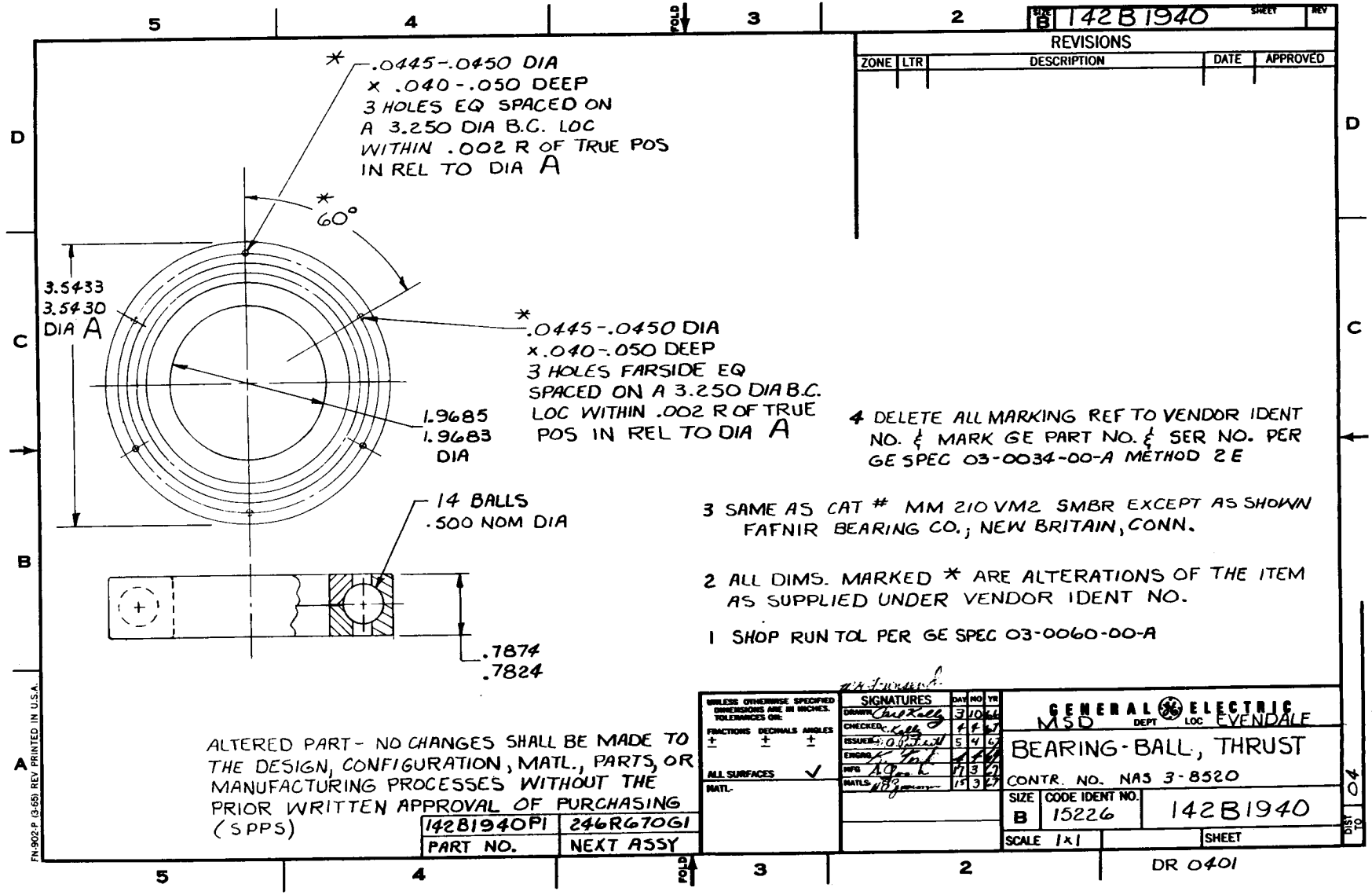

Figure 149. Ball Thrust Bearing. (142B1940)

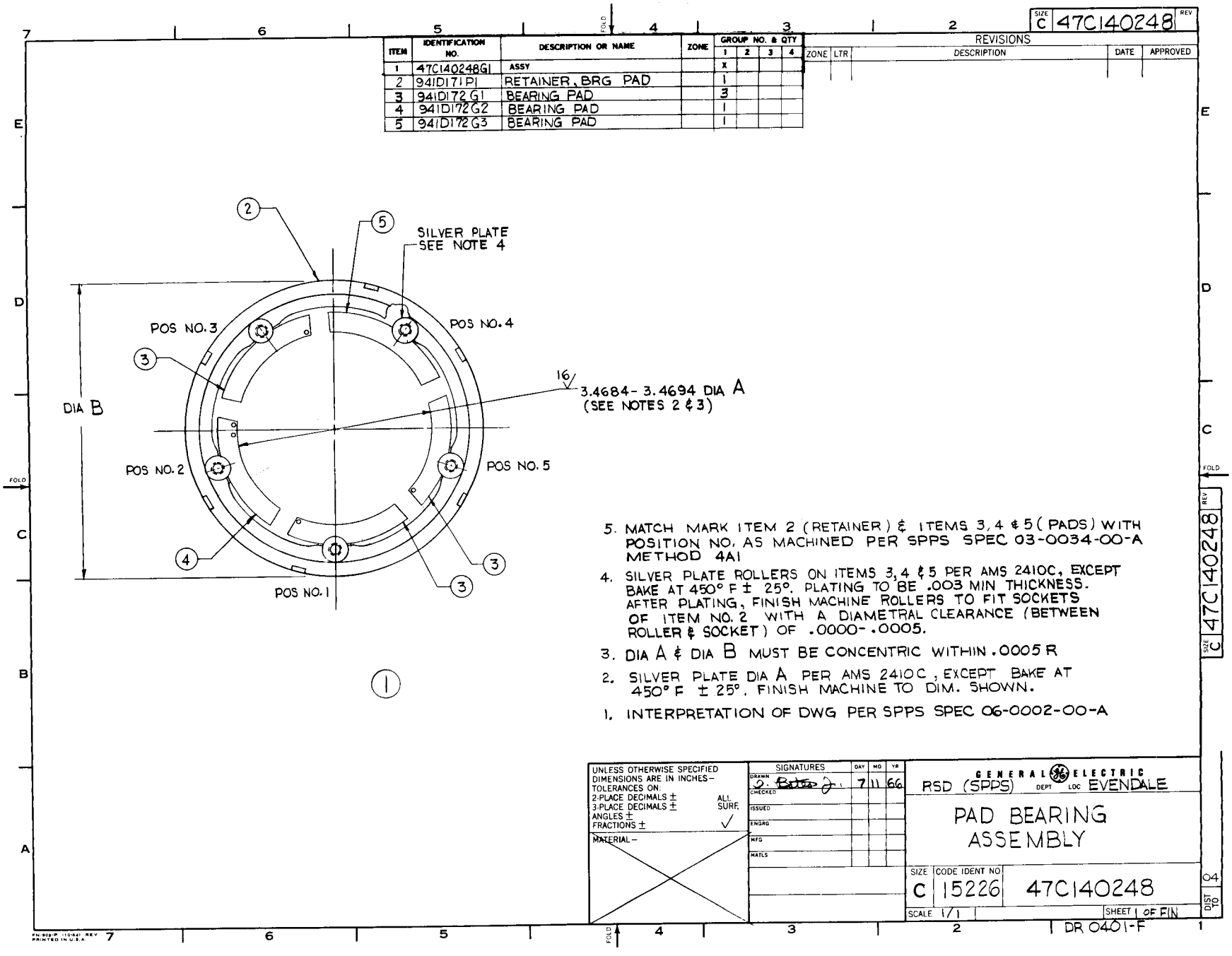

Figure 150. Pivoted Pad Bearing Assembly. (47C140248)

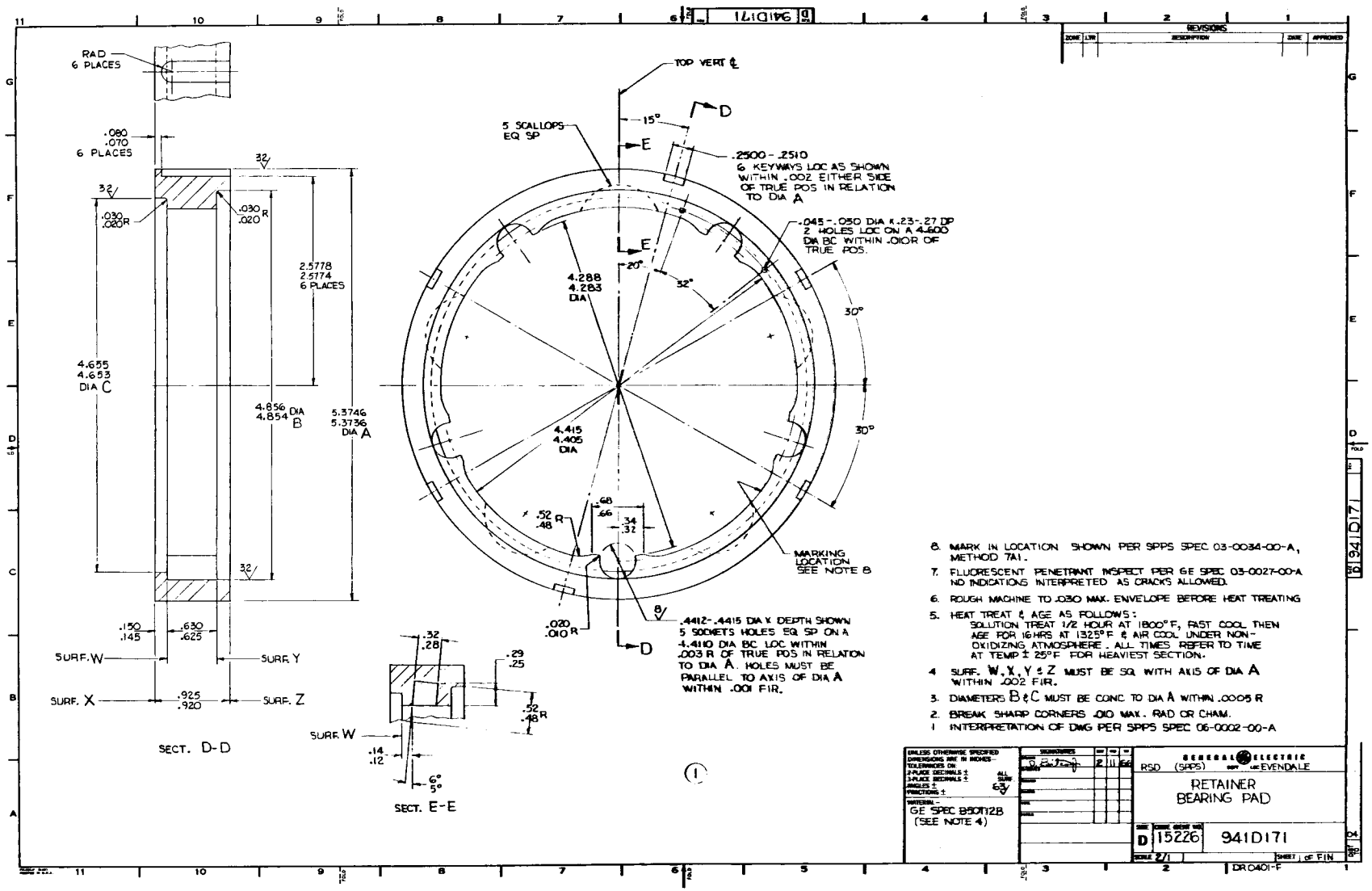

Figure 151. Pad Bearing Retainer Ring. (941D171)

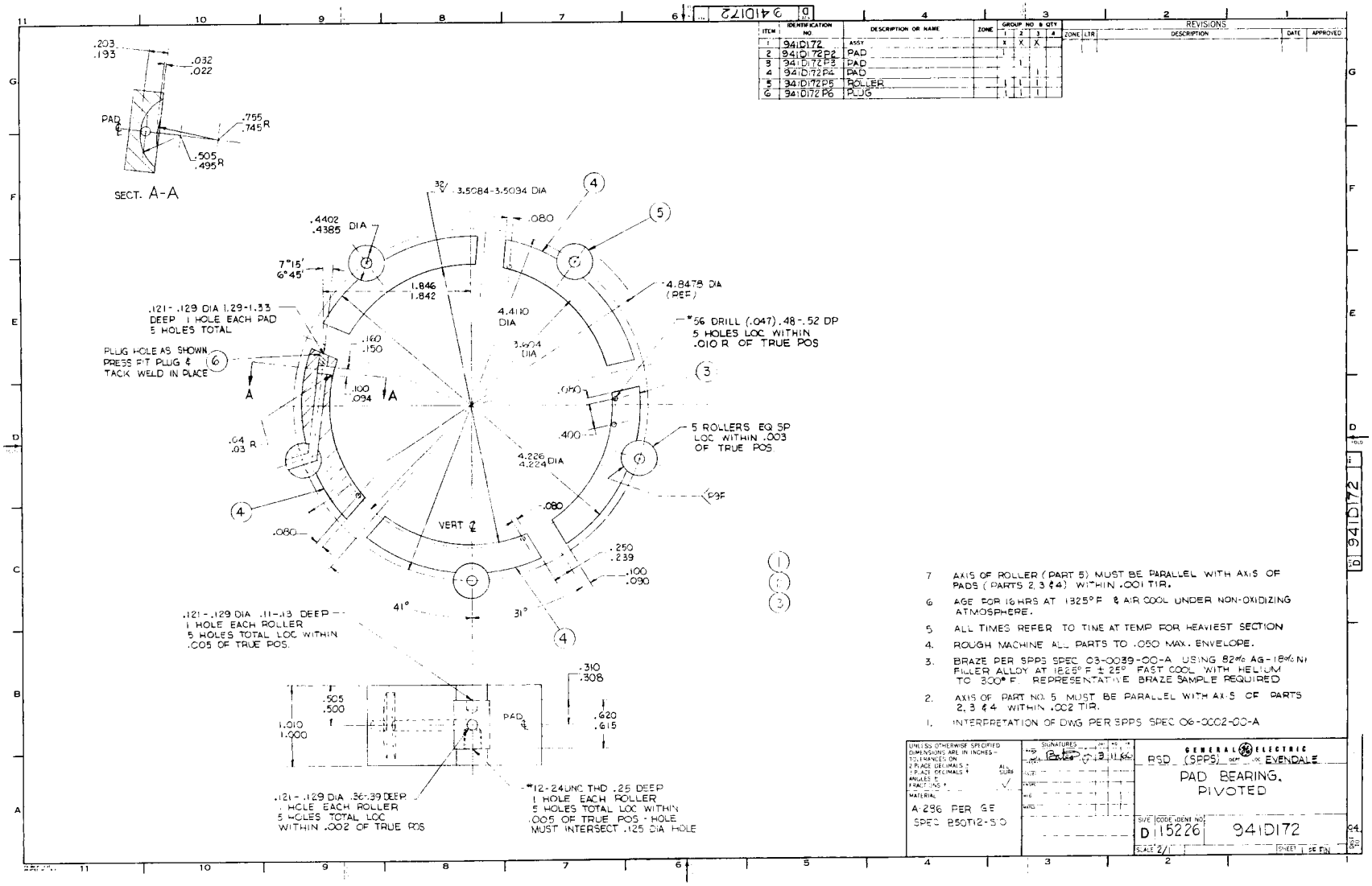

Figure 152. Bearing Pads. (941D172)

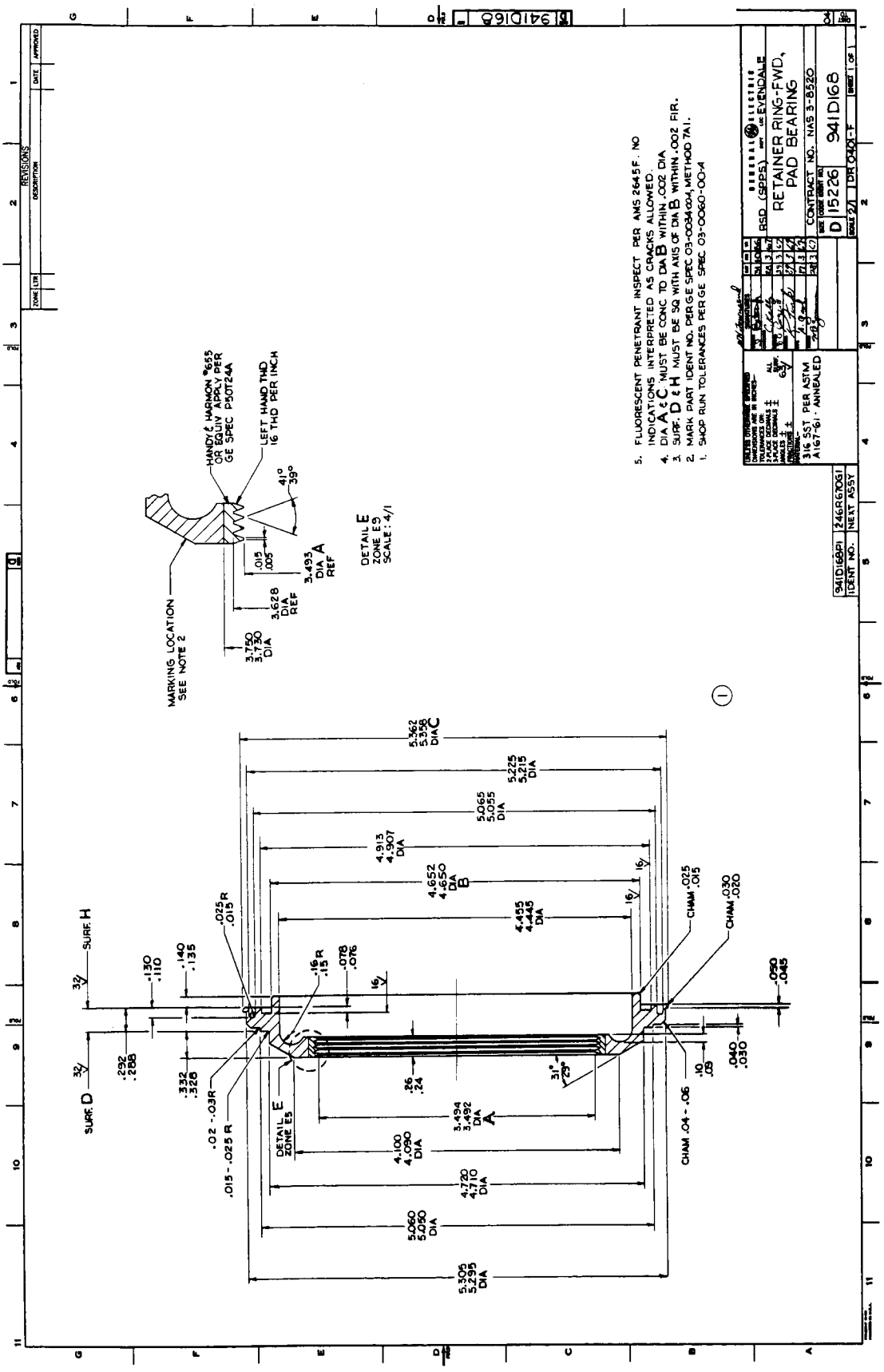

Figure 153. Pad Bearing Forward Screw Seal. (941D168)

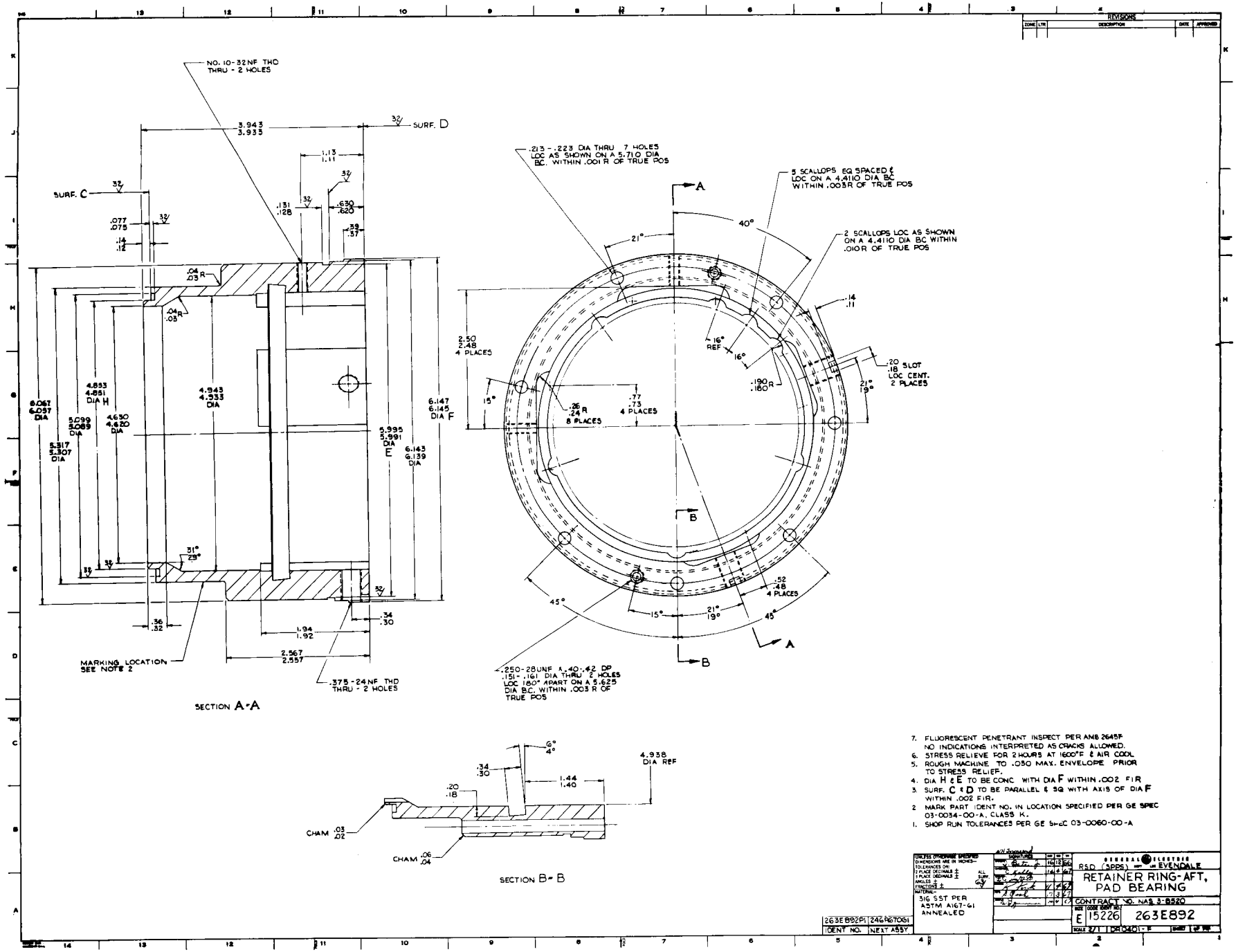

Figure 154. Pad Bearing Aft Retainer Ring. (263E892)

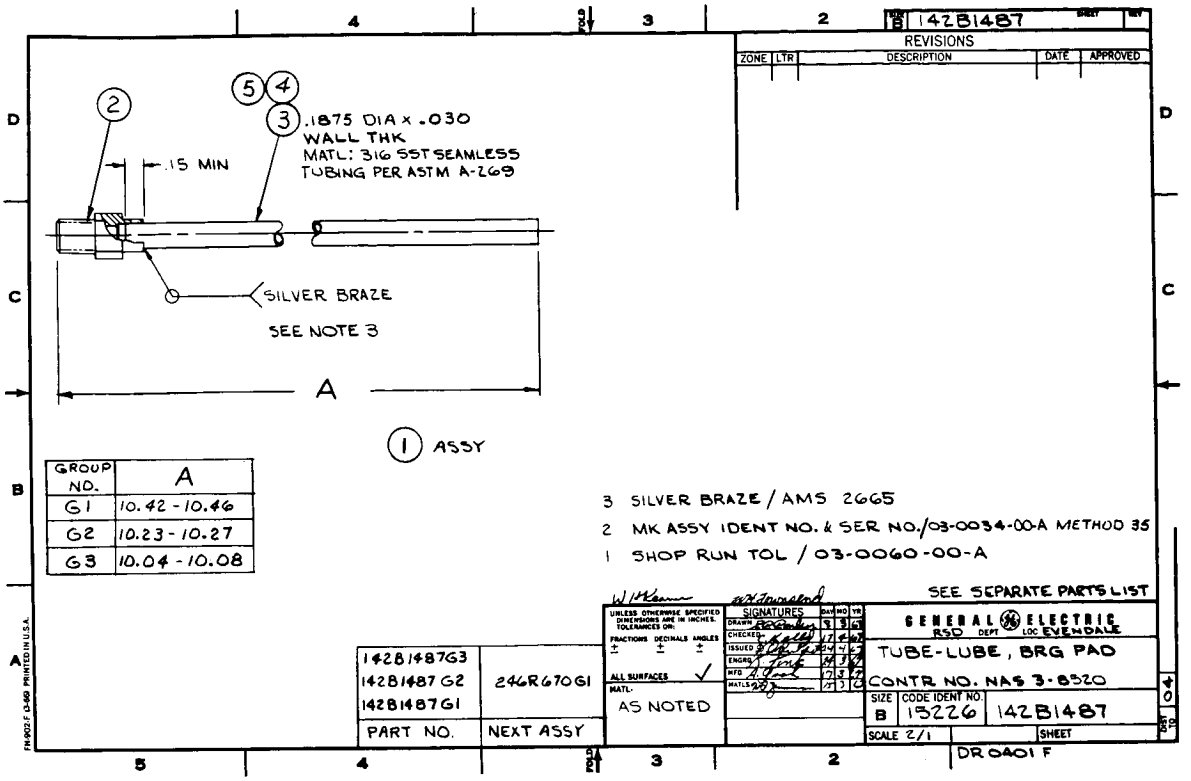

Figure 155. Lubrication Feed Tube for Pivoted Pad Bearing. (142B1487)

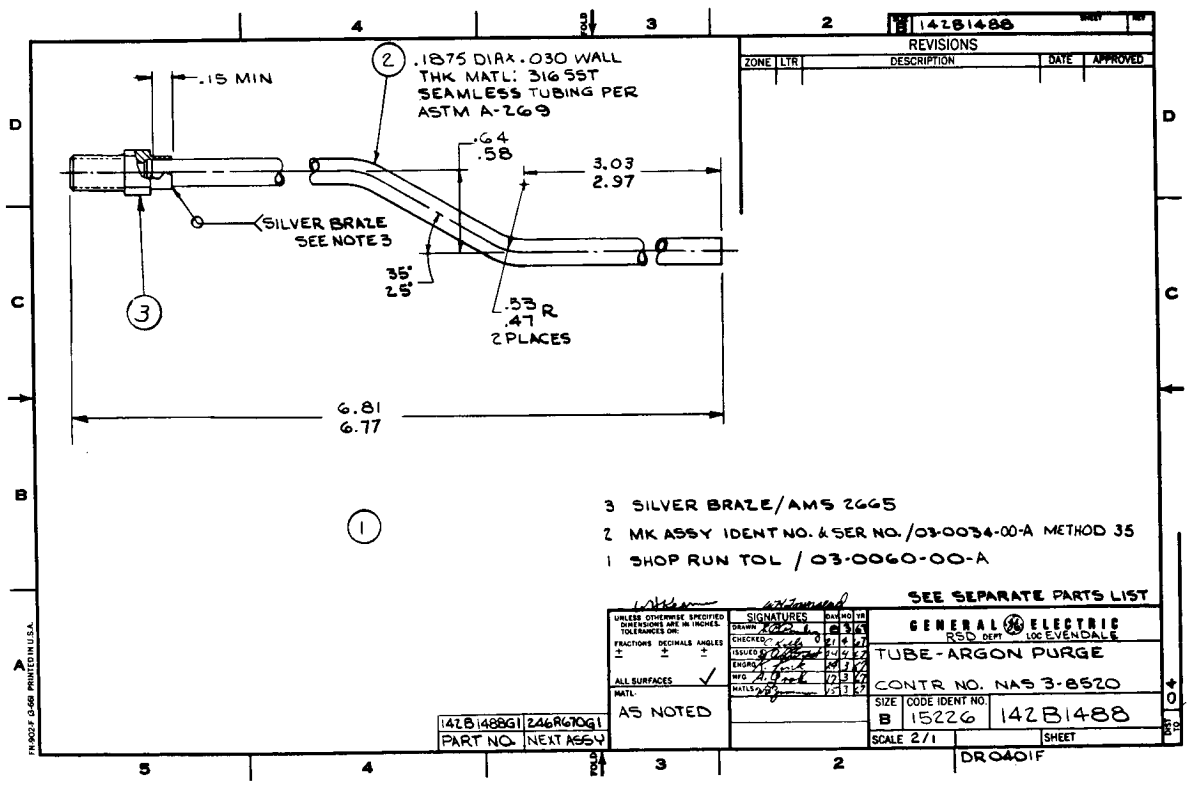

Figure 156. Argon Purge Flow Feed Tube for Region Behind Pad Bearing. (142B1488)

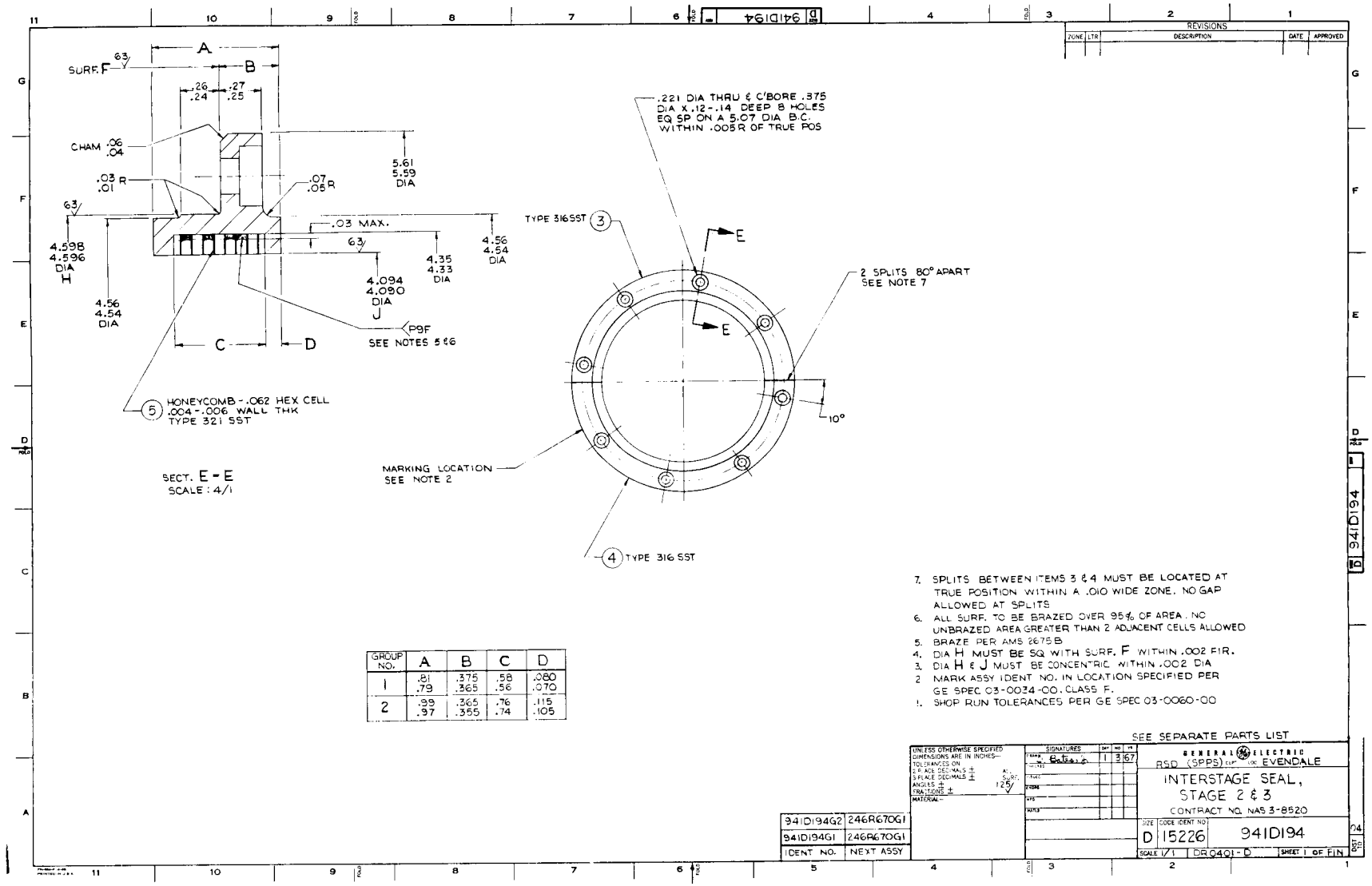

Figure 157. Interstage Honeycomb Seal. (941D194)

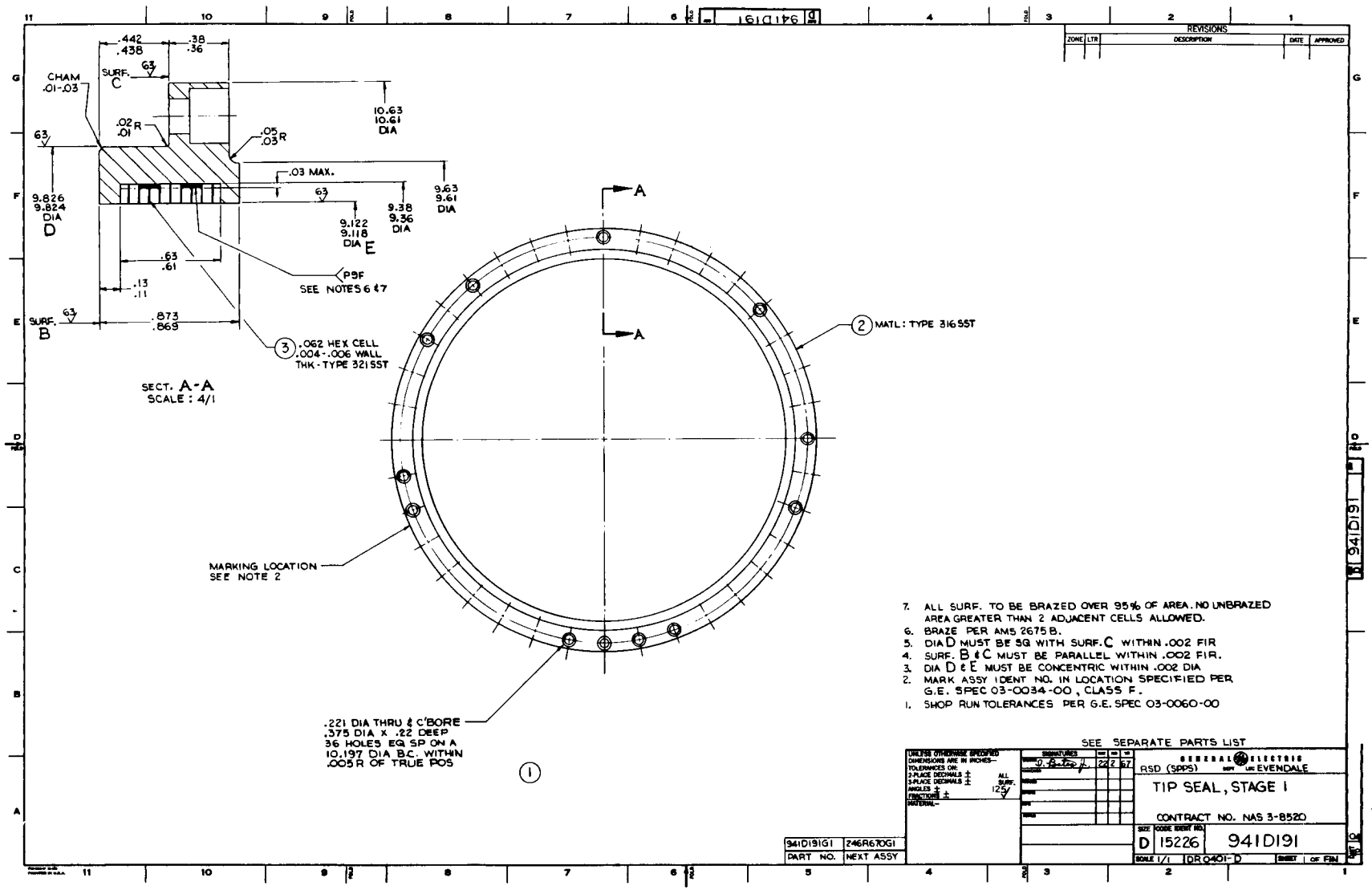

Figure 158. Stage 1 Honeycomb Tip Seal. (Phase I, Shrouded Design) (941D191)

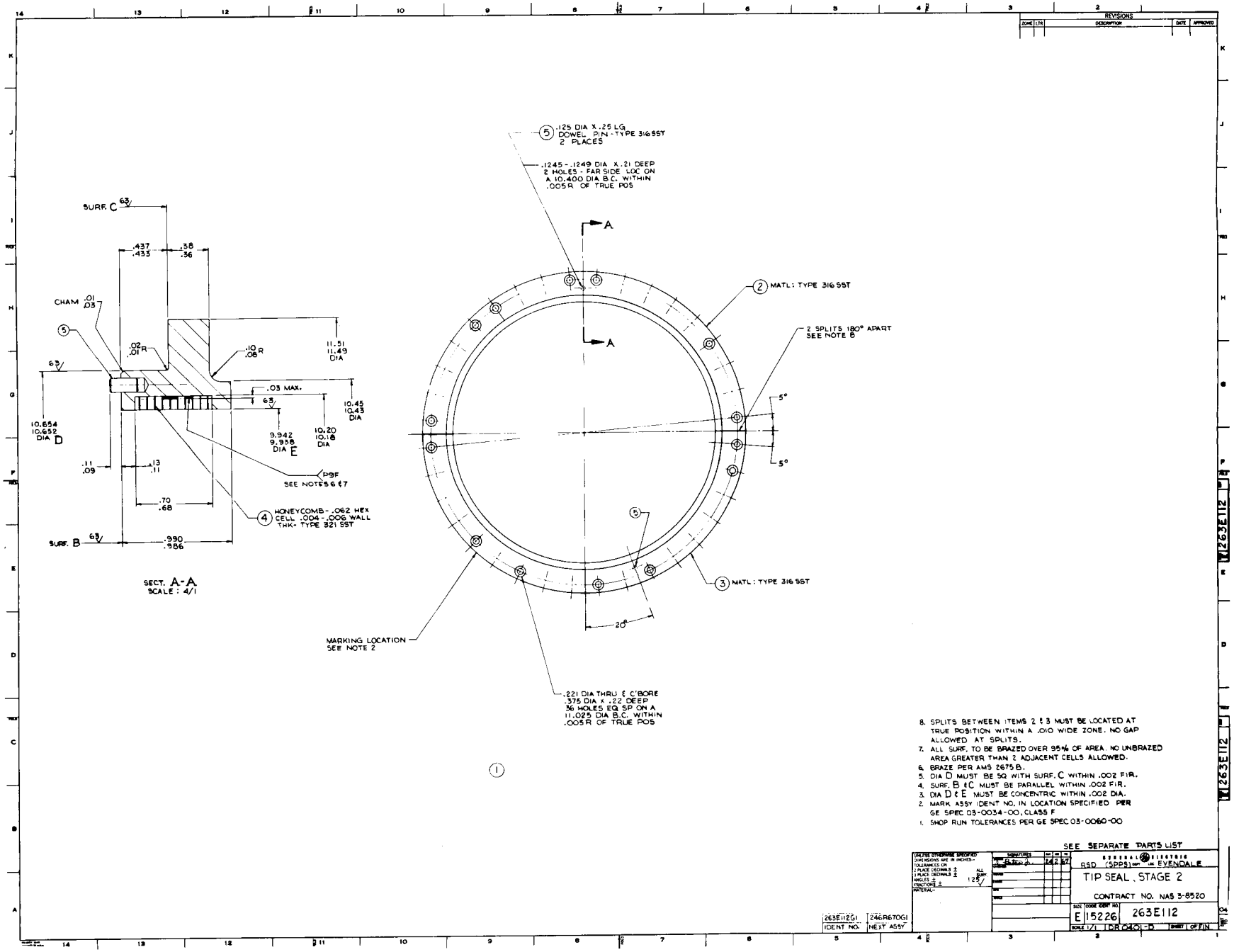

Figure 159. Stage 2 Honeycomb Tip Seal. (Phase I, Shrouded Design). (263E112)

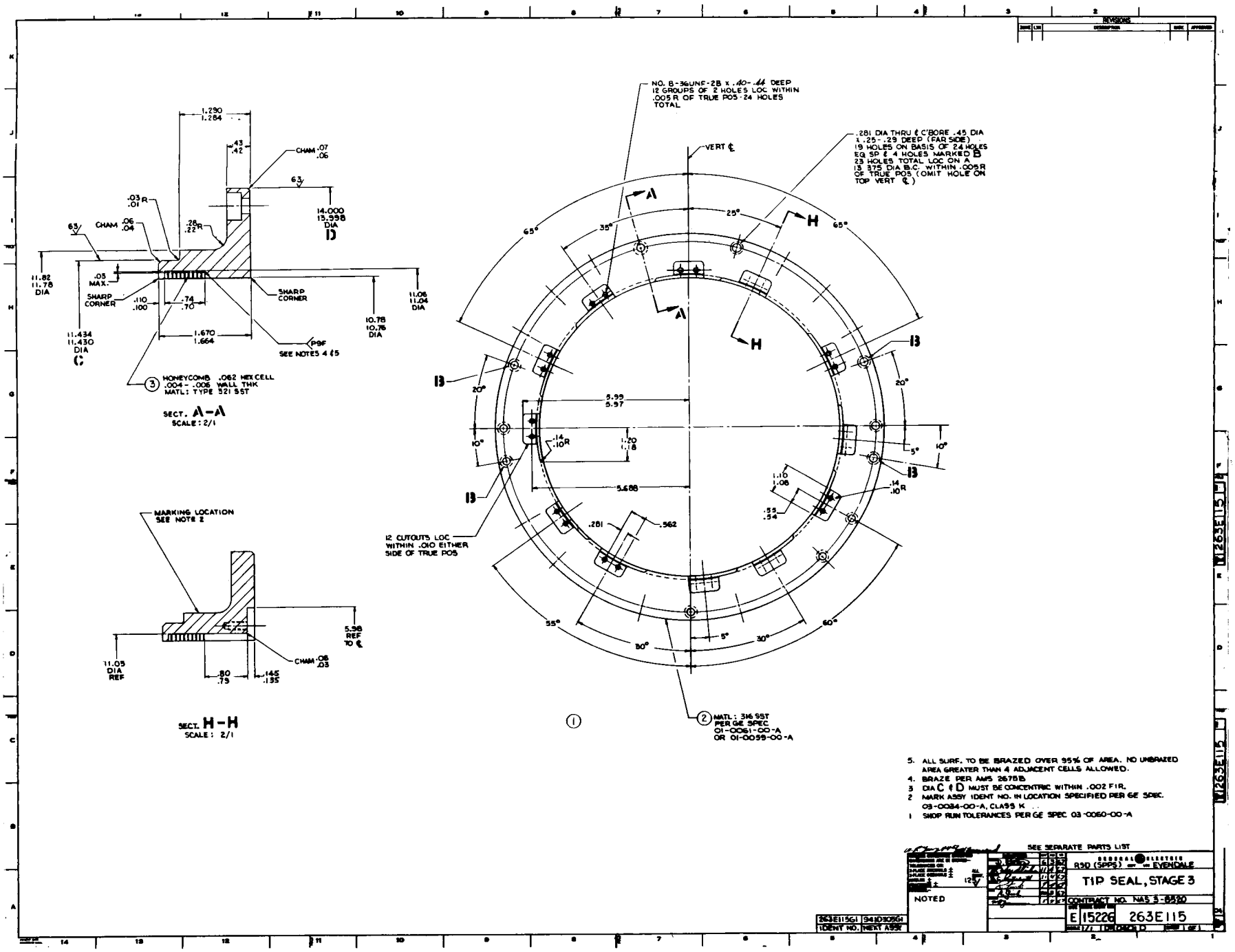

Figure 160. Stage 3 Honeycomb Tip Seal. (Phase I, Shrouded Design). (263E115).

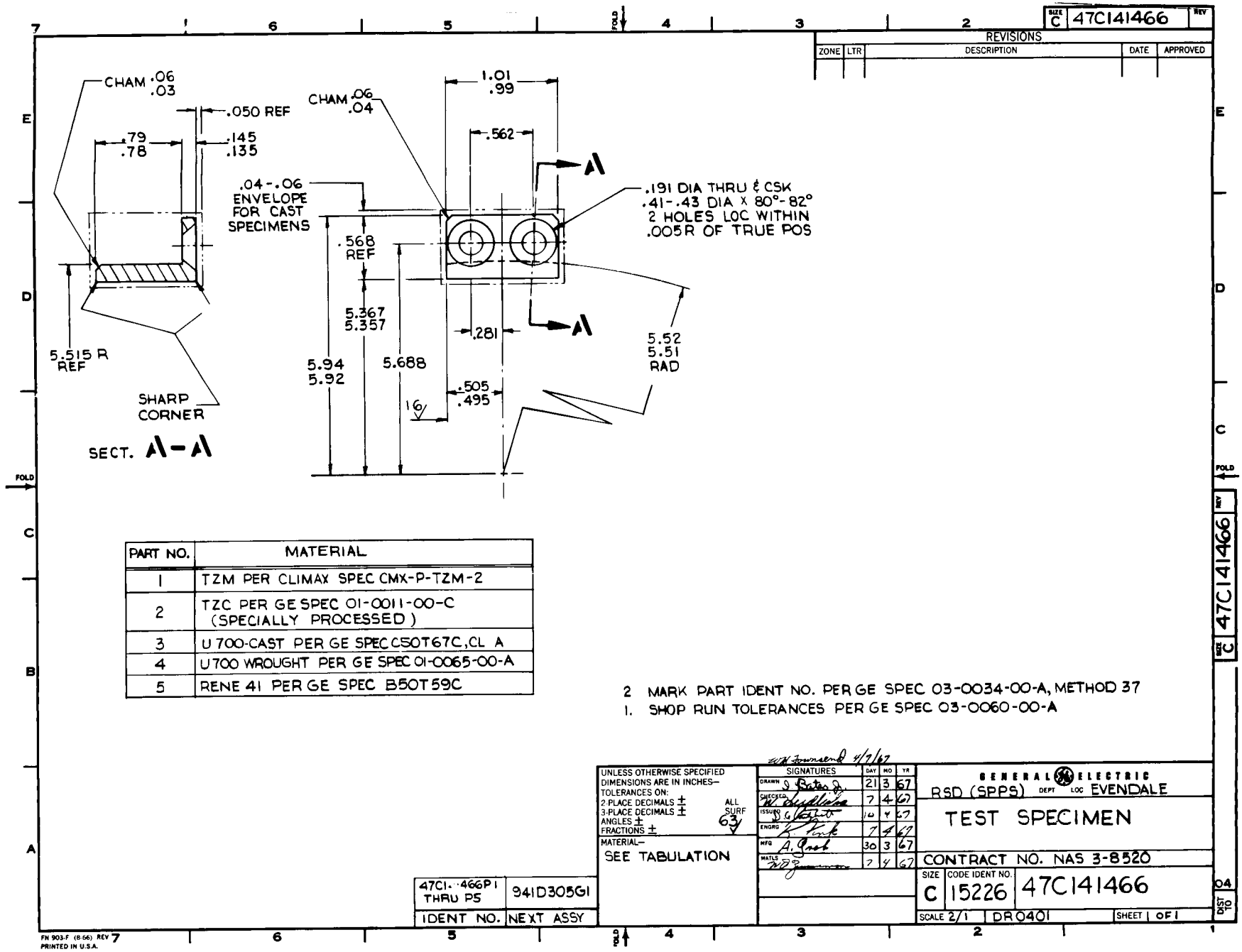

Figure 161. Erosion/Corrosion Material Test Insert. (Phase I, Shrouded Design) (47C141466)

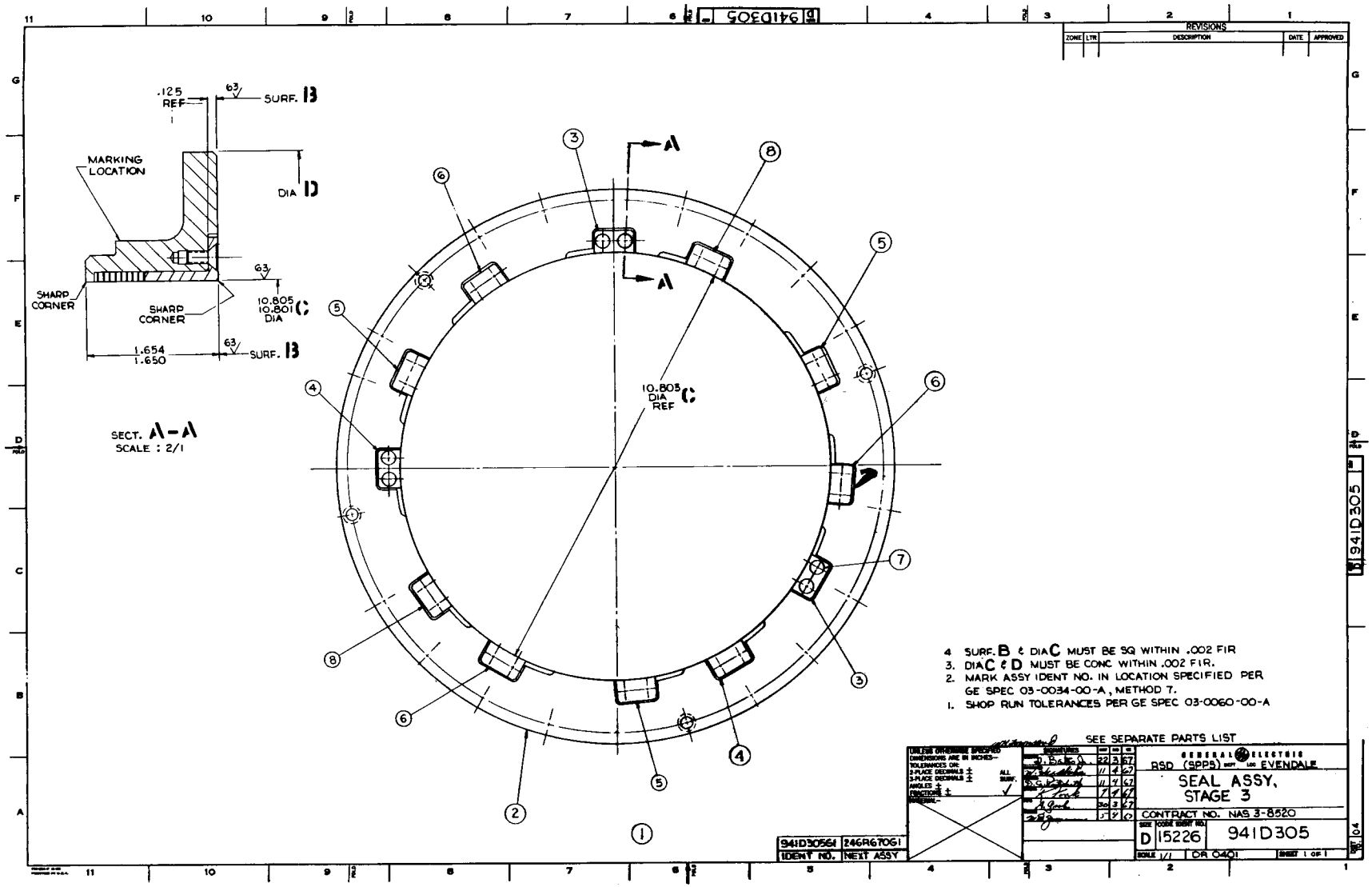

Figure 162. Stage 3 Honeycomb Tip Seal Assembly, Including Material Test Inserts. (Phase I, Shrouded Design) (941D305)

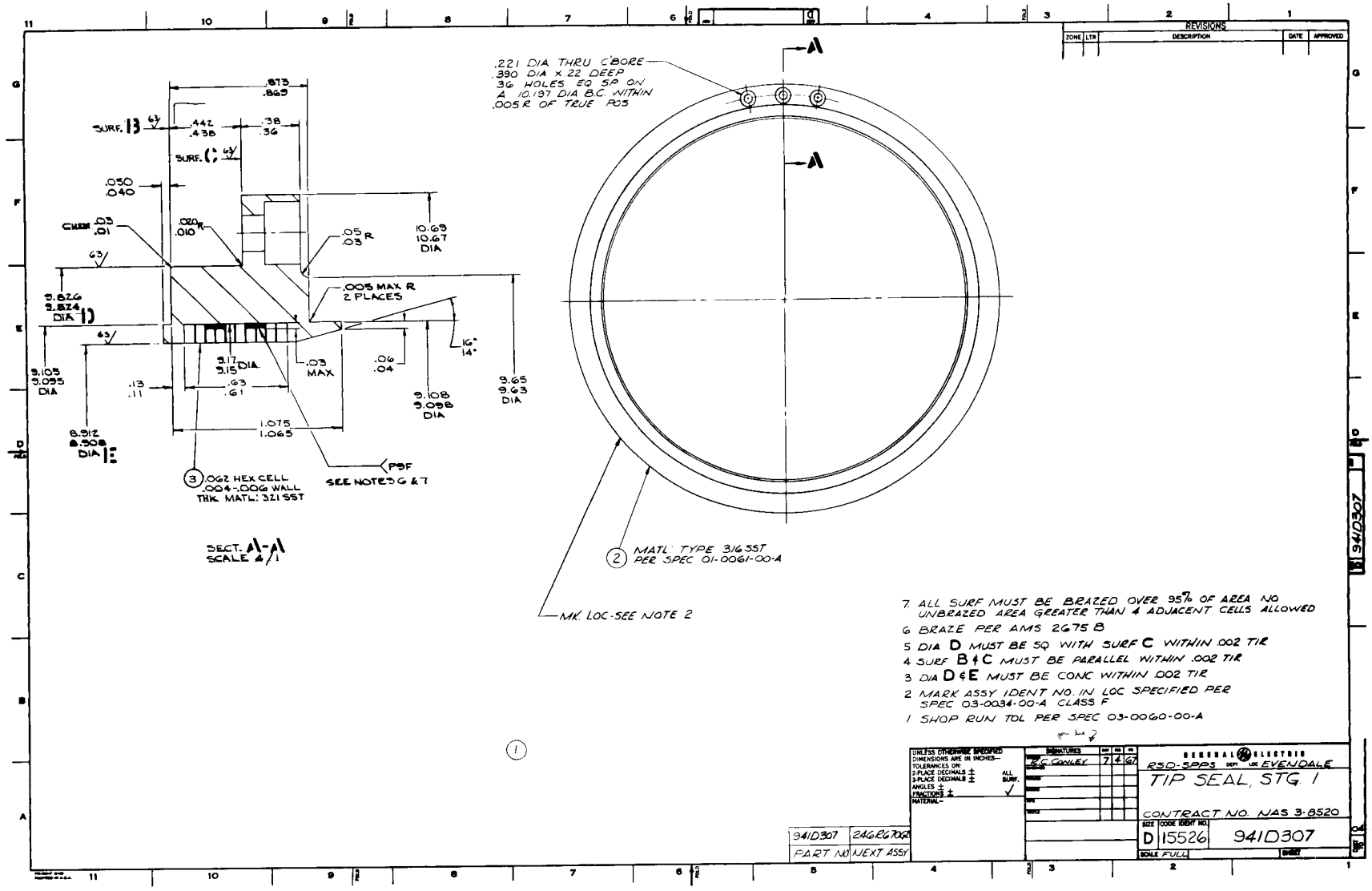

Figure 163. Stage 1 Honeycomb Tip Seal. (Phase II, Non-Shrouded Design). (941D307)

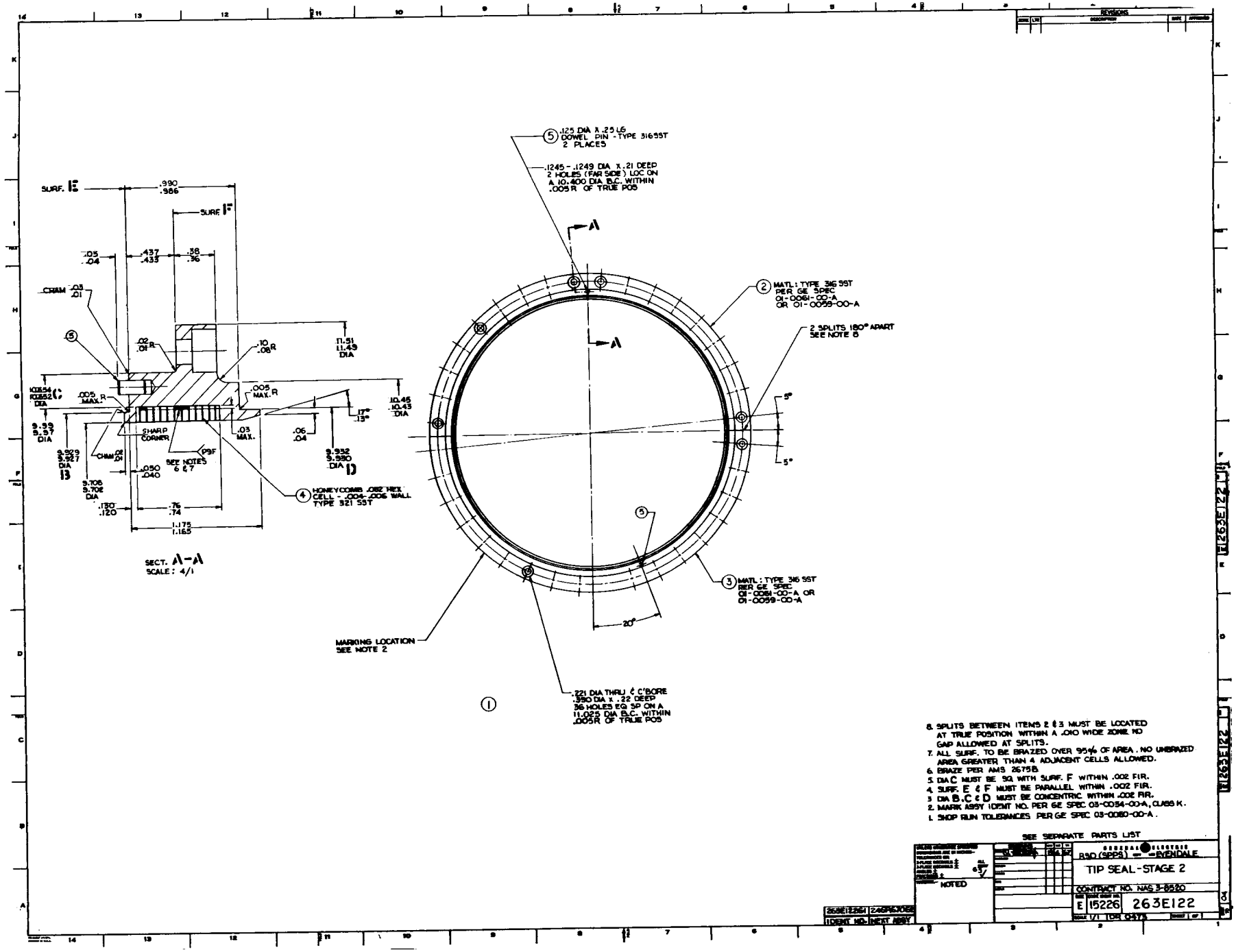

Figure 164. Stage 2 Honeycomb Tip Seal. (Phase II, Non-Shrouded Design). (263E122)

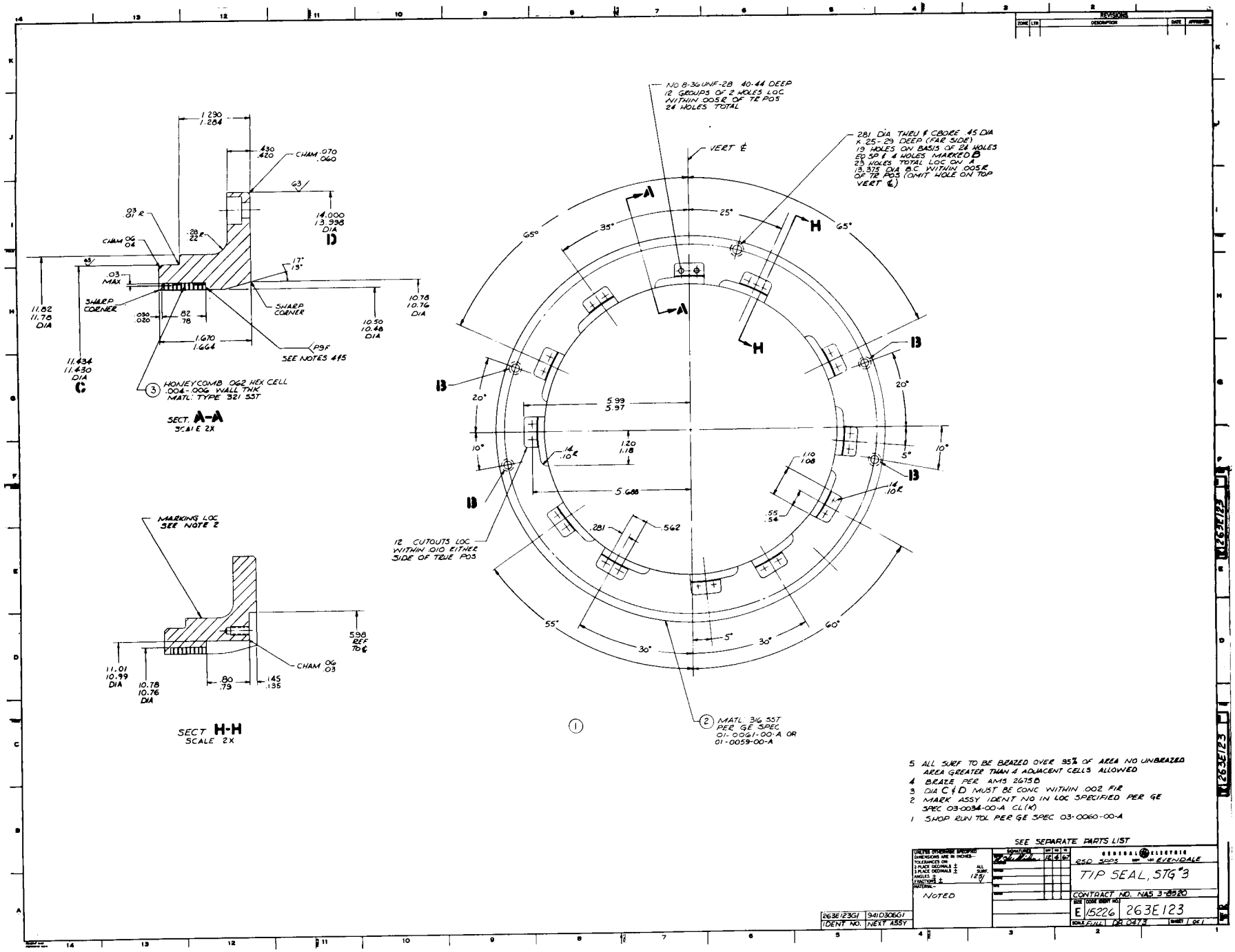

Figure 165. Stage 3 Honeycomb Tip Seal. (Phase II, Non-Shrouded Design). (263E123)

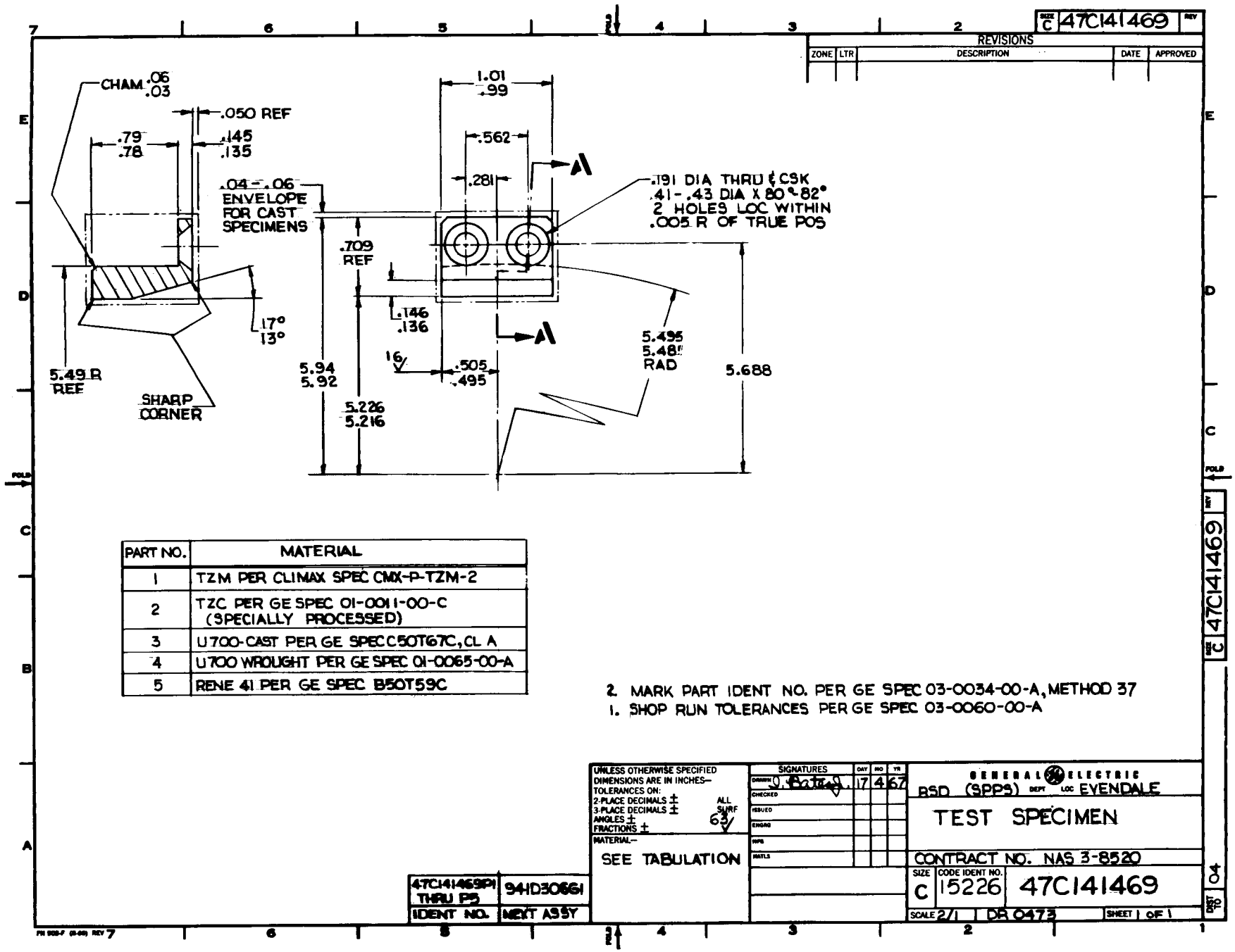

Figure 166. Erosion/Corrosion Material Test Insert. (Phase II, Non-Shrouded Design) (47C141469)

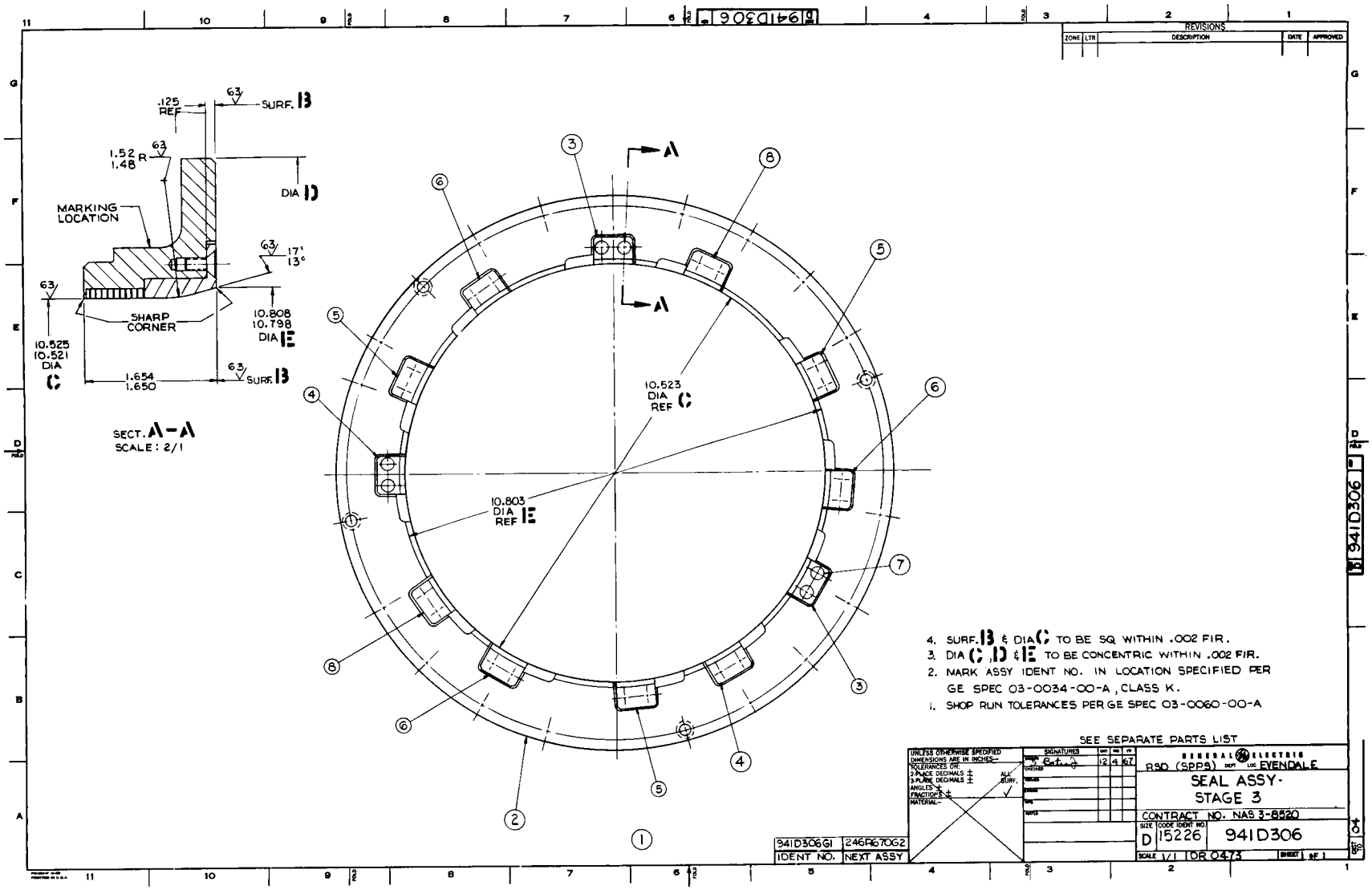

Figure 167. Stage 3 Honeycomb Tip Seal Assembly, Including Material Test Inserts. (Phase II, Non-Shrouded Design) (941D306)

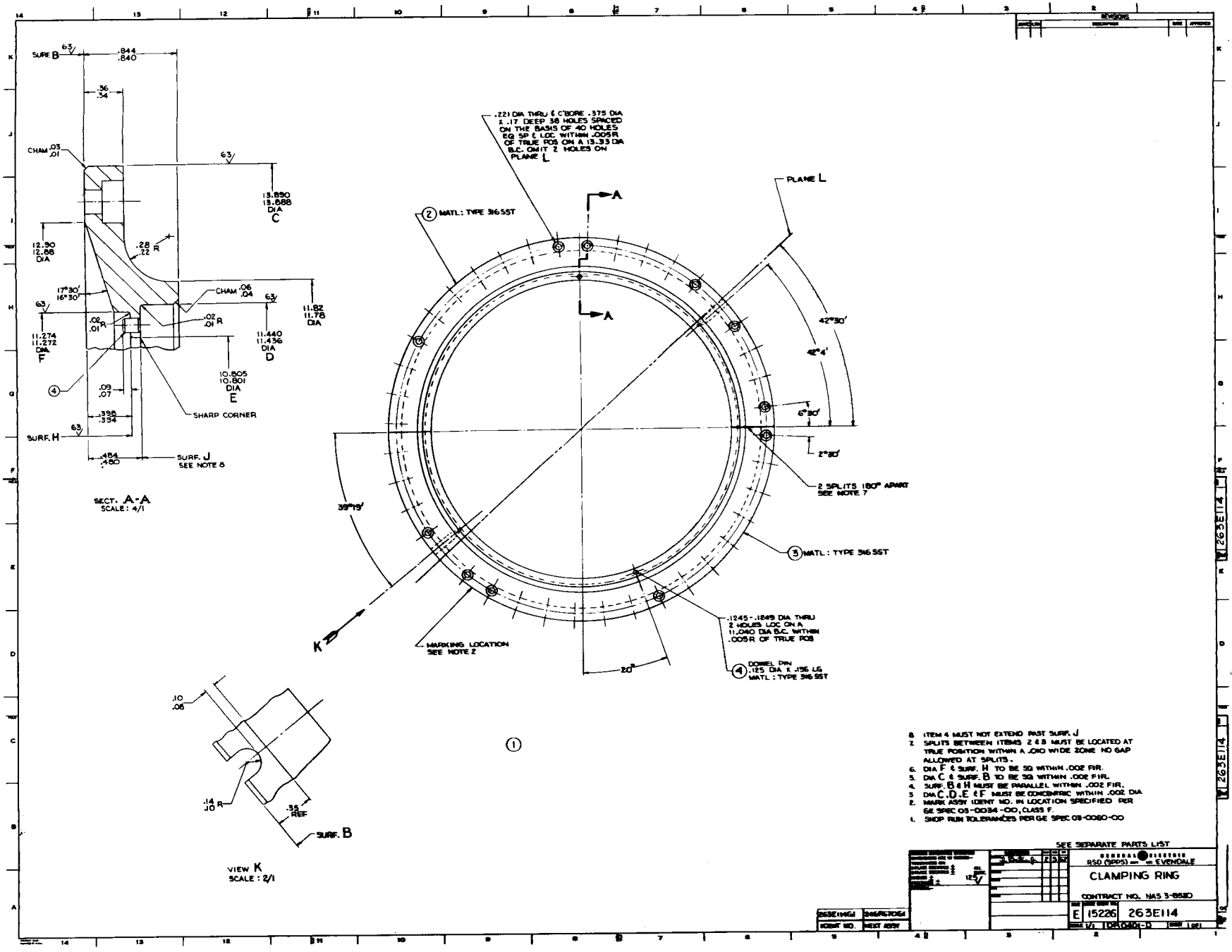

Figure 168. Stage 3 Nozzle Diaphragm Clamping Ring. (263E114)

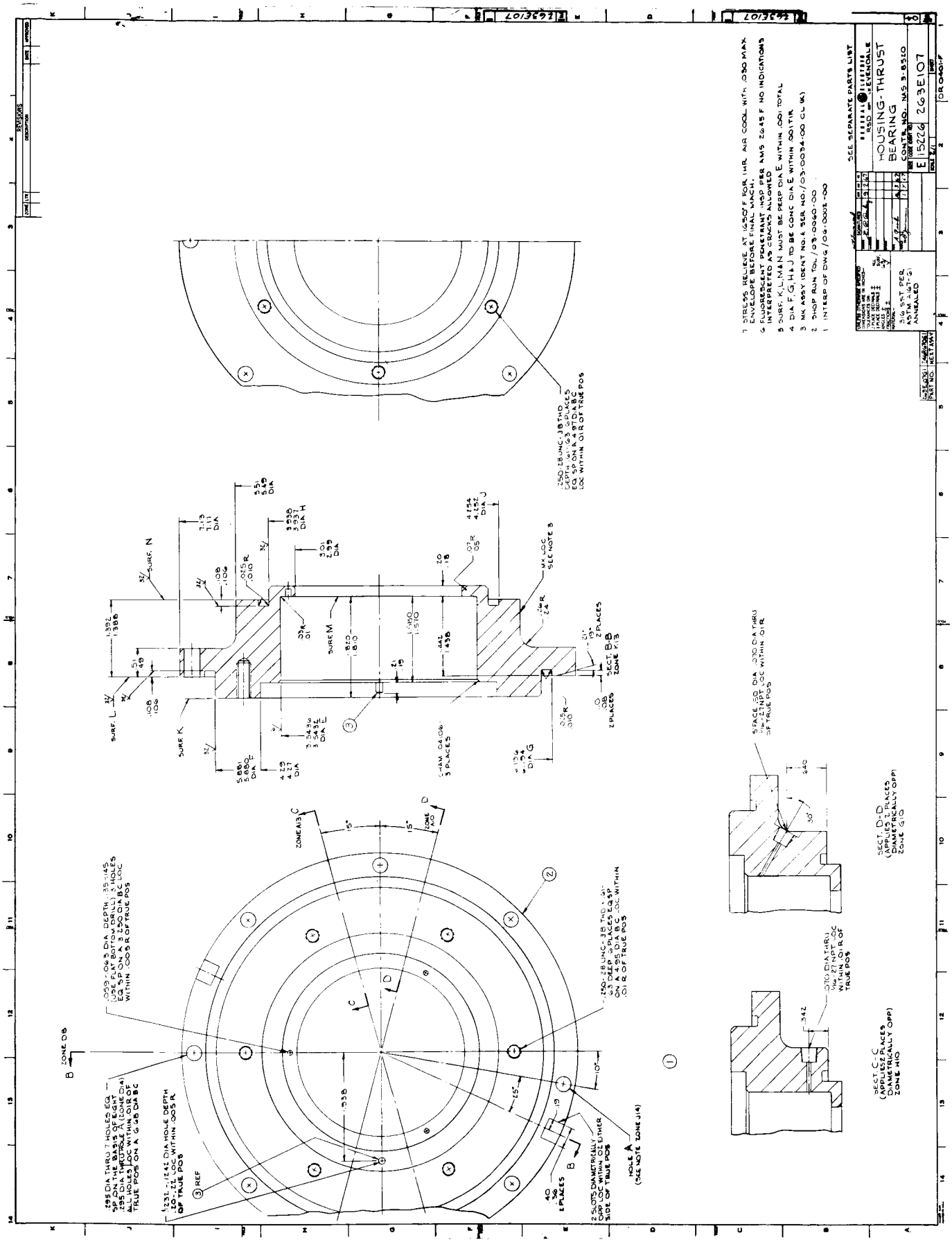

Figure 169. Thrust Bearing Housing. (263E107)

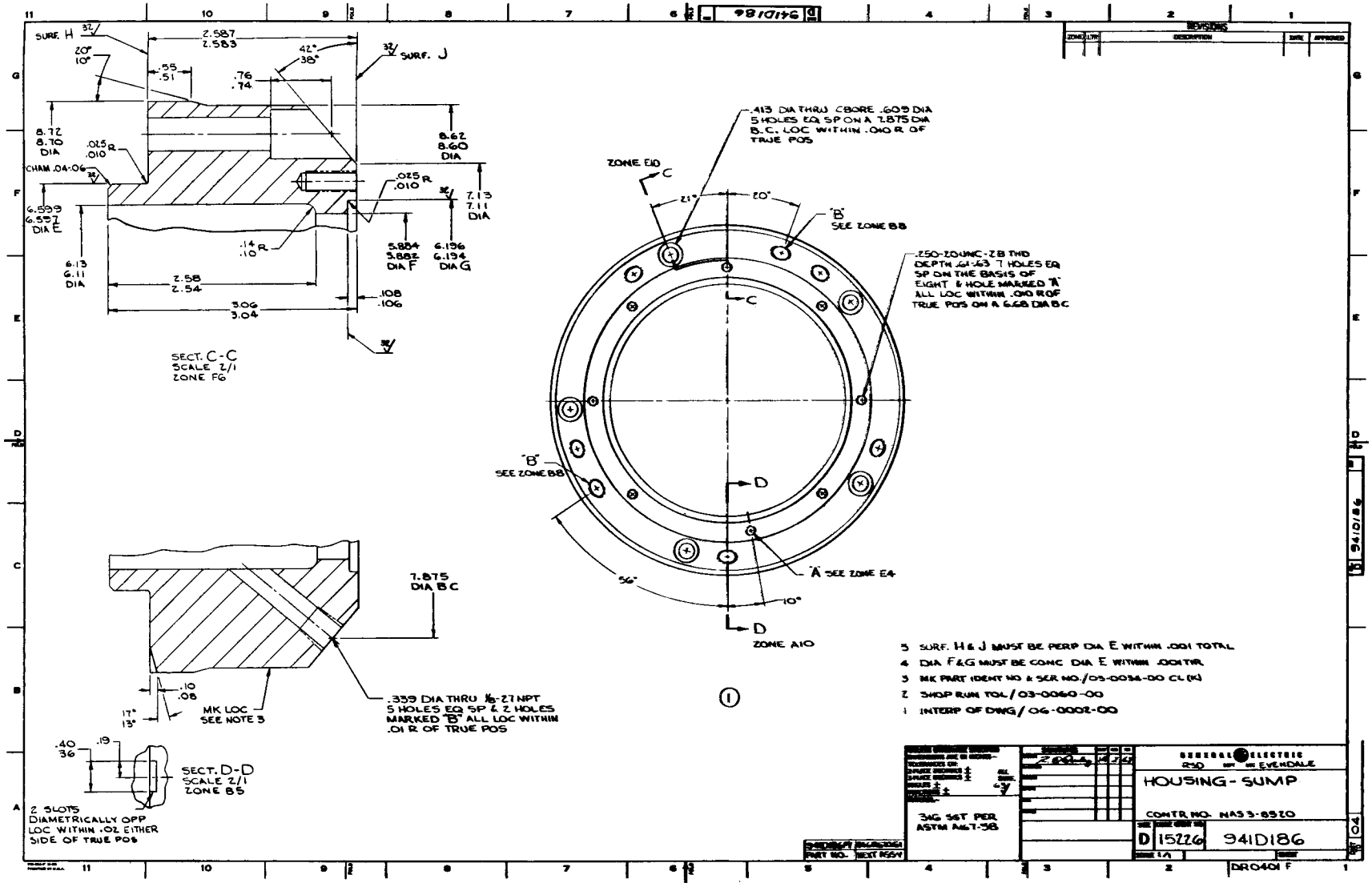

Figure 170. Ball Thrust Bearing Housing Sump. (941D186)

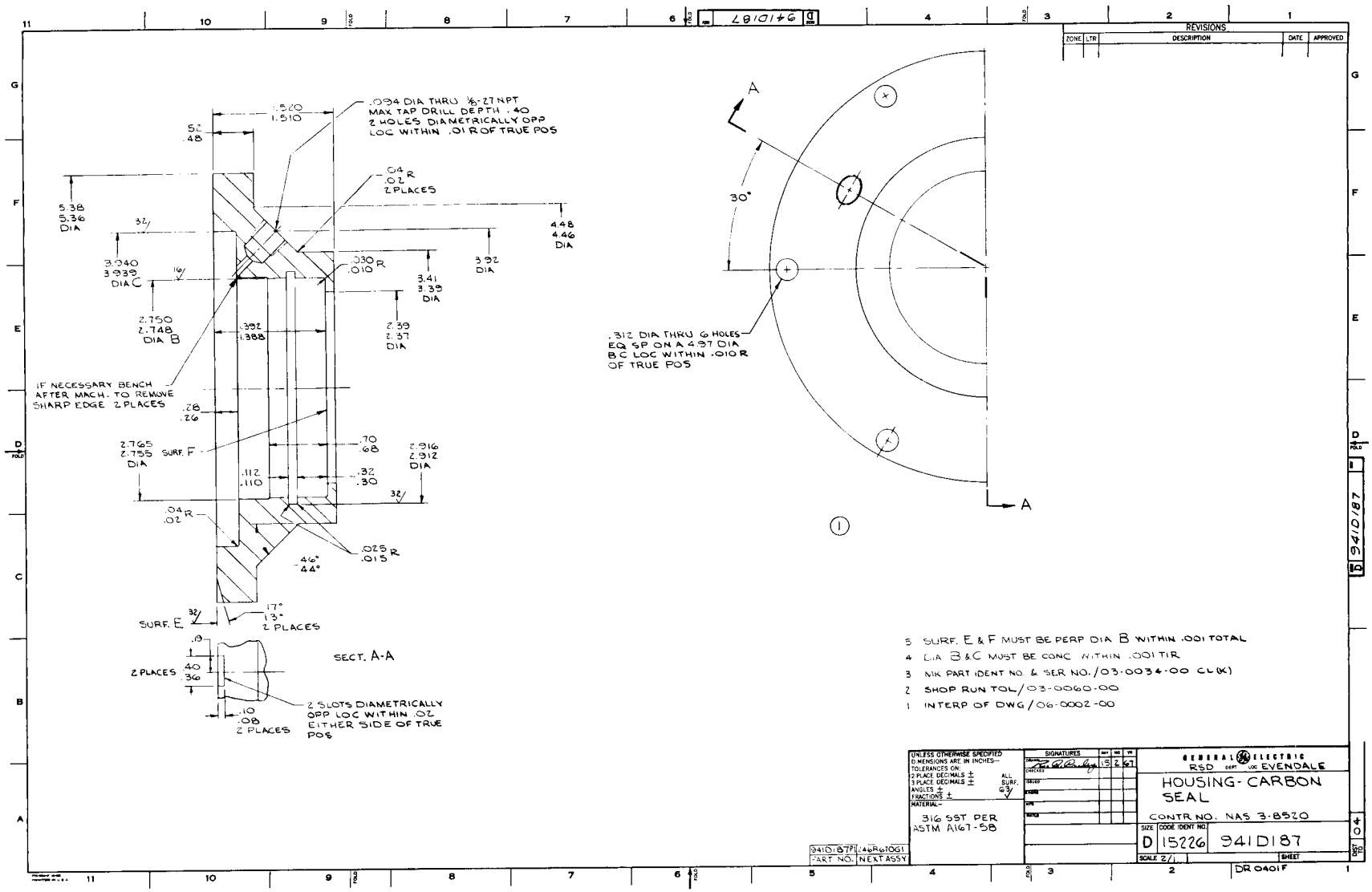

Figure 171. Carbon Face Seal Housing. (941D187)

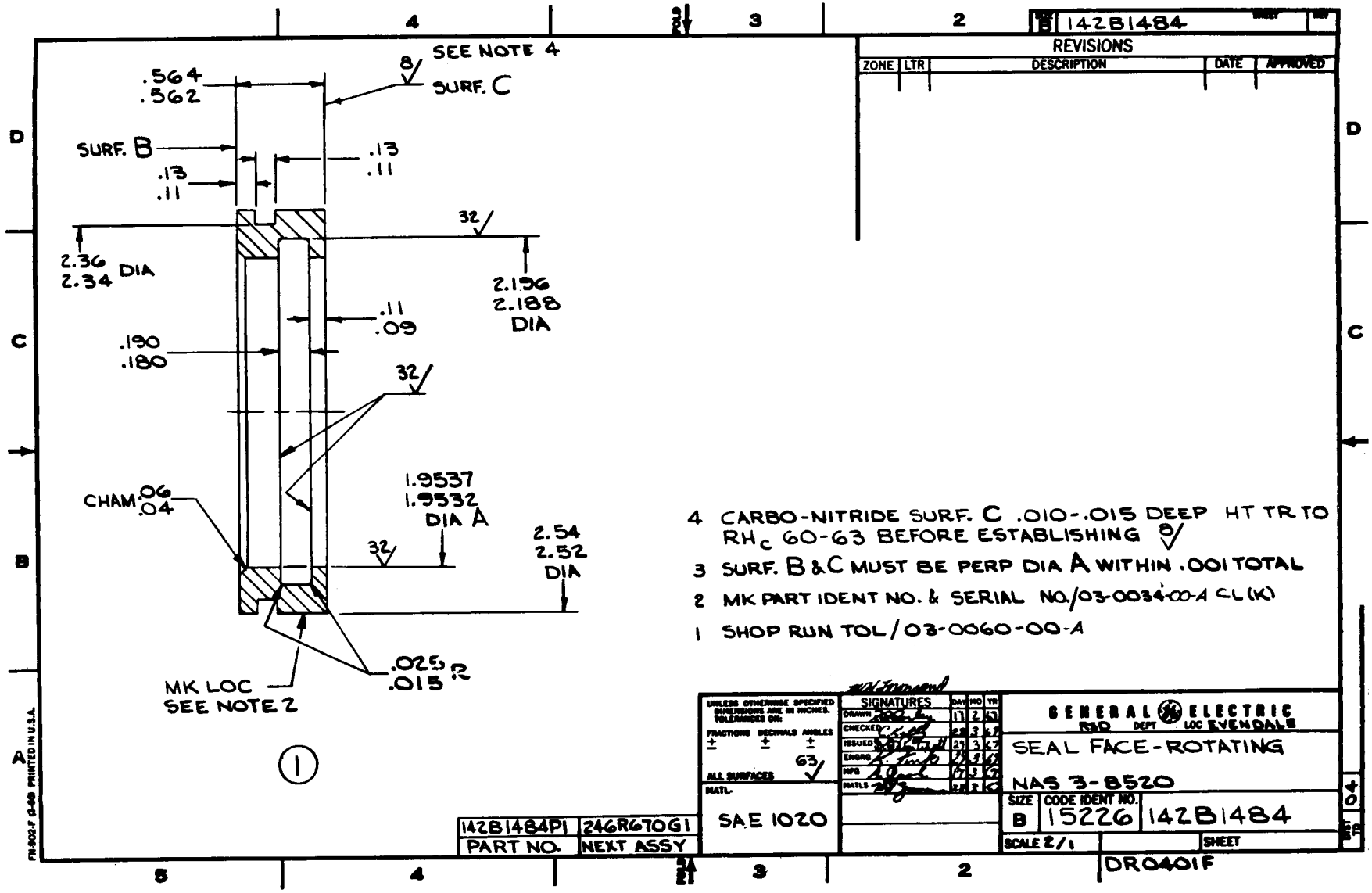

Figure 172. Rubbing Face for Carbon Seal. (142B1484)

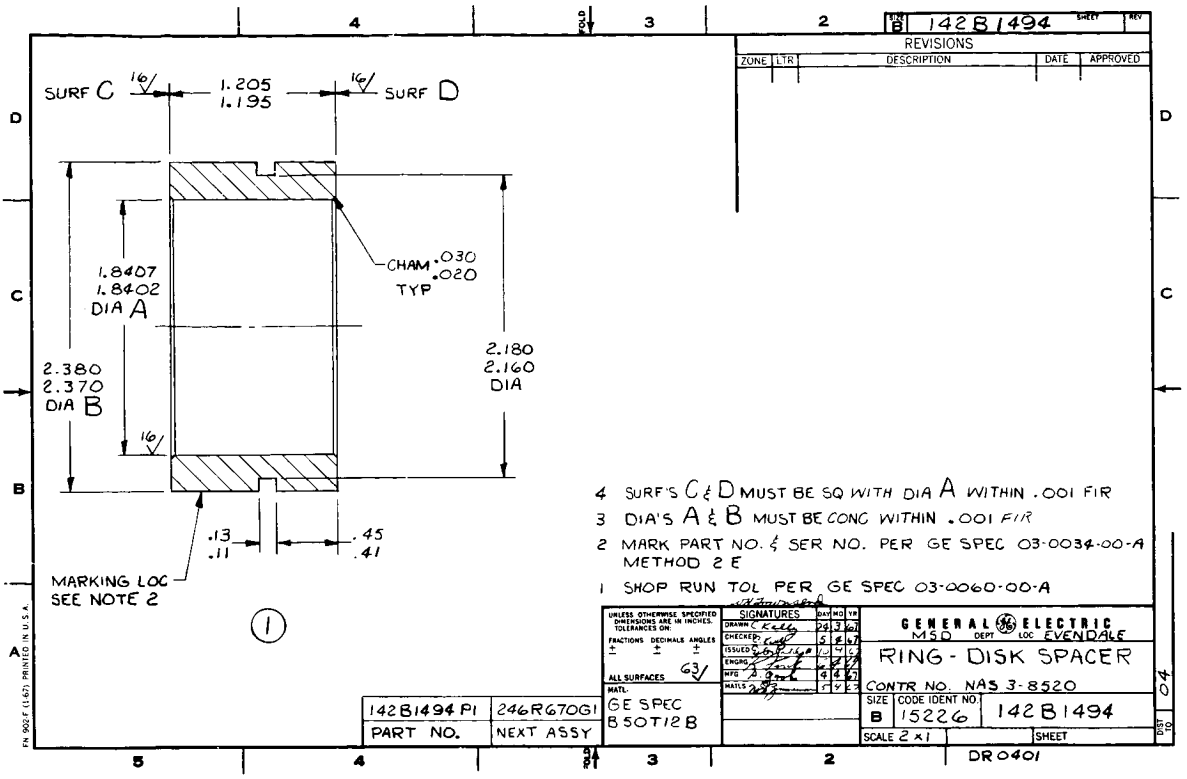

Figure 173. Spacer to Replace Disk Brake. (142B1494)

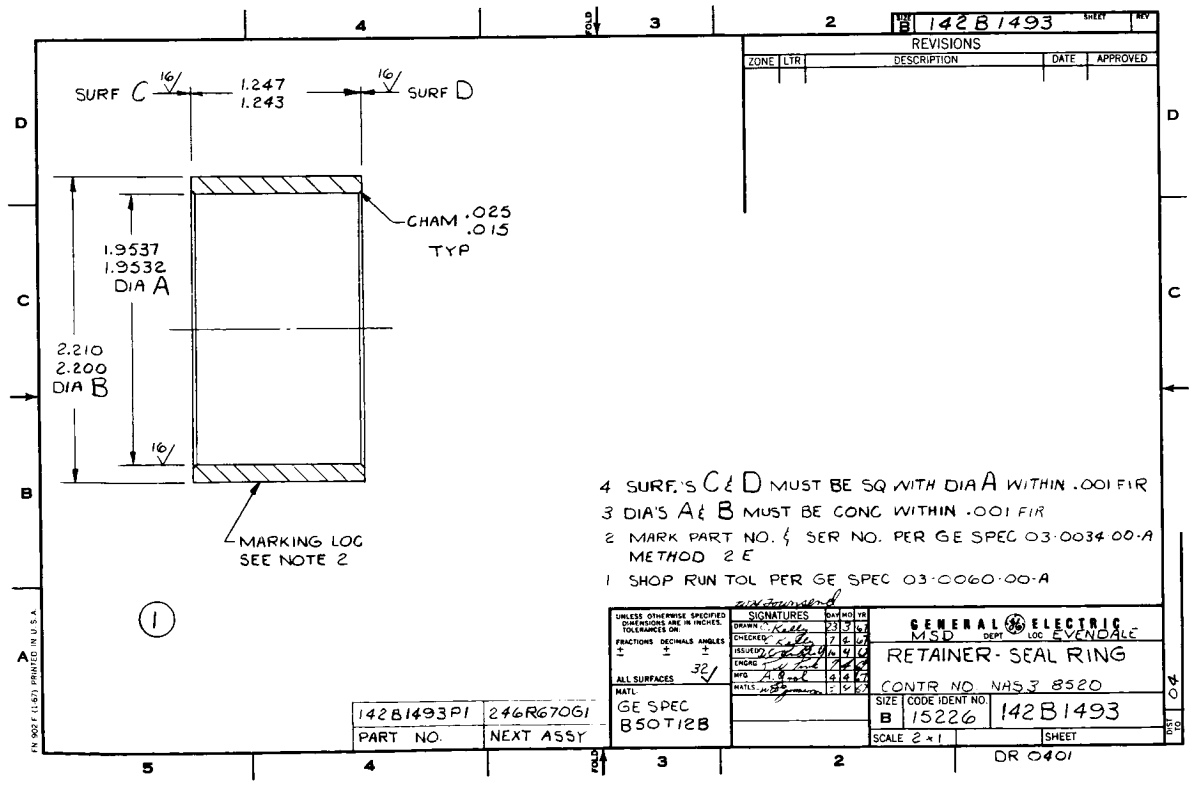

Figure 174. Retainer for Tie Bolt-to-Shaft Seal. (142B1493)

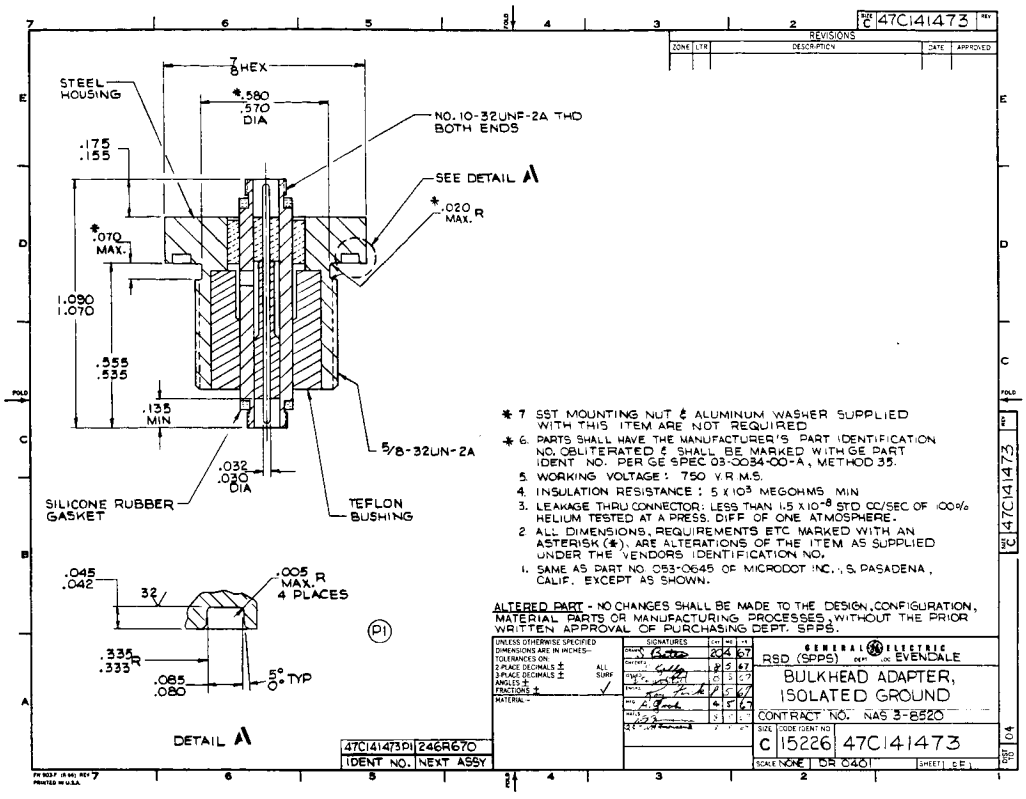

Figure 175. Instrumentation Lead-Through Retainer. (47C141473)

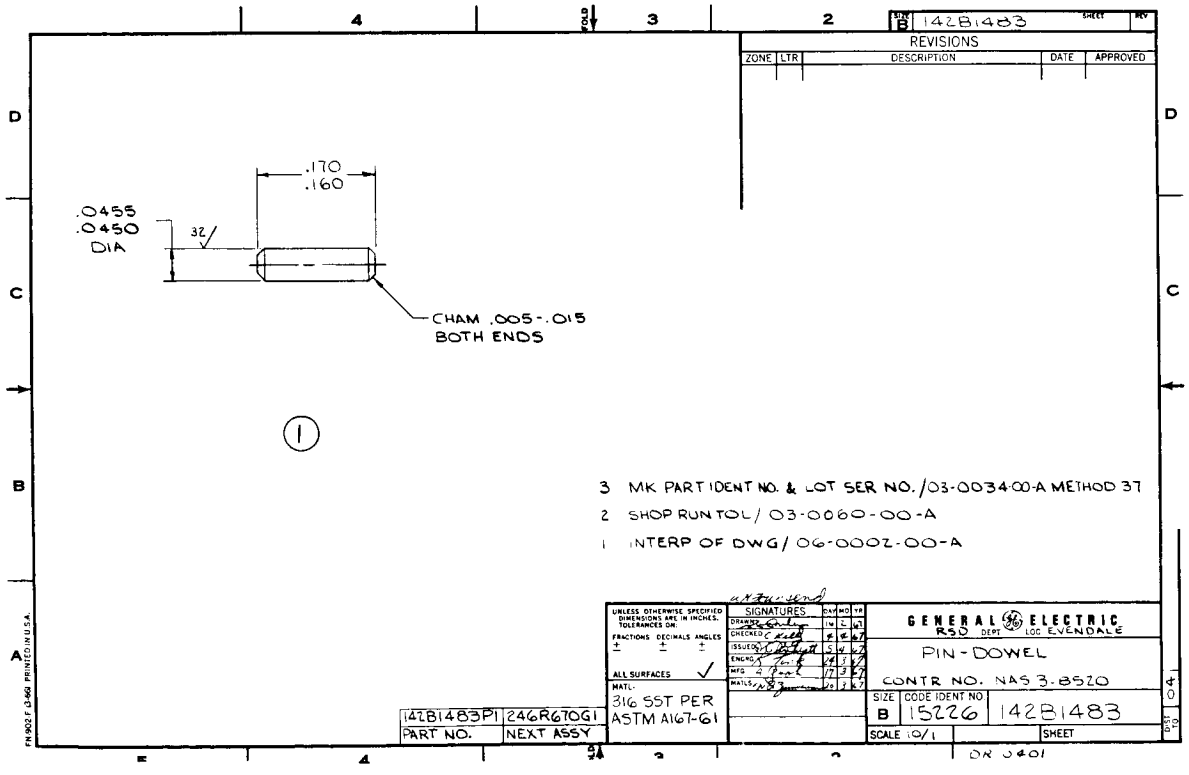

Figure 176. Dowel Pin for Nozzle Diaphragm Anti-Rotation. (142B1483)

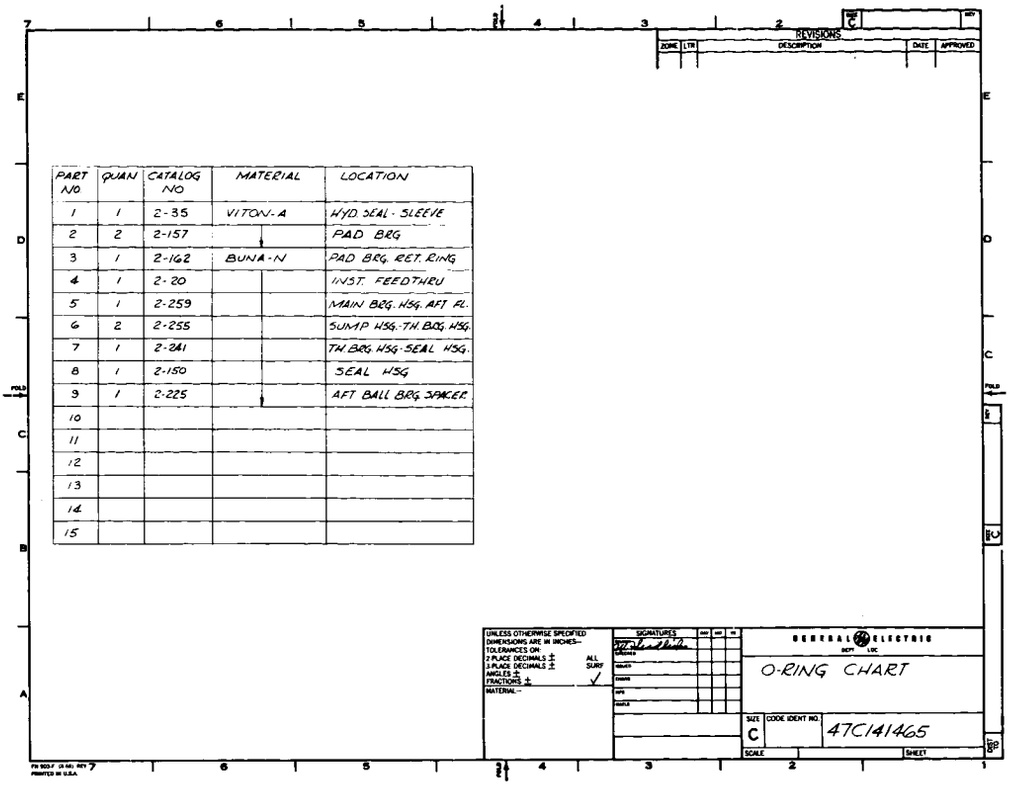

PART NO.	QUAN	CATALOG NO	MATERIAL	LOCATION
1	1	2-35	VITON-A	HYD. SEAL - SLEEVE
2	2	2-157		PAD BRG.
3	1	2-162	BUNA-N	PAD BRG. RET. RING
4	1	2-20		INST. FEEDTHRU
5	1	2-259		MAIN BRG. HSG. AFT FL.
6	2	2-255		SUMP HSG.-TH. BRG. HSG.
7	1	2-241		TH. BRG. HSG.-SEAL HSG.
8	1	2-150		SEAL HSG.
9	1	2-225		AFT BALL BRG. SPACER
10				
11				
12				
13				
14				
15				

Figure 177. Main O-Ring Chart. (47C141465)

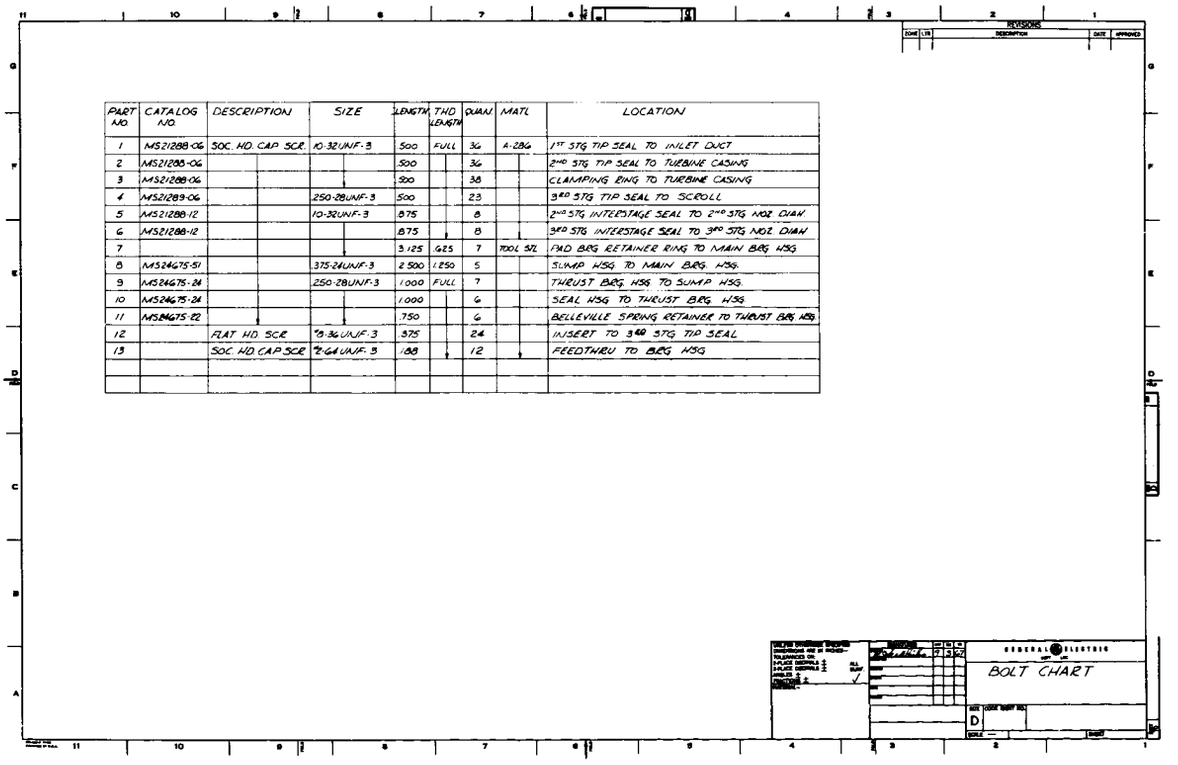

PART NO.	CATALOG NO.	DESCRIPTION	SIZE	LENGTH	THD LENGTH	QUAN	MATL	LOCATION
1	MS21288-06	SOC. HD. CAP SCR.	10-32UNF-3	.500	FULL	36	A-286	1ST STG TIP SEAL TO INLET DUCT
2	MS21288-06			.500		36		2ND STG TIP SEAL TO TURBINE CASING
3	MS21288-06			.500		38		CLAMPING RING TO TURBINE CASING
4	MS21289-06		250-28UNF-3	.500		23		3RD STG TIP SEAL TO SCROLL
5	MS21288-12		10-32UNF-3	.875		8		2ND STG INTERSTAGE SEAL TO 2ND STG NOZ. DIAN
6	MS21288-12			.875		8		3RD STG INTERSTAGE SEAL TO 3RD STG NOZ. DIAN
7				3.125	.625	7	TOOL STL	PAD BRG RETAINER RING TO MAIN BRG HSG
8	MS24675-51		375-24UNF-3	2.500	1.250	5		SUMP HSG TO MAIN BRG. HSG.
9	MS24675-24		250-28UNF-3	1.000	FULL	7		THRUST BRG. HSG TO SUMP HSG.
10	MS24675-24			1.000		6		SEAL HSG TO THRUST BRG HSG
11	MS24675-22			.750		6		BELLEVILLE SPRING RETAINER TO THRUST BRG HSG
12		FLAT HD. SCR	#8-36 UNF-3	.375		24		INSERT TO 3RD STG TIP SEAL
13		SOC. HD CAP SCR	1/4-64 UNF-3	.188		12		FEEDTHRU TO BRG HSG

Figure 178. Main Bolt Chart. (941D300)

INTRODUCTION

This report documents the metallurgical evaluation of six molybdenum alloy TZM pancake wheel forgings supplied by NASA to the Space Power and Propulsion Section of the General Electric Company. These forgings were intended for possible use in making a first and/or a second stage rotor wheel for the three stage potassium vapor turbine development program. Of these six forgings, one was to be selected for destructive testing to determine if the remaining forgings would meet the design requirements for long-time, high-temperature service, in this particular application. The design required that TZM wheels be operated for a life of 15000 hours at maximum wheel dovetail stresses of 32,798 psi at the 1445°F in the first stage and at stresses of 49,120 psi at 1335°F in the second stage. An additional requirement existed for a projecting interstage mechanical coupling located at the mid-radius sides of the wheels; a knowledge of the mechanical properties and low temperature ductility in this area was important since the grain flow would be transverse to this projecting part of the wheel and poor low temperature ductility would be expected.

Because of the concern for property variations as a function of grain flow, detailed macroetch studies were performed on the destructively analyzed wheel and additional surface macroetches were performed on the remaining wheels. The relationship between macrostructure and microstructure was also determined.

A program was conducted for determining the brittle-to-ductile transition temperature in various circumferential axial and radial locations within the wheel using impact, bend, smooth tensile and notched tensile testing methods. This information was intended to indicate the resistance of the material to low temperature brittle failure in the dovetail and curvic coupling areas during manufacturing, handling, assembly or testing and to determine the degree of turbine preheat which would be required to assure adequate ductility in these critical locations during turbine startup.

High temperature tensile tests were conducted to determine the material strength at the turbine operating temperatures between 1200°F and 1450°F; rupture testing was conducted at 2000°F for comparison of the rupture characteristics of this material with published TZM data.

A segment of the pancake forging was broached with dovetail tooling to evaluate this machining process for generating the dovetail slots with the required tolerances and surface finish.

were reinspected in order to select the least perfect forging for destructive testing. Ultrasonic testing was performed by the immersion technique at a frequency of 5 mc using focused transducers. Tests were performed using longitudinal and shear wave in both axial and the radial directions. Calibration was established on 0.020-inch diameter holes drilled radially inward at the rim at locations 1/4, 1/2, and 3/4 of the forging thickness. With the calibration holes established as 80% of the oscilliscope scale, a 60% defect indication constituted a 3% rejection limit. No unacceptable defects were found in any of the forgings. One forging having a 50% indication was selected for destructive testing.

Macroetching. The forging which was selected for destructive testing was sectioned along one diameter and one of the cut surfaces was then ground to approximately 32 rms surface finish and then etched with a solution of 47% HNO_3 and 2.5% HF. The structure, shown in Figure 2 (C66051950), was shown to be unsymetrical and indicated some gross shearing flow of the molybdenum during forging. One forging half was then cut at a 90° angle to the dimetrical surface, ground and etched. The resulting structure is shown also in Figure 2 (C660510108). Subsequently, all of the remaining forgings were surface ground and etched to determine if the structure revealed in the one forging was characteristic of all. Figure 3 (C66070883) shows the eccentric structure which was characteristic of all the forgings. Figure 4 shows graphically how this macrostructure could have been formed during the forging process.

Metallography. Metallographic specimens were selected from the forging rim as shown in Figure 5, and from the mid-radius area as shown in Figure 6.

A correlation between the macrostructure and microstructure is shown in Figure 7 where a diagonal trace of a macroetch flow line is indicated. The macroetch flow lines merely indicate the translation of position, during forging, of a given area of the original forging billet; since the individual grains of metal are subject to high shear forces, each grain assumes a final fiberous orientation in a plane parallel to the surface of the forging. It would be expected that the basic anisotropy exhibited in low temperature properites in the longitudinal and transverse (radial and axial) directions is a function basically of the microstructure and that the etched macrostructure flow lines exert a lesser effect in perturbatating the properties. In these pancake forgings the final grain flow is parallel to the surface. In a contoured forging grain flow could be induced in those directions in which improved ductility was required.

Test Specimen. A total of one hundred test specimens and three metallographic specimens were machined from the forging selected for destructive testing. The arrangement of these specimens as they were removed from the forgings are shown in Figure 8 where the type of specimen and its orientation are shown. Note that

A complete list of tests performed during this project is presented below:

1. Zyglo inspection
2. Ultrasonic inspection, all forgings
3. Hardness measurements, all forgings
4. Macroetch for surface structure, all forgings
5. Macroetch one diametric and one radial section, one forging
6. Metallographic structure comparisons with macrostructure
7. Brittle-to-ductile transition temperature in the circumferential, radial, and axial direction measurements by means of:

   Smooth bar Charpy impact tests
   Slow bend tests
   Smooth bar tensile tests
   Notch bar tensile tests

8. Tensile properties in the circumferential, radial, and axial directions at:

   Room temperature
   1200°F and 1400°F in vacuum

9. Rupture properties in the circumferential and radial directions at 2000°F
10. Dovetail broaching experiments

DATA AND RESULTS

Data concerning the procurement of the six TZM forgings by NASA are given in Table I; they indicate the acceptability of these forgings with respect to chemistry, hardness, heat treat condition, zyglo inspection and ultrasonic inspection. The forgings which were 12 inches in diameter were much larger than required to make the three stage turbine wheels; their thickness, which was 2.25 inches, was sufficient to make the first stage wheel, but not the second, as shown in Figure 1. Should a second stage TZM wheel be required, these forgings could be used in spite of their limited thickness by redesigning the location of the curvic coupling between the first and second stages to a position slightly aft of its present location. Figure 1 also indicates the optimum forged flow line configuration required to achieve low temperature ductility in the curvic coupling; it is likewise evident that machining the curvic coupling in a pancake forging, where the grain flow is parallel to the surface, would more likely result in cleavage failure at the base of the curvic coupling lugs.

Ultrasonic Inspection. An ultrasonic inspection was conducted by the forging vendor; however, because documentation of this test was incomplete the forgings

particular attention was paid to axial properties in the area of the curvic coupling and that all testing was limited within the nominal diameter of the three stage turbine wheels. Figure 9 shows a more detailed array of the test specimens and indicates both the arrangement of the specimens in depth and the number of each specimen.

The respective test specimen sizes were selected for maximum utilization of the material available in the critical area and the specimen length was selected as two inches so that specimens could be taken in the axial direction of the forging. The radial specimens were located so that the gauge portion of tensile specimens, for instance, would be centered in the area of interest. Circumferential specimens were located so that the gauge portion would be within the rim dimension of the machined wheel, likewise, the mid-radius specimens were located along the coupling diameter both for axial specimens and for the gauge portions of the tensile specimens. All specimens were zyglo inspected and then stress relieved for one hour at 2200°F after machining and prior to testing.

Impact Tests. The brittle-to-ductile transition temperature was determined using un-notched charpy impact specimens taken from the axial direction at the curvic coupling location and from the radial direction at the rim location. All machine marks and other possible stress risers were removed from the tension surface by lapping on a 600 grit paper. Tests were performed on a standard charpy machine having a maximum energy of 48 foot-pounds and an impacting velocity of 17 foot-pounds per second.

The brittle-to-ductile transition temperature for rim-radial specimens 77 through 84 was found to be approximately 590°F. The brittle-to-ductile transition temperature for mid-radius axial specimens 69 through 76 was found to be approximately 255°F. The impact data are shown plotted in Figure 10.

Slow Bend Tests. The brittle-to-ductile slow bend transition temperature was determined for the axial and radial direction at the curvic coupling location. As in the case of the impact specimens, all machine marks were removed from the tension surface by lapping on a 600 grit paper. Ductility was based on the ability of the specimen to bend 90° around a one (1) T radius without cracking. Bends were accomplished using a constant head speed of 0.05 inch per minute using 3-point loading over a one-inch span; the specimen was loaded on the 0.250-inch wide face of a 2.0 x 0.250 x 0.125-inch specimen.

The brittle-to-ductile transition temperature for the axially oriented specimens was found to be approximately 600°F. The brittle-to-ductile transition temperature for the radially oriented specimens was found to be approximately 75°F. A plot of bend angle versus test temperature for both directions is presented in Figure 11.

Tensile and Rupture Tests. All tensile and rupture specimens were designed so that the axial properties of the forging could be evaluated on an equivalent basis with the radial and circumferential properties. The specimens were machined into cylindrical blanks and then ground to the proper gauge dimension. Surface finish of the gauge section of all specimens was better than 16 rms. All specimens were zyglo inspected and stress relief heat treated for one (1) hour at 2200°F in a vacuum of 5×10^{-6} torr or better prior to testing.

Smooth Bar Tensile Tests: Initially, smooth bar tensile tests were conducted to determine the room temperature ductility; then, slightly above to determine brittle-to-ductile transition temperature. A minimum tensile ductility of 6% elongation was considered necessary for ductile behavior in a turbine based upon past experience in gas turbine technology. The remaining specimens were used to determine the material strength characteristics at the anticipated turbine operating temperature of 1450°F for the first stage wheel and 1350°F for the second stage wheel. Test temperatures of 1400°F and 1200°F were selected in order to compare the results with available published data. The specimen was strain loaded at 0.005 inch per minute head speed to 0.2% yield strain and then at 0.05 inch per inch per minute to failure. The tensile specimens were of a button head type with a 0.162-inch gauge diameter and a 1.1-inch gauge length.

The results for the smooth bar tensile tests are presented in Table II and plotted for comparison with available data in Figure 12 (Ultimate Tensile Strength) and Figure 13 (Yield Tensile Strength).

Notched-Bar Tensile Tests: Notched-bar tensile tests were performed on rim-circumferential, mid-radius radial and mid-radius axial specimens in order to determine at what temperature the material became notch strengthened. The notch factors ranged between 2.9 and 3.1.

The results which are presented in Table III show that notch strengthening occurred for the different locations as follows:

Rim-Circumferential: below 75°F
Mid-Radius Radial: between 75°F and 100°F
Mid-Radius Axial: between 75°F and 300°F

Rupture Tests: Stress-to-rupture tests were performed on rim-circumferential and mid-radius radial specimens at 2000°F in a vacuum of 5×10^{-5} torr. Tests were designed for less than 50 hours duration. Test results are presented in Table IV and plotted against a curve representing available published data in Figure 14.

Broaching Experiment. Broaching experiments were performed on a scrap

segment of the wheel forging which had been machined to provide one-inch thick specimens. The broach of a dovetailed form similar to that anticipated for the 3 stage turbine was employed. The tool had been used extensively in broaching A-286 alloy wheel dovetail slots. Two slots were made in the specimen without back-up provisions, one at a broach speed of 13 feet per minute and the other at 20 feet per minute. As can be observed in Figures 15 and 16, break-out occurred on the exit side approximately 0.025 to 0.030 inch deep. When a 1/4-inch thick unslotted steel back-up plate was employed for a third slot, break-out was practically eliminated. The surface finished of the three slots consisted of waves and tears and was considered poor, see Figure 17.

Break-out on the exit surface may be completely eliminated through the use of a pre-slotted, cast-iron back-up plate. Surface finish can be improved less easily; a study of lubricants and speed in addition to a broach designed expressly for the TZM alloy will be required. Present results are, however, encouraging.

DISCUSSION OF RESULTS

A summary of the data on brittle-to-ductile transition temperatures is given in Table V. As would be expected, the higher transition temperatures occur under the higher strain rate type of testing and in specimens taken in the axial rather than in the radial direction. In all cases, however, the transition temperatures are no greater than 590°F; by pre-heating the turbine to 700°F a high degree of reliability will be achieved in avoiding catostrophic brittle failure and in providing the measure of ductility required to plastically dispel peak stresses in dovetail slots or at the wheel bore as they develop. The problem of brittle behavior at room temperature during machining, handling and assembly will require an appreciation of the poor ductility particularly in the axial direction and under impact loads.

The unsymetrical appearance of the macroetch flowlines in the forging is apparently not of first order importance. This is attested to by the fact that among radial specimens subjected to impact test there was a variation in the orientation of macro flowlines from specimen to specimen but this did not result in erratic results in determining the radial impact transition temperature. The microstructure indicates that the fiber axis of the grain is parallel to the flat surface of the forging; it is this grain orientation which provides the basic anisotropy of properties at low temperatures as evidenced by a comparison of the transition temperatures for axial and radial specimens. As mentioned earlier, the macroetch flowlines indicate the gross movement of metal during forging. The shearing action during forging, however, results in a fiber grain texture directed parallel to the flat forging surface; the macro-flow lines represent a less significant perturbation in the size, shape and spacing of the well oriented fiber grain structure. While the above anisotropy is responsible for poor low temperature ductility in the axial

direction, and may be a ciritcal factor during manufacturing and assembly, the use of turbine preheat should prevent failure during operation as a result of this characteristic. The use of contoured forgings would tend to modify the fiber grain texture to provide improved low temperature ductility in certain required directions; but this would require a significant forging development program.

The high temperature tensile properties of this forging did not show anisotropy. The yield strengths and ultimate strengths when plotted as a function of temperature compared well with data on TZM forgings and bar stock as determined by other sources.*

CONCLUSIONS AND RECOMMENDATIONS

The following conclusions and recommendations have been reached after careful evaluation of the various test results:

Conclusions

1. The high temperature forgings are considered adequate for the intended use as first and second stage wheels of the three stage turbine. These forgings are considered usable for the first hardware.

2. The fiber grain microstructure appears to have the major influence on the low temperature ductility, and the unsymetrical character of the macroetched flow lines is probably not of major importance.

3. The poor low temperature ductility provides a high risk in manufacturing processes, in handling, and in subsequent assembly operations. Since only five forgings are available to make two each of both the first and second stage wheels, extreme care must be taken in manufacture, handling, and assembly to insure the availability of assembled turbine components for test.

4. It will be necessary to preheat the turbine facility to 700°F or higher to assure adequate ductility during turbine startup.

5. Pancake forgings with more uniform macrostructure could be made using extra caution in the forging process to minimize canting of the forge billet and to improve the initial distribution of metal flow; however, significant improvements in axial ductility would not be expected since the fiber grain structure is always oriented parallel to the flat surface of the forging. It would be desirable to have additional pancake forgings available as a backup to the limited member of forgings (4) now available for fabrication of 3-stage turbine components.

See List of References

Recommendations

1. It is recommended that contoured forgings be considered with controlled grain flow into the curvic coupling area for improved axial ductility and impact properties at this critical interstage coupling area.

TZM PANCAKE WHEEL FORGINGS
DATA AND PROCESSING HISTORY

Pieces Received

6 pieces @ 12-inch diameter x 2.25 inches thick

Source

NASA

Heat No.

3 pieces (A1-1,2,3) TZM-7491A
3 pieces (A2-1,2,3) TZM-7490A

Composition

	C	Si	Ni	Fe	Ti	Zr	N_2	O_2	H_2	Mo
TZM-7491A	.015	.002	.001	.001	.40	.10	.0002	.0005	.0001	ba.
TZM-7490A	.015	.002	.001	.001	.47	.10	.0002	.0002	.0001	ba.

Processing History

1. Forged from 7" round, stress relieved 2200°F one hour, air cooled
2. Zyglo inspected per MIL-T-6866
3. Ultrasonically inspected
4. Brinell hardness

Heat No. TZM-7491A (A1)

#1		#2		#3	
Edge	Center	Edge	Center	Edge	Center
258	240	258	240	249	240
249	258	258	240	258	258
258	240	258	240	249	240
258	258	249	240	249	258

Heat No. TZM-7490A (A2)

#1		#2		#3	
Edge	Center	Edge	Center	Edge	Center
258	240	258	240	258	240
258	240	258	240	258	240
249	249	249	240	249	240
258	240	258	240	258	240

TABLE II

SMOOTH BAR TENSILE TESTS

1. Rim, Circumferential

Specimen No.	Test Temp-°F	UTS-KSI	.2YS-KSI	% RA	% E	Acceptable Ductility
25	RT	102	99.0	1	2	No
27	RT	120	110	0	2	No
29	RT	104	102	2	1	No
30	RT	116	102	35	13	Yes
26	200	105	93.3	40.5	10.5	Yes
31	200	104	93.7	50	15	Yes
28	1400	84.9	69.7	74	11	Yes
32	1400	84.3	79.5	78	12	Yes

2. Rim, Radial

33	RT	116	102	12	8.5	Yes
37	RT	118	106	38	*	-
38	RT	117	102	39	14.5	Yes
40	300	100	89.6	54	16	Yes
34	1200	83.4	77.5	67	11	Yes
35	1400	83.6	78	74	11	Yes
39	1400	82.6	78.5	74	11	Yes
36	2000	72.8	67.5	76	12	Yes

*Specimen shattered at failure, elongation not determined.

TABLE II (CONTINUED)

3. Mid-Radius, Radial

Specimen No.	Test Temp-°F	UTS-KSI	.2YS-KSI	% RA	% E	Acceptable Ductility
41	RT	117	104	34	*	-
45	RT	118	105	38	15	Yes
46	RT	118	105	11	10.5	Yes
42	1200	85.9	82	70	11	Yes
48	1200	75.0	70.5	76	12	Yes
43	1400	81.5	77.5	77	11	Yes
47	1400	80.7	76.5	77	11	Yes
44	2000	68.1	65.5	77	11	Yes

4. Mid-Radius, Axial

49	RT	88.6	-	0	0	No
50	RT	100	99	0	0	No
51	350	95	85.1	1	1	No
53	500	92.2	79.3	70	13.5	Yes
52	700	88.0	81.3	80	11.5	Yes
54	1200	82.1	72.4	78	11	Yes
55	1400	79.1	71.0	79	12	Yes
57	1400	84.5	79.5	68	12	Yes
56	2000	68.5	62.2	78	12	Yes

*Specimen shattered at failure, elongation not determined.

TABLE III

NOTCH BAR TENSILE TEST RESULTS

1. Rim, Circumferential

Specimen No.	Test Temp-°F	UTS-KSI *	K_t
1	RT	138	3.1
2	125	149	3.1
5	RT	138	2.9
6	125	148	2.8

2. Mid-Radius, Radial

9	RT	61.5	2.6
10	200	140	3.1
11	150	157	3.2
12	125	141	3.0
13	100	153	3.1
14	RT	158	3.1
15	RT	156	3.1
16	RT	143	3.1

3. Mid-Radius, Axial

17	500	127	3.1
18	500	74.5**	3.1
19	350	78	3.1
21	400	102	3.3
23	RT	74.5	3.3
24	350	116	3.4

*Ultimate tensile strengths above 100 ksi indicate notch strengthening; values below 100 ksi indicate notch weakening.

**Failed in large diameter at specimen head.

TABLE IV

STRESS-TO-RUPTURE TEST RESULTS

	Specimen No.	Test Temp-°F	Stress-KSI	Life-Hours	% RA	% E
1. Mid-Radius, Radial						
	58	2000	66,000	17.2	81	16
	59	2000	66,000	13.4	81	16
2. Rim, Radial						
	62	2000	66,250	5.9	66	12
	64	2000	66,000	2.7	81	15
3. Rim, Circumferential						
	66	2000	66,000	19.9	79	15
	67	2000	66,000	23.5	82	15

TABLE V

DUCTILE-TO-BRITTLE TRANSITION TEMPERATURE FOR A NASA TZM WHEEL FORGING

Test Method	Specimen Direction	Transition Temperature-^{o}F
Charpy Impact	Radial	255
	Axial	590
Bend	Radial	75
	Axial	590
Smooth Tensile	Radial	75
	Axial	400
Notched Tensile	Radial	75*
	Axial	75/300*

*Transition from notch weakened to notch strengthened at failure.

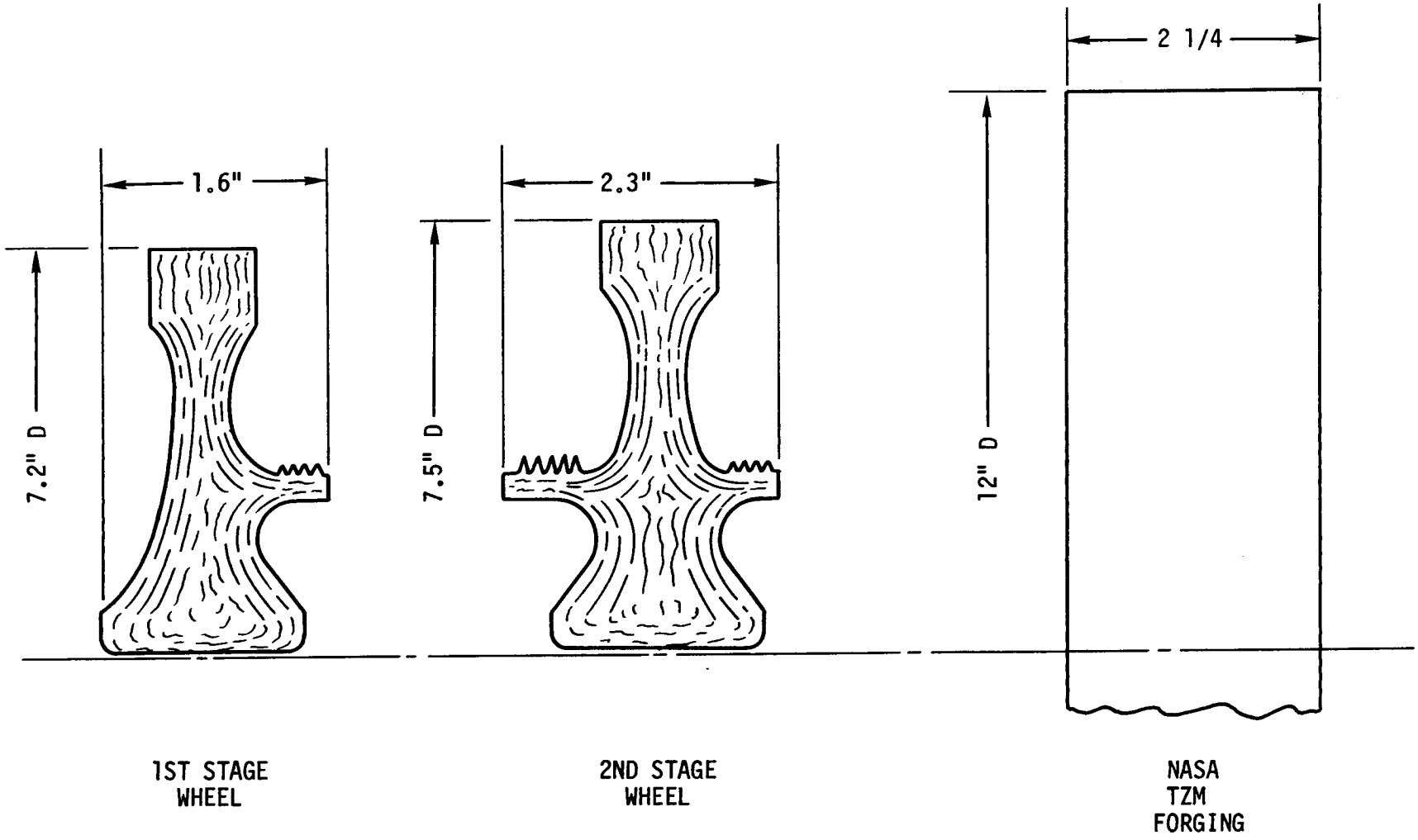

Figure 1. Turbine Wheel Shapes.

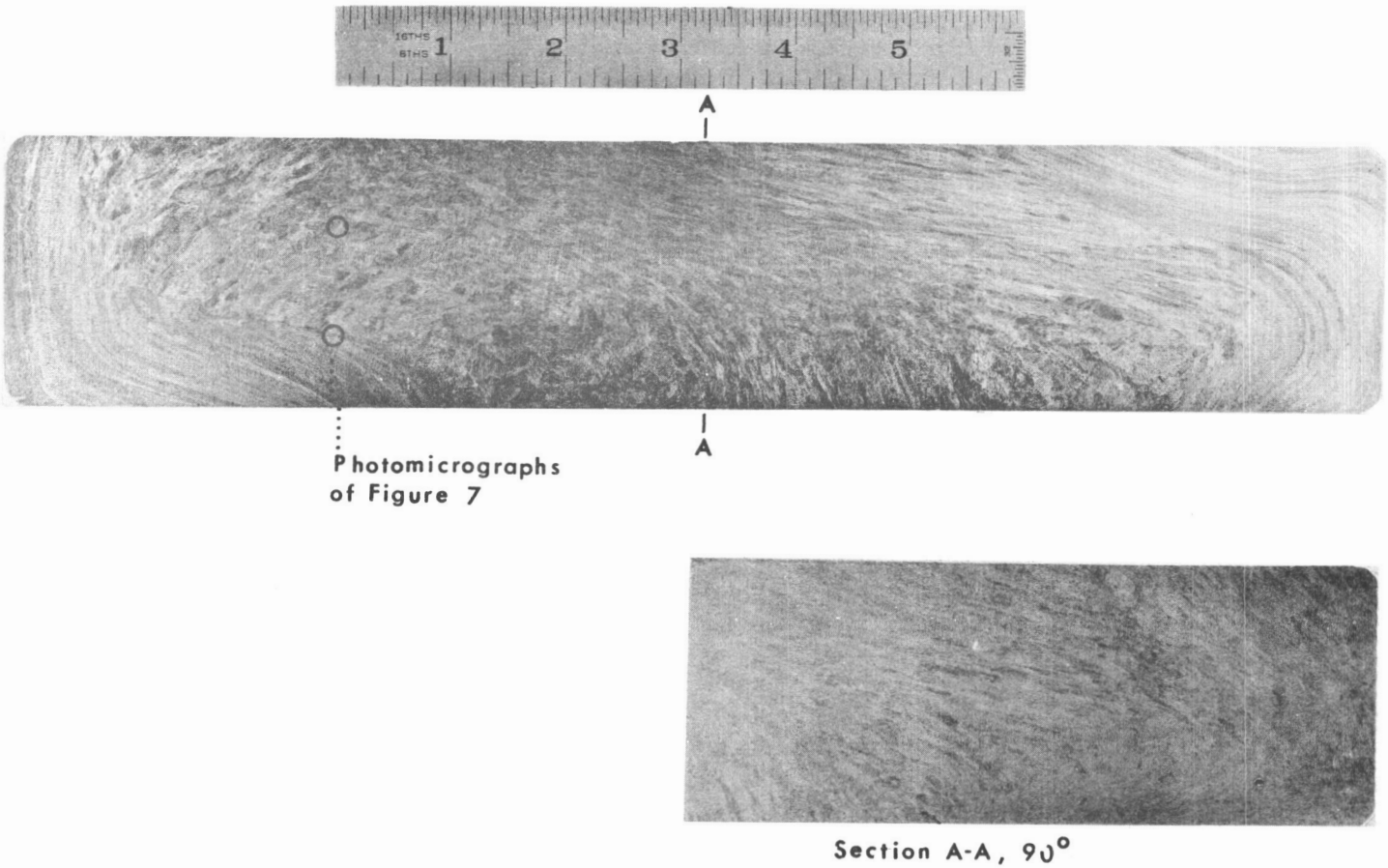

Figure 2. Cross Section of TZM Wheel Forging Macroetched With 47% HNO_3 + 2.5% HF Solution. (C66051950)

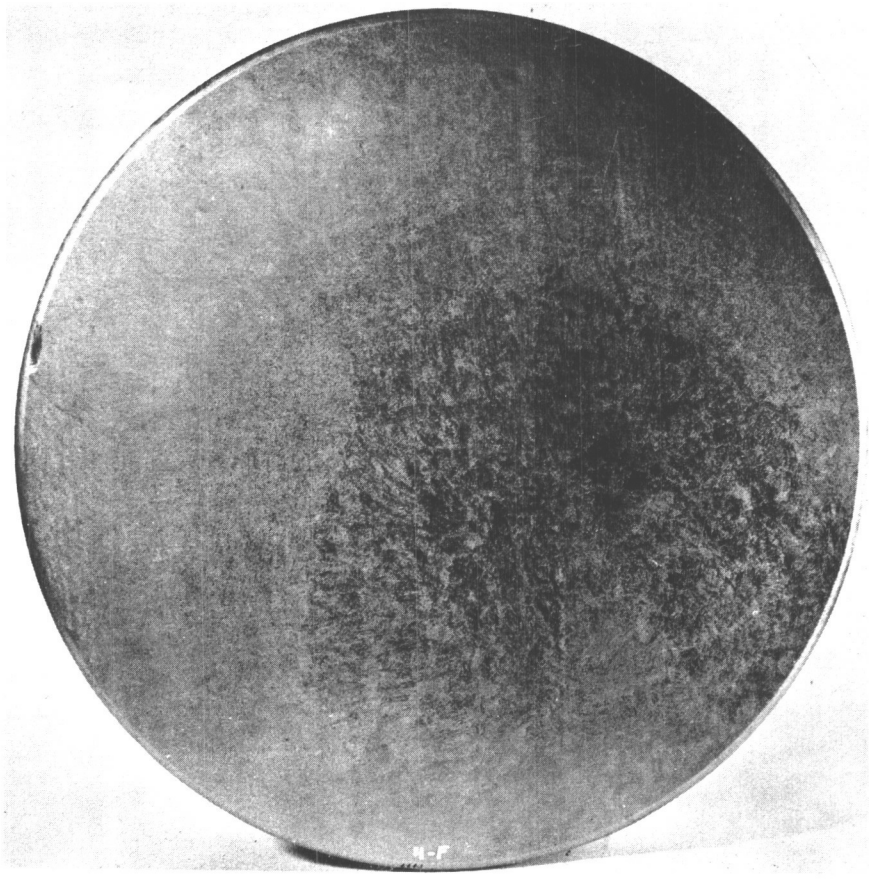

0°
FORE

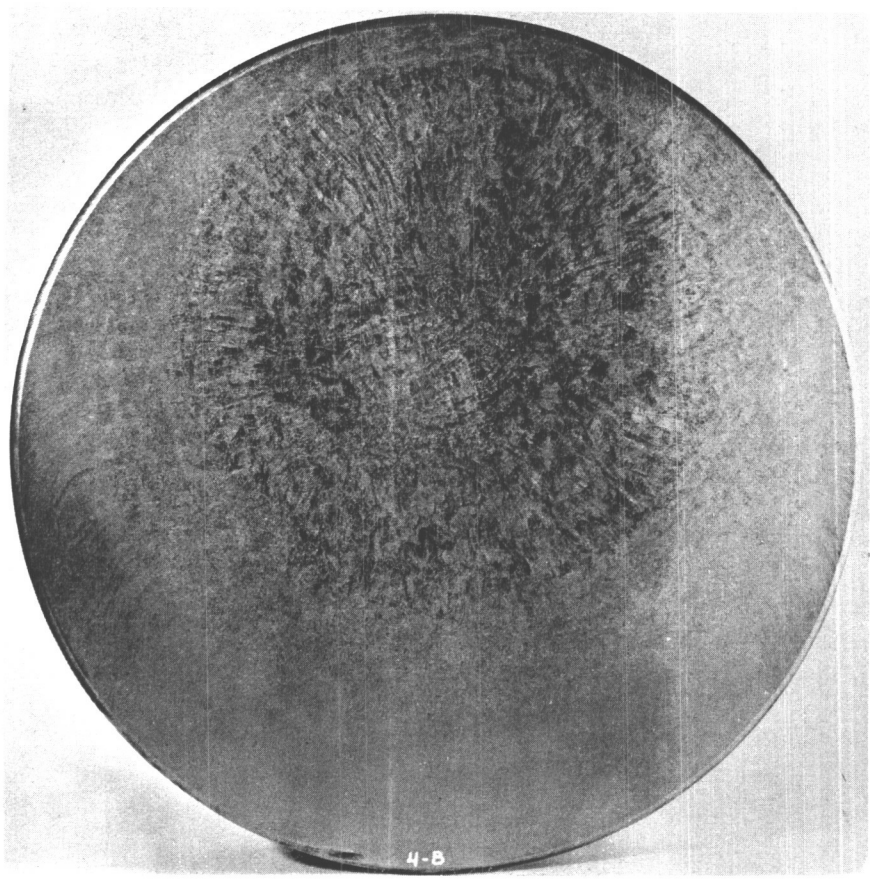

0°
AFT

Figure 3. Macroetch of Remaining Forgings.

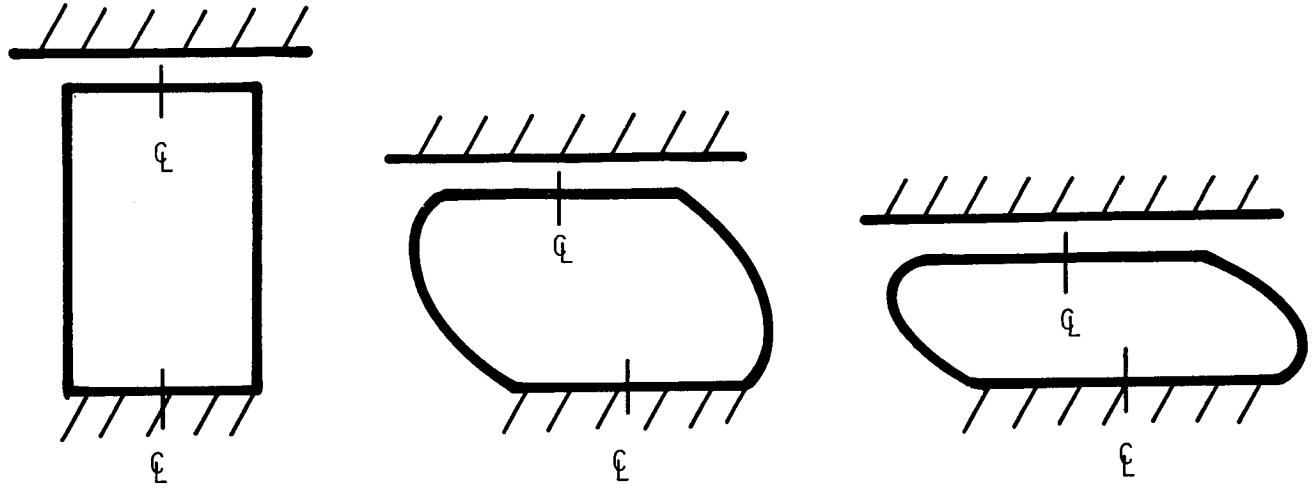

Figure 4. Apparent Forging Process.

Figure 5. Photo Micrographs of TZM Wheel Forging Sturcture at the Rim Location. Views Are Taken in the (a) Circumferential, (b) Axial, and (c) Radial Directions.

Etchant: Murakami's Etchant Mag: 100X

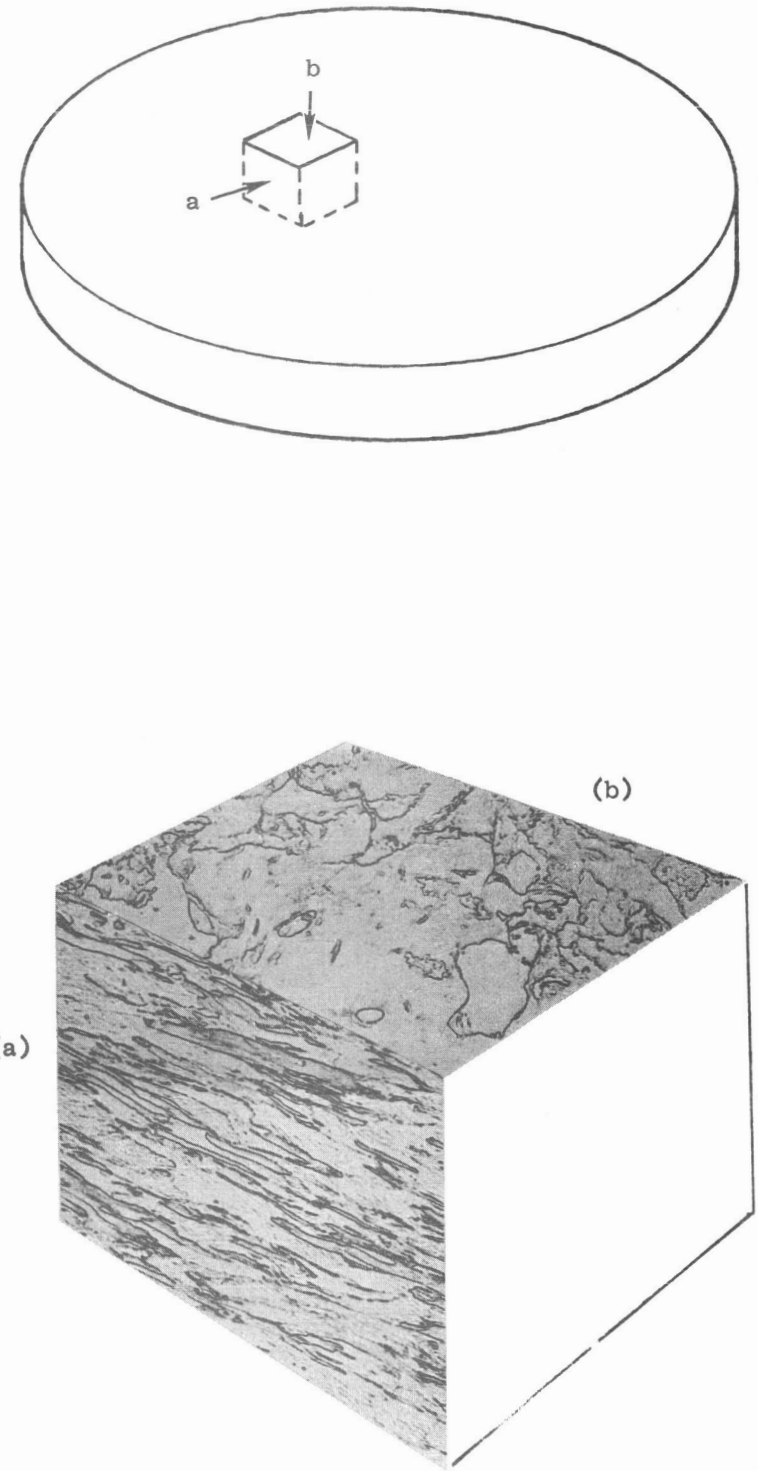

Figure 6. Photomicrographs of Structure at the Mid-Radius Location. Views are taken in the (a) Circumferential and (b) Axial Directions.

Etchant: Murakami's Etchant Mag: 100K

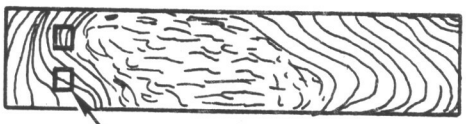

Area of Macroetch Indication

Area of Micrograph (See Figure 2)

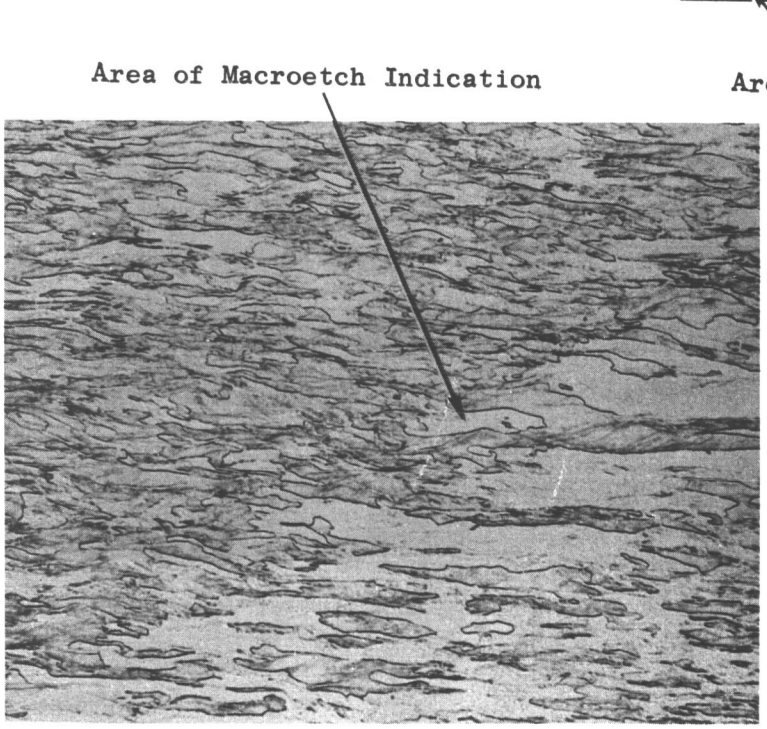

Figure 7. Photomicrographs of Grain Structure at Change of Grain Flow.
Etchant: Murakami's Reagent Mag: 100X

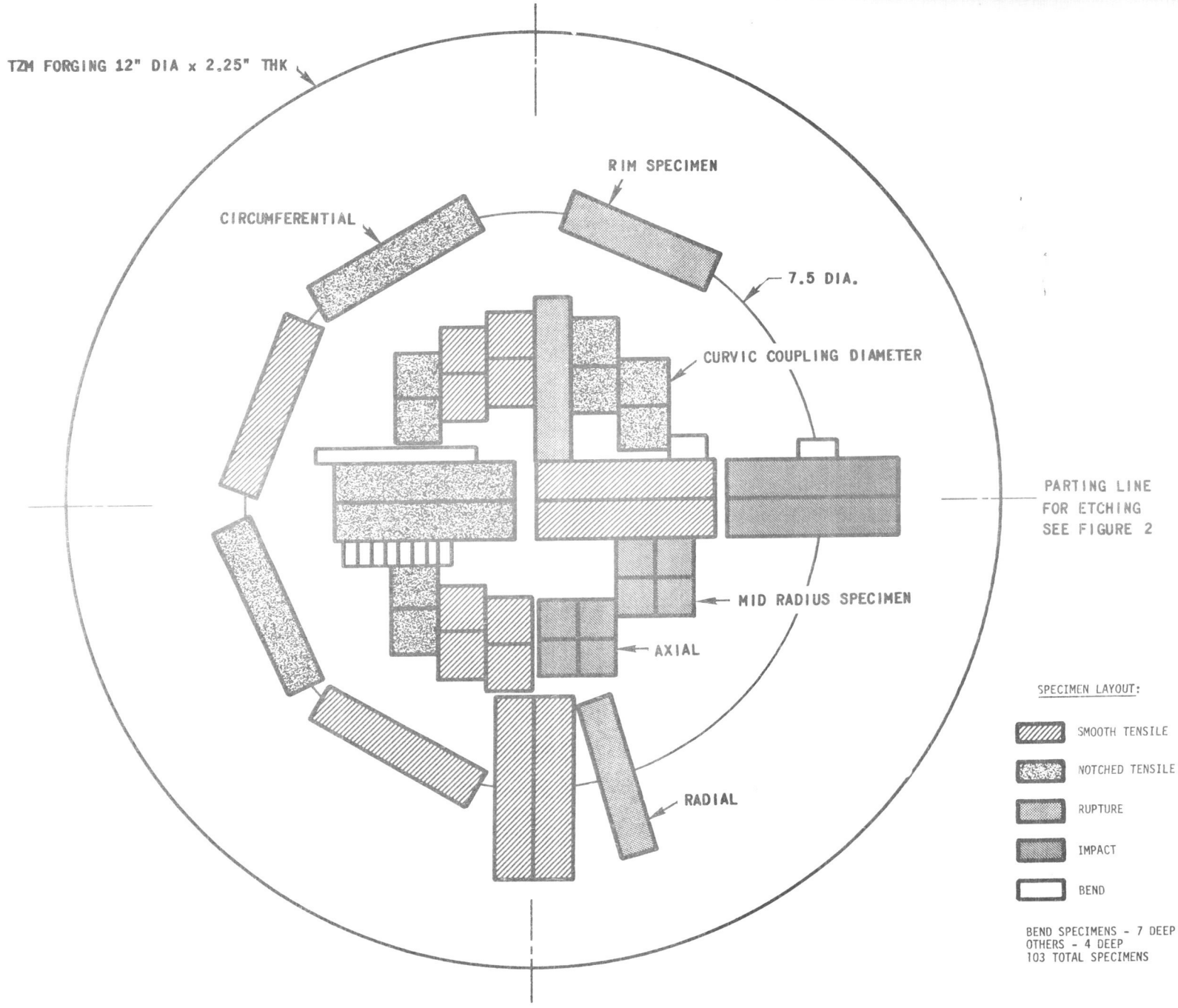

Figure 8. NASA TZM Forging Evaluation.

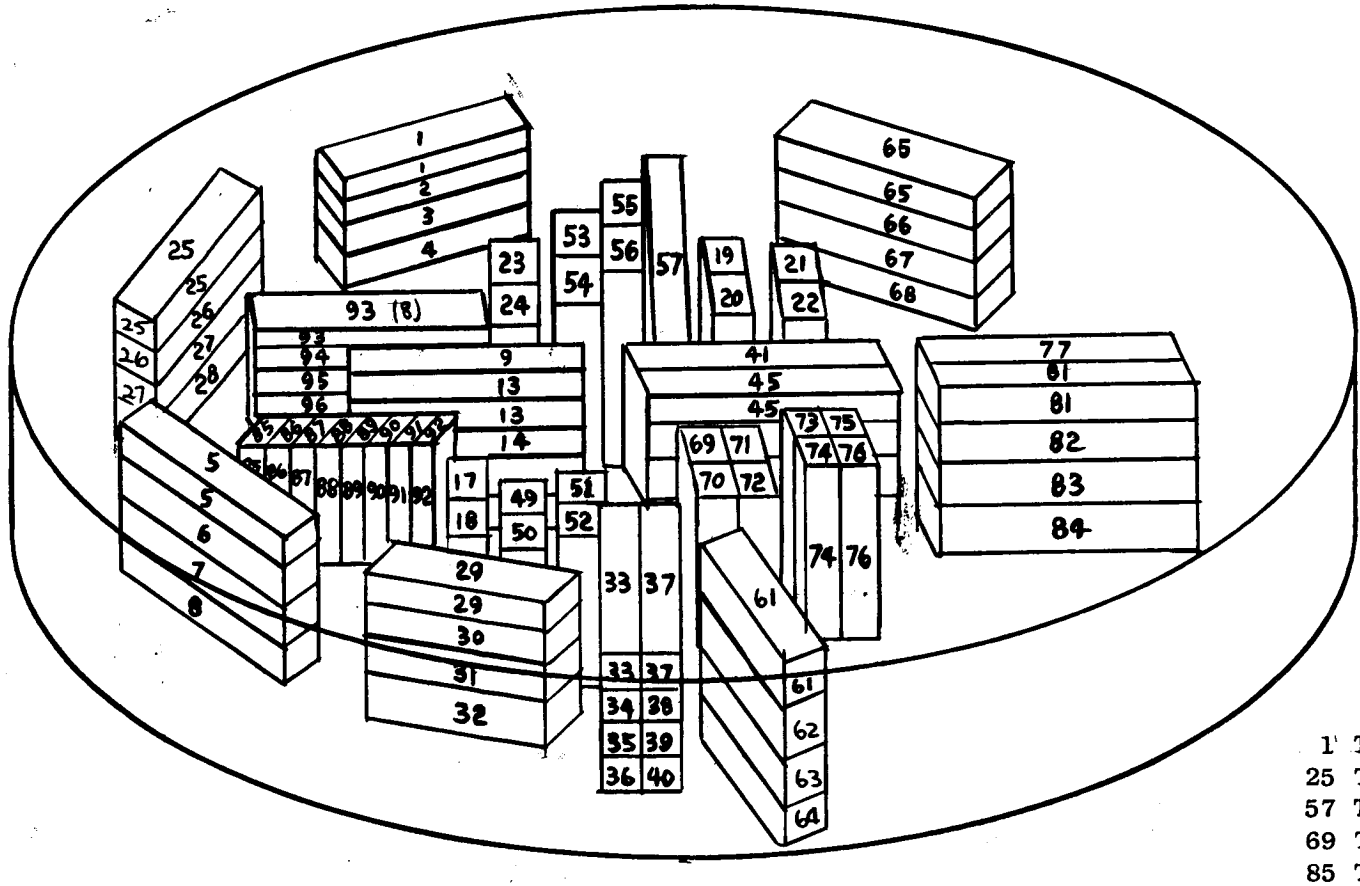

Figure 9. Specimen Location and Numbering Plan for Tensile, Rupture, Impact, and Bend Specimens from NASA TZM Forging for Three Stage Turbine.

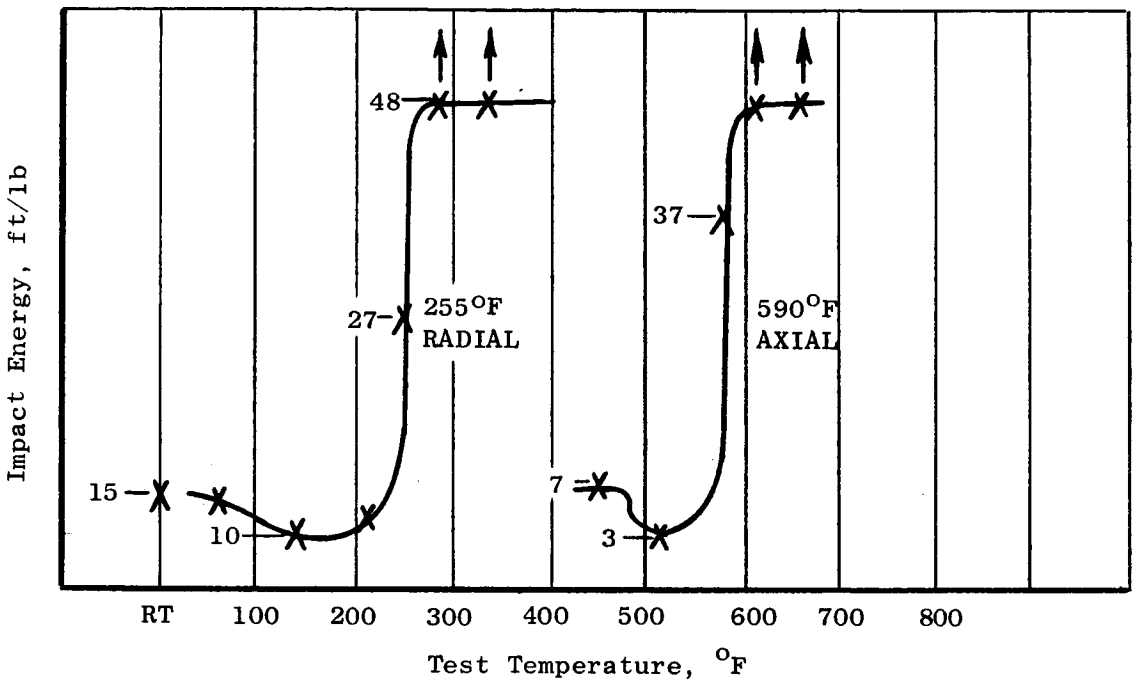

Figure 10. Impact Transition Temperature.

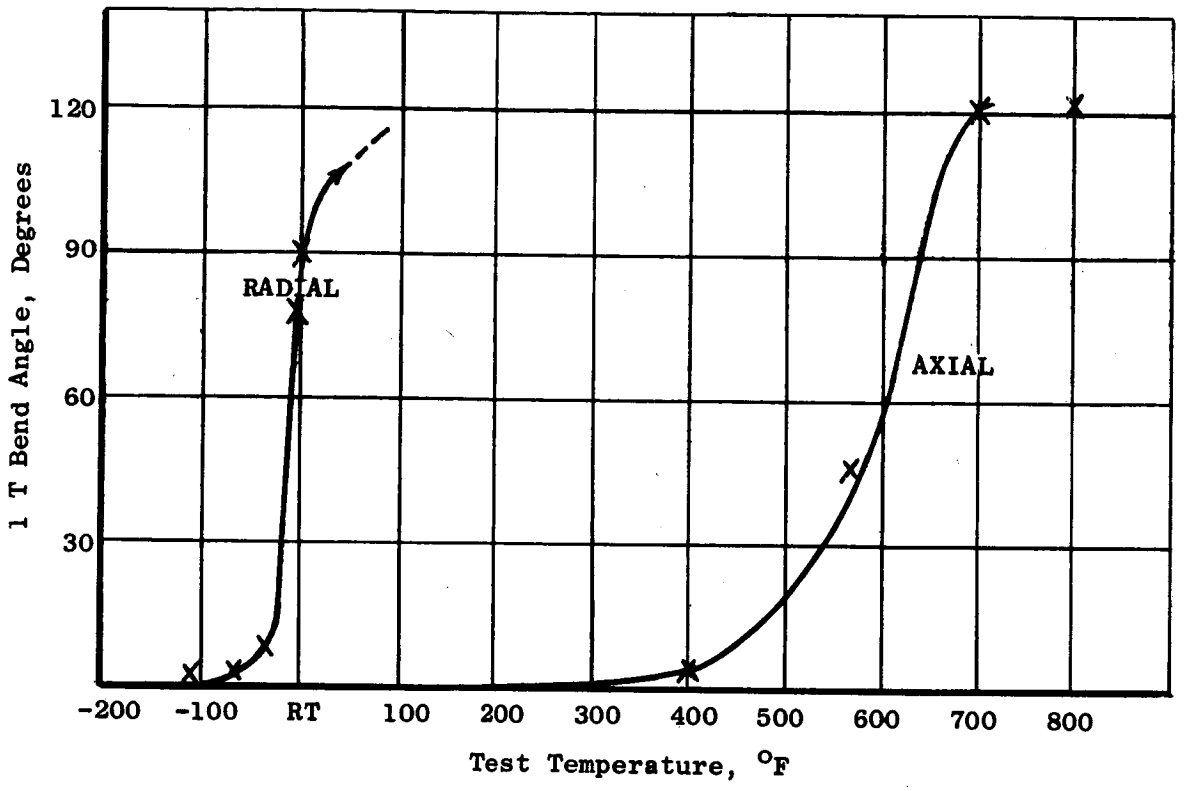

Figure 11. Slow Bend Transition Temperature.

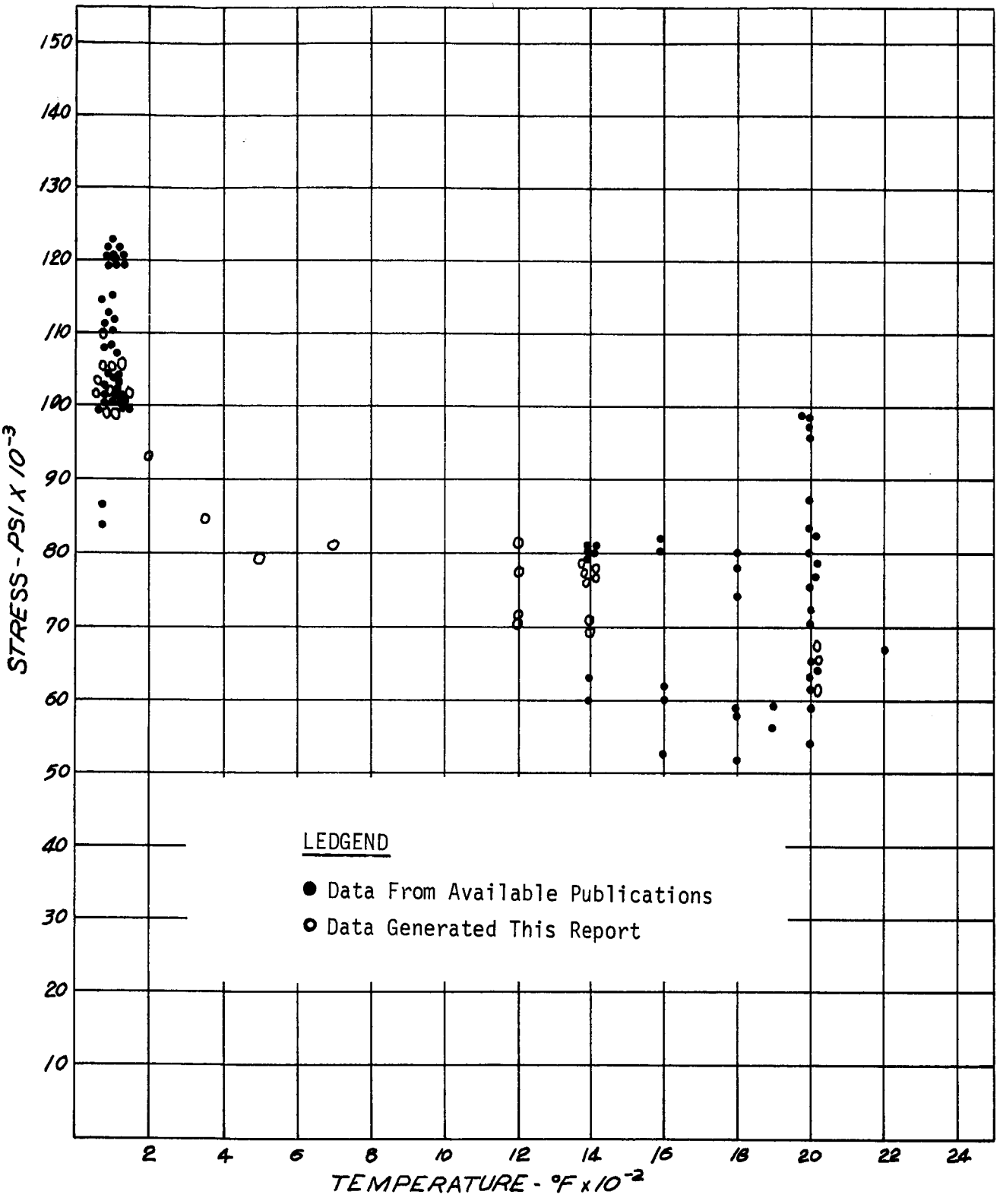

Figure 12. TZM Ultimate Tensile Strength.

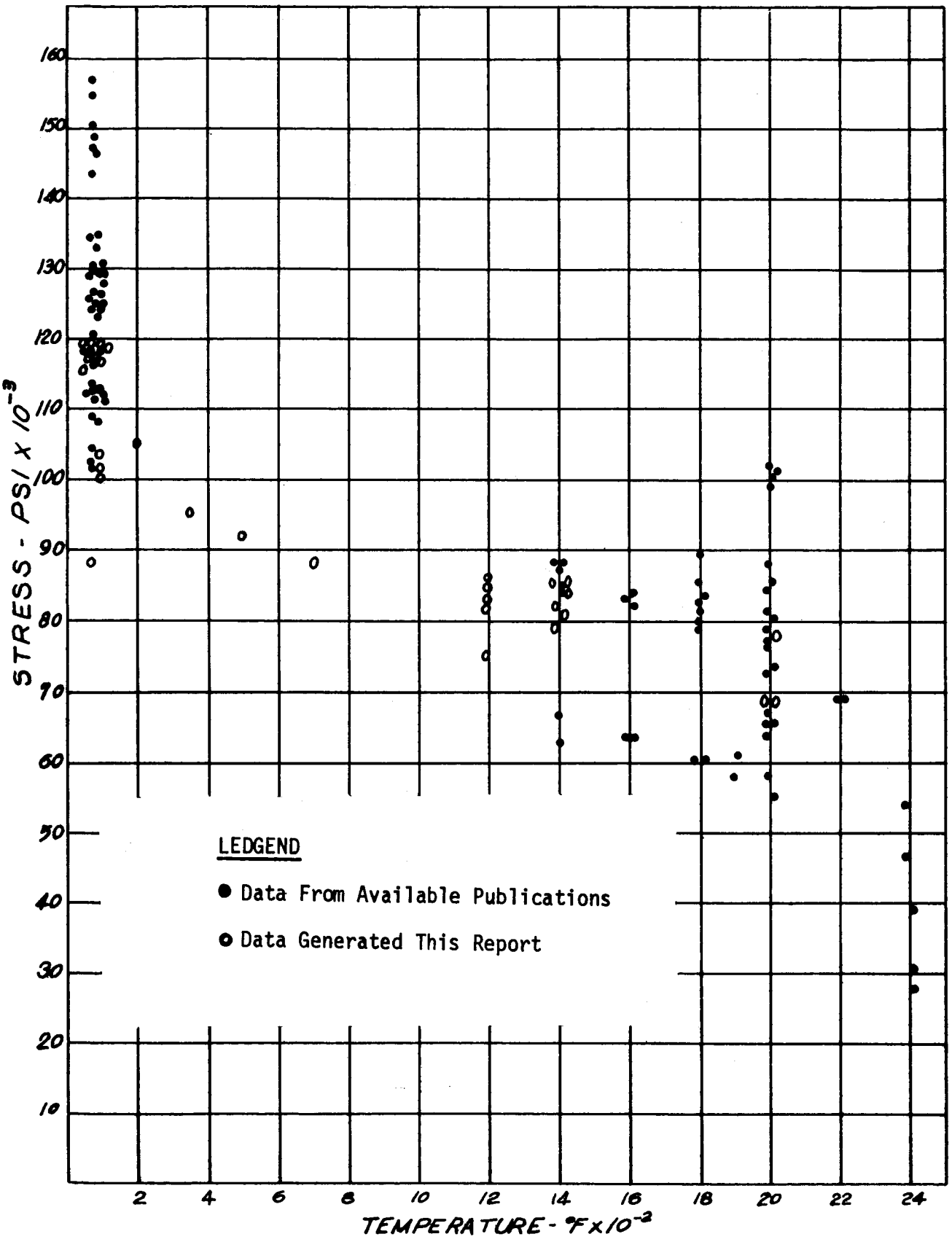

Figure 13. TZM Tensile Yield Strength.

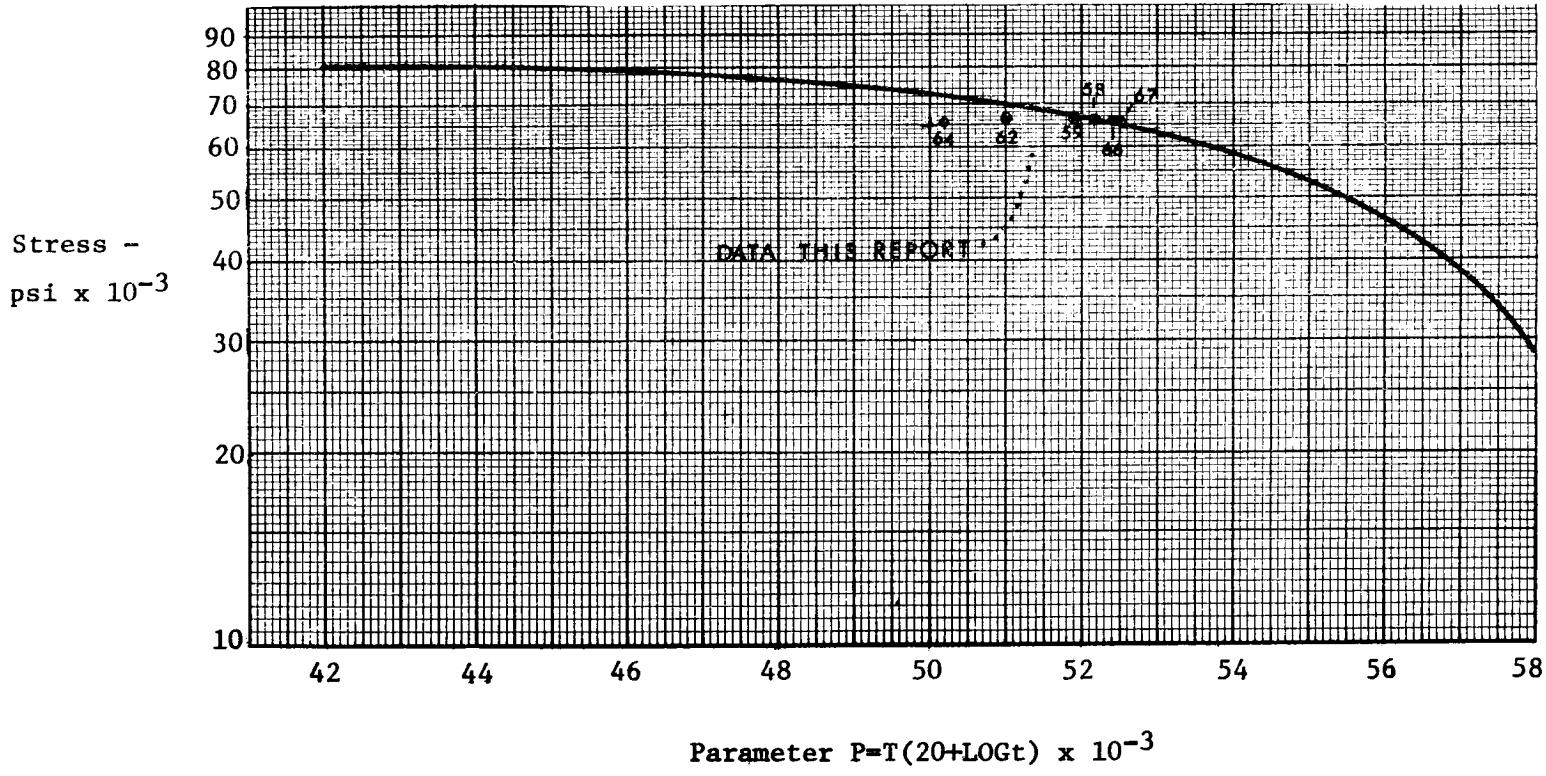

Figure 14. **TZM Rupture, Stress Relieved Bars & Forgings.**

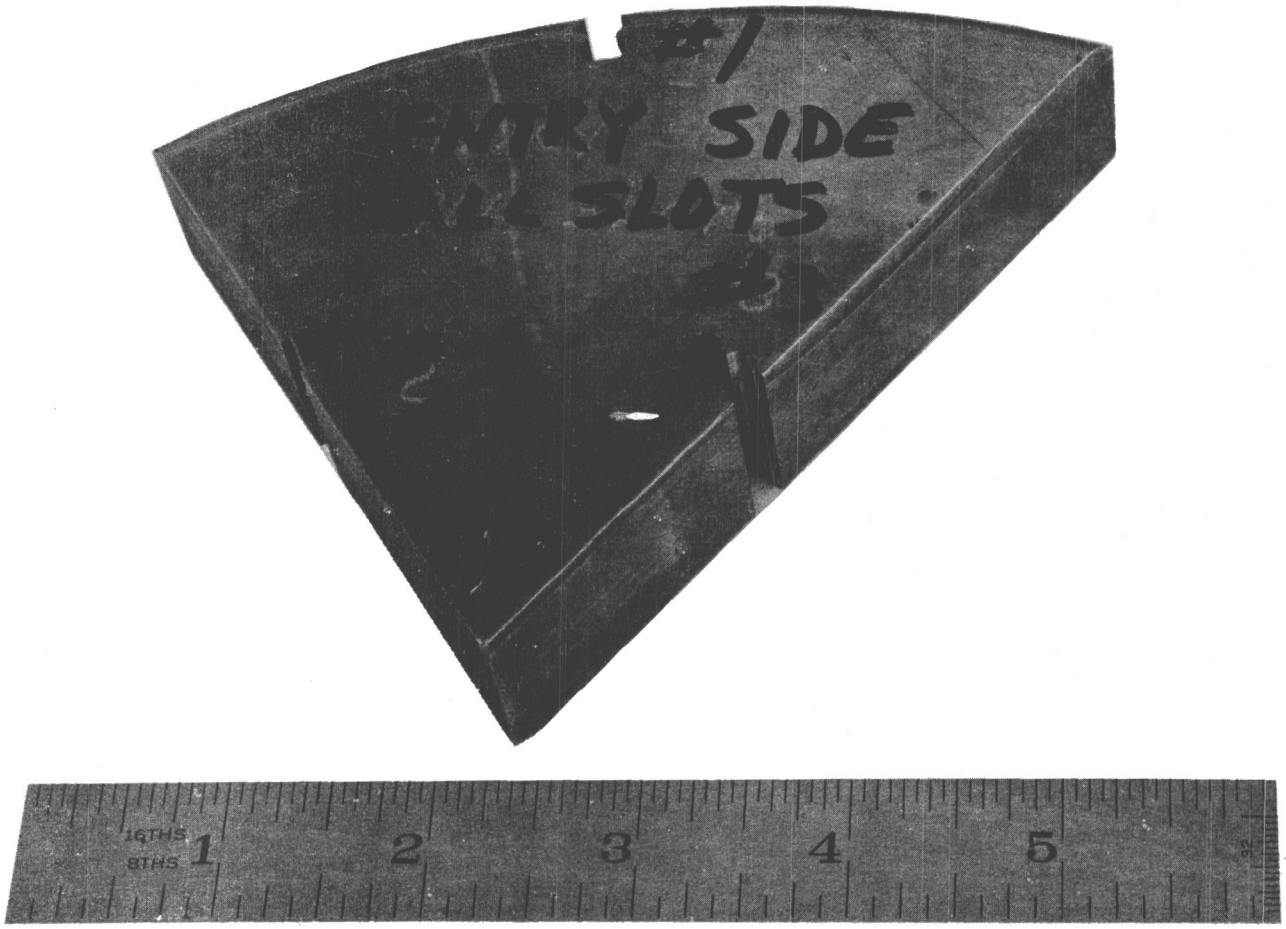

Figure 15. TZM Broach Specimen, Broach Entry Side. (C66100337)

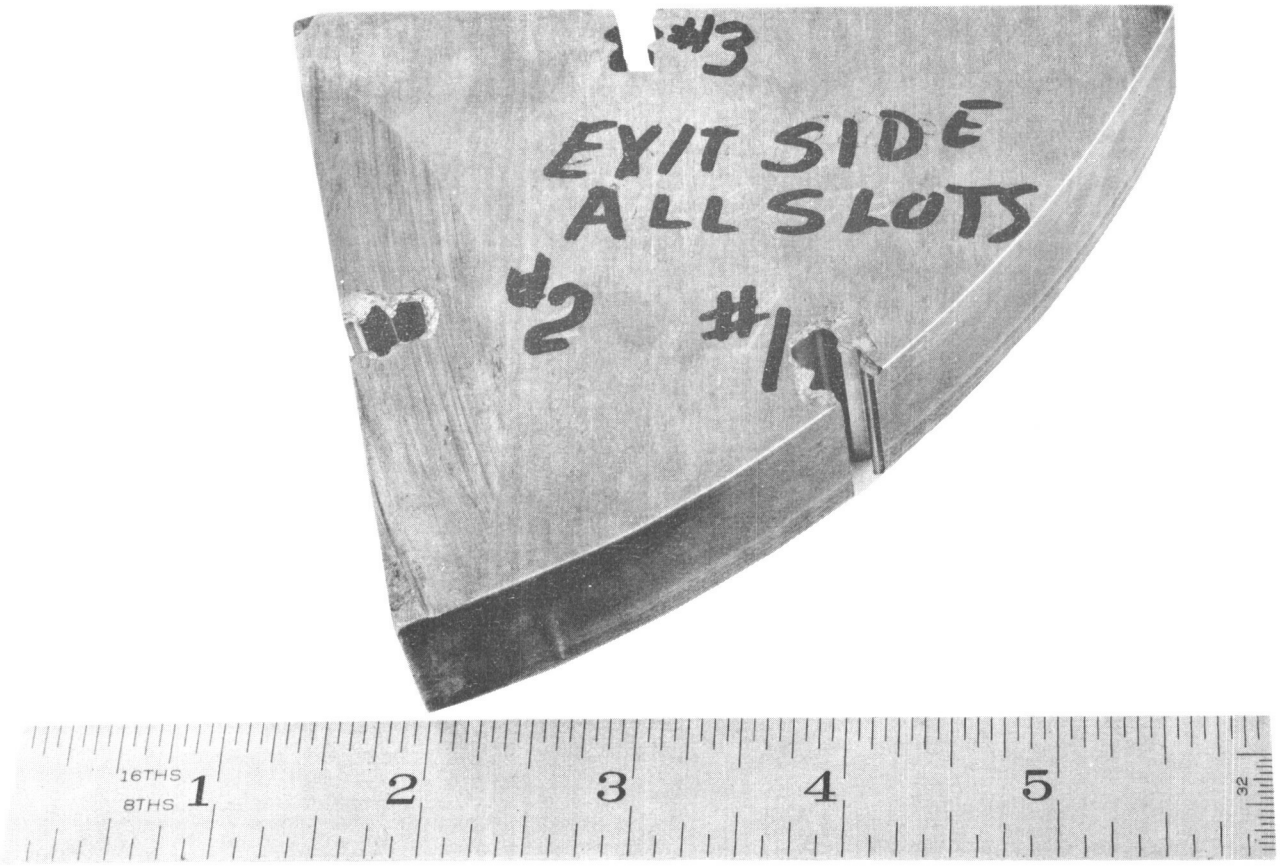

Figure 16. TZM Broach Specimen, Exit Slide All Slots. (C66100336)

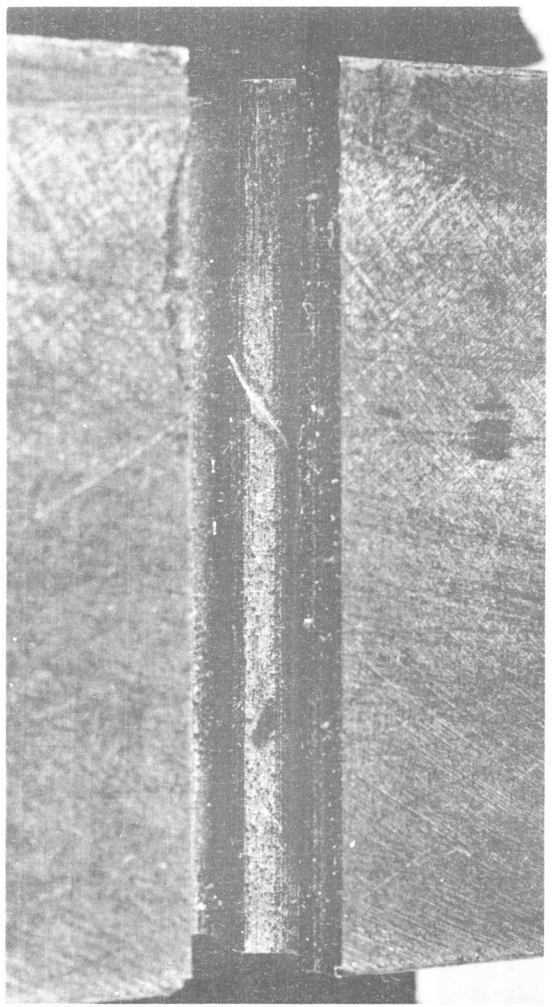

(C66101506)

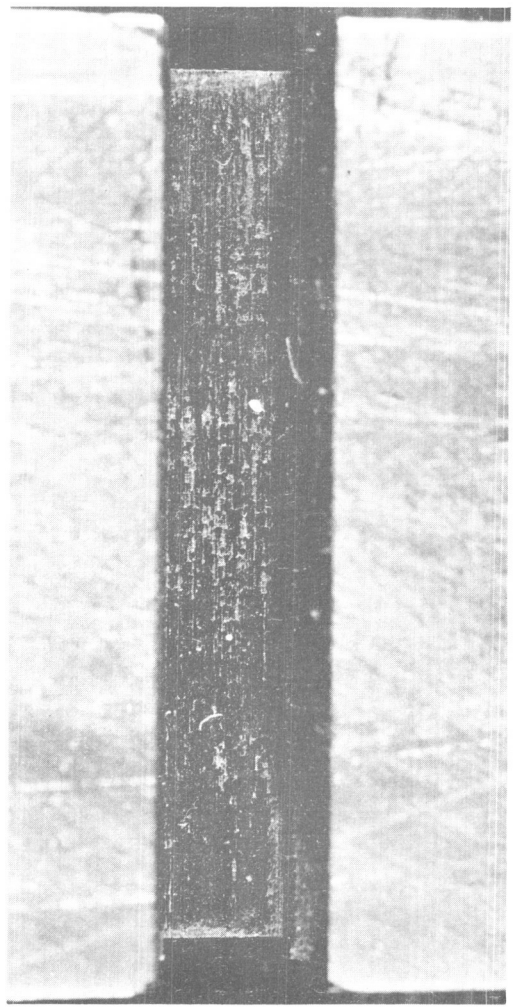

(C66101505)

Figure 17. Two Views of the Surface Finish of Slot #3 of the TZM Broached Specimen. Above, Bottom of Slot; Below, Lobe Surface. Mag: 5X

LIST OF DATA SOURCES FOR FIGURES

1. Semmel, Jr., J.W. et al, "Two-Stage Potassium Test Turbine, Volume I Materials Support", GE63FPD238, NAS 5-1143, May 8, 1963.

2. Anon., "Quarterly Technical Progress Report for Period Ending October 31, 1964, SNAP 50/SPUR Program", APS-5090-R3 Contract AF 33(615)1551, Air Research Manufacturing Company, April 17, 1964.

3. Anon., "Quarterly Technical Progress Report for Period Ending March 31, 1964, SNAP 50/SPUR Program", APS-5152-R2, Air Research Manufacturing Company, AF 33(615)2289, April 17, 1965.

4. Salley, R. L. and Kovacevich, E.A., "Materials Investigation, SNAP 50/SPUR Program, Pt. I Creep Rupture Properties of Stress Relieved TZM Alloy", APL TDR 64-116, Air Research Manufacturing Company, Contract AF 33(657)10922, October 1964.

5. Salley, R.L. and Kovacevich, E.A., "Materials Investigation SNAP 50/SPUR Program Mechanical Properties of TZM", AFAPL-TR-65-51, Air Research Manufacturing Company, Contract AF 33(615)2289, June 25, 1965.

6. Semchyshen, M. and Barr, R.Q., "Mechanical Properties of Molybdenum and Molybdenum-Base Alloy Sheet", ASTM STP272, 1959, pp. 12-13.

7. Anon., "Molybdenum Metal", Climax Molbydenum Company Data Sheet, 1959.

8. Sawyer, J.C. and Steigerwald, E.A., "Generation of Longtime Creep Data on Refractory Alloys at High Temperatures - Eighth Quarterly Report", Thompson Ramo Wooldridge, Inc., Contract NAS 3-2545, July 7, 1965.

9. Anon., "Quarterly Technical Progress Report for Period Ending June 30, 1966 SNAP 50/SPUR Program", APS-5152-R7, Air Research Manufacturing Company, Contract AF 33(615)2289, July 18, 1966.

APPENDIX B

BROACHING TZ MOLYBDENUM

BROACHING TZ MOLYBDENUM

* Conventional Broaching Data
* Metallography of Broached Specimens

C. E. Glynn, Manufacturing Engineer

P. A. Dion, Laboratory Technician

AME File #185

Advanced Manufacturing Engineering Laboratory
PMO - Manufacturing and Plant Engineering
Building 800, Mail Drop B-44

December, 1966

Introduction

This program was aimed at advancing the state-of-the-art for broaching TZ Molybdenum by defining tool geometry and machinability data that would generate 32 RMS surface finishes and acceptable broached slot exit edge conditions.

Earlier tests conducted by an independent testing vendor indicated surface finishing and exit edge conditions were problem areas.

Test results were to be documented with profilometer gage readings and photomicrographs of the microstructure of the broached surface, the entrance, and the exit edge of each slot produced.

Conclusions

1. Thirty to 50 RMS surface finishes can be broached in TZ Molybdenum alloy using conventional broaching methods. (See Figure I)

2. Photomicrographs do not show detrimental microstructural surface conditions as judged by the Advanced Manufacturing Engineering Laboratory. The surface, the entrance, and the exit edges of the four test slots showed microstructural surface "flow" (in the direction of the broaching force) in the order of one mil depth or less. (See Figure 2)

3. "Smearing" is a peculiarity of the visual appearance of broached TZ Molybdenum alloy surfaces. Each sample slot broached showed visual evidence of this "smearing". The microstructural "flow" was probable further indication of the smear.

4. The absence of a steel back-up plate at the exit edge of broached slots permits serious breakout of the TZ Molybdenum alloy.

Material Tested (1.0 Titanium, 0.5 Zr, bal. Mo)

The forging was made at Steel Improvement Company from a 7" round bar produced by the Climax Molybdenum Company. The Climax specification was CMX FB TZM-1. Normally, oxidation of TZ Molybdenum is prevented during forging by capsulation in stainless steel. The subject bar was reduced to a 2" thick forged wheel and thereafter split to a 1" thickness for the broaching tests. Hardness of the segments furnished to the laboratory was 24 Rc.

Recommendations

1. Machinability Data

Ram Speed:	13 surface feet per minute
Rise per Tooth:	.0023" roughing
	.0008" finishing

FIGURE I

BROACH TEST DATA SHEET

Test No. 7-254 — Date November 15, 1966

Tests By P. A. Dion

Material TZ-M (1.0 Ti., 0.5 Zr)
Hardness 24 Rc
Grain Size
Heat Treat
Thickness 1" with 1/2" steel back-up plate at the exit side of the slot
Avg. Chip Tk.
Type Test

Tool Overhang .375"
Tool Material T-15
Hardness 65 Rc
Cutting Fluid Sunicut 1225
Rise/Tooth .0023" and .0008"
Speed - L. Unl. 13 SFPM

Geometry & Sketch of Tool Form

1. Front Relief: 3° up sharp
2. Side Relief: 3°
3. Back Rake: 18° and 23°
4. Side Clearance: 1°
5. Shear Angle: 0°

Cutting Force #/in.^{2} at .005" wear
Radial Force #/in.^{2} at .005" wear

Test No.	No. Passes	Accum. Passes	Wear (c) Flank	Wear (c) Corn.	Edge B.U.	Chipping	Forces Cutting	Forces Radial	Specimen Finish	Type Chip	Chip Control	Test Condition Remarks
1	100	-	.004	.006	none	both corners			60 - 80 RMS			18° rake - .0023" R/T
2	100	-	.003	.006	slight	both corners			80 - 100 RMS			23° rake - .0023" R/T
(a) 3	100	-	.002	.003	none	one corner			30 - 50 RMS			18° rake - .0008" R/T
(a) 4	100	-	.002	.002	none	none			35 - 50 RMS (b)			23° rake - .0008" R/T

General Remarks (a) "Finishing Cut" type - Tests and #4 produced surface finishes that would generally classed as 32 RMS. This was the surface quality sired. (b) Finish checked by profilometer gage.) Crater wear on the tool interface was .002" to 004" wide - all four tests.

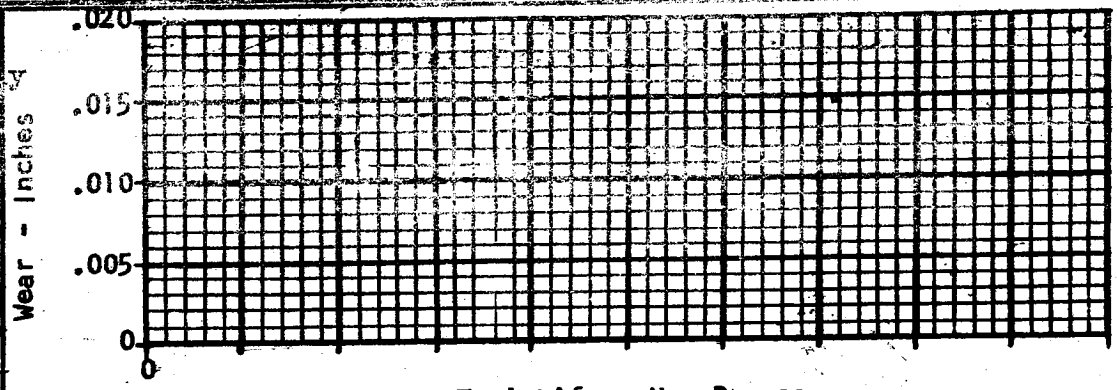

Figure I

1. Machinability Data - (Continued)

Tool Grade:	T-15 high speed steel
Tool Hardness:	65 Rc
Tool Chemistry:	12.0 W, 4.0 Cr, 5.0 V, and 5.0 Co
Tool Grind:	"low stress" wheel speed - 4000 surface feet per minute downfeed - .0005" per pass wheel grade - 38A80J 5VBE apply mist coolant
Tool Finish:	10 RMS
Tool Geometry:	(See Figure 1)
Cutting Oil:	Sunicut 1225
Chemistry:	8.5 Cl, 0.64 S, 5.0 sulfurized fatty oil with mineral oil base; 160 viscosity SUS 100

Discussion

1. The 30 to 50 RMS surface finishes were measured in the direction of the broached slot. Surface finishes across the slot could not be recorded with available profilometer styluses. However, a 30 to 50 RMS was judged to apply to the "across" surface finish also.

The conditions tested were conventional and can be duplicated in any broaching department. The Argonne National Laboratory reported that deep freeze machining of tungsten improves surface finishes and tool life. It is believed that deep freeze broaching of TZ Molybdenum would show similar improvements. The process is one of sub-zero cooling of a fluid containing 75% Stoddard Solvent and 25% Trichloroethylene. A contact at Argonne is Mr. P. J. Ziegelmeier. The Advanced Manufacturing Engineering Laboratory has a report on file from this source obtained by the Air Force Machinability Data Center of Cincinnati, Ohio.

It is my opinion that TZ Molybdenum can be broached by conventional methods. One hundred slots or more can be broached in TZ Molybdenum material, up to 1" thick, before resharpening of the tools becomes necessary.

2. Tests designed for this program were brief. It is possible that extensive testing would uncover machinability data for production of improved broached finishes and broach tool life. However, it is most apparent that the nature of TZ Molybdenum alloy was revealed as brittle and abrasive to broaching tools.

Discussion - (Continued)

The .062" radii on the broaching tools sustained .005" deep chipping after 100 strokes through TZ Molybdenum alloy. A .004" flank wear along the cutting edge in Test #1 (See Figure 1) indicated fairly rapid wear after 100 passes. As an example, Inconel 718 under similar broaching conditions, has been broached to recent tests 1200 slot passes before developing a .015" wearland.

TZ Molybdenum alloy must be supported with steel back-up plates. If the exit side of a given turbine wheel design was other than flat, a problem in "backing" would have to be solved. One test coupon was rejected because a serious break-out and laminar separation occurred as a result of allowing the TZ Molybdenum to overhang the steel.

3. A literature search uncovered a machinability report (T.I.S. #R56 AGT 199, titled "Broaching 0.5 Percent Titanium - Molybdenum," dated April 13, 1956). The machinability data in the earlier report are quite similar with the exception of back-up requirements. Apparently the difference lies in the alloying elements of the two materials.

Test Factors

Broaching Machine:	90" LaPointe
Test Material Coupons:	1.0 Ti., 0.5 Zr, balance Mo 1.0" x 1.5" x 1.5"
Back-up Material:	Mild Steel 0.5" x 1.5" x 1.5"
Fixture:	A special holder on the ram was fitted with suitable clamping to hold the TZ Molybdenum and steel coupons tightly together and well supported against tool forces.
Cutting Tools:	A single point tool made of T-15 high speed steel, 65 Rc, precision ground to:

Front Relief:	3° up sharp
Side Relief:	3° up sharp
Back Rake (hook):	18° and 23°
Side Clearance:	1°
Shear Angle:	0°

Test Factors - (Continued)

Rise Per Tooth:	Simulated by mounting the single point tool on the platen and upon each stroke of the ram advancing the platen the selected rise per tooth quantity. a. .0023" selected for representative roughing teeth - .0008" selected for representative finishing teeth.
Test End Point:	100 strokes (equivalent of 100 slots)
Test Pattern:	Test #1 18° rake .0023" R/T Test #2 23° rake .0023" R/T Test #3 18° rake .0008" R/T Test #4 23° rake .0008" R/T
Surface Finish Measurements:	profilometer
Visual Examinations:	10X, 20X, and 45X microscope a. Wearlands observed on flank, corners, and rake (hook) interface. (See Figure 1)

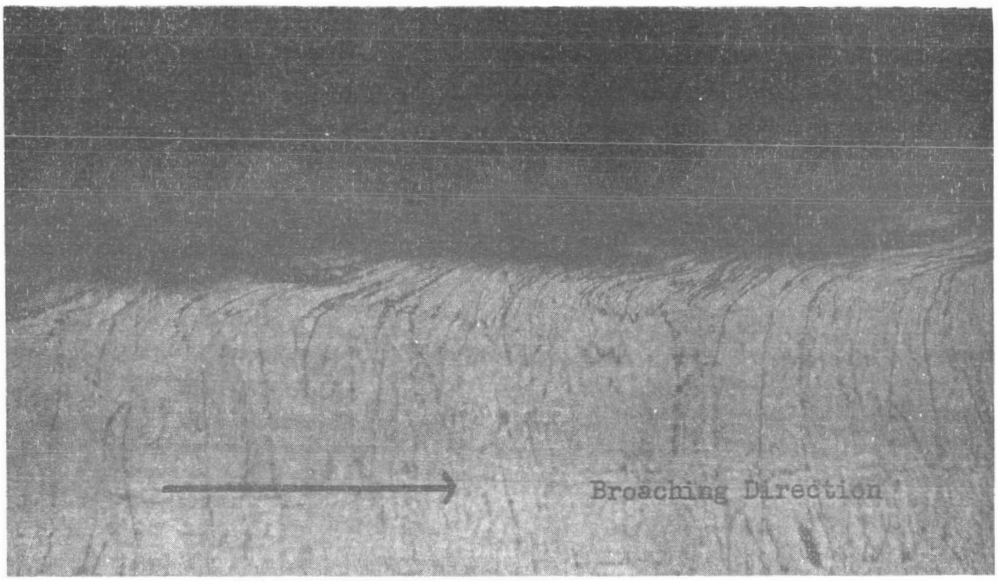

ROUGH CUT

23° Rake
.0023" Rise/Tooth

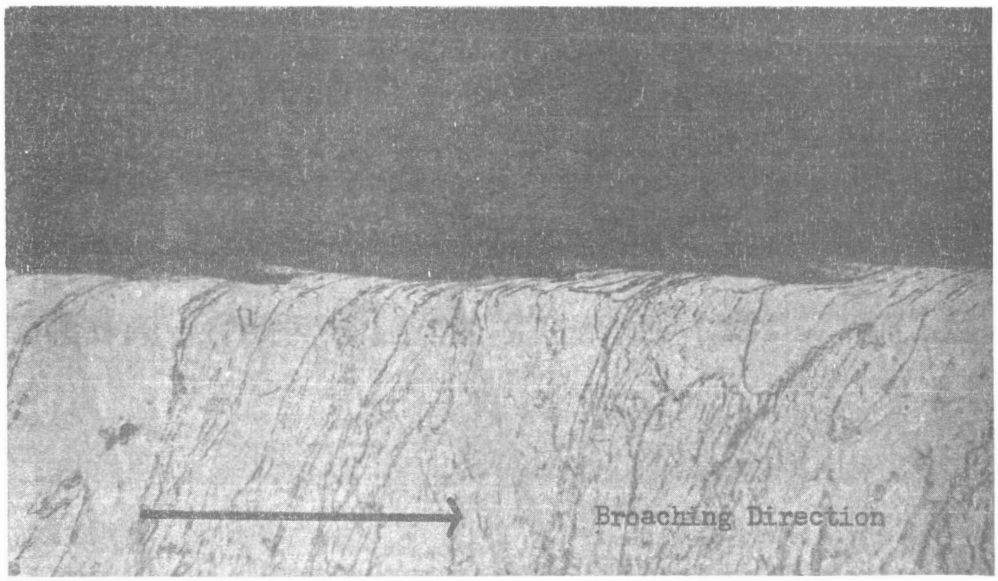

FINISH CUT

23° Rake
.0008" Rise/Tooth

35-50 RMS
250X

Figure 2. Sections through rough and finish type broaching cuts.

DISTRIBUTION LIST

NAS3-8520

National Aeronautics & Space Administration
Headquarters
Washington, D. C. 20546
ATTN: W. H. Woodward, Code RN

National Aeronautics & Space Administration
Headquarters
Washington, D. C. 20546
ATTN: Dr. Fred Schulman, Code RNP

National Aeronautics & Space Administration
Headquarters
Washington, D. C. 20546
ATTN: J. J. Lynch, Code RNP

National Aeronautics & Space Administration
Headquarters
Washington, D. C. 20546
ATTN: S. V. Manson, Code RNP

National Aeronautics & Space Administration
Headquarters
Washington, D. C. 20546
ATTN: H. D. Rochen, Code RNP

National Aeronautics & Space Administration
Scientific & Technical Information Facility
P.O. Box 33
College Park, Maryland 20740
ATTN: Acquisition Branch, (SQT-34054)
(2 + reproducible)

NASA - Lewis Research Center
21000 Brookpark Road
Cleveland, Ohio 44135
ATTN: Dr. B. Lubarsky (500-201)

NASA - Lewis Research Center
21000 Brookpark Road
Cleveland, Ohio 44135
ATTN: R. E. English (500-201)

NASA - Lewis Research Center
21000 Brookpark Road
Cleveland, Ohio 44135
ATTN: T. A. Moss (500-201)

NASA - Lewis Research Center
21000 Brookpark Road
Cleveland, Ohio 44135
ATTN: J. A. Heller (500-201)

NASA - Lewis Research Center
21000 Brookpark Road
Cleveland, Ohio 44135
ATTN: J. P. Joyce (500-201)

NASA - Lewis Research Center
21000 Brookpark Road
Cleveland, Ohio 44135
ATTN: H. O. Slone (500-201)

NASA - Lewis Research Center
21000 Brookpark Road
Cleveland, Ohio 44135
ATTN: J. H. Dunn (500-201)

NASA - Lewis Research Center
21000 Brookpark Road
Cleveland, Ohio 44135
ATTN: I. Pinkel (5-3)

NASA - Lewis Research Center
21000 Brookpark Road
Cleveland, Ohio 44135
ATTN: W. L. Stewart (77-2)

NASA - Lewis Research Center
21000 Brookpark Road
Cleveland, Ohio 44135
ATTN: J. E. Dilley (500-309)

NASA - Lewis Research Center
21000 Brookpark Road
Cleveland, Ohio 44135
ATTN: T. P. Moffitt (77-2)

NASA - Lewis Research Center
21000 Brookpark Road
Cleveland, Ohio 44135
ATTN: N. Musial (501-3)

NASA - Lewis Research Center
21000 Brookpark Road
Cleveland, Ohio 44135
ATTN: Library (60-3) (2)

NAS3-8520

NASA - Lewis Research Center
21000 Brookpark Road
Cleveland, Ohio 44135
ATTN: Report Control Office (5-5)

NASA - Lewis Research Center
21000 Brookpark Road
Cleveland, Ohio 44135
ATTN: P. E. Foster (3-19)

NASA - Lewis Research Center
21000 Brookpark Road
Cleveland, Ohio 44135
ATTN: F. J. Dutee (21-4)

NASA - Lewis Research Center
21000 Brookpark Road
Cleveland, Ohio 44135
ATTN: A. Glassman (77-2)

NASA - Lewis Research Center
21000 Brookpark Road
Cleveland, Ohio 44135
ATTN: V. F. Hlavin (3-14)

Lewis Research Center/SNAP-8 Field Office
Aerojet-General Corporation
Von Karman Center
P.O. Box 754
Azusa, California 91702
ATTN: J. G. Kennard

U. S. Atomic Energy Commission
Technical Information Service Extension
P.O. Box 62
Oak Ridge, Tennessee 37831

U S. Atomic Energy Commission
Washington, D. C. 20545
ATTN: Dr. Nicholas Grossman

U. S. Atomic Energy Commission
Washington, D. C. 20545
ATTN: Lt. Col. G. M. Anderson

Aerojet-General Corporation
Von Karman Center
P.O. Box 296
Azusa, California 91702
ATTN: Paul I. Wood

Atomics International
North Americal Aviation, Inc.
P.O. Box 309
Canoga Park, California 91304
ATTN: R. W. Dickinson

Battelle Memorial Institute
505 King Avenue
Columbus, Ohio 43201
ATTN: C. M. Allen

Brookhaven National Laboratory
Upton, Long Island, New York 11973
ATTN: Dr. O. E. Dwyer

Curtiss Wright Corporation
Wright Aeronautical Division
Wood Ridge, New Jersey 07075
ATTN: S. Lombardo

Defense Documention Center
Cameron Station
Alexandria, Virginia 22314

Ford Motor Company
Aeronutronic Division
Ford Road
Newport Beach, California 92660
ATTN: George P. Carver

Ford Motor Company
Aeronutronic Division
Ford Road
Newport Beach, California 92660
ATTN: Hans D. Linhardt

The Franklin Institute
Benjamin Franklin Parkway at 20th St.
Philadelphia, Pennsylvania 19103
ATTN: Otto Decker

The Garrett Corporation
AiResearch Mfg. Company
Phoenix, Arizona 85034
ATTN: Robert Gruntz

The Garrett Corporation
AiResearch Mfg. Company
Phoenix, Arizona 85034
ATTN: Librarian

Jet Propulsion Laboratory
California Institute of Technology
4800 Oak Grove Drive
Pasadena, California 91103
ATTN: Lance Hays

Lawrence Radiation Laboratory
P.O. Box 808
Livermore, California 94550
ATTN: Dr. James Hadley (2)

Massachusetts Institute of Technology
Engineering Projects Laboratory
Research Laboratory of Electronics
Cambridge, Massachusetts 02139
ATTN: Prof. George A. Brown

Mechanical Technology Incorporated
968 Albany-Shaker Road
Latham, New York 12110
ATTN: Dr. Beno Sternlicht

National Bureau of Standards
Washington, D. C. 20225
ATTN: C. W. Beckett

Power Information Center
University of Pennsylvania
3401 Market Street, Room 2107
Philadelphia, Pennsylvania 19104

Pratt and Whitney Aircraft
United Aircraft Corporation
East Hartford, Connecticut 06108
ATTN: Dr. W. Lueckel

Pratt and Whitney Aircraft
United Aircraft Corporation
East Hartford, Connecticut 06108
ATTN: W. H. Podelny

Southwest Research Institute
8500 Culebra Road
San Antonio, Texas 78206
ATTN: Dr. R. A. Burton

Sundstrand Aviation-Denver
Division of Sundstrand Corporation
Denver, Colorado 80221
ATTN: Robert Boyer

TRW Inc.
TRW-Electromechanical Division
7209 Platt Avenue
Cleveland, Ohio 44104
ATTN: Frank Bayer

TRW Inc.
TRW-Equipment Laboratory
23555 Euclid Avenue
Cleveland, Ohio 44117
ATTN: J. E. Taylor

Westinghouse Electric Corporation
Astronuclear Laboratory
P.O. Box 10864
Pittsburgh, Pennsylvania 15236
ATTN: R. T. Begley

Westinghouse Electric Corporation
Astronuclear Laboratory
P.O. Box 10864
Pittsburgh, Pennsylvania 15236
ATTN: W. D. Pouchot

Westinghouse Electric Corporation
Research Laboratories
Pittsburgh, Pennsylvania 15236
ATTN: J. Boyd

Aeronautical Systems Division
Aeromechanical Branch
Wright-Patterson AFB, Ohio 45433
ATTN: Charles Armbruster, ASRMFP-1

Aeronautical Systems Division
Wright-Patterson AFB, Ohio 45433
ATTN: George Sherman, API

Aeronautical Systems Division
Wright-Patterson AFB, Ohio 45433
ATTN: George E. Thompson, APIP-1

Aerospace Research Laboratory
Building 450
Wright-Patterson AFB, Ohio 45433
ATTN: Dr. G. Gyarmathy, ARN

NAS3-8520

Oak Ridge National Laboratory
P.O. Box X
Oak Ridge, Tennessee 37831
ATTN: William O. Harms
Metals & Ceramics Div.

Oak Ridge National Laboratory
P.O. Box Y
Oak Ridge, Tennessee 37831
ATTN: H. W. Savage

Oak Ridge National Laboratory
P.O. Box Y
Oak Ridge, Tennessee 37831
ATTN: Dr. Arthur Fraas